Spring 4-24-2014

Development of a MASH TL-3 Transition Between Guardrail and Portable Concrete Barriers

David A. Gutierrez

University of Nebraska-Lincoln, david.gutierrez24@huskers.unl.edu

Follow this and additional works at: http://digitalcommons.unl.edu/civilengdiss

Part of the Civil Engineering Commons, and the Structural Engineering Commons

DEVELOPMENT OF A MASH TL-3 TRANSITION BETWEEN

GUARDRAIL AND PORTABLE CONCRETE BARRIERS

by

David Anthony Gutierrez

A THESIS

Presented to the Faculty of

The Graduate College at the University of Nebraska

In Partial Fulfillment of Requirements

For the Degree of Master of Science

Major: Civil Engineering

Under the Supervision of Professor Ronald K. Faller

Lincoln, Nebraska

May, 2014

DEVELOPMENT OF A MASH TL-3 TRANSITION BETWEEN GUARDRAIL AND PORTABLE CONCRETE BARRIERS

David Anthony Gutierrez, M.S.

University of Nebraska, 2014

Advisor: Ronald K. Faller

Often, road construction causes the need to create a work zone. In these scenarios, portable concrete barriers (PCBs) are typically installed to shield workers and equipment from errant vehicles as well as prevent motorists from striking other roadside hazards. For an existing W-beam guardrail system installed adjacent to the roadway and near the work zone, guardrail sections are removed in order to place the portable concrete barrier system. The focus of this research study was to develop a proper stiffness transition between W-beam guardrail and portable concrete barrier systems. This research effort was accomplished through development and refinement of design concepts using computer simulation with LS-DYNA.

Several design concepts were simulated, and design metrics were used to evaluate and refine each concept. These concepts were then analyzed and ranked based on feasibility, likelihood of success, and ease of installation. The rankings were presented to the Technical Advisory Committee (TAC) for selection of a preferred design alternative. Next, a Critical Impact Point (CIP) study was conducted, while additional analyses were performed to determine the critical attachment location and a reduced installation length for the portable concrete barriers. Finally, an additional simulation effort was conducted in order to evaluate the safety performance of the transition system under reverse-direction impact scenarios as well as to select the CIP.

Recommendations were also provided for conducting a Phase II study and evaluating the nested MGS configuration using three Test Level 3 (TL-3) full-scale crash tests according to the criteria provided in the *Manual for Assessing Safety Hardware*, as published by the American Association of Safety Highway and Transportation Officials (AASHTO).

ACKNOWLEDGEMENTS

First, I would like to thank my advisor and committee chair, Dr. Ronald Faller. You always made time to ensure that all of my questions and concerns were answered no matter how busy your schedule was. You ensured me that this was not an impossible task even when things looked overwhelming to me.

I would also like to thank the other members of my committee, Dr. Daniel Linzell and Dr. John Reid. Dr. Linzell, I wish that I had the opportunity to take one of your classes because I know that you are very knowledgeable and have our program headed toward being one of the finest in the nation. Dr. Reid, I learned everything that I know about computer simulation from your classes. You taught me that hard work pays off and to always be inquisitive.

I owe a big thank you to the whole Midwest Roadside Safety Facility staff. I appreciate having learned and grown as both an engineer and person with you. Thank you, Bob Bielenberg, for being my mentor and guide through this whole process. You took the time to answer every question and explain every foreign concept with patience and diligence.

Lastly, I want to thank my family and friends. My parents, Henry and Penny Gutierrez, have supported me through thick and thin. This opportunity could not be possible without your love and care every day of my life. Thank you to my friends for allowing me to forget about the stresses of graduate school and remember to still enjoy life along the way.

TABLE OF CONTENTS

LIST OF FIGURES

LIST OF TABLES

CHAPTER 1 INTRODUCTION

1.1 Problem Statement

In practice, portable concrete barriers (PCBs) must be connected and transitioned to many types of barriers. Sometimes, portable concrete barriers are connected to similarly-shaped permanent concrete barriers. At other times, portable concrete barriers must be connected to dissimilar barriers, such as vertical concrete barriers, tubular steel bridge railings, W-beam guardrail, thrie beam guardrail, and open concrete bridge railings. Unfortunately, very little research has been devoted to this transition need. The only previously-developed portable concrete barrier transitions have involved attachment to permanent, safety-shape concrete roadside and median barriers [1-4].

Previously, researchers at the Midwest Roadside Safety Facility (MwRSF) conducted a survey of the members participating in the Midwest States Regional Pooled Fund program in order to identify the most prominent transition needs involving portable concrete barriers. The results, as shown in Table 1, identified a transition between portable concrete barriers and W-beam guardrail as the second highest need. As noted above, a transition from portable concrete barriers to permanent concrete safety-shape barriers has been previously developed. Thus, the focus of this research study was to investigate stiffness transitions between portable concrete barriers and W-beam guardrail.

A transition between portable concrete barriers and W-beam guardrail is necessary when roadway construction creates a work zone adjacent to existing W-beam guardrail. In this situation, a portion of W-beam guardrail is often removed, and portable concrete barriers are installed to create a work zone. The area where these two barriers meet can create a potential hazard, especially if a proper transition is not installed, as shown in Figure 1.

Table 1. Summary of State DOT Survey for Portable Concrete Barrier Transitions [2]

Transition Type - Temporary Concrete Safety Shape Barrier Transitioning to:	Usefulness Summary: (1)					Percent (2)	Rank (3)
	Not Useful	Somewhat Useful			Very Useful		
W-Beam Guardrail	1	2	3	4	**5**	30%	2
Thrie-Beam Guardrail	1	**2**	3	4	5	0%	6
Permanent Concrete Vertical Barrier	1	2	3	**4**	5	15%	3
Permanent Concrete Safety Shape Barrier	1	2	3	4	**5**	40%	1
Temporary Concrete Safety Barrier	1	2	3	4	**5**	10%	4
Tubular Steel Bridge Railing	**1**	2	3	4	5	0%	7
Open Concrete Bridge Railing	1	2	3	**4**	5	5%	5
Box-Beam Guardrail	**1**	2	3	4	5	0%	8
Other:							
	1	2	3	4	5		

Note: States completing the survey were asked to:
(1) Identify how useful the development of the listed transition would be to your state by circling a number from 1 to 5.
(2) Include the approximate percentage of portable concrete barrier transitions which are comprised of the listed transitions.
(3) Rank the transition types in order of their benefit to your state with 1 being the most beneficial.
(4) Include pictures, details, and drawings concerning portable concrete barrier transitions, including all those listed above.

www.manaraa.com

Figure 1. Unsafe Connection between Guardrail and Portable Concrete Barriers

Some of the primary concerns associated with a transition between W-beam guardrail and portable concrete barriers correspond to the difference in barrier deflections and functionality of two barrier types. A strong-post, W-beam guardrail system is a semi-rigid installation with typical permanent set deflections ranging between 36 in. (914 mm) and 48 in. (1,219 mm) for high-speed impacts with passenger vehicles. However, a portable concrete barrier system is often placed as a temporary installation to create and protect work zones, which may have a permanent set deflection as high as 80 in. (2,032 mm) under similar impact scenarios. This drastic difference in barrier deflection could lead to unwanted vehicle snag, pocketing, vehicle instability, or occupant risk. Therefore, researchers determined that a proper transition in lateral barrier stiffness and strength was necessary between the two systems. Unfortunately, a crashworthy stiffness transition is currently unavailable.

1.2 Research Objectives

The research objectives were to (1) determine performance and design criteria and (2) develop a stiffness transition between portable concrete barriers and W-beam guardrail that will significantly improve safety for the motoring public and workers within construction zones. The transition system was designed to meet the Test Level 3 (TL-3) safety performance criteria set forth in the American Association of State Highway and Transportation Officials (AASHTOs) *Manual for Assessing Safety Hardware* (MASH) [5].

1.3 Scope

The research objectives were achieved through the completion of several tasks. First, a literature review was performed on previous testing of free-standing portable concrete barrier systems, pinned and anchored portable concrete barriers, W-beam guardrail, transitions between different barrier types, and various barrier stiffening techniques. Next, performance and design criteria were developed that would allow the researchers to determine the likelihood of success for each design concept. Then, several design concepts for guardrail to PCB transitions were developed, discussed, and prioritized. A computer simulation effort was undertaken to analyze, refine, and evaluate several of the design concepts using LS-DYNA, a 3-D nonlinear finite element code [6]. Since ease of installation was a desired trait of the transition system, the simplest design concepts were simulated first. Based on the simulation results, complexity was later added on an incremental basis in order to meet the performance and design criteria. For each selected transition design concept, an FEA model was configured. Subsequently, an LS-DYNA analysis and design effort was conducted in order to evaluate the transition

concepts under MASH TL-3 impact scenarios, modify the configurations, and determine the Critical Impact Points (CIPs) for the transition. Finally, conclusions pertaining to the success potential of each proposed design was made, and recommendations for full-scale crash testing were provided.

CHAPTER 2 LITERATURE REVIEW

2.1 Introduction

Before transition design concepts were formulated and simulated, a literature search was conducted in order to review (1) prior guardrail to PCB and PCB to permanent barrier transition configurations, (2) barrier deflections, and (3) other barrier stiffening techniques. A brief summary for the relevant research studies are provided below and include test descriptions, test conditions, as well as dynamic and permanent set deflections for actual and simulated tests. These results aided in the formulation of design concepts for the transition between W-beam guardrail and portable concrete barriers. Please note that the purpose of this literature review was to identify similar research and gain knowledge of barrier deflections and transition stiffening techniques. However, a historical summary for all barrier transitions is not included herein.

2.2 Crash Testing and Simulation Studies on Free-Standing PCBs

2.2.1 National Crash Analysis Center Finite Element Study

In 2007, the National Crash Analysis Center (NCAC) conducted an extensive LS-DYNA computer simulation study to evaluate the performance of portable concrete barriers (PCBs), including different combinations of PCB shapes, lengths, and connection types [7]. As illustrated by the simulation matrix in Figure 2, 160 different combinations were examined under the National Cooperative Highway Research Program (NCHRP) Report No. 350 safety guidelines for Test Level 3 (TL-3). This investigation required that each simulation be setup for an impact with a 4,409-lb (2,000-kg) pickup truck at an angle of 25 degrees and an impact velocity of 62.1 mph (100 km/h). For this effort, full-scale crash test results and findings from previous studies were used to develop and

validate the computer models. Each PCB system was evaluated for occupant ridedown acceleration, occupant impact velocity, barrier displacement, and rotation angle. Full results of the study can be found in the charts located in Appendix A.
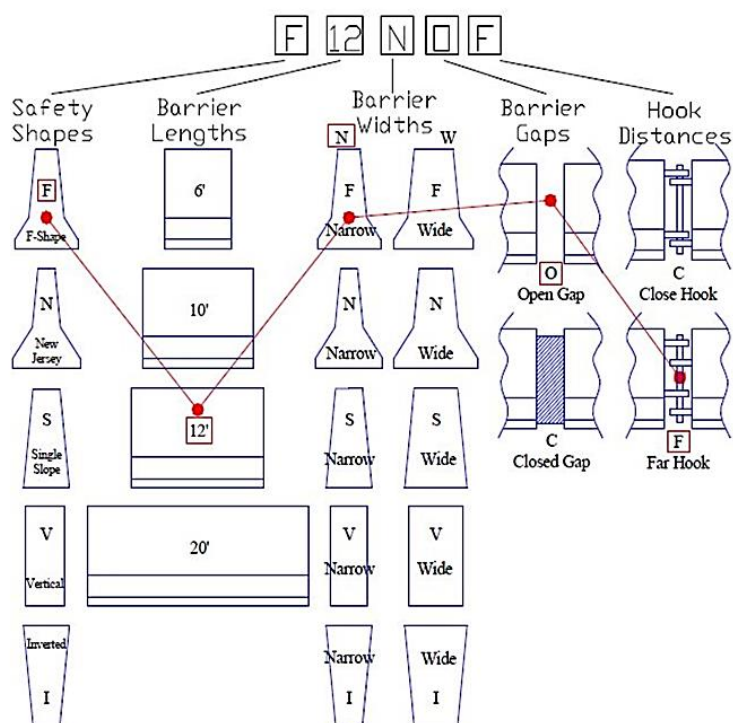
Figure 2. Simulation Matrix for NCAC Study [7]

2.2.2 Development of MwRSF F-Shape PCB

In 1996, researchers at Midwest Roadside Safety Facility (MwRSF) developed an F-shape PCB for the Midwest States Regional Pooled Fund program [8]. Prior to this effort, PCB configurations varied significantly from state to state. As such, contractors that worked in multiple states were required to either maintain inventories of several PCB configurations or seek approval to use alternate designs on a project-by-project basis. Therefore, a need existed to develop, test, and evaluate one, standardized, PCB design that met the TL-3 impact safety standards provided in NCHRP Report No. 350. The F-

shape PCB was chosen, as shown in Figure 3, and two full-scale crash tests were conducted and are discussed below.
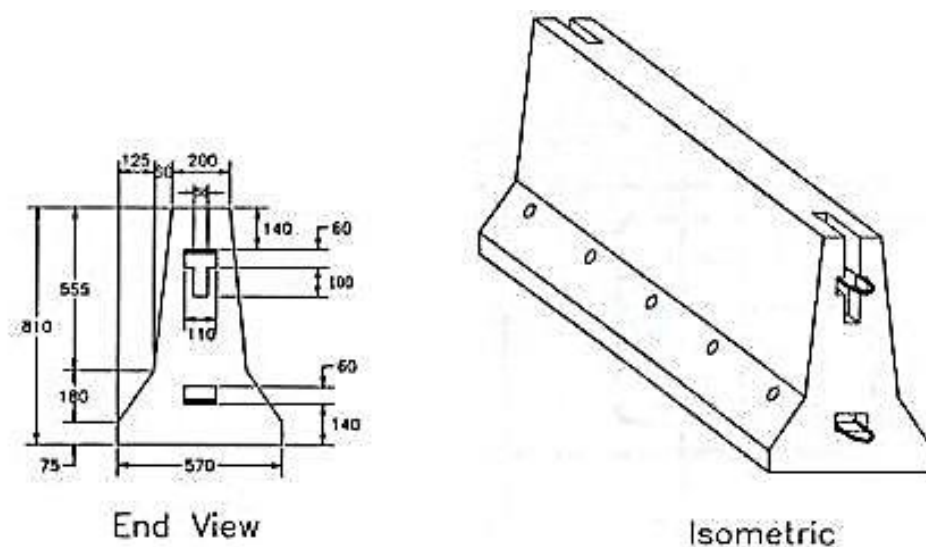
Figure 3. Initial Prototype for F-Shape PCB Segment (ITMP-1) [8]

The initial system consisted of sixteen 12-ft 5½-in. (3,800-mm) long, F-shape PCB segments for a total system length of 203 ft – 3¾ in. (62.0 m). The PCB system was free-standing on a concrete surface and utilized a pin and loop barrier-to-barrier connection. During test no. ITMP-1, a 4,409-lb (2,000-kg) pickup truck impacted the PCB system at a speed of 64.1 mph (103.1 km/h) and at an angle of 27.6 degrees using a point 3 ft – 9¼ in. (1,150 mm) upstream from the joint between barrier nos. 8 and 9. Upon impact, the vehicle climbed and overrode the system, and the test was deemed unsuccessful.

Upon inspection of the damaged barrier system, it was discovered that considerable damage occurred at the barrier joints. It was determined that this damage was likely caused by the weakened recessed areas located at the top end of each barrier segment. The recessed areas were incorporated for future use in implementing a rigid

joint for permanent barrier installations. In order to reduce joint rotations and prevent barrier uplift, it was necessary to strengthen the barrier ends by eliminating the recessed areas. This retrofit was completed in a three step process, as shown in Figure 4.
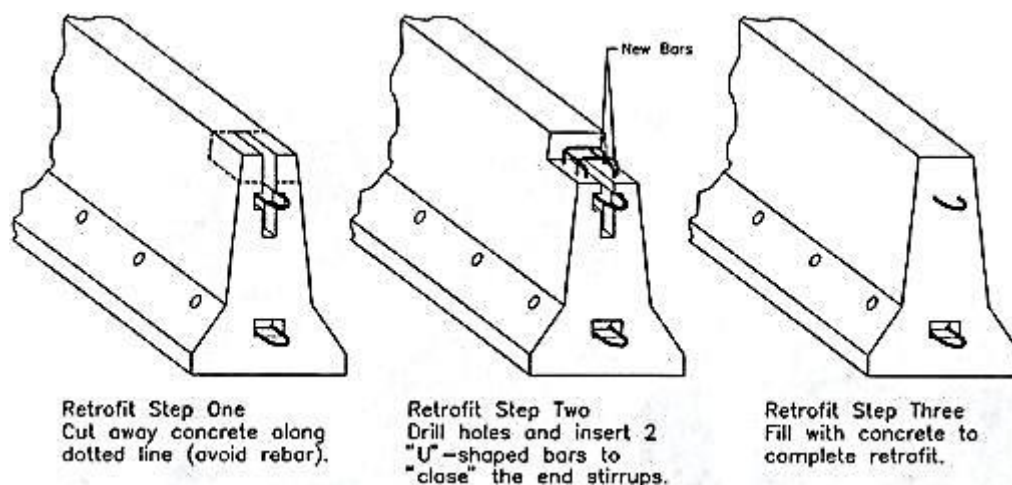
Figure 4. Retrofit to F-Shape PCB Sections [8]

The second system consisted of twenty-one 12-ft 5½-in. (3,800-mm) long, F-shape PCB segments for a total system length of 267 ft − 5½ in. (81.5 m). The PCB system was free-standing on a concrete surface and utilized a pin and loop barrier-to-barrier connection. During test no. ITMP-2, a 4,420-lb (2,005-kg) pickup truck impacted the PCB system at a speed of 62.3 mph (100.3 km/h) and at an angle of 27.1 degrees using a point 3 ft − 11¼ in. (1,200 mm) upstream from the joint between barrier nos. 8 and 9. The system contained and redirected the vehicle with maximum lateral dynamic and permanent set deflections of 3 ft − 9¼ in. (1,150 mm) and 3 ft − 8⅞ in. (1,140 mm), respectively, and was determined to be successful according to TL-3 of NCHRP Report No. 350.

2.2.3 F-Shape PCB Evaluation under Update to NCHRP Report No. 350

With the vehicle fleet constantly changing and growing, standards for testing and evaluating roadside safety hardware must also change. Thus, NCHRP Report No. 350

was being updated to include heavier vehicles with higher centers of gravity. In 2006, MwRSF researchers conducted another crash test under the impact conditions outlined in the Update to NCHRP Report No. 350 (i.e., future MASH) on the F-shaped PCB system that had been previously tested [9].

The system consisted of sixteen 12-ft 6-in. (3,810-mm) long, F-shape PCB segments for a total system length of 204 ft − 6 in. (62.3 m). The PCB system was free-standing on a concrete surface and utilized a pin and loop barrier-to-barrier connection. During test no. 2214TB-2, a 5,000-lb (2,268-kg) pickup truck impacted the system 48 in. (1,219 mm) upstream of the joint between barrier nos. 8 and 9 at a speed of 61.9 mph (99.6 km/h) and at an angle of 25.4 degrees. The system contained and redirected the vehicle with maximum lateral dynamic and permanent set deflections of 6 ft − 7⅝ in. (2,023 mm) and 6 ft − 1 in. (1,854 mm), respectively, and was found to be successful according to the TL-3 criteria published in the Update to NCHRP Report No. 350.

2.3 Testing of Pinned and Anchored PCBs

2.3.1 Limited-Slip PCB Connection

In 1993, researchers at TTI conducted a study into limited-displacement PCB systems immediately adjacent to vertical drop-offs for the Texas Department of Transportation (TxDOT) [10]. There are circumstances that require PCB systems to be positioned immediately adjacent to vertical drop-offs in temporary work zones. During these cases, there is insufficient lateral space for displacement of free-standing PCB systems during crash events. Two different barrier-to-barrier connection types were used in this study, and test results from free-standing and anchored configurations were compared. The two different barrier-to-barrier connection types included a channel/angle

splice connection and a grid-slot connection. Five full-scale tests were conducted using 30-ft (9.14-m) long, New Jersey safety-shape PCB segments and are discussed below.

The first system consisted of four 30-ft (9.1-m) long segments for a total system length of 120 ft (36.6 m), which were placed immediately adjacent to a vertical drop-off. The PCB system was pinned to the concrete surface through the front toe of each PCB with four evenly-spaced 1¼-in. (32-mm) diameter x 20½-in. (521-mm) long steel pins at an angle of 53.1 degrees from the horizontal plane, as shown in Figure 5. The PCB system utilized a channel/angle splice barrier-to-barrier connection. During test no. 1959A-1, a 4,410-lb (2,000-kg) pickup truck impacted the system 5 ft (1,524 mm) upstream from the joint between barrier nos. 2 and 3 at a speed of 60.3 mph (97.0 km/h) and at an angle of 25.7 degrees. The vehicle rolled upon exiting the PCB system, and the test was determined to be unsuccessful according to TL-3 of NCHRP Report No. 350. Researchers analyzed the test and determined that a longer PCB system would likely have contained the vehicle.
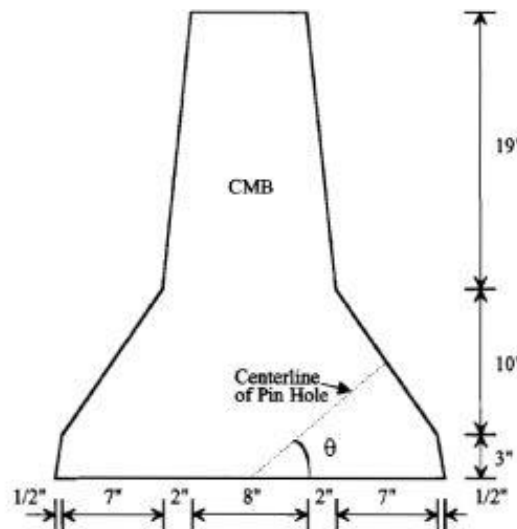
Figure 5. Limited-Slip Pin Placement Angle [10]

The second system consisted of nine 30-ft (9.1-m) long segments for a total system length of 270 ft (82.3 m), which were placed immediately adjacent to a vertical drop-off. The PCB system was free-standing on a concrete surface and utilized a channel/angle splice barrier-to-barrier connection. During test no. 1959A-2, a 4,409-lb (2,000-kg) pickup truck impacted the system 5 ft (1,524 mm) upstream from the end of barrier no. 4 at a speed of 61.9 mph (99.6 km/h) and at an angle of 26.1 degrees. All of the PCB segments downstream from the impact location were displaced off the vertical drop-off. Subsequently, test no. 1959A-2 was considered unsuccessful according to TL-3 of NCHRP Report No. 350.

The third system consisted of nine 30-ft (9.1-m) long segments for a total system length of 270 ft (82.3 m), which were placed immediately adjacent to a vertical drop-off. The PCB system was pinned to the concrete surface through the front toe of each PCB with four evenly spaced 1¼-in. (32-mm) diameter x 20½-in. (521-mm) long steel pins at an angle of 40.1 degrees from the horizontal plane. The PCB system utilized a channel/angle splice barrier-to-barrier connection. During test no. 1959A-3, a 4,409-lb (2,000-kg) pickup truck impacted the system 5 ft (1,524 mm) upstream from the end of barrier no. 4 at a speed of 60.6 mph (97.5 km/h) and at an angle of 26.2 degrees. The system contained and redirected the vehicle with a maximum lateral permanent set deflection of 5 in. (127 mm) and was considered successful according to TL-3 of NCHRP Report No. 350.

The fourth system consisted of nine 30-ft (9.1-m) long segments for a total system length of 270 ft (82.3 m), which were placed immediately adjacent to a vertical drop-off. The PCB system was pinned to the concrete surface through the front toe of each PCB

with four, evenly-spaced, 1¼-in. (32-mm) diameter x 20½-in. (521-mm) long steel pins at an angle of 40.1 degrees from the horizontal plane. The PCB system utilized a grid-slot barrier-to-barrier connection. During test no. 1959A-4, a 4,409-lb (2,000-kg) pickup truck impacted the system 5 ft (1,524 mm) upstream from the end of barrier no. 2 at a speed of 60.9 mph (98.0 km/h) and at an angle of 23.7 degrees. The vehicle came to a rest on top of the PCB system with a maximum lateral permanent set barrier deflection of 9 in. (229 mm) and was considered successful according to TL-3 of NCHRP Report No. 350.

The fifth system consisted of nine 30-ft (9.1-m) long segments for a total system length of 270 ft (82.3 m), which were placed immediately adjacent to a vertical drop-off. The PCB system was free-standing on a concrete surface and utilized a grid-slot connection. During test no. 1959A-5, a 4,409-lb (2,000-kg) pickup truck impacted the system 4 ft – 6 in. (1,372 mm) upstream of the end from barrier no. 2 at a speed of 44.6 mph (71.8 km/h) and at an angle of 25.0 degrees. Two PCB segments were displaced off the vertical drop-off, and the vehicle rolled upon exiting the PCB system. The test was considered unsuccessful for installation in a low-speed work zone according to TL-2 of NCHRP Report No. 350.

2.3.2 K-Rail Used in Semi-Permanent Installations

In 1999, researchers at the California Department of Transportation (Caltrans) conducted compliance testing of the California K-Rail (New Jersey safety shape) PCB in semi-permanent applications [11]. The California K-Rail had previously been tested in free-standing applications according to NCHRP Report No. 350, but in the interest of limiting deflections of the PCB system, a semi-permanent installation was developed. In

compliance with NCHRP Report No. 350, two full-scale crash tests were conducted on the semi-permanent application.

Both systems consisted of eight 20-ft (6,096-mm) long segments for a total system length of 160 ft (48.8 m). The PCB systems were pinned in all four corners to an asphalt concrete surface. The pins were 1-in. (25-mm) diameter x 24-in. (610-mm) long steel stakes. The PCB system utilized a pin and loop barrier-to-barrier connection. During test no. 551, a 4,445-lb (2,016-kg) pickup truck impacted the system at the joint between barrier nos. 4 and 5 at a speed of 62.5 mph (100.6 km/h) and at an angle of 25.0 degrees. The system contained and redirected the vehicle with a maximum lateral permanent set deflection of 2¾ in. (70 mm) and was considered successful according to TL-3 of NCHRP Report No. 350. During test no. 552, a 1,861-lb (844-kg) small car impacted the system at the joint between barrier nos. 4 and 5 at a speed of 63.2 mph (101.7 km/h) and at an angle of 20.0 degrees. The system contained and redirected the vehicle with a maximum lateral permanent set deflection of 1 in. (25 mm) and was considered successful according to TL-3 of NCHRP Report No. 350. Due to a misinterpretation of the original drawings, the pins were cut to a length of 24 in. (610 mm) instead of the intended 39.4 in. (1000 mm). So, after evaluation of both tests, the California K-Rail was recommended for use with four 1-in. (25-mm) diameter x 39.4-in. (1000-mm) long steel stakes in each corner of the PCBs, as shown in Figure 6.
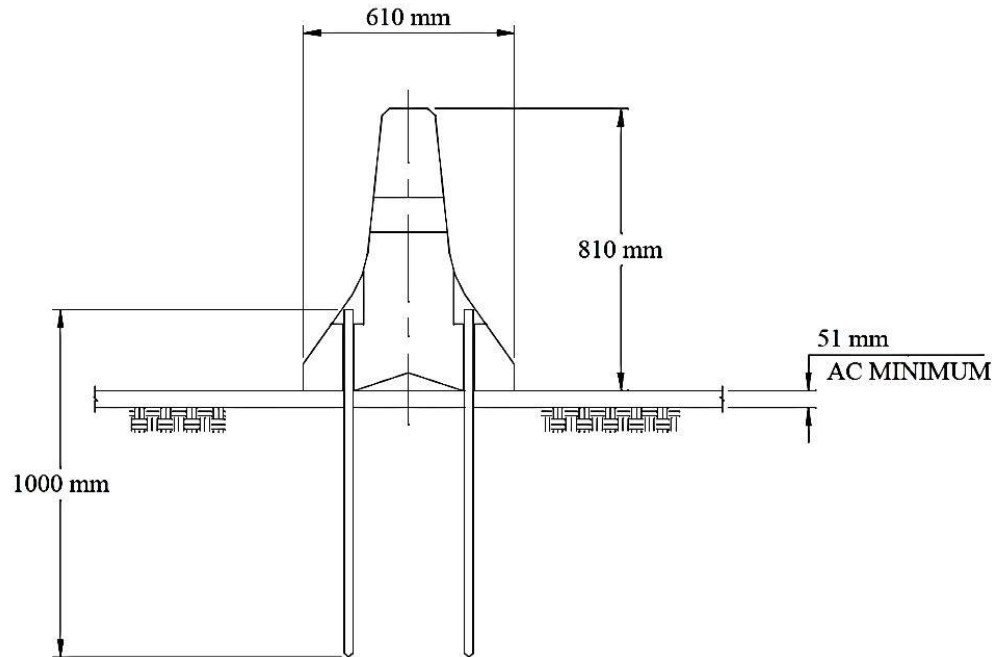
Figure 6. California K-Rail Steel Stake Setup [11]

2.3.3 Development of a Tie-Down System for F-Shape PCBs

In 2002, MwRSF researchers developed a tie-down system for PCBs [12]. During bridge construction, PCBs are often placed adjacent to the edge of a bridge deck. However, free-standing PCB systems near vertical drop-offs are at risk of being displaced off of the bridge deck when impacted by an errant vehicle. In order to decrease this risk, researchers developed a steel tie-down strap that could be placed on the connection pin at the PCB joints and anchored to the bridge deck using drop-in anchors. Following a series of LS-DYNA computer simulations as well as component testing of the steel tie-down strap, researchers pursued full-scale crash testing with the design shown in Figure 7. The design consisted of a 3-in. (76-mm) wide x ¼-in. (6-mm) thick x 36-in. (914-mm) long piece of ASTM A36 steel bent into a trapezoidal shape. The straps were attached to the bridge deck using two Red Head ¾-in. (19-mm) diameter drop-in anchors and ¾-in. (19-mm) diameter x 2¼-in. (57-mm) long ISO Class 8.8 bolts.

Figure 7. Steel Tie-Down Strap [12]

The test installation consisted of sixteen 12-ft 6-in. (3,810-mm) long, F-shape PCB segments placed 12 in. (305 mm) away from a simulated bridge deck edge. The tie-down straps were installed at eleven joints, beginning at barrier no. 2 and ending at barrier no. 13. During test no. ITD-1, a 4,435-lb (2,012-kg) pickup truck impacted the system 3 ft – 11¼ in. (1,200 mm) upstream from the joint between barrier nos. 8 and 9 at a speed of 60.6 mph (97.5 km/h) and at an angle of 24.3 degrees. The PCB system contained and redirected the vehicle with maximum lateral dynamic and permanent set barrier deflections of 3 ft – 1¾ in. (960 mm) and 2 ft – 9½ in. (851 mm), respectively. The tie-down straps were designed to support the dead weight of three PCB segments. In test no. ITD-1, only one PCB segment was displaced completely off the bridge deck with two PCB segments partially displaced off the bridge deck. Thus, the results from test no. ITD-1 were successful according to TL-3 of NCHRP Report No. 350.

2.3.4 Development of Tie-Down System for Redesigned F-Shape PCB

In 2003, MwRSF researchers developed a tie-down system for redesigned F-shape PCBs that incorporated a bolt-through detail [13]. The redesigned F-shape PCBs

incorporated a three loop connection that provided double shear at two locations on each pin. The bolt-through, tie-down system consisted of three 1⅛-in. (29-mm) diameter ASTM A307 anchor bolts with heavy hex nuts and 3-in. (76-mm) x 3-in. (76-mm) x ½-in. (13-mm) thick washers spaced evenly across the traffic side of each PCB segment, as shown in Figure 8. Each anchor bolt was epoxied into the concrete with an embedment depth of 12 in. (305 mm).

The test installation consisted of sixteen 12-ft 6-in. (3,810-mm) long, redesigned F-shape PCB segments placed adjacent to a simulated bridge deck edge with a total system length of 204 ft (62.2 m). During test no. KTB-1, a 4,448-lb (2,018-kg) pickup truck impacted the system 5 ft – 5 in. (1,651 mm) upstream from the joint between barrier nos. 8 and 9 at a speed of 62.0 mph (99.8 km/h) and at an angle of 25.3 degrees. The system contained and redirected the vehicle with maximum lateral dynamic and permanent set deflections of 11.3 in. (287 mm) and 3½ in. (89 mm), respectively, and was considered successful according to TL-3 of NCHRP Report No. 350.
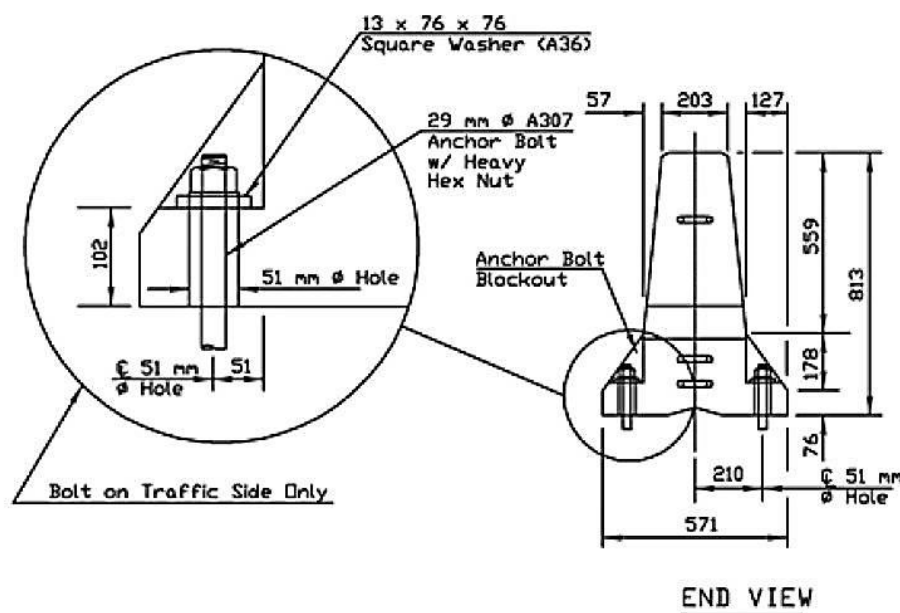
Figure 8. Tie-Down System for Redesigned F-Shape PCB [13]

2.3.5 Tie-Down and Transition for PCBs on Asphalt Road Surfaces

In 2006, MwRSF researchers developed a tie-down system for PCBs on an asphalt road surface [1]. Previous tie-down systems had been developed, but only tested on concrete surfaces and thus were not appropriate for use on asphalt road surfaces. The tie-down system consisted of F-shape PCB segments placed on a 2-in. (51-mm) thick asphalt pad with three 1½-in. (38-mm) diameter x 36-in. (914-mm) long, A36 steel pins installed through the holes on the traffic-side toe of the PCB segments.
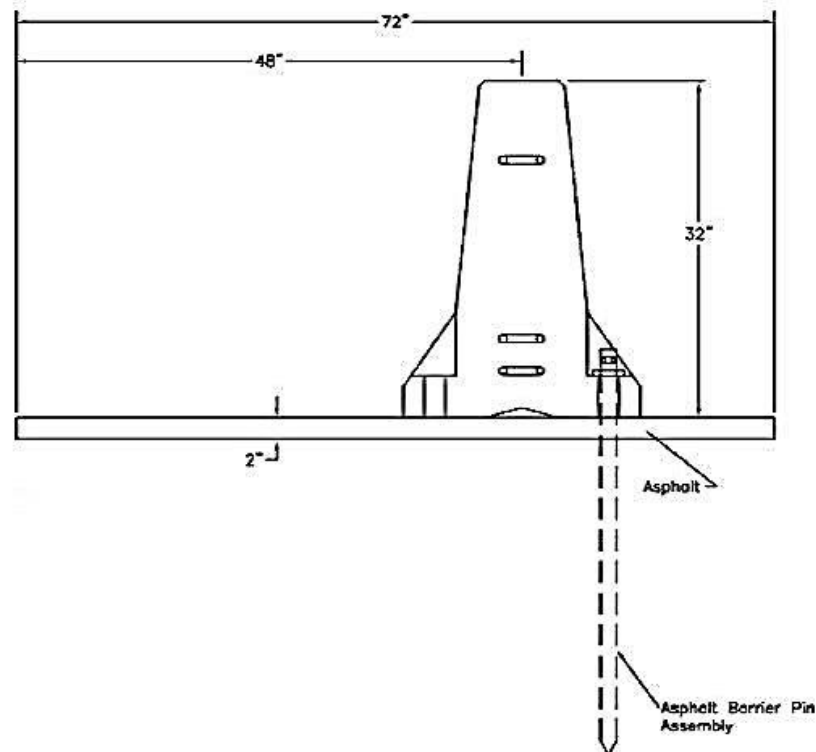
Figure 9. Asphalt Pin Assembly [1]

The test installation consisted of sixteen 12-ft 6-in. (3,810-mm) long, F-shape PCB segments placed 6 in. (152 mm) from a 3-ft (914-mm) wide x 3-ft (914-mm) deep trench. The tie-down pins were installed on the middle ten PCB segments. During test no. FTB-1, a 4,434-lb (2,011-kg) pickup truck impacted the system 4 ft (1,219 mm) upstream from the joint between barrier nos. 8 and 9 at a speed of 61.3 mph (98.7 km/h) and at an

angle of 25.4 degrees. The tie-down PCB system contained and redirected the vehicle with maximum lateral dynamic and permanent set barrier deflections of 21.8 in. (554 mm) and 11⅛ in. (283 mm), respectively. A portion of the soil and asphalt fractured and separated away from the road surface beneath the PCB system due to loading of the tie-down pins. The separated area was approximately 23 ft – 6 in. (7.16-m) long and had an average separation of 7 in. (178 mm). However, this separation did not adversely affect the performance of the system, and researchers determined that test no. FTB-1 was successful according to TL-3 of NCHRP Report No. 350.

A second aspect of the research pertained to a transition between barrier systems. When a free-standing PCB system is connected to a rigid barrier, a transition between the two barrier systems may be required. The final transition utilized a varied spacing of the same asphalt tie-down pins from FTB-1 over a series of four PCB segments to create a transition in stiffness, as shown in Figure 10. The first barrier in the transition had a single pin in the downstream end. The second barrier had pins installed at the two outside hole locations. The final two barriers had all three pins installed. In addition, either 10-gauge (3.42-mm) or nested 12-gauge (2.66-mm) thrie beam was bolted across both sides of the joint between the pinned barriers and the rigid barrier system in order to reduce the potential for vehicle snag at the joint.
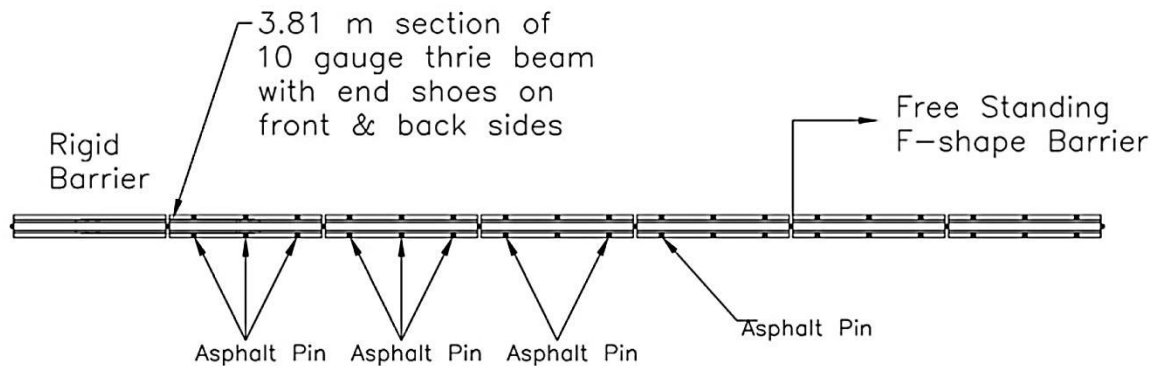
Figure 10. PCB Transition from Free-Standing to Rigid [1]

The test installation consisted of twenty-two 12-ft 6-in. (3,810-mm) long, F-shape PCB segments: five rigidly constrained barriers; four transition barriers; and thirteen free-standing barriers. All four transition barriers and twelve of the free-standing barriers were installed on a 2-in. (51-mm) thick asphalt pad, while the five rigidly-constrained barriers and one free-standing barrier were installed on a concrete surface. During test no. FTB-2, a 4,475-lb (2,030-kg) pickup truck impacted the system 4 ft (1,219 mm) upstream from the joint between barrier nos. 8 and 9 at a speed of 63.8 mph (102.7 km/h) and at an angle of 26.1 degrees. The tie-down PCB transition system contained and redirected the vehicle with maximum lateral dynamic and permanent set barrier deflections of 18⅜ in. (467 mm) and 5¼ in. (133 mm), respectively, and was determined to be successful according to TL-3 of NCHRP Report No. 350.

2.3.6 PCB Transition to Tall Permanent Concrete Median Barrier

In 2010, MwRSF researchers developed a transition between a free-standing PCB system and a permanent concrete barrier for median applications [2]. The permanent concrete barrier chosen for testing was the 42-in. (1,067-mm) tall, single-slope median barrier, while the PCB was a 32-in. (813-mm) tall F-shape barrier. The system consisted of eight free-standing barriers, four transition barriers, and a rigid parapet. The free-

standing and transition barriers were installed on a 3-in. (76-mm) thick asphalt pad. The transition barriers used a varied spacing of asphalt pins to create a transition in stiffness over four barriers. The asphalt pins used were 1½-in. (38-mm) diameter x 38½-in. (978-mm) long ASTM A36 steel pins with a steel cap plate on the top. The first barrier in the transition (adjacent to the free-standing barrier) had a single pin at the downstream end through both the front- and back-side toes. The second barrier had pins installed at the two outermost hole locations on both the front- and back-side toes. The third and fourth transition barriers had all three pins installed on both the front- and back-side toes. In order to prevent vehicle snag, nested 12-gauge (2.66-mm) thrie beam sections were installed on both the front and back sides of the joint between the pinned barriers and the rigid parapet, as shown in Figure 8.

Figure 11. Transition from PCB to Permanent Concrete Barrier [2]

Using finite element modeling, two critical impact locations were identified for full-scale crash testing. Thus, two full-scale crash tests were conducted on the system described above. During test no. TCBT-1, a 5,175-lb (2,347-kg) pickup truck impacted the transition barrier 56⅜ in. (1,432 mm) away from the upstream end of the permanent concrete barrier at a speed of 62.5 mph (100.6 km/h) and at an angle of 24.7 degrees. The system safely contained and redirected the vehicle with maximum lateral dynamic and permanent set barrier deflections of 2⅝ in. (67 mm) and ¼ in. (6 mm), respectively, and subsequently was deemed successful according to TL-3 of MASH. During test no. TCBT-2, a 5,160-lb (2,341-kg) pickup truck impacted the system at 3 ft − 5¼ in. (1,048 mm) upstream from the end of barrier no. 5 at a speed of 62.2 mph (100.1 km/h) and at an angle of 26.2 degrees. The system safely contained and redirected the vehicle with maximum lateral dynamic and permanent set barrier deflections of 34 in. (864 mm) and 34 in. (864 mm), respectively, and subsequently was deemed successful according to TL-3 of MASH.

2.3.7 Evaluation of 12-ft 6-in. Pinned F-Shape PCB

In 2006, TTI researchers evaluated mechanisms for limiting deflections of 12-ft 6-in. (3,810-mm) long, F-shape PCB systems installed near extreme drop-offs [14]. From the currently available PCB restraining or anchoring mechanisms, most designs required through-deck bolting, anchor bolts with adhesive bonding, or other constraining straps. The goal of this research was to develop an easy to install restraining mechanism to limit PCB deflections while minimizing the damage to the bridge deck. The design incorporated two 1½-in. (38-mm) diameter × 21¼-in. (540-mm) long ASTM A36 steel drop-pins placed into 1⅞-in. (48-mm) diameter holes cast into the toe of each PCB

segment at an angle of 40 degrees from the horizontal. The embedment depth of the drop-pins was 6¼ in. (159 mm) when measured vertically. Each of the holes for the drop-pins was located 16 in. (406 mm) away from the ends of the barrier segments on the traffic-side of the PCBs.

The test installation consisted of eight 12-ft 6-in. (3,810-mm) long, pinned F-shape PCB segments placed adjacent to a simulated bridge deck edge with a total system length of 100 ft (30.5 m). During test no. 405160-3-2a, a 4,674-lb (2,120-kg) pickup truck impacted the system 4 ft (1,219 mm) upstream from the joint between barrier nos. 3 and 4 at a speed of 62.7 mph (100.9 km/h) and at an angle of 25.4 degrees. The tie-down PCB transition system contained and redirected the vehicle with maximum lateral dynamic and permanent set barrier deflections of 11½ in. (292 mm) and 5¾ in. (146 mm), respectively, and was determined to be successful according to TL-3 of NCHRP Report No. 350.

2.3.8   Pinned Anchorage System for New York State's PCBs

In 2009, MwRSF researchers evaluated mechanisms for limiting deflections of New York State's New Jersey shape PCB system [15]. For PCBs located adjacent to vertical drop-offs, NYSDOT found it desirable to utilize vertical pins through the back-side toe of the PCBs in order to reduce barrier deflections as well as to reduce the need for workers to be positioned on the traffic-side face of the system when installing anchors. In an attempt to reduce construction costs and damage to bridge decks, vertical pins were placed in every other PCB segment in order to evaluate whether the barrier deflections would be maintained to reasonable levels. Four 1-in. (25-mm) diameter x 15½-in. (394-mm) long, hot rolled ASTM A36 steel rods were used to pin the PCB

segments to the concrete surface through the back-side toe. Each anchor rod was inserted into a 1⅛-in. (29-mm) diameter, drilled hole in the rigid concrete surface using an embedment depth of 5 in. (127 mm), as shown in Figure 12.

The full-scale crash test consisted of ten 20-ft (6,096-mm) long, New Jersey shape PCB segments with a total system length of 200 ft (61.0 m). The PCB system utilized an I-beam key connector barrier-to-barrier connection and only PCB segment nos. 1, 3, 5, 7, and 9 were pinned to the concrete surface. During test no. NYTCB-4, a 5,172-lb (2,346-kg) pickup truck impacted the system 51 3/16 in. (1,300 mm) upstream from the joint between barrier nos. 4 and 5 at a speed of 62.3 mph (100.3 km/h) and at an angle of 24.3 degrees. The pinned PCB system contained and redirected the vehicle with maximum lateral dynamic and permanent set barrier deflections of 64.8 in. (1,646 mm) and 53½ in. (1,359 mm), respectively, and was determined to be successful according to TL-3 of MASH.
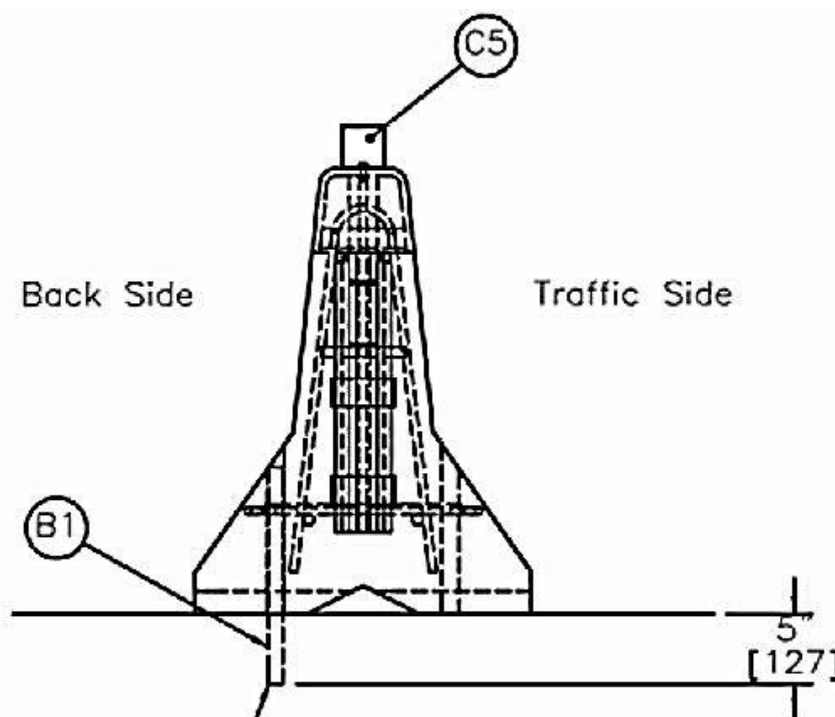
Figure 12. NYSDOT Pinned PCB Setup [15]

2.3.9 Pinned Anchorage System for New York State's PCBs – Phase II

Previous research was conducted to reduce deflections of New York State's New Jersey shape PCB system by anchoring alternating PCB segments to the concrete surface with vertical steel pins placed through the back-side toe [15]. However, significant barrier deflections were observed during the full-scale crash test, which may need to be reduced for work zones with restricted space. In 2010, MwRSF conducted further research on New York State's New Jersey shape PCB system with every PCB segment anchored to the concrete surface [16]. Four 1-in. (25-mm) diameter x 15½-in. (394-mm) long, hot rolled ASTM A36 steel rods were used to pin the PCB segments to the concrete surface through the back-side toe. Each anchor rod was inserted into a 1⅛-in. (29-mm) diameter, drilled hole in the rigid concrete surface to an embedment depth of 5 in. (127 mm), as shown in Figure 13.
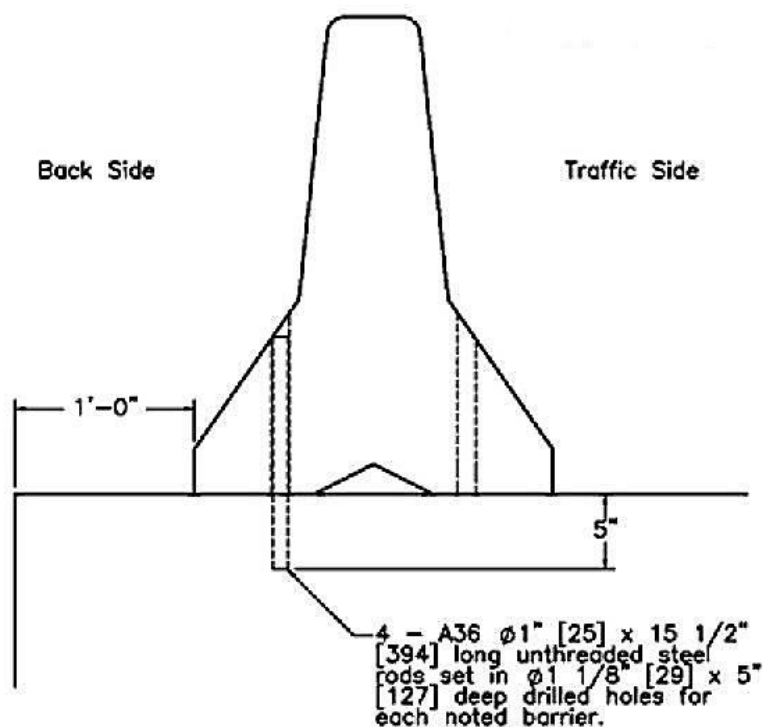
Figure 13. NYSDOT Pinned PCB, Phase II Setup [16]

The test installation consisted of ten 20-ft (6,096-mm) long, New Jersey shape PCB segments with a total system length of 200 ft (61.0 m). The PCB system utilized an I-beam key connector barrier-to-barrier connection, and the system was placed 12 in. (305 mm) laterally from the edge of a simulated bridge deck. During test no. NYTCB-5, a 5,124-lb (2,324-kg) pickup truck impacted the system 4 ft - 3 3/16 in. (1,300 mm) upstream from the joint between barrier nos. 4 and 5 at a speed of 64.3 mph (103.5 km/h) and at an angle of 26.2 degrees. The pinned PCB system contained and redirected the vehicle with maximum lateral dynamic and permanent set barrier deflections of 20½ in. (521 mm) and 9 in. (229 mm), respectively, and was determined to be successful according to the TL-3 of MASH.

2.3.10 Termination and Anchorage of PCBs

In 2009, MwRSF researchers at MwRSF investigated termination and end anchorages for PCB systems [17]. The impact behavior of PCBs, when struck near the upstream end of the system, had never been investigated. In order to determine impact loads for future analysis and design of the termination anchor system, computer simulations were conducted using the non-linear finite element code, LS-DYNA.

Upon determination of the design loads, several concepts were explored, and a driven steel anchor post concept was chosen for full-scale testing. The upstream-most PCB segment was installed with 36 in. (914 mm) of its downstream end placed on a concrete surface and the remainder of the PCB segment resting on soil. This end barrier was anchored by two cable assemblies that connected the end connector pin to two driven steel anchor posts. Each of the two anchor posts utilized an 8-ft (2,438-mm) long, W6x25 (W152x37.2) steel section with a 24-in. (610-mm) x 24-in. (610-mm) x ½-in. (13-mm)

thick soil plate welded to the front flange and a ½-in. (13-mm) thick plate welded to the top of the post. The anchor posts were installed in soil with an embedment depth of 8 ft (2,438 mm). One post was located along the longitudinal axis of the system, 45⅜ in. (1,153 mm) upstream of the first barrier. The second post was located 29⅜ in. (746 mm) upstream of the first barrier and offset 11½ in. (292 mm) laterally from the traffic side face of the barrier.

Cable brackets were bolted to the top of the anchor posts, which were assembled from multiple ½-in. (13-mm) thick, A36 steel plates welded together. The cable assemblies were comprised of a ¾-in. (19-mm) diameter, 7x19 wire rope, BCT cable end fittings, a Crosby heavy-duty HT thimble, and a 115-HT mechanical splice. One 54¾ in. (1,391 mm) long cable assembly was aligned with the longitudinal axis of the barrier system. This cable assembly was attached with one end fixed between the lower barrier loops on an additional connection pin on the upstream end of the barrier and the other end attached to the anchor post. The end connector pin utilized a second 2½-in. (64-mm) wide x 4-in. (102-mm) long x ½-in. (13-mm) thick ASTM A36 steel plate and a ½-in. (13-mm) diameter x 10-in. (254-mm) long Grade 8 hex bolt and nut at the bottom of the pin to prevent it from pulling out of the barrier loops when loaded. The second cable assembly measured 48⅜-in. (1,229-mm) long, and it was attached from just below the top barrier loop on the connector pin on the end of the barrier to the offset anchor post. A pin sleeve, made from 1½-in. (38-mm) Schedule 40 pipe, was used to keep the anchor cables in the correct vertical positions. The as-tested PCB end anchorage is shown in Figure 14.

The test installation consisted of twelve 12-ft 6-in. (3,810-mm) long, F-shape PCB segments that utilized the end anchorage design above for a total system length of

156 ft – 6 in. (47.7 m). The PCB system utilized a pin and loop barrier-to-barrier connection. During test no. TTCB-1, a 4,991-lb (2,264-kg) pickup truck impacted the system 9 ft - ⅝ in. (2,759 mm) downstream from the upstream end of barrier no. 1 at a speed of 62.9 mph (101.2 km/h) and at an angle of 25.5 degrees. The maximum dynamic anchor deflections were 5.3 in. (135 mm) for the offset anchorage and 6.2 in. (157 mm) for the in-line anchorage, measured from string potentiometers mounted on the anchors. The PCB end anchorage system contained and redirected the vehicle with a maximum lateral permanent set barrier deflection of 66½ in. (1,689 mm), and was determined to be successful according to the TL-3 of MASH.

Figure 14. PCB End Anchorage [17]

2.4 Testing of W-beam Guardrail Systems

2.4.1   Guardrail Deflection Analysis – Phase I

In 2011, TTI researchers reviewed literature on previous full-scale crash tests of beam guardrails tested in accordance with the criteria set forth in National Cooperative Highway Research Program (NCHRP) Report No. 350 and *Manual for Assessing Safety Hardware* (MASH) test 3-11 [18]. The guardrail systems were divided into one of five categories: single 12-gauge (2.66-mm) W-beam rail; thrie beam rail; nested W-beam rail; 13-gauge (2.28-mm) Buffalo W-beam rail; and W-beam rail designed for special applications. The single 12-gauge (2.66-mm) W-beam rail category was of particular interest for this research, and the TTI findings can be found in Appendix B. A performance summary of the 27¾-in. (705-mm) and 31-in. (787-mm) tall guardrail systems can be found in Tables 2 and 3, respectively. Based on this information, an average dynamic deflection of 39.7 in. (1,008 mm) and 41.4 in. (1,052 mm) was calculated for the 27¾-in. (705-mm) and 31-in. (787-mm) tall guardrail systems, respectively. An average permanent set deflection of 24.3 in. (617 mm) and 28.4 in. (721 mm) was also calculated for the 27¾-in. (705-mm) and 31-in. (787-mm) tall guardrail systems, respectively.

Table 2. System Performance of 27¾-in. (705-mm) Tall Guardrail Systems

Test Agency	Test Name	Test Designation	Permanent Set Deflection, in. (mm)	Dynamic Deflection, in. (mm)	System Configuation
TTI	405421-1	NCHRP 350 3-11	27.6 (701)	39.4 (1,001)	Modified W-beam, strong post G4(1S) guardrail
TTI	405391-1	NCHRP 350 3-11	31.1 (790)	43.3 (1,100)	Round wood post G4(2W) guardrail
TTI	400001-MPT-1	NCHRP 350 3-11	28.3 (719)	44.5 (1,130)	Modified G4(1S) with recycled blockouts
TTI	439637-1	NCHRP 350 3-11	17.7 (450)	29.5 (749)	Modified G4(1S)
TTI	400001-APL-1	NCHRP 350 3-11	31.3 (795)	53.6 (1,361)	Modified G4(2W) with Amitty plastic's recycled posts
TTI	404201-1	NCHRP 350 3-11	33.9 (861)	40.6 (1,031)	G4(2W) with 100 mm asphaltic curb
TTI	400001-CFI1	NCHRP 350 3-11	12.8 (325)	31.9 (810)	G4 with HALCO X-48 steel posts and recycled plastic blockouts
TTI	400001-ILP2	NCHRP 350 3-11	13.4 (340)	31.1 (790)	G4(2W) guardrail with imperial 5-Lam posts and blockouts
E-TECH Inc.	41-1655-001	NCHRP 350 3-11	27.6 (701)	51.2 (1,300)	G4 guardrail with light weight HALCO X-40 steel posts and recycled plastic blockouts
TTI	400001-MON1	NCHRP 350 3-11	10.4 (264)	33.0 (838)	Modified G4(1S) with Mondo Polymer blockouts
MwRSF	PR-1	NCHRP 350 3-11	N/A	38.2 (970)	Strong W-beam guardrail with posts installed in rock
SwRI	N/A_1	NCHRP 350 3-11	N/A	40.6 (1,031)	O-Post as an alternative to a standard W6x8.5 steel post for use for W-beam guardrail
SwRI	N/A_2	NCHRP 350 3-11	N/A	43.7 (1,107)	O-Post impacting at the open side
E-TECH Inc.	41-1792-001	NCHRP 350 3-11	23.6 (599)	27.6 (701)	G4 guardrail with light weight, strong HALCO X-44 steel posts and recycled plastic blockouts
MwRSF	2214WB-2	MASH 3-11	33.3 (846)	47.1 (1,196)	Modified G4(1S) guardrail

Table 3. System Performance of 31-in. (787-mm) Tall Guardrail Systems

Test Agency	Test Name	Test Designation	Permanent Set Deflection, in. (mm)	Dynamic Deflection, in. (mm)	System Configuation
MwRSF	NPG-4	NCHRP 350 3-11	25.7 (653)	43.1 (1,095)	Modified Midwest Guardrail System
MwRSF	NPG-5	NCHRP 350 3-11	24.1 (612)	40.3 (1,024)	MGS with 6 in. tall concrete curb
MwRSF	NPG-6	NCHRP 350 3-11	12.0 (305)	17.6 (447)	MGS with reduced post spacing
MwRSF	2214MG-1	MASH 3-11	42.9 (1,090)	57.0 (1,448)	Midwest Guardrail System
MwRSF	2214MG-2	MASH 3-11	31.6 (803)	43.9 (1,115)	MGS with reduced post spacing
TTI	220570-2	MASH 3-11	28.7 (729)	40.9 (1,039)	W-beam guardrail on SYLP
SwRI	GMS-1	MASH 3-11	22.0 (559)	35.0 (889)	Modified G4(1S) longitudinal barrier with GMS fastener
MwRSF	MGSDF-1	NCHRP 350 3-11	35.5 (902)	60.2 (1,529)	MGS with Douglas Fir wood posts
MwRSF	MGSPP-1	NCHRP 350 3-11	27.8 (706)	37.6 (955)	MGS with round Ponderosa Pine posts
TTI	400001-TGS1	MASH 3-11	31.0 (787)	38.4 (975)	Trinity Guardrail System (TGS)
Holmes Solution	57073112	MASH 3-11	31.5 (800)	41.3 (1,049)	Nucor Strong Post W-beam guardrail system without blockouts

2.5 Testing of Transitions Between Different Barrier Types

2.5.1 Two Approach Guardrail Transitions for Concrete Safety Shape Barriers

In 1996, MwRSF researchers developed two guardrail to concrete safety-shape barrier transitions [19]. One transition design was constructed using W6x9 (W152x13.4) steel posts, and the other system was constructed using 6-in. x 8-in. (152-mm x 203-mm) wood posts. For both systems, a varied post spacing consisted of one at 11½ in. (292 mm), five at 18¾ in. (476 mm), and three at 37½ in. (953 mm). The steel- and wood-post versions of the approach transition are shown in Figures 15 and 16, respectively. Two full-scale crash tests were conducted on each approach transition design for a total of four tests.

The first full-scale crash test utilized steel posts with an embedment depth of 43 in. (1,092 mm) in the thrie beam area. During test no. ITNJ-1, a 4,396-lb (1,994-kg) pickup truck impacted the system 7 ft – 11⅞ in. (2,435 mm) upstream from the end of the concrete barrier at a speed of 62.1 mph (99.9 km/h) and at an angle of 25.0 degrees. The system experienced larger than expected deflections, which caused pocketing upstream of the bridge rail end. The pocketing caused a high exit angle and eventually resulted in vehicle rollover. Subsequently, the performance of test no. ITNJ-1 was deemed unsuccessful according to TL-3 of NCHRP Report No. 350.

Upon investigation of the results from test no. ITNJ-1, it was determined that the system was not stiff enough near the bridge end. In order to increase the stiffness and strength, the post embedment depth in the thrie beam area was increased to 49 in. (1,245 mm). Also, the upstream corner on the traffic-side of the concrete bridge rail was chamfered in order to mitigate vehicle snag. During test no. ITNJ-2, a 4,359-lb (1,977-

kg) pickup truck impacted the system at 7 ft – 11⅞ in. (2,435 mm) upstream from the end of the concrete barrier at a speed of 63.1 mph (101.6 km/h) and at an angle of 25.7 degrees. The modified steel-post transition system contained and smoothly redirected the vehicle with maximum lateral dynamic and permanent set barrier deflections of 5¼ in. (133 mm) and 3⅝ in. (92 mm), respectively and was determined to be a success according to TL-3 of NCHRP Report No. 350.

The third full-scale crash test utilized wood posts with an embedment depth of 43 in. (1,092 mm) in the thrie beam area. During test no. ITNJ-3, a 4,381-lb (1,987-kg) pickup truck impacted the system 7 ft – 11⅞ in. (2,435 mm) upstream from the end of the concrete barrier at a speed of 63.4 mph (102.0 km/h) and at an angle of 26.9 degrees. Similar to test no. ITNJ-1, the system experienced larger than expected deflections, which caused vehicle instabilities and eventually rollover. Subsequently, the performance of test no. ITNJ-3 was deemed unsuccessful according toTL-3 of NCHRP Report No. 350.

In order to lower deflections of the transition system with wood-post configuration, the post embedment depth in the thrie beam area was increased to 52 in. (1,321 mm). During test no. ITNJ-4, a 4,407-lb (1,999-kg) pickup truck impacted the system at 7 ft – 11⅞ in. (2,435 mm) upstream from the end of the concrete barrier at a speed of 63.6 mph (102.4 km/h) and at an angle of 24.6 degrees. The wood-post transition system contained and smoothly redirected the vehicle with maximum lateral dynamic and permanent set barrier deflections of 3.8 in. (99 mm) and 1¼ in. (32 mm), respectively, and was determined to be a success according to TL-3 of NCHRP Report No. 350.
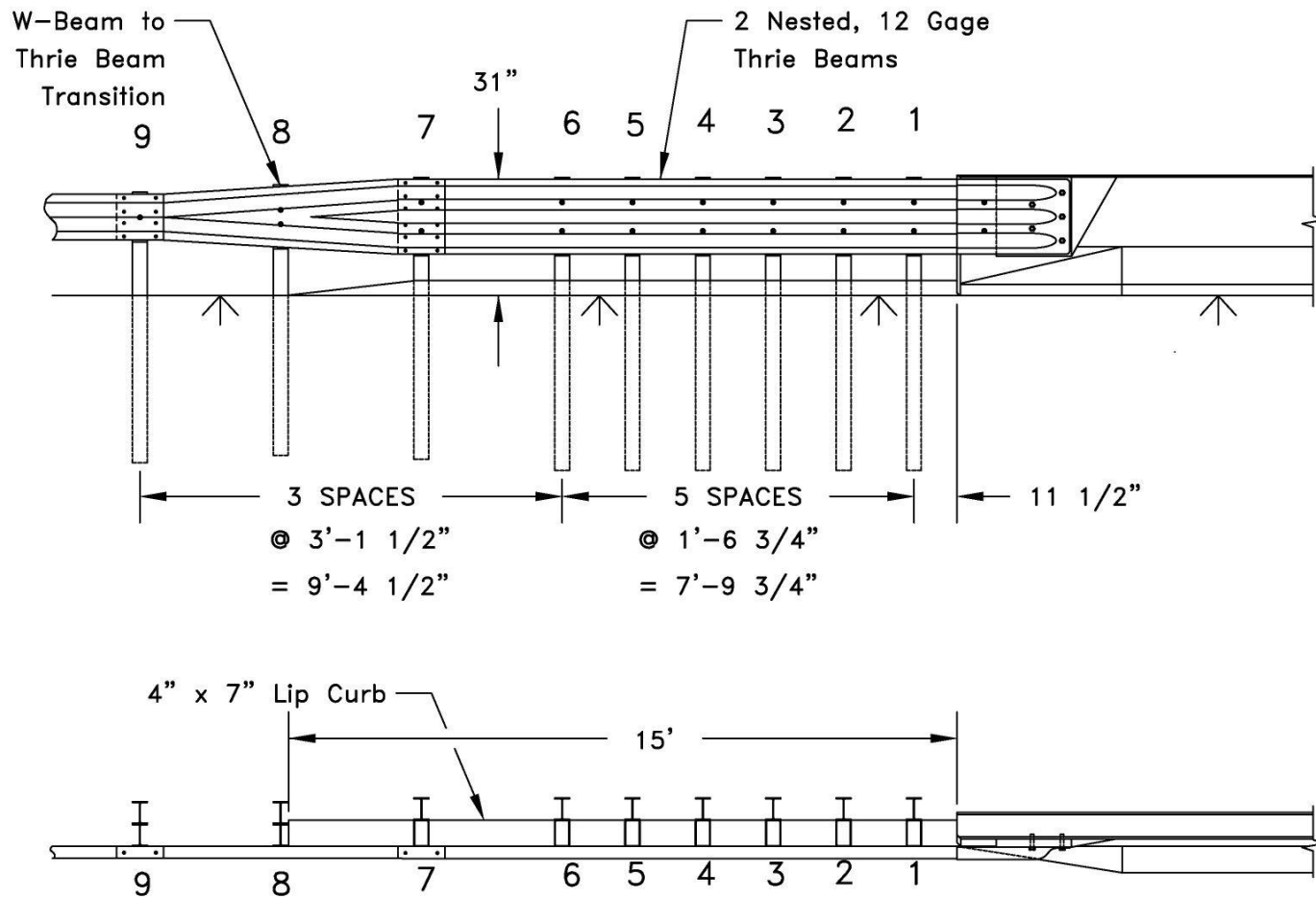
Figure 15.Steel Post Approach Transition – ITNJ-2 [19]

www.manaraa.com
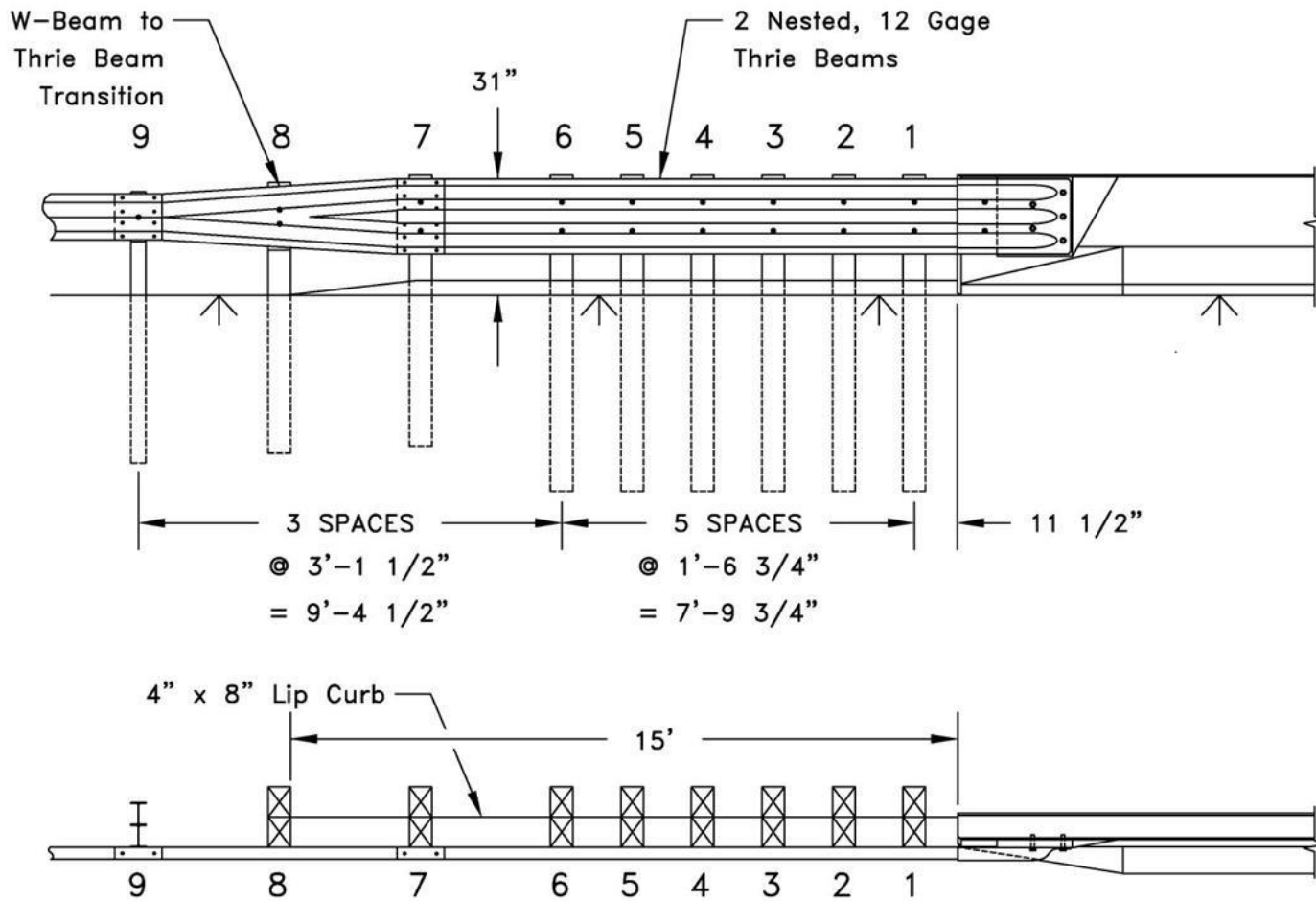
Figure 16. Wood Post Approach Transition – ITNJ-4 [19]

www.manaraa.com

2.5.2 Evaluation of Guardrail to Concrete Barrier Transition

With the vehicle fleet constantly changing and growing, standards for testing roadside safety hardware must also change. Thus, NCHRP Report No. 350 was updated to include heavier vehicles with higher centers of gravity. In 2006, MwRSF researchers conducted another crash test under the impact conditions outlined in the Update to NCHRP Report No. 350 on the guardrail to concrete barrier transition system that had been previously tested [20].

The transition design was constructed using W6x9 (W152x13.4) steel posts with a length of 6 ft (1,829 mm) for post nos. 3 through 10 and 6 ft – 6 in. (1,981) for post nos. 11-17 [20]. A varied post spacing consisted of one at 10½ in. (267 mm), five at 18¾ in. (476 mm), and three at 37½ in. (953 mm). During test no. 2241T-1, a 5,083-lb (2,306-kg) pickup truck impacted the system at 7 ft – 11⅞ in. (2,435 mm) upstream from the end of the concrete barrier at a speed of 60.3 mph (97.0 km/h) and at an angle of 24.8 degrees. The steel-post transition system contained and smoothly redirected the vehicle with maximum lateral dynamic and permanent set barrier deflections of 11.4 in. (289 mm) and 7⅝ in. 194 mm), respectively and was determined to be a success according to TL-3 found in the Update to NCHRP Report No. 350.

2.5.3 Stiffness Transition Between W-Beam Guardrail and Thrie Beam

In 2007, MwRSF researchers investigated stiffness transitions from W-beam guardrail to thrie beam approach guardrail transitions [21]. Prior testing of symmetric W-beam to thrie beam transition elements had been conducted according the guidelines set forth in NCHRP Report No. 350, but the system did not successfully pass the 2000P light pickup truck test [22]. This study was conducted to alleviate some of the stiffness

concerns associated with the previously-tested transition design. This study included four full-scale crash tests that utilized a varied post spacing that consisted of post nos. 1 through 7 spaced 75 in. (1,905 mm), post nos. 7 through 19 spaced 37.5 in. (953 mm), and post nos. 19 through 21 spaced 75 in. (1,905 mm).

For the first full-scale crash test, the W-beam rail had a nominal top rail height of 27¾ in. (705 mm), while the thrie beam had a nominal top rail height of 31⅝ in. (803 mm). The approach transition is shown in Figure 17. During test no. MWT-3, a 4,456-lb (2,021-kg) pickup truck impacted the system 8 in. (203 mm) upstream from the centerline of post no. 9 at a speed of 63.9 mph (102.9 km/h) and at an angle of 24.8 degrees. The transition system contained but did not safely redirect the vehicle; since, the vehicle rolled over upon exiting the system. Therefore, test no. MWT-3 was determined to be unsuccessful according to TL-3 of NCHRP Report No. 350.

Upon investigation of the results from test no. MWT-3, researchers concluded that the roll behavior was due to the relatively higher center of gravity of the 2000P vehicle combined with the relatively low rail height for the 27¾-in. (705-mm) tall standard guardrail. The proposed solution was to switch the approach guardrail to the 31-in. (787-mm) high Midwest Guardrail System (MGS). Since the MGS utilized a 31-in. (787-mm) rail height, a new asymmetric transition element was needed. The new transition element was fabricated by cutting a triangular piece out of the bottom of a standard 12-gauge (2.66-mm) thrie beam rail, as shown in Figure 18. During test no. MWT-4, a 4,448-lb (2,018-kg) pickup truck impacted the system at 9 in. (229 mm) upstream from the centerline of post no. 9 at a speed of 61.0 mph (98.1 km/h) and at an angle of 25.3 degrees. The system did not safely contain nor redirect the vehicle; since,
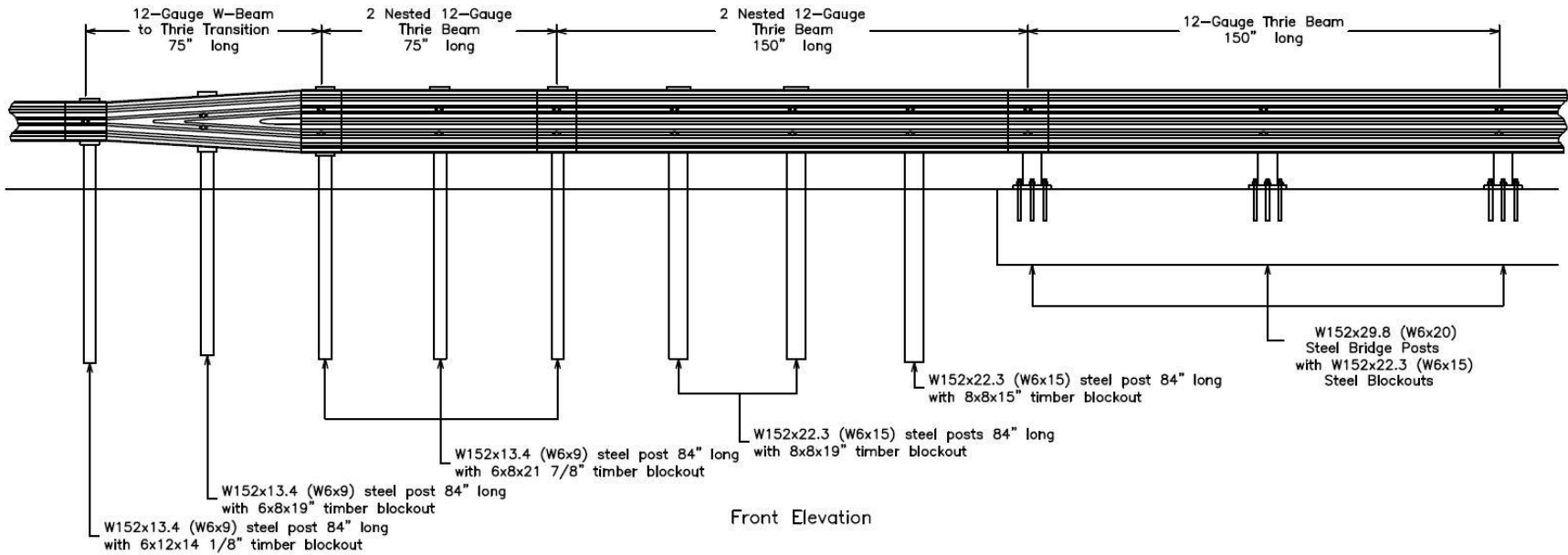
Figure 17. Approach Transition for Test No. MWT-3 [21]

the vehicle penetrated the system due to rail rupture. Subsequently, test no. MWT-4 was deemed unsuccessful according to TL-3 of NCHRP Report No. 350.

Figure 18. Asymmetric Transition Element for Test No. MWT-4 [21]

Upon investigation of the results of test no. MWT-4, researchers concluded that increasing the post size and embedment depth of posts within the transition region would eliminate pocketing. For test no. MWT-5, post nos. 9 through 15 were W6x12 (W152x17.9) section measuring 7-ft 6-in. (2,286-mm) long. Additionally, the post embedment depth for post nos. 9 through 15 was 58 in. (1,473 mm). The fabricated asymmetrical W-beam to thrie beam transition was also replaced with a new 10-gauge (3.43-mm) MGS asymmetrical transition element, shown in Figure 19. During test no. MWT-5, a 4,431-lb (2,010-kg) pickup truck traveling at 61.5 mph (99.0 km/h) impacted the system 13 in. (330 mm) upstream of the centerline of post no. 9 at an angle of 24.9 degrees. The system safely contained and redirected the vehicle with maximum lateral

dynamic and permanent set barrier deflections of 23⅞ in. (605 mm) and 14¾ in. (375 mm), respectively, and subsequently was deemed successful according to NCHRP Report No. 350.

Figure 19. MGS Stiffness Transition with Asymmetrical Element [21]

The fourth full-scale crash test utilized the same system setup used for test no. MWT-5 but now tested with a small car. During test no. MWT-6, a 1,992-lb (904-kg) small car impacted the system 12½ in. (318 mm) upstream from the centerline of post no. 10 at a speed of 65.5 mph (105.3 km/h) and at an angle of 20.4 degrees. The system safely contained and redirected the vehicle with maximum lateral dynamic and permanent set barrier deflections of 12⅜ in. (313 mm) and 12⅜ in. (313 mm), respectively, and subsequently was deemed successful according to NCHRP Report No. 350.

2.5.4 Evaluation of Thrie Beam Transition without Curb

In 2013, TTI researchers conducted a performance evaluation of a modified thrie beam transition to rigid concrete barrier without a curb element below the transition rail [23]. The rigid concrete barrier was a 36-in. (914-mm) tall, single-slope traffic rail that

was 7½-in. (191-mm) wide at the top and 14½-in. (368-mm) wide at the bottom. The approach guardrail transition consisted of a nineteen W6x8.5 (W152x12.6) posts with lengths of 72 in. (1,829 mm) for post nos. 3-13 and 84 in. (2,134 mm) for post nos. 14 to 19. The 12-gauge (2.66-mm) W-beam guardrail was positioned from post no. 1 to post no. 11 and then an asymmetric W-to-thrie transition element spanned from post no. 11 to post no. 13. Then, nested 12-gauge (2.66-mm) thrie beam rail extended from post no. 13 to the attachment location on the rigid concrete barrier, as shown in Figure 20.

During test no. 490022-4, a 5,002-lb (2,269-kg) pickup truck impacted the system 7 ft – 5 in. (2,261 mm) upstream from the rigid concrete barrier at a speed of 62.6 mph (100.7 km/h) and at an angle of 23.9 degrees. The transition system contained but did not safely redirect the vehicle; since, the vehicle rolled over upon exiting the system. The maximum dynamic and permanent set deflections were 5.9 in. (150 mm) and 4.5 in. (114 mm), respectively, with a working width of 22.8 in. (579 mm). Test no. 490022-4 was determined to be unsuccessful according to TL-3 of MASH due to vehicle rollover.

Figure 20. Thrie Beam Transition without Curb [23]

2.5.5 MGS Approach Guardrail Transition Using Standardized Steel Posts

Previously, MwRSF developed and crash tested a stiffness transition between MGS and thrie beam AGTs utilizing an asymmetrical transition element and three different steel post types under TL-3 of NCHRP Report No. 350. However, many State Departments of Transportation (DOTs) viewed the system as too complicated, and they do not use W6x12 (W152x17.9) steel posts. Therefore, a simplified transition was developed using only W6x15 (W152x22.3) and W6x9 (W152x13.4) steel posts [24].

The system consisted of three bridge rail posts and eighteen guardrail posts. The guardrail posts utilized a varied post spacing of 75 in. (1,905 mm) for post nos. 1 through 8, 37½ in. (953 mm) for post nos. 8 through 12, 18¾ in. (476 mm) for post nos. 12 through 16, and 37½ in. (953 mm) for post nos. 16 through 19. Post nos. 3 through 15 were galvanized ASTM A36 W6x9 (W152x13.4) steel sections measuring 6-ft (1,829-mm) long. Post nos. 16 through 18 were galvanized ASTM A36 W6x15 (W152x22.3) steel sections measuring 7-ft (2,134-mm) long. The soil embedment depths for post nos. 3 through 15 and 16 through 18 were 40 in. (1,016 mm) and 55⅛ in. (1,400 mm), respectively. During test no. MWTSP-1, a 5,169-lb (2,345-kg) pickup truck impacted the system 71 in. (1,803 mm) upstream from post no. 9 at a speed of 61.5 mph (99.0 km/h) and at an angle of 24.7 degrees. The system adequately contained but did not safely redirect the vehicle. The vehicle came to an abrupt stop due to pocketing that formed in the system. Subsequently, MWTSP-1 was deemed unsuccessful according to TL-3 of MASH.

Upon investigation of test no. MWTSP-1, post no. 1, a Breakaway Cable Terminal (BCT) wood anchor post, fractured early in the impact event. Inspection of the

post revealed significant checking through the wide faces of the post along with a critically placed knot on the upstream, back-side corner of the post. Researchers concluded that these post deficiencies were the cause of early post fracture. Researchers also concluded that without this early post fracture, the system would have adequately contained and redirected the vehicle. So a retest was conducted using the system layout shown in Figure 21. During test no. MWTSP-2, a 5,158-lb (2,340-kg) pickup truck impacted the system 74½ in. (1,892 mm) upstream from post no. 9 at a speed of 61.2 mph (98.5 km/h) and at an angle of 26.3 degrees. The system adequately contained and redirected the vehicle with maximum lateral dynamic and permanent set barrier deflections of 32.8 in. (833 mm) and 25¾ in. (654 mm), respectively, and was subsequently deemed successful according to TL-3 of MASH.

The MGS stiffness transition to thrie beam AGTs was also subjected to crash testing with a 1100C small car according to MASH in order to investigate potential underride tendencies. During test no. MWTSP-3, a 2,591-lb (1,175-kg) small car impacted the system 93¾ in. (2,381 mm) upstream from post no. 9 at a speed of 61.0 mph (98.2 km/h) and at an angle of 25.7 degrees. The system adequately contained and redirected the vehicle with maximum lateral dynamic and permanent set barrier deflections of 34.8 in. (883 mm) and 27 in. (686 mm), and was subsequently deemed successful according to TL-3 of MASH.
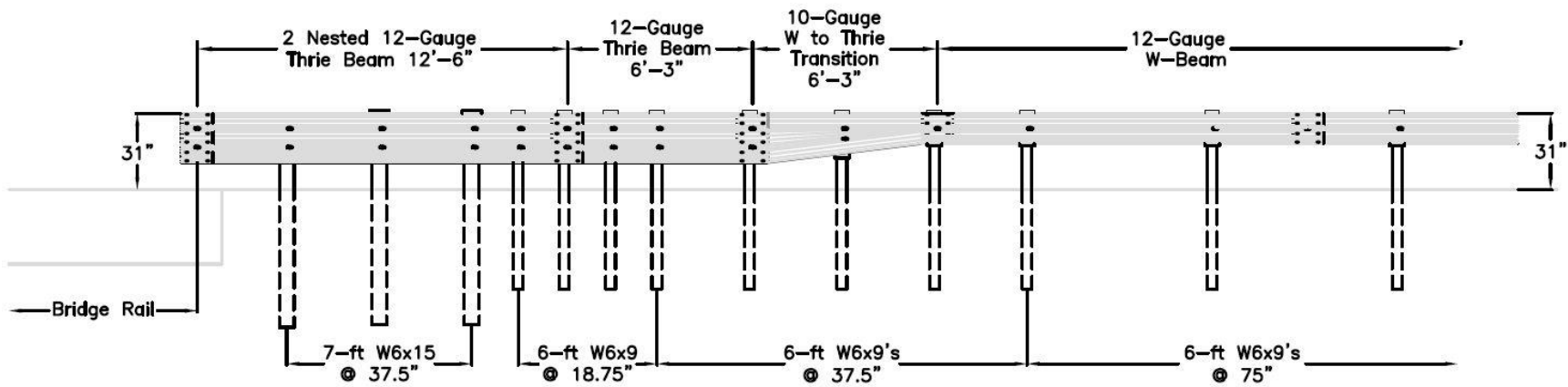
Figure 21. MGS Approach Transition to Thrie Beam [24]

2.5.6 Roadside Barriers for Bridge-Pier Protection

In 1983, New York State Department of Transportation developed a roadside barrier for the protection of concrete bridge piers near the pavement edge [3-4]. Seven full-scale crash tests were conducted following the evaluation guidelines found in NCHRP Report No. 230. The barrier system consisted of four 15-ft (4,572-mm) long half-section, safety-shape concrete barriers and 6-in. (152-mm) x 6-in. (152-mm) x 3/16-in. (4.76-mm) box-beam guiderail. One concrete barrier was installed in front of and parallel to two simulated bridge piers. The remaining three concrete barriers were installed at an 8H:1V flare rate away from the roadway upstream from the bridge piers. The concrete barriers were rigidly installed with continuity connectors at barrier joints and driven steel backup posts for the first four full-scale tests and soil-backfill for the final three full-scale tests.

For the first four full-scale tests, the box-beam guiderail attached to the face of the second concrete barrier with a total system length of 130 ft − 6 in. (39.8 m). During test no. 60, a 4,450-lb (2,018-kg) sedan impacted the box-beam guiderail 55 ft − 6 in. (16.9 m) downstream from its end at a speed of 55.7 mph (89.6 km/h) and at an angle of 25.0 degrees. The system safely contained and redirected the vehicle with maximum lateral dynamic and permanent set barrier deflections of 2.6 ft (792 mm) and 1.7 ft (518 mm), respectively, and subsequently was deemed successful according to NCHRP Report No. 230. During test no. 61, a 1,600-lb (726-kg) sedan impacted 12.2 ft (3,719 mm) upstream from the box-beam attachment to the concrete barrier at a speed of 59.0 mph (95.0 km/h) and at an angle of 14.0 degrees. The system safely contained and redirected the vehicle with maximum lateral dynamic deflection of 6 in. (152 mm) and no permanent set barrier

deflection, and subsequently was deemed successful according to NCHRP Report No. 230. During test no. 62, a 4,500-lb (2,041-kg) sedan impacted 12.2 ft (3,719 mm) upstream from the box-beam attachment to the concrete barrier at a speed of 54.3 mph (87.4 km/h) and at an angle of 29.0 degrees. The system safely contained and redirected the vehicle with maximum lateral dynamic and permanent set barrier deflections of 0.25 ft (76 mm) and 0.19 ft (58 mm), respectively, and subsequently was deemed successful according to NCHRP Report No. 230. During test no. 63, a 4,730-lb (2,145-kg) sedan impacted 7.7 ft (2,347 mm) upstream from the joint between barrier nos. 1 and 2 at a speed of 57.1 mph (91.9 km/h) and at an angle of 26.0 degrees. The vehicle climbed the face of the concrete barrier and rolled upon exiting the system and was deemed unsuccessful according to NCHRP Report No. 230.

In order to prevent vehicle climb on the concrete barriers, the box-beam guiderail was installed across the face of the most downstream concrete barrier and continuing past the simulated bridge piers. During test no. 76, a 1,800-lb (816-kg) sedan impacted 4.3 ft (1,311 mm) upstream from the joint between barrier nos. 1 and 2 at a speed of 58.3 mph (93.8 km/h) and at an angle of 20.0 degrees. The system safely contained and redirected the vehicle with no lateral dynamic or permanent set barrier deflections and subsequently was deemed successful according to NCHRP Report No. 230. During test no. 77, a 4,650-lb (2,109-kg) sedan impacted 4.3 ft (1,311 mm) upstream from the joint between barrier nos. 1 and 2 at a speed of 61.2 mph (98.5 km/h) and at an angle of 29.0 degrees. The system safely contained and redirected the vehicle with no lateral dynamic deflection and a permanent set barrier deflection of 0.19 ft (58 mm) and subsequently was deemed successful according to NCHRP Report No. 230.

For the final full-scale crash test, the box beam installed in front of the most downstream concrete barrier was removed, and test no. 63 was repeated with full-height bridge piers to evaluate the severity of vehicle contact with the bridge piers. During test no. 78, a 4,500-lb (2,041-kg) sedan impacted 3.2 ft (975 mm) upstream from the joint between barrier nos. 1 and 2 at a speed of 63.7 mph (102.5 km/h) and at an angle of 30.0 degrees. The vehicle climbed the face of the concrete barriers and impacted both simulated bridge piers and rolled upon exiting the system and subsequently was deemed unsuccessful according to NCHRP Report No. 230.

It was therefore recommended by the New York State Department of Transportation that the box-beam guiderail should be installed across the face of the most downstream concrete barrier in order to adequately contain and redirect the vehicle without impact with the bridge piers.

2.5.7 Development of Low Profile to F-Shape Transition Barrier Segment

In 2006, TTI researchers developed a low-profile to F-shape transition barrier segment [25]. Low-profile barriers are used in low-speed work zones to allow drivers increased visibility of traffic and pedestrians. However, areas where speed limits transition from low-speed to high-speed or high-speed to low-speed require a transition from the low-profile barrier to the taller F-shape PCB. For this study, the transition barrier segment was 32 in. (813 mm) tall on the side that connected to the F-shape PCB and transitioned to the low-profile barrier height of 20 in. (508 mm) over a length of 10 ft (3,048 mm), as shown in Figure 22. The transition barrier segment was connected to the F-shape PCB using a cross-bolt connection, while the transition segment used a standard bolted connection to attach to the low-profile barrier. Through finite element modeling,

two critical impact conditions were identified, and two full-scale crash tests were conducted.

Figure 22. Low-Profile to F-Shape Transition Barrier Segment [25]

During test no. 455276-1, a 4,725-lb (2,143-kg) pickup truck impacted the transition barrier 25.6 in. (650 mm) downstream from the joint between the F-shape PCB and the transition barrier at a speed of 44.0 mph (70.8 km/h) and at an angle of 25.1 degrees. The system safely contained and redirected the vehicle with maximum lateral dynamic and permanent set barrier deflections of 10¼ in. (260 mm) and 10¼ in. (260 mm), respectively, and subsequently was deemed successful according to TL-2 of NCHRP Report No. 350. During test no. 455276-2, a 4,744-lb (2,152-kg) pickup truck impacted the system at the joint between the low-profile barrier and the transition barrier at a speed of 44.7 mph (71.9 km/h) and at an angle of 25.9 degrees. The system safely contained and redirected the vehicle with maximum lateral dynamic and permanent set barrier deflections of 7 in. (177 mm) and 6⅝ in. (168 mm), respectively, and subsequently was deemed successful according to the TL-2 of NCHRP Report No. 350.

2.6 Testing of Various Barrier Stiffening Techniques

2.6.1 Concrete Median Barriers with Corrugated Ends and Tensioned Cables

In 1978, CALTRANS researcher investigated a new barrier type that could be used in both temporary and permanent installations [26]. The barrier segments were 12-ft 6-in. (3,810-mm) long, New Jersey shape PCBs with corrugated ends. A continuous 2½-in. (64-mm) diameter hole was cast 10 in. (254 mm) vertically from the bottom of each PCB segment through the longitudinal cross-section. In order to limit barrier deflections, a cable was threaded through the hole in each PCB and tensioned at the exterior ends.

For the first full-scale crash test, the system utilized ten PCB segments for a total system length of 125 ft (38.1 m). The PCB system was placed on polystyrene pads, and the cable was tensioned to 17,640 lb (78,467 N) on the upstream end of the system and 14,780 lb (65,745 N) on the downstream end of the system. During test no. 331, a 4,680-lb (2,123-kg) sedan impacted the PCB system at 5.5 ft (1,676 mm) upstream from the upstream of joint no. 5 at a speed of 63.0 mph (101.4 km/h) and at an angle of 25.0 degrees. The vehicle became airborne and was on top of the PCB system. Subsequently, test no. 331 was found to be unsuccessful according to the safety criteria provided in NCHRP Report No. 153.

For the second full-scale crash test, the system utilized ten PCB segments for a total system length of 125 ft (38.1 m). The PCB system was placed on grout pads, and the cable was tensioned to 4,880 lb (21,707 N) throughout the system. During test no. 332, a 4,600-lb (2,087-kg) sedan impacted the PCB system 11.7 ft (3,566 mm) upstream from joint no. 5 at a speed of 60.0 mph (96.6 km/h) and at an angle of 25.0 degrees. The grout

pads were ineffective in limiting barrier deflections and the PCB segment design was determined to be structurally inadequate according to NCHRP Report No. 153.

2.6.2 Channel-Beams Spanning a Gap in Continuous Concrete Median Barrier

In 1979, CALTRANS researchers investigated systems for spanning gaps in continuous concrete median barriers where storm drain catch basins were located [27]. The permanent New Jersey shape concrete median was 32 in. (813 mm) tall with a 4-ft (1,219-mm) gap cutout. Threaded rods with $\frac{7}{8}$-in. (22-mm) diameter were cast into the ends of the permanent concrete median barriers at an embedment depth of 5 in. (127 mm). Hanger brackets were cut from pieces of C6x8.2 (C150x12.2) steel channel rubrail and bolted on the ends of the permanent concrete median barriers. The channel beams, C6x8.2 (C150x12.2), were bolted onto the hanger brackets, as shown in Figure 23. During test no. 361, a 4,410-lb (2,000-kg) sedan impacted the concrete median barrier system 5.9 ft (1,798 mm) upstream from the gap at a speed of 61.0 mph (98.2 km/h) and at an angle of 23.0 degrees. The gap beam sustained minimal damage, and the vehicle was safely contained and redirected. Subsequently, test no. 361 was determined to be a success according to Transportation Research Circular (TRC) Report No. 191.
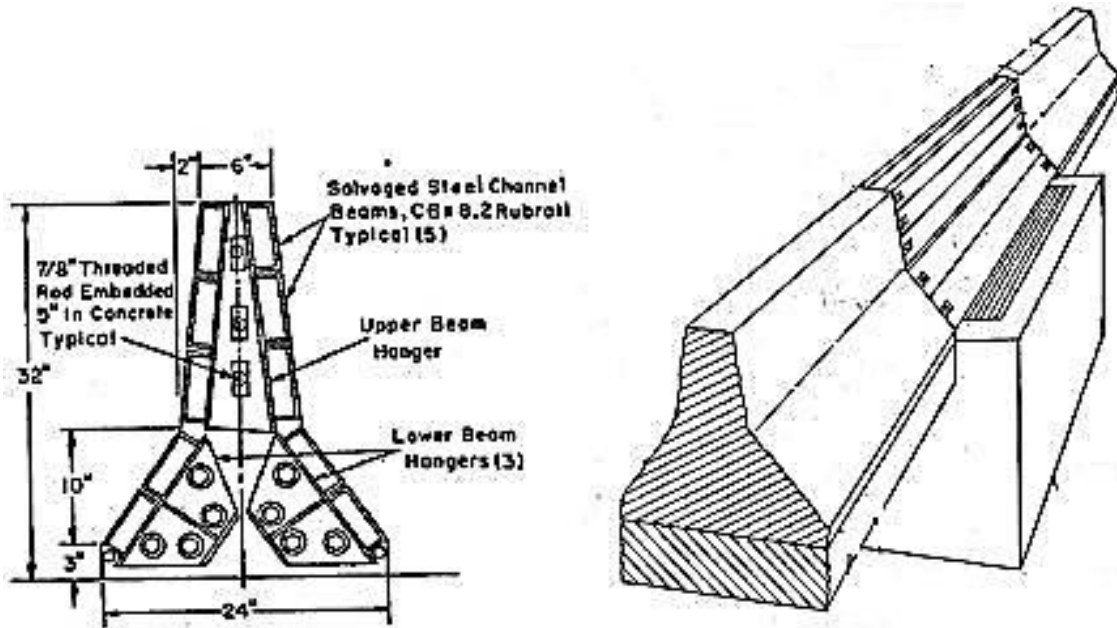
Figure 23. Hanger Bracket and Steel Channel Beam Design [27]

2.6.3 PCB System for Off-Road Applications

In 1996, MwRSF researchers developed a PCB system for placement on a soil foundation [28]. PCB systems are typically placed on concrete or bituminous surfaces, but it is often impractical and costly to follow this practice. Therefore, it was determined that development of a PCB system capable of placement on soil foundations or native fill with slopes 10H:1V or flatter would be economical. In order to mitigate the potential of barrier tipping, a ski system was developed. The design called for two ski systems to be attached to each PCB segment. The maximum overturning moment of a PCB during a crash test was estimated to be 3.3 kip-ft (4.5 kN-m), and each ski system was designed to resist half of this moment. A 2-ft (610-mm) x 2-ft (610-mm) square piece of ¾-in. (19-mm) thick plywood was placed under the ski to prevent it from gouging into the soil. The ski was attached to the plywood with a ¼-in. (6-mm) long wood screw. The ski design is shown in Figure 24.
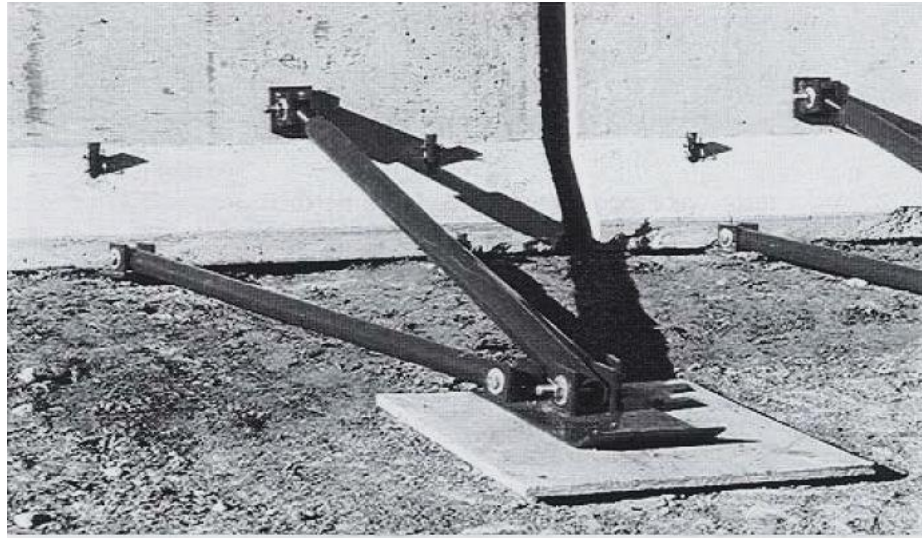
Figure 24. PCB Ski Design [28]

The test installation consisted of seventeen 12-ft 6-in. (3,810-mm) long, F-shape PCB segments for a total system length of 203 ft – 5½ in. (62.0 m). The ski configuration was connected to barrier nos. 5 through 14. During test no. KTS-1, a 4,405-lb (1,998-kg) pickup truck impacted the PCB system 47¼ in. (1,200 mm) upstream from the joint between barrier nos. 8 and 9 at a speed of 61.9 mph (99.6 km/h) and at an angle of 26.9 degrees. The system contained and redirected the vehicle with a maximum lateral permanent set deflection of 45 11/16 in. (1,160 mm) and was considered successful according to TL-3 of NCHRP Report No. 350.

2.6.4 Box-Beam Stiffening of Unanchored PCBs

In 2008, MwRSF researchers tested a PCB stiffening system for the New York Department of Transportation using box beams bolted across barrier joints on the backside of the system in order to limit system deflections [29]. Anchoring of PCB systems with pins or bolted-through connections had been previously tested, but this process is time consuming and may result in damage to the bridge. NYSDOT personnel

developed a concept of using box-beam stiffeners that would minimize barrier deflections while preventing bridge deck damage.

The first test installation consisted of ten 20-ft (6,096-mm) long, New Jersey shape PCB segments for a total system length of 200 ft (61.0 m). The PCB system was free-standing with both end segments anchored to the tarmac with nine 1-in. (25-mm) diameter x 15½-in. (394-mm) long, A36 steel rods – five anchors on the traffic-side and four anchors on the back-side. Each anchor rod was driven into a hole drilled in the concrete to an embedment depth of 5 in. (127 mm). The PCB system utilized an I-beam key connector barrier-to-barrier connection. The three joints between barrier nos. 4 and 7 were stiffened with box beams. Each box beam stiffener consisted of a 6-in. (152-mm) x 6-in. (152-mm) x ⅛-in. (3-mm) ASTM A500 Grade C box beam, which was 12 ft (3,658 mm) long. Two ¾-in. (19-mm) holes were drilled through the barriers at an angle of 6 degrees in order to mount the box beam stiffeners. The box beams were connected to the barriers with ¾-in. (19-mm) diameter x 17-in. (432-mm) long, Grade 5 continuously threaded rod. The PCB with box beam stiffeners is shown in Figure 25. During test no. NYTCB-1, a 5,016-lb (2,275-kg) pickup truck impacted the box-beam stiffened PCB system 51.2 in. (1,300 mm) upstream from the end of barrier no. 4 at a speed of 61.8 mph (99.5 km/h) and at an angle of 24.6 degrees. The system contained and redirected the vehicle with maximum lateral dynamic and permanent set deflections of 27.6 in. (700 mm) and 26 in. (660 mm), respectively, and was considered successful according to TL-3 in the Update to NCHRP Report No. 350.

For the purpose of comparison, the second full-scale crash was identical to the first except with the box-beam stiffeners removed. The system was constructed with

identical PCB segments, I-beam key connectors, and anchored ends. During test no. NYTCB-2, a 5,024-lb (2,279-kg) pickup truck impacted the free-standing PCB system 51.2 in. (1,300 mm) upstream from the end of barrier no. 4 at a speed of 61.2 mph (98.5 km/h) and at an angle of 25.8 degrees. The system contained and redirected the vehicle with maximum lateral dynamic and permanent set deflections of 40¼ in. (1,023 mm) and 39½ in. (1,003 mm), respectively, and was considered successful according to TL-3 in the Update to NCHRP Report No. 350.

Figure 25. NYSDOT Box-Beam Stiffener System [29]

The third full-scale crash test utilized a system that was identical to test no. NYTCB-1, except with more robust box-beam stiffeners and placement of the system 12 in. (305 mm) away from the edge of a simulated bridge deck. For this installation, each box-beam stiffener consisted of a 6-in. (152-mm) x 8-in. (203-mm) x ¼-in. (6-mm) ASTM A500 Grade C box beam, which was 12 ft (3,658 mm) long. The stiffeners were connected to the barrier segments utilizing similar connecting rods used in test no. NYTCB-1, except that the length was increased to 19 in. (483 mm). During test no.

NYTCB-3, a 5,001-lb (2,268-kg) pickup truck impacted the box-beam stiffened PCB system 51.2 in. (1,300 mm) upstream from the end of barrier no. 4 at a speed of 63.5 mph (102.2 km/h) and at an angle of 24.4 degrees. The system contained and redirected the vehicle with maximum lateral dynamic and permanent set deflections of 30.9 in. (784 mm) and 26 in. (660 mm), respectively, while all of the PCB segments remained on the simulated bridge deck. Subsequently test no. NYTCB-3 was considered successful according to TL-3 in the Update to NCHRP Report No. 350.

2.6.5 Retrofit of Existing Approach Guardrail Transitions

In 2012, MwRSF researchers established guidance for retrofitting existing approach guardrail transitions for the State of Wisconsin [30]. A survey determined that several transition systems were installed in a manner that deviated from the as-tested design details. These deviations included: missing transition posts; transition posts installed near or at slope break point of fill slope; insufficient soil backfill/grading behind transition posts; wood posts installed in asphalt surfacing; and the presence of drainage structures below the rail. The purpose of the research was to determine if these deficiencies degraded the performance of the 18-ft 9-in. (5,715-mm) long and the 31-ft 3-in. (9,525-mm) long approach guardrail transitions.

Missing transition posts were believed to have the potential to cause system failure and allow a vehicle to snag on the upstream end of the bridge rail. Whenever possible, the best option for repairing this deficiency is to re-install an appropriate post in the prescribed location. However, for some cases where this is not possible, three retrofit designs were developed. The first retrofit corresponded to a missing post near a blunt-end parapet, which consisted of a horizontal cantilever beam off of the back-side of the bridge

rail that would be vertically centered with the thrie beam at a height of 21.7 in. (551 mm). The second retrofit corresponded to a missing post near a sloped-end parapet, which was similar to the first retrofit with modifications to the blockout and anchor plate. The third retrofit corresponded to missing posts not adjacent to a parapet, which consisted of two surrogate posts linked by a horizontally-mounted beam. The horizontally-mounted beam attached at the mid-span to the thrie beam transition at the location of the missing post with the use of several blockouts. The three missing transition post retrofits are shown in Figure 26.

Transition posts installed near or at slope break points of fill slopes with insufficient level terrain behind the guardrail transition have the potential to cause excessive barrier deflections, vehicle pocketing, and vehicle snag on the upstream end on the bridge rail. In order to provide adequate soil resistance, it was recommended that affected wood posts positioned on a 2H:1V sloped terrain should be supplemented with 8-ft 6-in. (2,591-mm) long, W6x16 (W152x23.8) steel posts. Affected wood posts positioned on a 3:1 sloped terrain should be supplemented with 12-ft (3,658-mm) long, W6x12 (W152x17.9) steel posts, as shown in Figure 27.
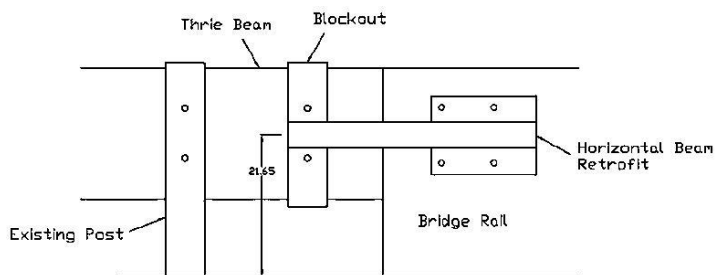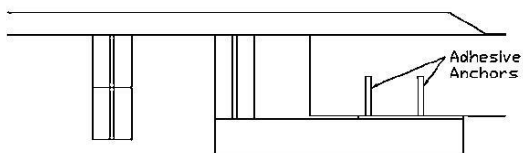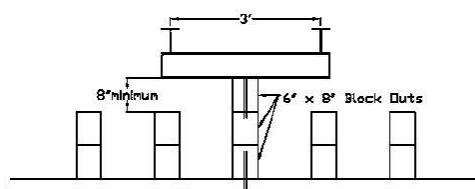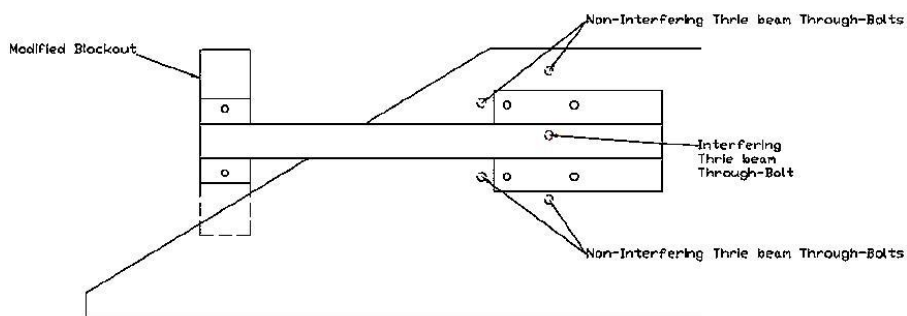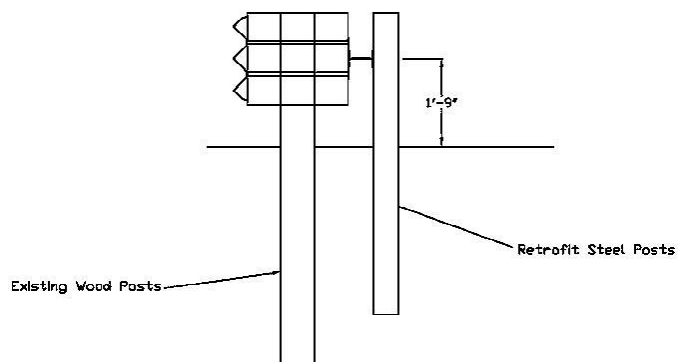
Figure 26. Missing Transition Post Retrofits [30]
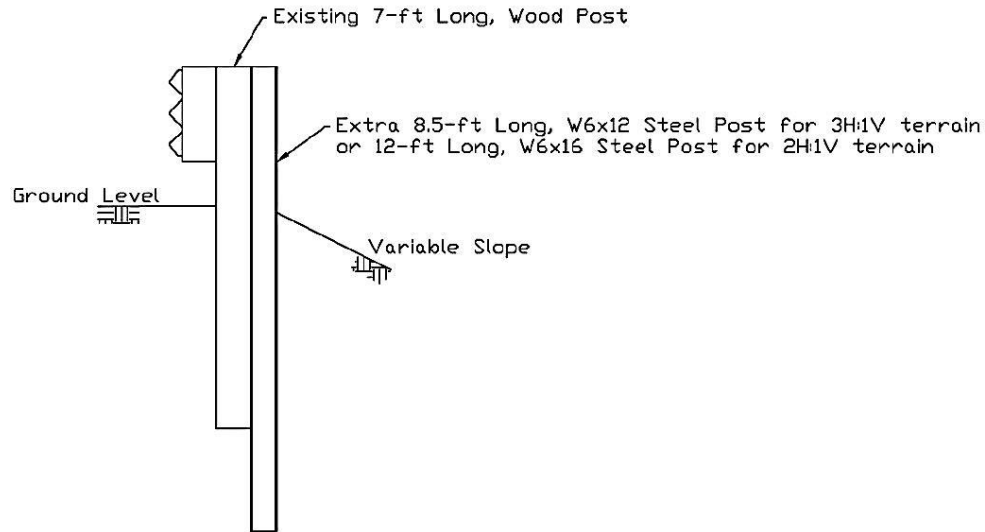
Figure 27. Driven Post Design [30]

Transition posts embedded in asphalt surfaces show potential to hinder post rotation and cause wood posts to prematurely fracture during impact events. Upon investigation of photograph evidence provided by the Wisconsin DOT of common approach transition installations, it was discovered that asphalt usage was more prevalent on sloped terrain in order to prevent soil erosion. A series of four bogie tests were conducted on 6-in. (152-mm) x 8-in. (203-mm) x 84-in. (2,134-mm) long wood posts confined in 2-in. (51-mm) thick asphalt with an embedment depth of 50 in. (1,270 mm) at the slope break point of either a 2H:1V or 4H:1V fill slope. It was determined that for wood posts positioned on a 2H:1V fill slope, a 2-in. (51-mm) thick asphalt confinement was not shown to negatively affect post behavior. However, since the forces observed in the two bogie tests did not reach the design loads for the approach transition system, it was determined that wood posts confined in asphalt on a 2H:1V slope break point should be supplemented with an additional steel post, as shown previously in Figure 26. For wood posts positioned on a 4H:1V fill slope, a 2-in. (51-mm) thick asphalt confinement was shown to negatively affect post behavior. It was recommended that transition

systems should not be installed on 4H:1V or flatter slopes while confined in 2-in. (51-mm) thick asphalt pavement.

Transition systems installed with drainage structures below the installation show potential to cause severe vehicle instabilities during vehicle containment, capture, and redirection. Survey data and photograph evidence indicated that the majority of approach transitions utilized a 6-in. (152-mm) tall, vertical curb. Based on previous full-scale crash testing of comparable transition systems, it was determined that for 18-ft 9-in. (5,715-mm) long and 31-ft 3-in. (9,525-mm) long transition systems, the use of a 4-in. (102-mm) tall triangular curb below the thrie beam transition is required. Also, the adverse effect of a lateral drainage flume curb below an approach transition installation was investigated. It was believed that the height and shape of the 6-in. (152-mm) tall curb could lead to an increased propensity for vehicle instability. Also, the 3-in. (76-mm) deep swell near the lateral curb opening may promote bumper or wheel snag as vehicles wedge under the thrie beam rail and potentially result in system underride. It was strongly recommended that no additional approach guardrail transitions with a lateral drainage flume curb below the system be installed until full-scale crash testing was conducted.

CHAPTER 3 DEVELOPMENT OF DESIGN CONCEPTS

3.1 Design Constraints

Upon consultation with the Technical Advisory Committee (TAC) members, it was determined that this TL-3 transition was necessary for situations where road construction created a work zone adjacent to existing W-beam guardrail systems. In this scenario, a portion of the W-beam guardrail would need to be removed. Subsequently, PCBs would be used to shield the work zone and installed at a 15H:1V flare rate. In order to limit damage to the roadway surface and reduce installation time, it was preferred that none of the PCBs be anchored or pinned to the roadway surface. Although the primary configuration considered a transition from W-beam guardrail to PCBs, there was potential for reverse-direction impacts, which should be investigated during a critical impact point (CIP) study.

Soil grading and roadside terrain were also considered; since, several transition design concepts would require that PCBs be installed behind the existing W-beam guardrail system. When PCBs are installed on native soil, they may settle or gouge into the soil, potentially resulting in a large overturning moment and/or barrier tipping upon impact. For these situations, a compacted crushed limestone base, or similar, would be required for a minimum lateral width of 4 ft (1,219 mm) and at a 10V:1H cross slope behind the transition installation. Since the transition could likely be installed on a concrete, asphalt, or compacted crushed limestone base, all three foundations need to be considered during the concept development and full-scale crash testing phases of the study.

Two different W-beam guardrail systems were considered in this research: the modified G4(1S) guardrail system and the Midwest Guardrail System (MGS). The PCBs consisted of 32-in. (813-mm) tall, F-shape PCBs that were developed through the Midwest Pooled Fund Program [1].

3.1.1 W-Beam Guardrail Systems

3.1.1.1 Modified G4(1S) Guardrail

It was determined that the initial W-beam guardrail system used in this research should be representative of the most common guardrail system found on the roadside, which was the modified G4(1S) guardrail system. It was also determined that the modified G4(1S) guardrail would provide a more critical impact scenario due to its relatively low top rail height and a higher center of gravity for the 2270P test vehicle. Researchers also felt confident that a successful transition from modified G4(1S) guardrail to PCBs could successfully be adapted to the MGS with minor modifications.

The modified G4(1S) guardrail system utilized A992 Grade 50 W6x9 (W152x13.4) steel posts measuring 72-in. (1,829-mm) long, 12-ft 6-in. (3,810-mm) long 12-gauge (2.66-mm) W-beam rail sections, and 6-in. (152-mm) wide x 8-in. (203-mm) deep x 14¼-in. (362-mm) long wood blockouts to space the rail away from the front face of the steel posts. The top rail height was 27¾ in. (706 mm) with a 21⅝-in. (550-mm) center mounting height, and the steel guardrail posts were spaced at 6 ft − 3 in. (1,905 mm) on center. A typical cross-section is shown in Figure 28.
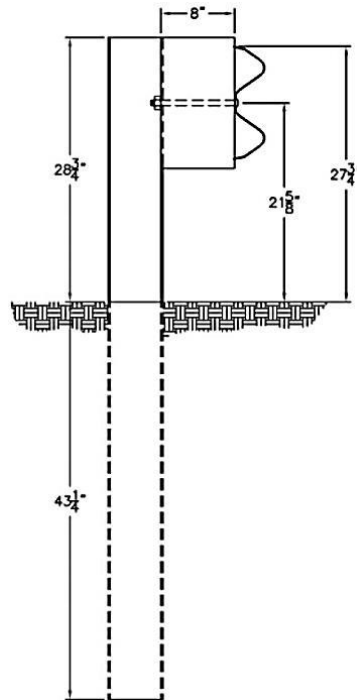
Figure 28. Typical Cross-Section of Modified G4(1S) Guardrail

3.1.1.2 Midwest Guardrail System (MGS)

The second W-beam guardrail system that was considered was the Midwest Guardrail System (MGS) [31]. Due to its taller top rail mounting height and history of improved performance over the modified G4(1S) guardrail system, researchers felt confident that an MGS-based transition system would improve system performance and the likelihood of success.

The MGS utilized A992 Grade 50 W6x9 (W152x13.4) steel posts measuring 72-in. (1,829-mm) long, 12-ft 6-in. (3,810-mm) long 12-gauge (2.66-mm) W-beam rail sections, and 6-in. (152-mm) wide x 12-in. (305-mm) deep x 14¼-in. (362-mm) long wood blockouts to space the rail away from the front face of the steel posts. The top rail height was 31 in. (787 mm) with a 24⅞-in. (632-mm) center mounting height. The MGS used a standard 6-ft 3-in. (1,905-mm) post spacing, and the splice locations were moved

to the center of the span between guardrail posts. A typical cross-section is shown in Figure 29.
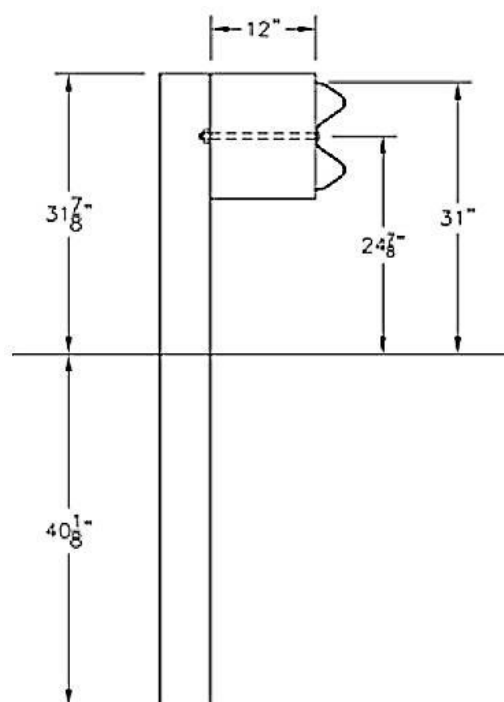
Figure 29. Typical Cross-Section of Midwest Guardrail System (MGS)

3.1.2 F-Shape Portable Concrete Barrier

A 32-in. (813-mm) tall F-shape PCB was chosen for this research study, which is representative of the typical PCBs used by NDOR to create work zones [1,8,13]. Each PCB segment measured 12 ft – 6 in. (3,810 mm) long and utilized a pin and loop barrier-to-barrier connection, as shown in Figure 30. The PCB system was installed at a 15H:1V flare rate, which is a typical flare used by NDOR.
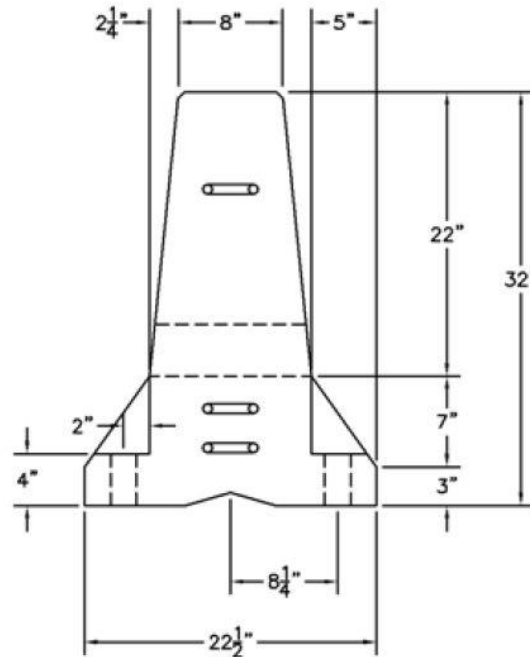
Figure 30. Cross-Section of 32-in. (813-mm) Tall F-Shape PCB [1]

3.2 Design Concepts

Taking into account all of the design considerations, several design concepts were brainstormed and discussed. The top five design concepts were formulated, and drawings were developed and presented to the TAC members for consideration. Following discussion, the concepts were ranked by feasibility, likelihood of success, and ease of installation. The rankings were to provide guidance through concept evaluation and the simulation process. A description of each design concept along with pros and cons are presented below. The TAC members advised that the simplest transition in regards to installation time and number of components was considered a high priority. Therefore, each design concept was presented in its simplest form, and complexity was added as needed based on the simulation results to improve the safety performance of the transition system.

3.2.1 Flared PCB – Modified G4(1S)

The first design concept was comprised of three components: modified G4(1S) guardrail; W-beam end shoe connection; and F-shape PCBs. The modified G4(1S) guardrail attached to a 15H:1V flared F-shape PCB system using a W-beam end shoe connection to the third PCB segment. Three 15H:1V flared PCB segments extended behind the modified G4(1S) guardrail system, and the posts that interfered with the installation of the PCBs were removed, as shown in Figure 31. The two posts that remained in front of the PCB system would aid in the displacement of the PCB system. Upon impact, the remaining two posts would rotate backward into the PCBs and initiate displacement of the PCB system, which may reduce vehicle climb and instabilities. Based on the simulation results, several modifications could be made to the transition system to improve its likelihood of success. These modifications included: a transition to thrie beam; removal of posts in front of PCB system; installation of blockouts between the rail and PCBs; installation of a cantilever beam to the front face of the most upstream PCB; and nesting of rail.

One positive for this design concept considered the use of an existing modified G4(1S) guardrail system without significant changes. It was also highly desirable to attach the modified G4(1S) system directly to a 15H:1V flared PCB system in order to alleviate the need to incorporate PCB segments at different flare rates. However, one downside for this design concept was the presence of a single point connection between the modified G4(1S) and the PCB system using a W-beam end shoe. One potential modification involved the installation of blockouts at standard post spacings to allow for more connection points between the modified G4(1S) system and the PCB system, which
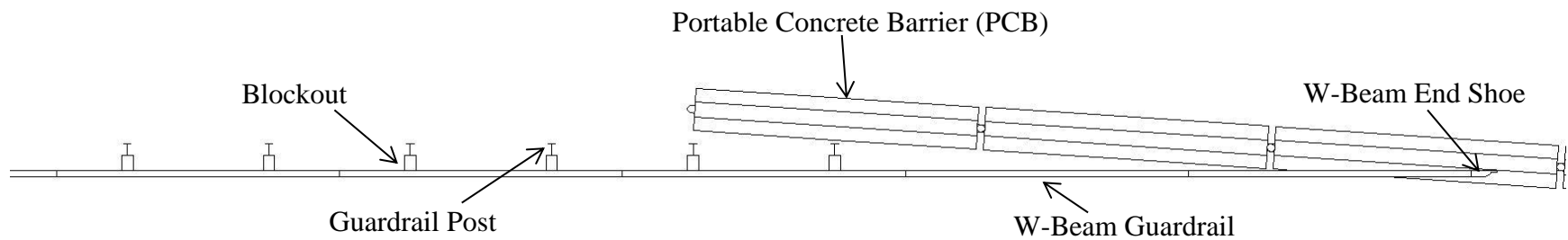
Portable Concrete Barrier (PCB)

Blockout

W-Beam End Shoe

Guardrail Post

W-Beam Guardrail

Notes:
(1) Thrie beam may be utilized in transition area.
(2) Posts installed in front of PCB system may be removed.
(3) May require blockouts between W-beam guardrail and PCBs where post removal was required.
(4) Cantilever beam may be installed on most upstream PCB.
(5) Nesting of rail components may be required.

Figure 31. Flared PCB – Modified G4(1S) Design Concept

should reduce the loading on the W-beam end shoe connection.

3.2.2 PCBs Parallel PCB – Modified G4(1S)

The next design concept utilized three components: modified G4(1S) guardrail; W-beam end shoe connection; and F-shape PCBs. Two PCB segments were placed parallel to and behind the modified G4(1S) guardrail system before the PCB system was flared at 15H:1V to create the work zone, as shown in Figure 32. The modified G4(1S) was attached to the fifth PCB segment using a W-beam end shoe connection. Five posts remained in front of the PCB system, and posts that interfered with the installation of the 15H:1V flared PCBs were removed. The posts that remained in front of the PCB system were expected to rotate backward into the PCBs and initiate displacement of the PCB system. Based on the simulation results, several modifications could be made to the transition system to improve its likelihood of success. These modifications included: a transition to thrie beam; removal of posts in front of PCB system; installation of blockouts between the rail and PCBs; installation of a cantilever beam to the front face of the most upstream PCB; and nesting of rail components.

One concern for this design concept was that placing PCBs segments parallel to and behind the modified G4(1S) may accentuate wheel snag on the end of the PCB system during vehicle impacts upstream from the PCB system. Along with wheel snag, rail pocketing was a concern upstream from the end of the PCB system due to the inertial force required to initiate PCB displacement. Further, the attachment location may vary based on the actual location of the PCB system relative to the guardrail system. An alternative attachment location will alter the distance between the PCB segments placed parallel to and behind the modified G4(1S) system, thus affecting system performance.
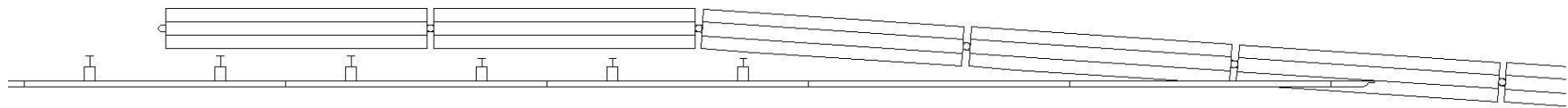
Notes:
(1) Thrie beam may be utilized in transition area.
(2) Posts installed in front of PCB system may be removed.
(3) May require blockouts between W-beam guardrail and PCBs where post removal was required.
(4) Cantilever beam may be installed on most upstream PCB.
(5) Nesting of rail components may be required.

Figure 32. Parallel PCB − Modified G4(1S) Design Concept

One positive for this design concept considered use of an existing modified G4(1S) W-beam guardrail system without significant changes.

3.2.3 Beam Attachment Between PCB and Modified G4(1S)

The third design concept utilized four components: modified G4(1S) guardrail; W-beam end shoe connection; F-shape PCBs; and either a box beam or horizontal post. This design concept explored the use of an end-to-end connection between the two systems. In order to encourage the two systems to displace together, the systems would be connected to one another. This behavior would be achieved by attaching a box beam rail to the backside of the most upstream PCB and extending it to the backside of the most downstream guardrail post. Alternatively, a horizontal post could be attached to the backside of the most upstream PCB and extending it to the web of the most downstream guardrail post. Both designs are shown in Figure 33.

Researchers also took note of the high probability for wheel snag on the upstream end of the PCB system, which could accentuate vehicle instabilities and elevated occupant risk values. Researchers decided that the best way to mitigate wheel snag concerns would be to design and fabricate a special chamfered-end, PCB segment, as shown in Figure 34. Based on the simulation results, several modifications could be made to the transition system to improve its likelihood of success. These modifications included: a transition to thrie beam; nesting of the rail components; and installation of a chamfered-end PCB segment. Note that this design does not incorporate the 15H:1V flare rate, often used to create a work zone. However, it was decided that the PCB system could run parallel to the modified G4(1S) guardrail system for a distance and then transition to the 15H:1V flared PCB system.
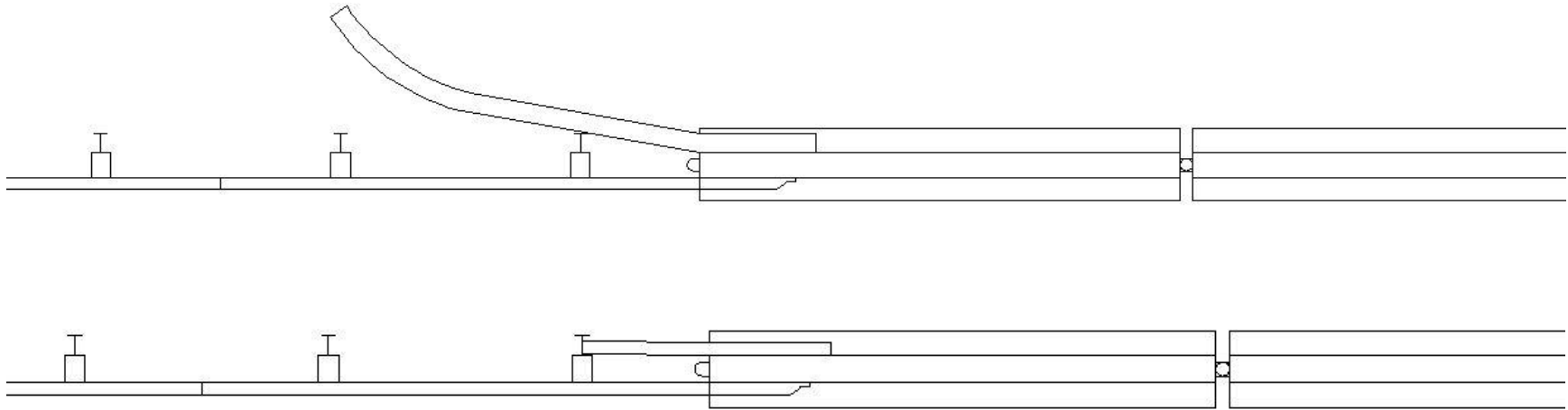
Notes:

(1) Thrie beam may be utilized in transition area.

(2) Nesting of rail sections may be required.

(3) May require a special chamfered PCB section in order to prevent wheel snag on upstream end of PCB system.

Figure 33. Beam Attachment Between PCB and Modified G4(1S) Design Concept

Figure 34. Chamfered End PCB Segment

One concern associated with this design concept was the cost associated with designing and fabricating a special chamfered-end PCB segment. Similar to the previous design concept, the attachment location may vary based on the actual location of the PCB system relative to the guardrail system, which may affect performance. One positive for this design concept was that it would likely be the shortest system and easiest to install for all of the transition design concepts. It also includes the existing modified G4(1S) guardrail system with no significant modifications which reduces the complexity of the transition design.

3.2.4 PCB Offset From Modified G4(1S)

The fourth design concept utilized three components: modified G4(1S) guardrail; W-beam end shoe connection; and F-shape PCBs. This design concept is similar to the Parallel PCB − Modified G4(1S) design concept. In this design concept, the PCB segments located behind the modified G4(1S) guardrail are installed to replace the guardrail posts that would be installed in front of the PCB system. The PCB segments are installed behind the modified G4(1S) guardrail system and blocked away from the rail using spacers at locations where guardrail posts were removed. This design concept is shown in Figure 35. The primary reasoning behind guardrail post removal and blockout installation was to allow for the blockouts to initiate PCB displacement and provide a smooth transition in lateral stiffness from the modified G4(1S) to the PCBs. The blockout depths would remain 8 in. (203 mm) with a slight taper to fit the sloped face of the F-shape PCBs. Since the PCBs would be installed to replace the guardrail posts and would be blocked away from the guardrail, the attachment to the PCB system would be different than the previous design concepts. The rail would need to taper back toward the face of the PCB system over one rail section, and smaller tapered blockouts would be required in
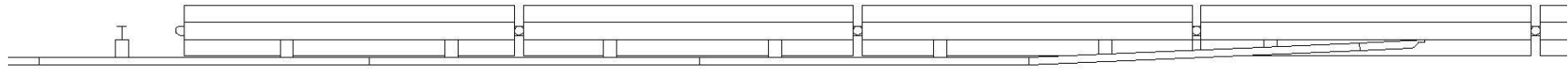
Notes:
(1) Thrie beam may be utilized in transition area.
(2) Cantilever beam may be installed on most upstream PCB.
(3) Nesting of rail components may be required.
(4) May require a special chamfered PCB section in order to prevent wheel snag on upstream end of PCB system.

Figure 35. PCB Offset from Modified G4(1S) Design Concept

the attachment area. Based on the simulation results, several modifications could be made to the transition system to improve its likelihood of success. These modifications included: a transition to thrie beam; installation of a cantilever beam off of the most upstream PCB segment; nesting of rail components; or installation of a special chamfered-end, PCB segment. Note that this design does not incorporate a 15H:1V flare that is often used to create a work zone. However, it was decided that the PCB system could run parallel to and behind the modified G4(1S) guardrail system for a distance and then transition to the 15H:1V flared PCB system.

One concern associated with this design concept was the potential for wheel snag on the upstream end of the PCB system, which may require the use of a special chamfered-end, PCB segment. The cost associated with the design and fabrication of a chamfered-end PCB segment also made this design concept less desirable. Also, similar to previous design concepts, the attachment location may vary based on the actual location of the PCB system relative to the guardrail system, which may affect performance. One positive for this design concept is that it would use standard 8-in. (203-mm) deep blockouts instead of oversized blockouts, which may be required to attach W-beam to flared PCB segments. It also includes the existing modified G4(1S) guardrail system with no significant changes, which reduces the complexity of the transition design.

3.2.5 Stiffened PCB and Modified G4(1S)

The final design concept utilized three components: modified G4(1S) guardrail; W-beam end shoe connection; and F-shape PCBs. The approach for this design concept was to stiffen the area where the two systems attached to each other, thus forcing the

systems to deflect together and eliminating the need to match deflection behaviors. In order to increase the stiffness of the modified G4(1S) system, guardrail posts would be installed at 37½ in. (953 mm) or at half-post spacings leading up to the PCB attachment location. In addition, either pins or tie-downs would be installed in the PCBs to limit the deflections. If the PCB system were installed on a compacted crushed limestone base, guardrail posts could be driven behind the PCB system to accomplish the same goal, which is shown in Figure 36. As the PCB system progressed downstream, the PCBs would be transitioned to a free-standing system at a 15H:1V flare by variable placement of either the driven guardrail posts or the pins or tie-downs. Upstream, the modified G4(1S) guardrail system would be transitioned from 37½ in. (953 mm) half-post spacing to 75 in. (1905 mm) full or standard post spacing. Based on the simulation results, several modifications could be made to the transition system to improve its likelihood of success. These modifications included: a transition to thrie beam and nesting of rail components.

One concern associated with this design concept was the installation of new posts, which would increase system cost and make this concept less desirable. Also, a stiffened transition could potentially have adverse effects on the vehicle stability and occupant risk values. One positive for this design concept was that it does not require fabrication of new components, such as a cantilever beam or the chamfered-end PCB segment. Pocketing would not likely be a concern due to its increased lateral stiffness.
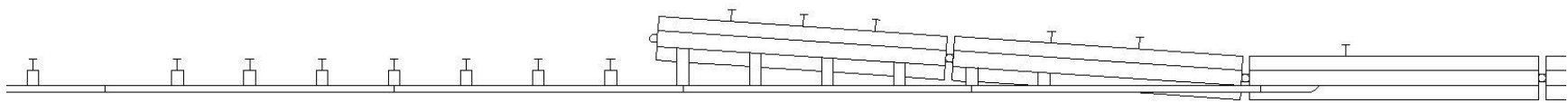
Notes:
(1) Thrie beam may be utilized in transition area.
(2) Nesting of rail components may be required.
(3) May require tie-downs or pins through toe of PCBs.

Figure 36. Stiffened PCB and Modified G4(1S) Design Concept

3.3 Design Concept Summary

Once all of the design concepts were presented to the Nebraska TAC members, the pros and cons for each design concept were discussed and weighed. The TAC members determined that the use of the modified G4(1S) guardrail was preferred. However, a transition to thrie beam would be feasible and would not require extensive time or effort to install. Thus, design concepts that utilize a transition to thrie beam may be considered. The fabrication of a cantilever beam was also determined to be favorable based on the idea that the safety improvements would outweigh the cost of fabrication. However, the design and fabrication of a chamfered-end PCB segment would be far too extensive and expensive. Thus, design concepts that would potentially use it were deemed less desirable. The installation of new guardrail posts and pinning or anchoring PCB segments would require significant time and extra equipment. These design concepts were also deemed less desirable. Based on the feasibility, likelihood of success, ease of installation and component fabrication, all design concepts were ranked and simulated in this order:

(1) Flared PCB − Modified G4(1S);

(2) Parallel PCB − Modified G4(1S);

(3) Beam Attachment Between PCB and Modified G4(1S);

(4) PCB Offset From Modified G4(1S); and

(5) Stiffened PCB and Modified G4(1S).

Due to project constraints, only the first two design concepts were simulated in the initial investigation.

CHAPTER 4 TEST CONDITIONS AND EVALUATION CRITERIA

4.1 MASH TL-3 Simulated Test Conditions

Transition systems must satisfy impact safety standards defined in MASH in order to be accepted by the Federal Highway Administration (FHWA) for use on the roadside. According to TL-3 of MASH, longitudinal barriers must be impacted at a nominal speed and angle of 62.1 mph (100 km/hr) and 25 degrees, respectively. Therefore, each candidate design was subjected to simulated impacts according to these parameters and at several impact locations ranging from the connection point between the guardrail and the PCB system to four posts upstream of the PCB system. The design concepts were simulated using LS-DYNA. Each simulation was subjected to a MASH TL-3 impact scenario, and metrics were extracted, compiled, and compared.

4.2 Evaluation Criteria

It was necessary to determine evaluation criteria for which to properly analyze and rank the concepts as well as determine the likelihood of success. The evaluation criteria included vehicle behavior, occupant risk, and rail pocketing, which are described in greater detail below.

4.2.1 Vehicle Behavior

Vehicle behavior is examined to evaluate the potential for safe vehicle containment and redirection without excessive roll or complete rollover. The transition system should capture and smoothly redirect the vehicle. Also, the vehicle should not penetrate, underride, or override the transition system, while remaining upright during and after the impact event. Vehicle behavior was evaluated after calculating of several parameters, including maximum roll, pitch, and yaw angles. According to MASH, the maximum roll and pitch angles are not to exceed 75 degrees [5]. It was also determined

that wheel snag on the upstream end of the PCB system could affect vehicle behavior and cause rapid deceleration, so it was documented for each simulation.

4.2.2 Occupant Risk

Occupant risk evaluates the degree of hazard to occupants in the impacting vehicle. In order to quantify this hazard, maximum longitudinal and lateral occupant impact velocities (OIVs) as well as maximum longitudinal and lateral occupant ridedown accelerations (ORAs) were calculated for each simulation. According to MASH, longitudinal and lateral OIVs should fall below the maximum allowable value of 40.0 ft/s (12.2 m/s). MASH also states that longitudinal and lateral ORAs should fall below the maximum allowable value of 20.49 g's [5]. Occupant compartment damage was not measured in this study. To date, there has been no extensive validation efforts that have focused on the occupant compartment of the Chevrolet Silverado pickup model.

4.2.3 Pocketing Angle

Maximum pocketing angles are a primary concern for the transition design due to the relatively high initial deflection of the guardrail system and the relatively low initial deflection of the PCB system. Excessive pocketing angles can affect a system's capability to safely contain, and redirect a test vehicle without rupture of the rail components. The maximum pocketing angle for each simulation was calculated by tracking adjacent nodes on the rail to determine barrier deflections as well as to calculate maximum slopes in advance of the vehicle. The maximum pocketing angle should fall below 23 degrees, which has previously been shown to be associated with degraded barrier performance, including rail rupture [22].

CHAPTER 5 FINITE ELEMENT BARRIER AND VEHICLE MODELS

5.1 Introduction

Finite element modeling is a very robust tool that is used to evaluate roadside safety hardware. Accurate finite element modeling can be used to preliminarily evaluate potential design concepts prior to conducting expensive full-scale vehicle crash testing. Four finite element models were used in order to evaluate potential design concepts for the transition between W-beam guardrail and PCBs. A previously-developed MGS model [32] was used to configure several design concepts. The MGS model was altered to configure a model of the modified G4(1S) guardrail system. A previously-developed F-shape PCB model [1] was used to configure both tangent and 15H:1V flared PCBs within a work-zone environment. A Chevrolet Silverado vehicle model was chosen to be representative of 2270P pickup truck test vehicles.

5.2 Midwest Guardrail System (MGS) Model

A second generation MGS LS-DYNA model was developed by researchers at MwRSF. Goals of the new model were to: (i) improve end anchorage design to better match full-scale system construction and results; (ii) refine system mesh for improved barrier deflection performance; and (iii) improve vehicle-to-barrier interaction and results. The second generation model has been shown to improve model performance in simulating full-scale vehicle crash tests [32]. A list of MGS model parts and associated LS-DYNA modeling parameters are shown in Table 4. A comparison between the actual and finite element model end anchorage and full MGS system is shown in Figures 37 and 38, respectively.

Table 4. Summary of MGS Model Parts and LS-DYNA Parameters [32]

Part Name	Element Type	Element Formulation	Material Type	Material Formulation
Anchor Cable	Beam	Belytschko-Schwer, Resultant Beam	6x19 3/4" Wire Rope	Moment, Curvature Beam
Anchor Post Bolt	Solid	Constant Stress Solid Element	ASTM A307	Rigid
Anchor Post Bolt Heads	Shell	Belytschko-Tsay	ASTM A307	Rigid
Anchor Post Washers	Solid	Constant Stress Solid Element	ASTM F844	Rigid
BCT Anchor Post	Solid	Fully Integrated, S/R	Wood	Plastic Kinematic
Bearing Plate	Solid	Constant Stress Solid Element	ASTM A36	Rigid
Blockout	Solid	Fully Integrated, S/R	Wood	Elastic
Blockout Bolts	Shell	Belytschko-Tsay	ASTM A307	Rigid
Bolt Springs	Discrete	DRO=Translational Spring/Damper	ASTM A307	Spring, Non-Linear Elastic
Ground-Line Strut	Shell	Belytschko-Tsay	ASTM A36	Piecewise, Linear Plastic
Post Soil Tubes	Shell	Belytschko-Tsay	Equivalent Soil	Rigid
Soil Springs	Discrete	DRO=Translational Spring/Damper	Equivalent Soil	Spring, General Non-Linear
W-Beam Guardrail Section	Shell	Fully Integrated, Shell Element	AASHTO M180, 12-Ga. Galvanized Steel	Piecewise, Linear Plastic
W6x9 Post	Shell	Fully Integrated, Shell Element	ASTM A992 Gr. 50	Piecewise, Linear Plastic

(a)
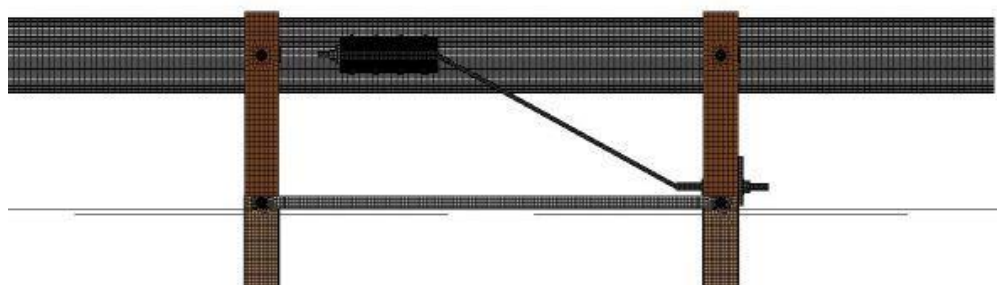
(b)

Figure 37. MGS End Anchorage (a) Actual (b) Finite Element Model

(a)
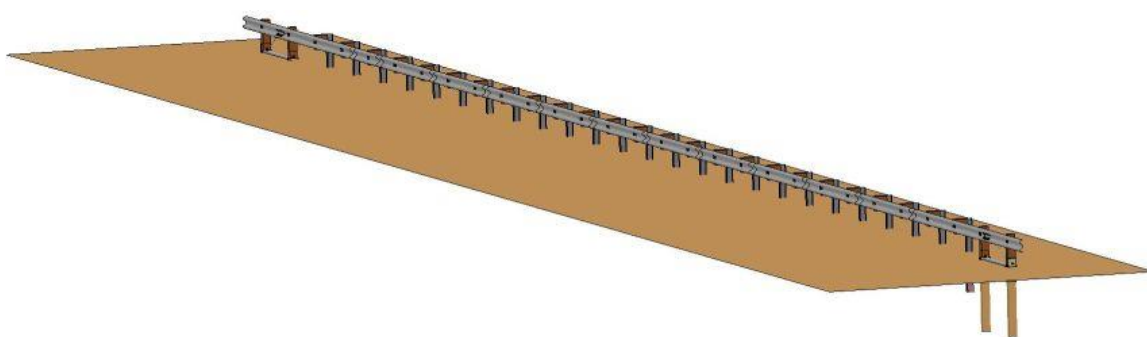
(b)

Figure 38. MGS Full System (a) Actual (b) Finite Element Model

5.3 Modified G4(1S) Guardrail Model

The 31-in. (787-mm) tall MGS model was modified in several ways to represent

the modified G4(1S) guardrail system with nominal top rail height of 27¾ in. (705 mm)

and 8-in. (203-mm) deep blockouts. This alteration process was accomplished in several

steps, as described below:

1. Translating the W6x9 (W152x13.4) guardrail line posts 3¼ in. (83 mm) vertically in order to increase the post embedment depth from 40 in. (1,016 mm) to 43¼ in. (1,099);

2. Translating the corrugated rail and mounting hardware 3¼ in. (83 mm) vertically to align with the new height of the W6x9 (152x13.4) guardrail line posts;

3. Scaling the wood blockouts, guardrail bolts, and guardrail bolt hole nulls in order to decrease the blockout depth from 12 in. (305 mm) to 8 in. (203 mm);

4. Translating the corrugated rail and mounting hardware 4 in. (102 mm) to align the decreased depth blockouts with the front face of the W6x9 (W152x13.4) guardrail line posts;

5. Scaling BCT anchor post elements between rail mounting hole and groundline hole vertically in order to decrease the BCT anchor post height 3¼ in. (83 mm) in order to align mounting holes with the rail; and

6. Re-drawing and re-meshing the upstream anchor cable to align with the new rail height and groundline mounting locations.

These steps were followed in order to decrease the top rail height from 31 in. (787 mm)

to 27¾ in. (705 mm) and decrease the blockout depth from 12 in. (305 mm) to 8 in. (203

mm), as shown in Figures 39 and 40, respectively.
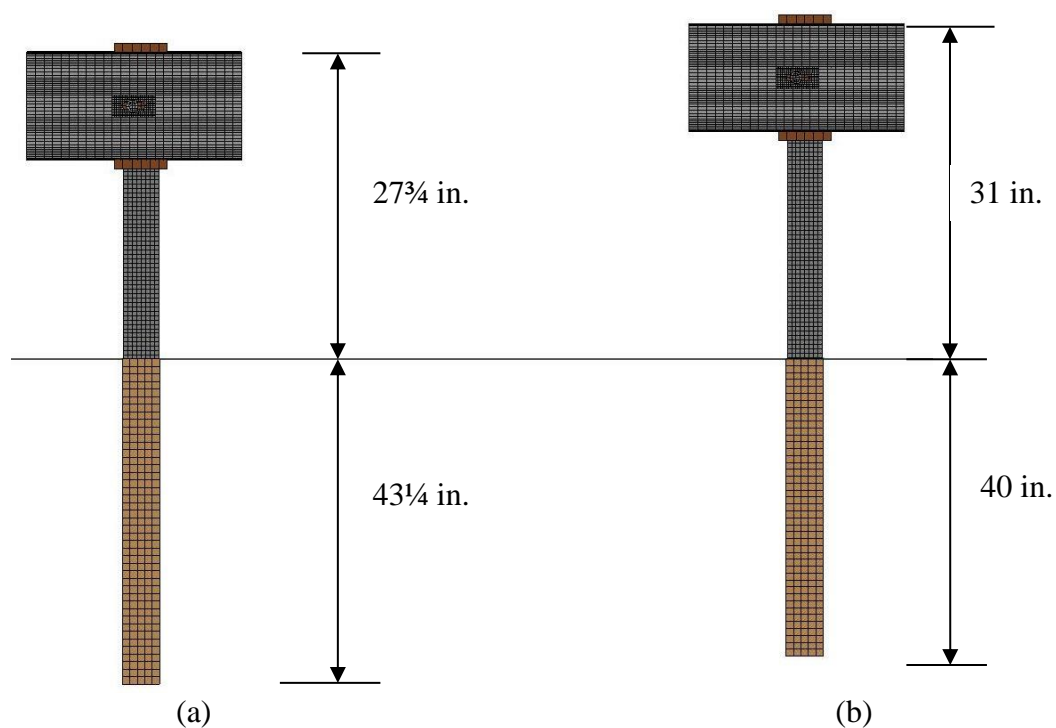
Figure 39. Top Rail Height and Embedment Depth Comparison for (a) Modified G4(1S) Guardrail and (b) Midwest Guardrail System
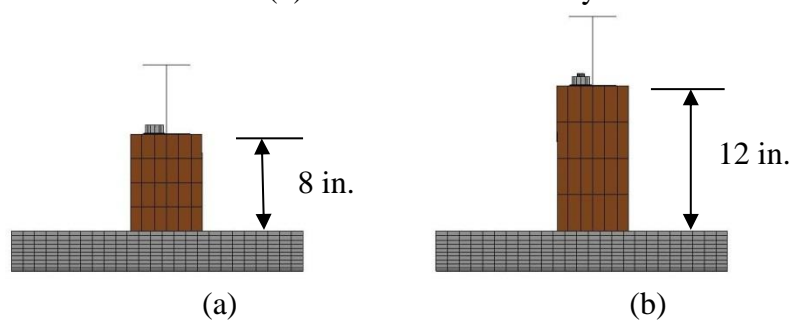
Figure 40. Blockout Depth Comparison for (a) Modified G4(1S) Guardrail and (b) Midwest Guardrail System

5.3.1 Downstream Anchorage Removal

A typical guardrail system requires anchorage on both its upstream and downstream ends in order to provide adequate rail tension. However, for this research, the downstream end of the guardrail system will be transitioned to a PCB system. Therefore, removal of the downstream anchorage was necessary, which required removal of several components: downstream BCT posts; BCT anchor tubes; groundline strut and

yoke; anchor cable; attachment hardware; and end section of W-beam guardrail. The modified G4(1S) guardrail system with downstream anchorage removed is shown in Figure 41.
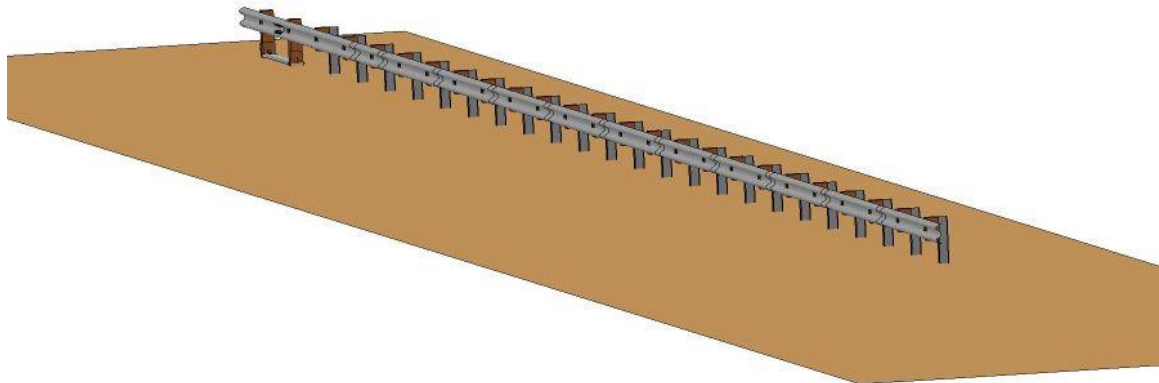
Figure 41. Modified G4(1S)Guardrail System with Downstream Anchorage Removed

5.4 F-Shape PCB Model

A modified F-shape PCB model was developed by researchers at MwRSF. The PCB model required minor modifications to the previously-developed model. First, the original model used solid elements with rigid material definition to represent the F-shape PCB. This approach was originally taken because the proper mass properties and geometry of the barrier was captured. However, the use of solid elements does not provide a robust contact surface when used with shell elements of the existing 2270P pickup model. Therefore, a modified F-shape PCB model was created using shell elements with a rigid material definition. The rigid material definition allowed the proper mass and rotational inertias to be defined for the barrier even though it was essentially hollow. The use of the shell elements improved the overall contact behavior between the barrier and the vehicle. In addition, the use of shell elements made it easier to fillet the corners and edges of the barrier. By rounding off the barrier edges, edge contacts and penetrations were reduced, thus further improving the contact interface. The geometry of

the barrier was also modified to include holes in the face of the barrier for use with driven steel pins in asphalt. The loops in the barrier model were also modified to match the current configuration, which consisted of two sets of three rebar loops. The modified F-shape PCB model was validated using previous F-shape PCB testing [1]. A list of F-shape PCB model parts and associated LS-DYNA modeling parameters are shown in Table 5. A comparison between the actual and finite element model F-shape PCB is shown in Figure 42.

Table 5. Summary of F-Shape PCB Model Parts and LS-DYNA Parameters

Part Name	Element Type	Element Formulation	Material Type	Material Formulation
Barrier Loops	Solid	Fully Integrated, S/R	ASTM A706	Rigid
Connection Pins	Solid	Fully Integrated, S/R	ASTM A36	Piecewise, Linear Plastic
Connection Pin Plate	Shell	Belytschko-Tsay	ASTM A36	Piecewise, Linear Plastic
F-Shape PCB	Shell	Belytschko-Tsay	Concrete	Rigid

(a)
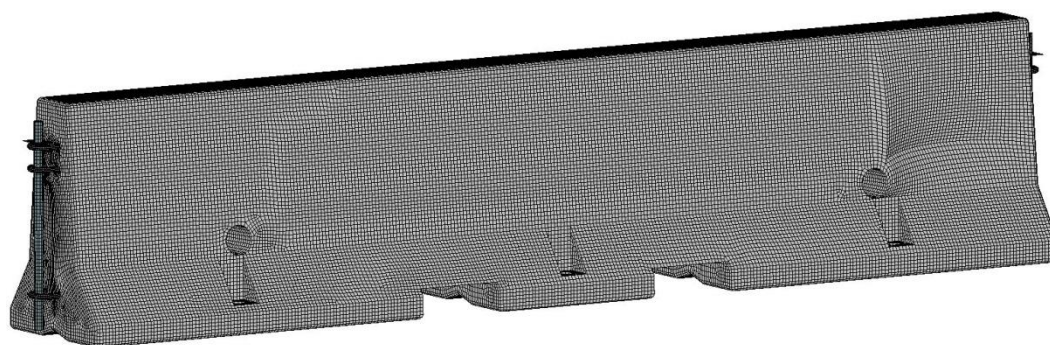
(b)

Figure 42. F-Shape PCB (a) Actual (b) Finite Element Model

5.4.1 F-Shape PCB Rotation

In order to create a safe and usable work zone, an F-shape PCB system is often installed with a 15H:1V flare relative to the roadway. When creating a transition between guardrail and F-shape PCBs, it was necessary to rotate the PCB model 3.81 degrees relative to the guardrail system. The rotated PCB model is shown in Figure 43.
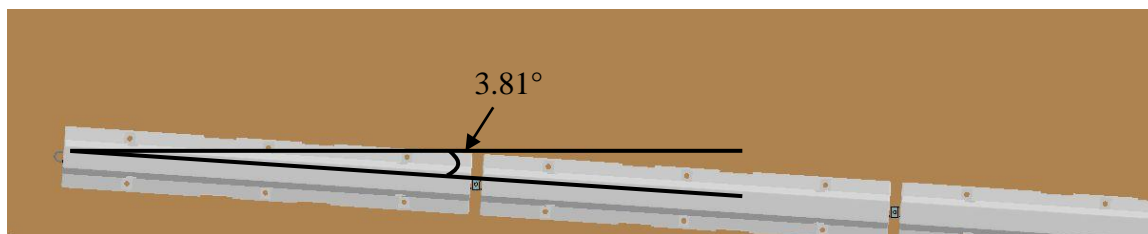
Figure 43. Rotated F-Shape PCB Model

5.5 Chevrolet Silverado Vehicle Model

The Chevrolet Silverado vehicle model was chosen for the research and simulation study. MASH denotes that a TL-3 longitudinal barrier must be subjected to impacts with the 2270P pickup truck and the 1100C small car. However, the 2270P test vehicle was deemed more critical than the 1100C small car due the likelihood of increased barrier deflections, rail and anchor loads, rail pocketing, and wheel snag. Further, vehicle instabilities have been exhibited during full-scale crash tests involving 2270P pickup trucks with F-shape PCB systems due to vehicle climb. The Silverado vehicle model was originally created by the National Crash Analysis Center (NCAC) and later modified by MwRSF personnel for use in roadside safety applications. The Chevrolet Silverado vehicle model is shown in Figure 44.

Figure 44. Chevrolet Silverado Vehicle Model

CHAPTER 6 BASELINE SIMULATION – MODIFIED G4(1S) GUARDRAIL ACROSS PCBs

6.1 Introduction

A baseline study was conducted in order to better understand the inherent risks associated with a barrier installation without using a proper transition from guardrail to PCBs. The baseline model consisted of the modified G4(1S) guardrail system with a minimum overlap in front of the 15H:1V flared PCB system without system-to-system connection to provide continuity. The simulation study consisted of impacts at the final six post locations in the modified G4(1S) guardrail system, as depicted in Figure 45.
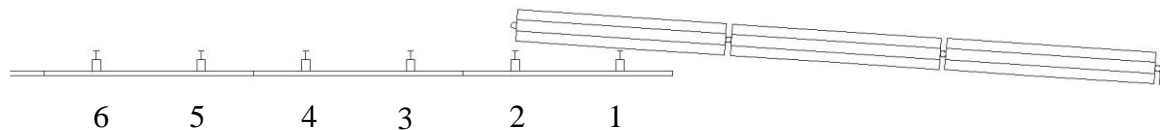
Figure 45. Baseline Simulation – Impact Locations

6.2 Vehicle Behavior

Based on the simulation results, it was found that satisfactory vehicle behavior was a very large concern for the baseline system. The vehicle behavior results and evaluation criteria for all six impact locations are found in Table 6. Generally, W-beam guardrail systems have anchorage on both the upstream and downstream ends of the system to develop rail tension, which enables the system to capture and redirect the vehicle. The lack of downstream anchorage in this system allowed the rail components to disengage away from the posts very early in the impact event, which diminished any capability to capture and redirect the vehicle. This early rail disengagement allowed the vehicle to penetrate and override the modified G4(1S) guardrail system. As the vehicle overrode the guardrail system, it engaged several guardrail posts prior to and during impact with the PCB system. The combination of vehicle impact with guardrail posts and

an unanchored upstream end of the PCB system caused severe vehicle instabilities. The roll values exceeded the MASH limits for impact location nos. 1-3, as shown in Table 6. The concern for vehicle rollover as well as wheel snag on PCBs demonstrated that an overlay of modified G4(1S) across PCBs without system-to-system connection was inadequate.

Table 6. Vehicle Behavior Results – Baseline System

Impact Location	Roll	Pitch	Yaw	Wheel Snag on PCBs?
1	90.9°[1]	23.9°	45.8°	No
2	106.4°[1]	42.7°[1]	47.0°	No
3	87.8°[1]	27.0°[1]	53.7°	No
4	16.6°	27.7°[1]	90.1°[1]	Yes
5	16.2°[1]	10.9°	8.9°	Yes
6	16.6°[1]	6.9°	15.2°[1]	Yes
MASH Limits	< 75°	< 75°	N/A	N/A

[1]Maximum value was not reached prior to conclusion of simulation
*Yellow cells denote values within 20% of MASH or recommended limits
*Red cells denote values that exceed MASH or recommended limits

6.3 Occupant Risk

The lack of rail tension diminished the capability for the modified G4(1S) guardrail to capture and redirect the vehicle. For impact locations upstream from the end of the PCB system, the vehicle contacted the upstream end of the PCB system. This end-on impact scenario caused elevated occupant risk values for impact location nos. 4 to 6. The vehicle snag on the upstream end of the PCB system resulted in rapid decelerations.

The rapid deceleration exposed potential occupants to longitudinal ORAs that exceeded the MASH limits for impact location nos. 4 to 6, as shown in Table 7.

Table 7. Occupant Risk Results – Baseline System

Impact Location	OIV ft/s (m/s)		ORA g's	
	Longitudinal	Lateral	Longitudinal	Lateral
1	-14.53 (-4.43)	-19.42 (-5.92)	-13.29	-11.87
2	-20.08 (-6.12)	-19.49 (-5.94)	-10.85	-15.75
3	-28.18 (-8.59)	-15.19 (-4.63)	-13.58	-14.38
4	-38.68 (-11.79)	-12.80 (-3.90)	-46.12	15.10
5	-13.85 (-4.22)	-8.79 (-2.68)	-81.87	17.27
6	-15.81 (-4.82)	-9.81 (-2.99)	-21.35	6.86
MASH Limits	≤ 40 (12.2)	≤ 40 (12.2)	≤ 20.49	≤ 20.49

*Yellow cells denote values within 20% of MASH or recommended limits
*Red cells denote values that exceed MASH or recommended limits

The sequentials, as shown in Figures 46 and 47, show the impact event associated with impact location no. 5. At 100 ms, the guardrail had disengaged from the line posts. By 300 ms, the vehicle had overridden the guardrail system and impacted the upstream end of the PCB system. The impact with the end of the PCB caused an abrupt vehicle deceleration which, led to a longitudinal ORA of -81.87 g's. Similar end-on impact behavior was seen at location nos. 4 and 6, which also had longitudinal ORAs exceeding the MASH limit. These ORA results indicated that the baseline system would likely fail the MASH occupant risk criteria if subjected to actual crash testing.

0 ms

100 ms

200 ms

300 ms

400 ms
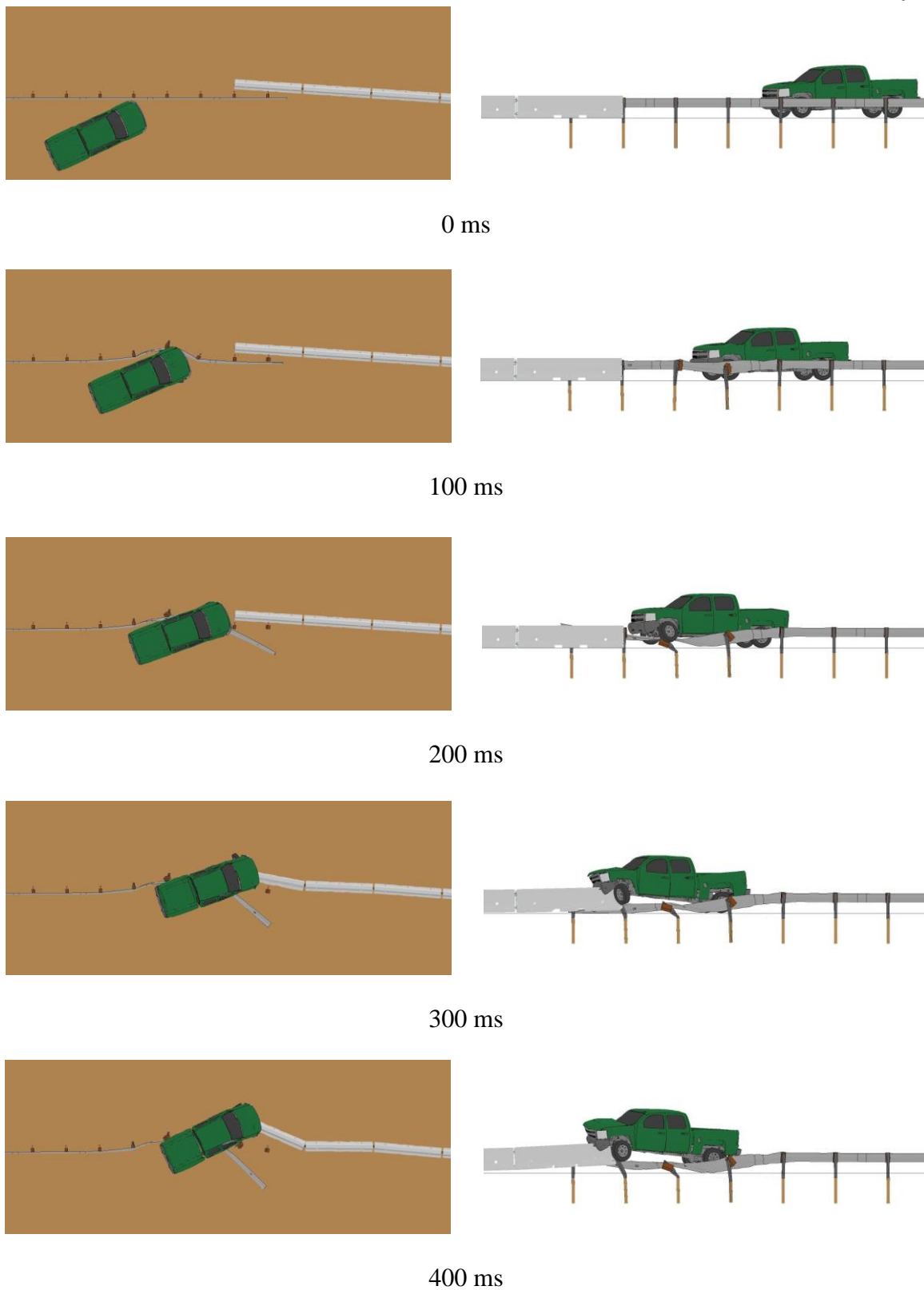
Figure 46. Baseline System Sequentials, Impact Location No. 5

500 ms

600 ms
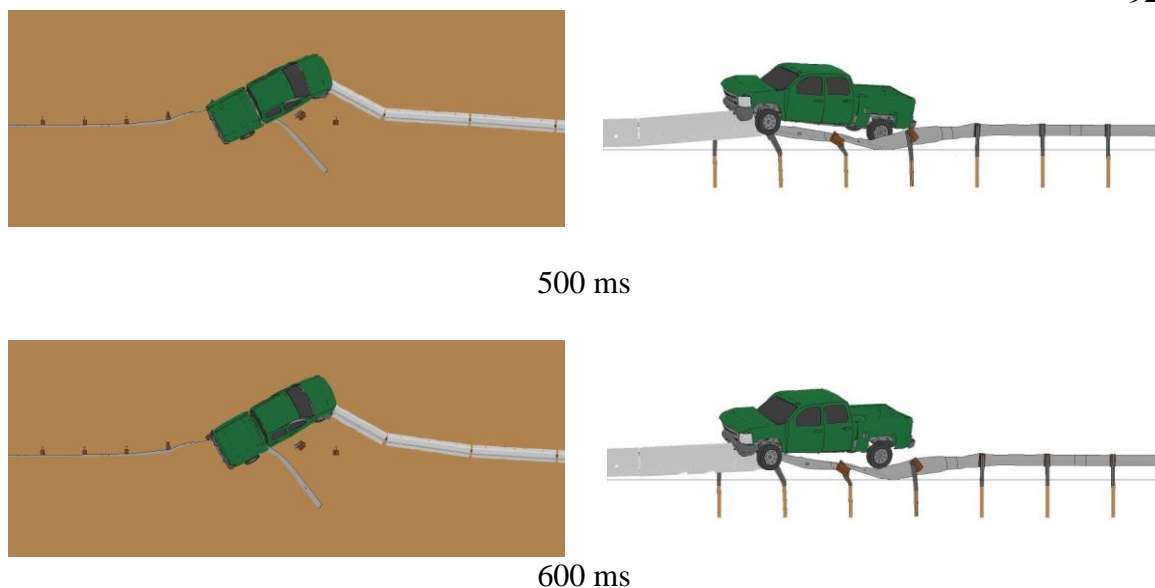
Figure 47. Baseline System Sequentials, Impact Location No. 5 (cont.)

6.4 Pocketing Angle

Due to the fact that there was no system-to-system connection between the modified G4(1S) guardrail system and the PCBs, pocketing angles could not be measured and evaluated.

6.5 Discussion

Upon full investigation of the simulation results, it was determined that a proper stiffness transition was required between the two barrier systems. Due to the lack of downstream anchorage for the modified G4(1S) guardrail system, there was inadequate rail tension to capture and redirect the vehicle. The lack of rail tension led to early disengagement away from the downstream guardrail posts as well as vehicle penetration into the barrier system and an end-on impact with the upstream end of the PCB system. The next step was to provide the increased rail tension in the modified G4(1S) guardrail by implementing a system-to-system connection using a W-beam end shoe.

.

CHAPTER 7 MODIFIED G4(1S) END SHOE

7.1 Introduction

Based on the results from the baseline system, downstream anchorage of the modified G4(1S) guardrail was required in order to provide adequate tension in the rail. Thus, the guardrail was extended and connected to the PCB system using a W-beam end shoe, as shown in Figure 48. The modified G4(1S) end shoe configuration was simulated and evaluated at the same six impact locations used for the baseline model.
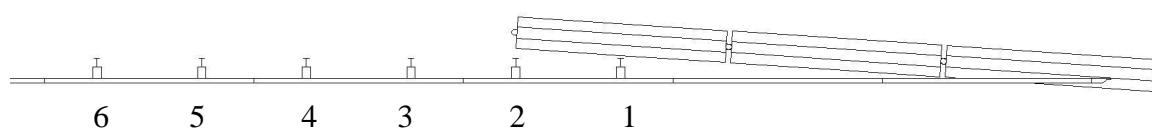
Figure 48. Modified G4(1S) End Shoe – Impact Locations

7.2 Model Modifications

Three additional components were required in order to attach the modified G4(1S) guardrail system to the PCB system: two 12-ft 6-in. (3,810-mm) long 12-gauge (2.66-mm) W-beam sections and a 30-in. (762-mm) long, 12-gauge (2.66-mm) W-beam end shoe, as shown in Figure 49. The two W-beam guardrail sections were attached to the downstream end of the existing guardrail system. Then, the W-beam end shoe was used to attach the W-beam guardrail system to the third PCB segment.
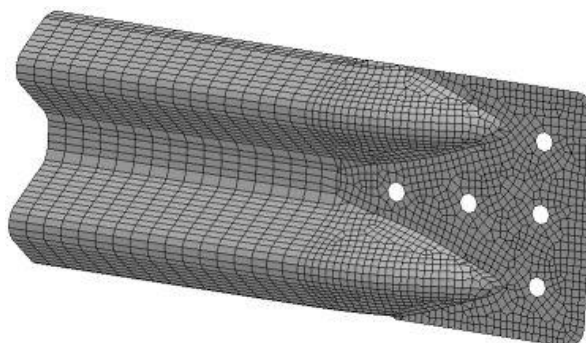
Figure 49. W-Beam End Shoe

An actual W-beam end shoe could likely be bolted directly to the face of the F-shape PCB segment with very little trouble. However, due to the sloped face of the F-shape PCB in combination with limitations in modeling capabilities, a small attachment wedge rigidly attached the W-beam end shoe to the PCB segment, as shown in Figure 50. The attachment wedge was constructed of the same rigid concrete material as the PCBs in order to mimic, as closely as possible, a real W-beam end shoe attachment.
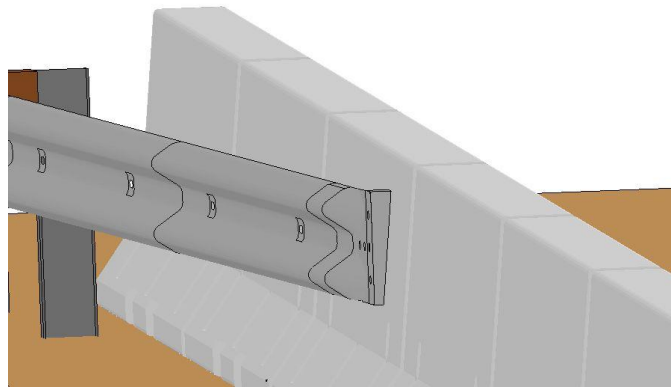
Figure 50. W-Beam End Shoe Attachment with Wedge

7.3 Vehicle Behavior

The vehicle behavior results and evaluation criteria for the six impact locations were compiled and analyzed for the modified G4(1S) end shoe configuration, as shown in Table 8. It can be seen that the maximum roll angle exceeded the MASH limit at impact location nos. 1, 3, and 6. Wheel snag on the upstream end of the PCB system was a concern at impact location no. 4. However, the W-beam end shoe connection restored rail tension, which allowed the vehicle to be successfully captured at all six impact locations.

Table 8. Vehicle Behavior Results – Modified G4(1S) End Shoe

Impact Location	Roll	Pitch	Yaw	Wheel Snag on PCBs?
1	78.4°[1]	21.8°[1]	37.5°	No
2	49.9°[1]	19.5°[1]	41.6°[1]	No
3	81.5°[1]	29.8°[1]	35.6°	No
4	47.6°[1]	24.6°[1]	41.2°	Yes
5	30.5°	8.1°	23.6°	No
6	133.6°[1]	32.6°	44.2°	No
MASH Limits	$< 75°$	$< 75°$	N/A	N/A

[1]Maximum value was not reached prior to conclusion of simulation
*Yellow cells denote values within 20% of MASH or recommended limits
*Red cells denote values that exceed MASH or recommended limits

Upon investigation of the results, the primary cause for elevated roll angles corresponded with the guardrail posts installed in front of the PCB system. The guardrail posts installed in front of the PCB system rotated into the PCBs, which initiated PCB displacement, as predicted. However, these posts wedged against the face of the PCBs and allowed the vehicle to climb up and above the modified G4(1S) guardrail system, as shown in the sequentials for impact location no. 4 in Figures 51 and 52. At 200 ms, the vehicle had run over the weak axis of post no. 2. At 300 ms, the vehicle had ridden up post no. 1 that was wedged against the PCB system. By 400 ms, the vehicle had become airborne and started to roll toward the PCB system.

Vehicle climb was exhibited in the simulations at all six impact locations. Post wedging was the cause of some of the vehicle climb, but the low top rail height of the modified G4(1S) guardrail system was also a concern. A higher top rail height would likely provide a more stable vehicle capture and redirection.

0 ms
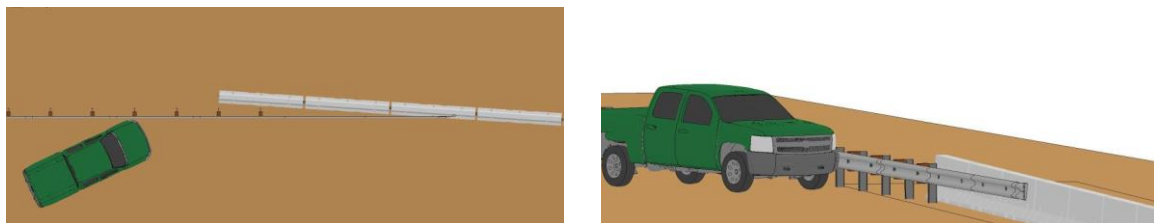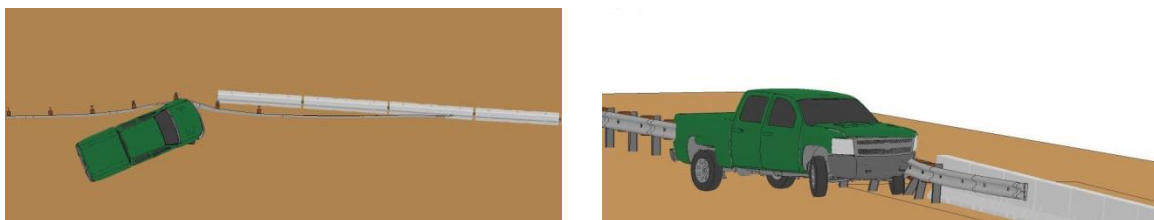
100 ms
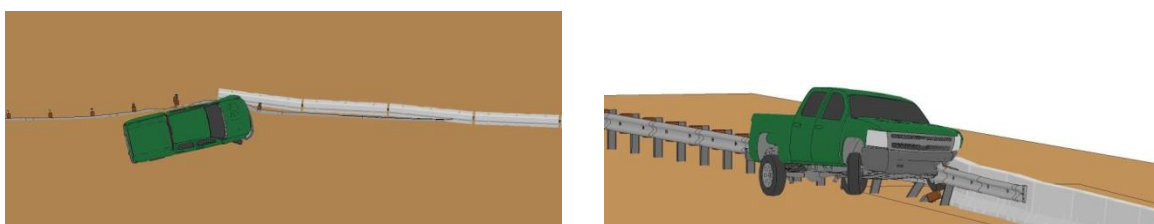
200 ms
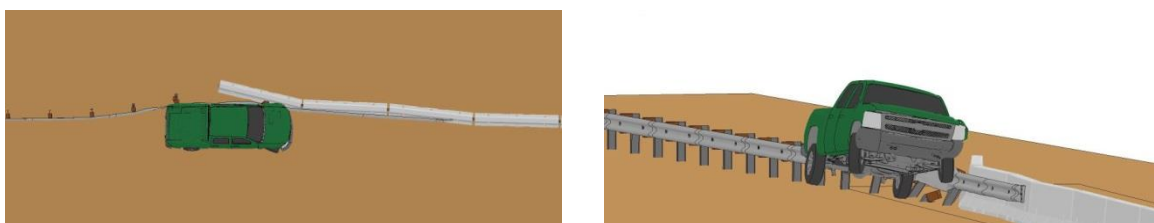
300 ms
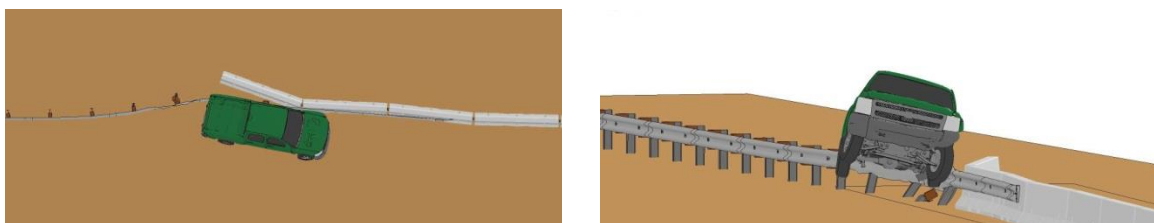
400 ms
Figure 51. Modified G4(1S) End Shoe Sequentials, Impact Location No. 4
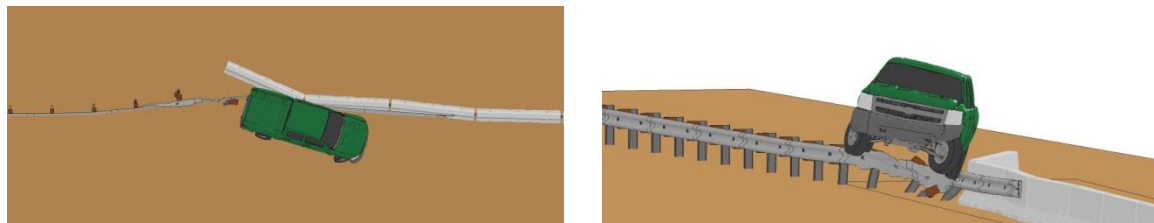
500 ms
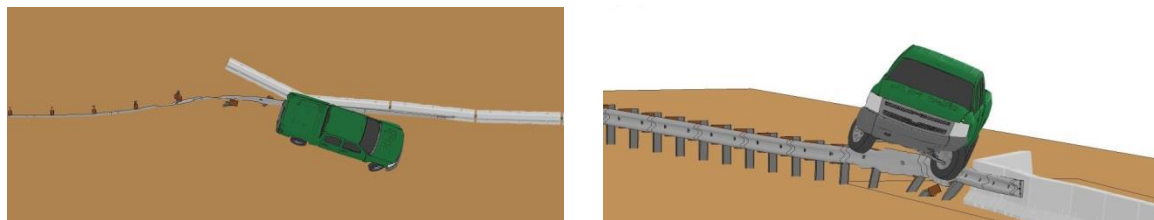
600 ms
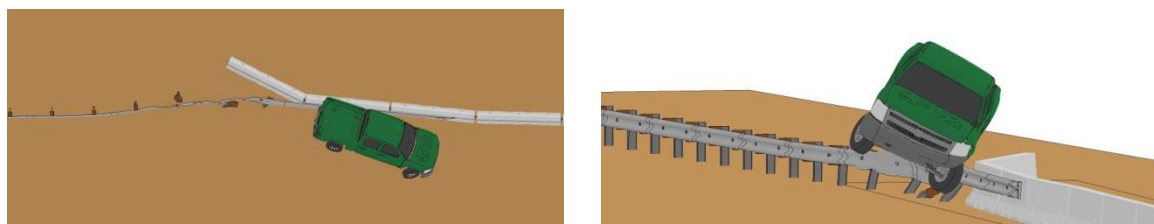
700 ms
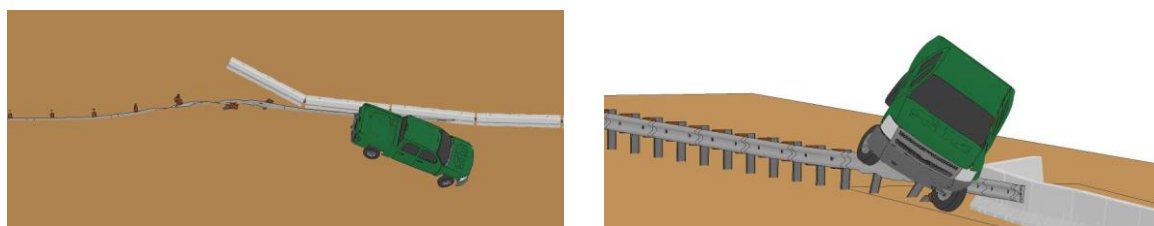
800 ms
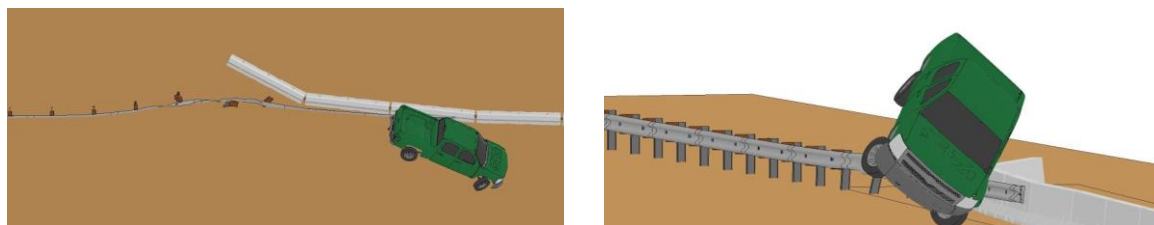
900 ms

Figure 52. Modified G4(1S) End Shoe Sequentials, Impact Location No. 4 (cont.)

7.4 Occupant Risk

The modified G4(1S) end shoe configuration improved vehicle capture and prevented vehicle impact into the upstream end of the PCB system, which resulted in reduced occupant risk values, as shown in Table 9. Neither the longitudinal nor the lateral OIVs were within 20% of the MASH limits for any of the six impact locations. However, the longitudinal ORAs for impact location no. 5 was -23.62 g's, which exceeded the MASH limit of 20.49 g's. A lack of a connection between the modified G4(1S) guardrail and the PCB system for an extended length contributed to outward bowing of the rail and slow rotation of the guardrail posts downstream of the impact location. This behavior allowed the vehicle to run over the weak axis of two guardrail posts. This, in combination with high rail pocketing angles, led to a high longitudinal ORA at impact location no. 5.

Table 9. Occupant Risk Results – Modified G4(1S) End Shoe

Impact Location	OIV ft/s (m/s)		ORA g's	
	Longitudinal	Lateral	Longitudinal	Lateral
1	-15.12 (-4.61)	-20.44 (-6.23)	-16.24	-7.32
2	-28.02 (-8.54)	-14.80 (-4.51)	-10.56	-8.84
3	-20.73 (-6.32)	-18.70 (-5.70)	-9.50	-10.36
4	-21.16 (-6.45)	-17.55 (-5.35)	-12.46	8.03
5	-16.31 (-4.97)	-17.03 (-5.19)	-23.62	-11.42
6	-16.99 (-5.18)	-16.50 (-5.03)	-10.49	-8.45
MASH Limits	≤ 40 (12.2)	≤ 40 (12.2)	≤ 20.49	≤ 20.49

*Red cells denote values that exceed MASH or recommended limits

7.5 Pocketing Angle

The pocketing angle for impact location no. 4 exceeded the recommended value of 23.0 degrees, as shown in Table 10. Also, the pocketing angles for impact location nos. 5 and 6 were within 20% of the recommended limited. As previously mentioned, the lack of a blocked connection between the modified G4(1S) guardrail and the PCBs resulted in outward bowing of the rail and limited rotation of the guardrail posts installed in front of the PCBs. The limited post rotation contributed to elevated pocketing angles at impact location nos. 4 to 6.

Table 10. Pocketing Angle Results – Modified G4(1S) End Shoe

Impact Location	Pocketing		
	Angle	**Time (ms)**	**Location**
1	10.6°	360	7 ft – 8.9 in. Upstream of the End Shoe
2	10.9°	470	14 ft – 4.3 in. Upstream of the End Shoe
3	17.9°	120	2 ft – 6.8 in. Downstream of Centerline of Post No. 2
4	23.1°	210	2 ft – 6.8 in. Downstream of Centerline of Post No. 2
5	20.7°	220	2 ft – 9 in. Upstream of Centerline of Post No. 2
6	22.1°	310	2 ft – 7.4 in. Downstream of Centerline of Post No. 3
Recommended Limits	23.0°	N/A	N/A

*Yellow cells denote values within 20% of MASH or acceptable limits
*Red cells denote values that exceed MASH or acceptable limits

7.6 Discussion

Upon full investigation of the simulation results from all six impact locations, it was determined that the modified G4(1S) end shoe configuration provided an inadequate transition system. Wedging of posts against the PCBs increased the propensity for vehicle climb and generated vehicle instability. Also, vehicle climb concerns were attributed to the low top mounting height of the W-beam guardrail and less effective vehicle capture of the modified G4(1S) guardrail. Pocketing was also observed at impact location nos. 4 to 6 due to limited post rotation caused by outward bowing of the rail. Due to concerns for vehicle climb, inadequate guardrail height, and pocketing, researchers determined that the modified G4(1S) end shoe configuration had a low likelihood of successfully meeting the TL-3 MASH full-scale crash testing criteria. In order to mitigate these problems, researchers decided to utilize and investigate the stiffer and taller thrie beam rail section.

CHAPTER 8 THRIE BEAM END SHOE

8.1 Introduction

A transition from W-beam to thrie beam was incorporated into the design in order to aid in the capture and stable redirection of the vehicle. The higher nominal rail height along with the increased stiffness of the thrie beam should allow for increased capture and stable redirection of the vehicle, while simultaneously reducing rail pocketing. Thrie beam should also decrease the amount of wheel snag on guardrail posts as well as decrease wheel interaction with the face of PCBs, which may decrease vehicle climb. The thrie beam end shoe configuration layout and its nine impact locations are shown in Figure 53.
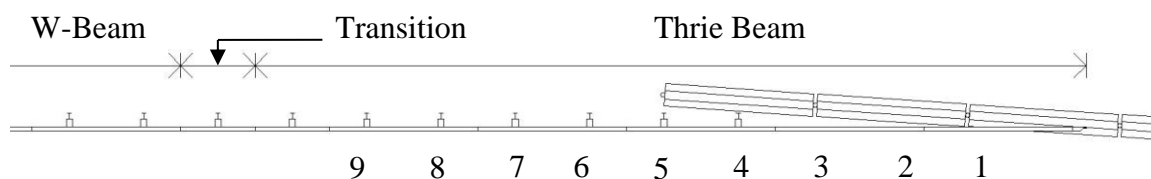
Figure 53. Thrie Beam End Shoe – Impact Locations

8.2 Model Modifications

8.2.1 Symmetric W-Beam to Thrie Beam Transition Element

A symmetric 6-ft 3-in. (1,905-mm) long 12-gauge (2.66-mm) transition element was required to transition from modified G4(1S) guardrail to thrie beam. The transition element was meshed to match the mesh of the W-beam guardrail on the upstream end and to match the mesh of the thrie beam on the downstream end, which allowed for ease of connection between the rail elements, as shown in Figure 54. The area around the bolt-slot openings utilized a finer mesh in order to allow for a better contact interface between the rail and the guardrail bolt.
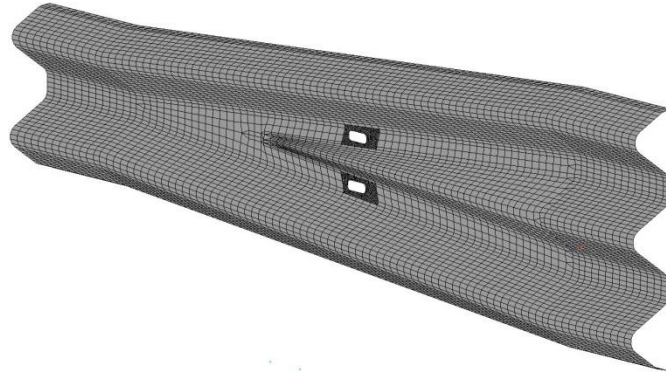
Figure 54. Symmetric W-Beam to Thrie Beam Transition Element Model

8.2.2 Thrie Beam

The last five rail sections in the modified G4(1S) guardrail system were replaced with thrie beam sections. Each of the thrie beam sections, as shown in Figure 55, measured 12 ft − 6 in. (3,810 mm) long and had a 12 gauge (2.66 mm) thickness. The thrie beam sections were meshed to have similar sized elements as the W-beam guardrail elements in order to match the contact interfaces with the blockouts, guardrail bolts, and vehicle.
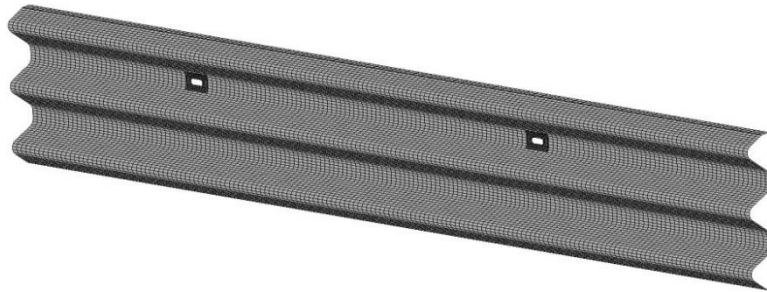
Figure 55. Thrie Beam Model

8.2.3 Increased Nominal Rail Height

The nominal rail height for thrie beam installation was 31⅝ in. (803 mm), as shown in Figure 56. In order to increase the nominal rail height, the post embedment depth was decreased 3⅞ (98 mm) from 43¼ in. (1,099 mm) to 39⅜ in. (1,000 mm). The increased nominal rail height along with the increased stiffness of the rail was intended to

allow for improved vehicle behavior. The blockouts measured 6 in. (152 mm) wide x 8 in. (203 mm) deep x 14¼ in. (362 mm) tall. The blockouts did not run the entire height of the thrie beam section, because they were designed to allow the lower thrie beam to fold underneath the blockout upon impact. This action has allowed the wheel of the vehicle to protrude underneath thrie beam rail and blockout, which allowed for improved capture of the vehicle and reduced wheel and floor board loading and deformation [33].

31⅝ in.   31⅝ in.

(a)   (b)
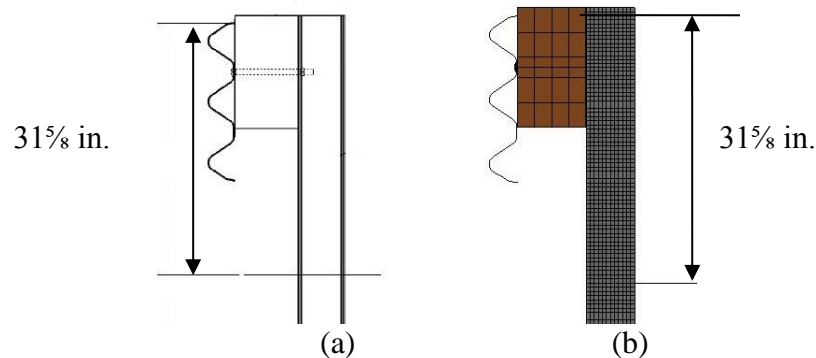
Figure 56. Thrie Beam Top Mounting Height (a) Actual (b) Model

8.3 Vehicle Behavior

The increased nominal rail height of the thrie beam along with its increased stiffness and strength allowed for a much more stable capture and redirection of the vehicle. The transition to thrie beam also eliminated wheel snag on the upstream end of the PCB system. The roll, pitch, and yaw angles for all impact locations yielded results that were well below and not within 20% of the MASH limits, as shown in Table 11. As researchers further investigated each impact location, it was discovered that the roll values at impact location nos. 5, 8, and 9 are very close to being within 20% of the MASH limit. At impact location no. 5, the roll angle was still increasing at the conclusion of the simulation, and researchers concluded that the vehicle would have likely rolled over.

This slight vehicle instability was caused by posts in front of the PCB system wedging against the face of the PCBs and promoting vehicle climb, as shown in Figure 57. Researchers determined that posts located in front of the PCB system could result in vehicle climb and instabilities.

Table 11. Vehicle Behavior Results – Thrie Beam End Shoe

Impact Location	Roll	Pitch	Yaw	Wheel Snag on PCBs?
1	33.0°	24.6°[1]	39.5°	No
2	30.2°	12.7°	41.1°	No
3	22.6°	20.3°	38.8°	No
4	25.7°	15.2°	38.3°	No
5	56.5°[1]	17.5°	41.4°[1]	No
6	30.5°	19.7°[1]	37.2°	No
7	33.0°	18.0°	40.2°	No
8	52.2°	17.9°	40.7°	No
9	53.3°	16.7°	38.6°	No
MASH Limits	< 75°	< 75°	N/A	N/A

[1]Maximum value was not reached prior to conclusion of simulation
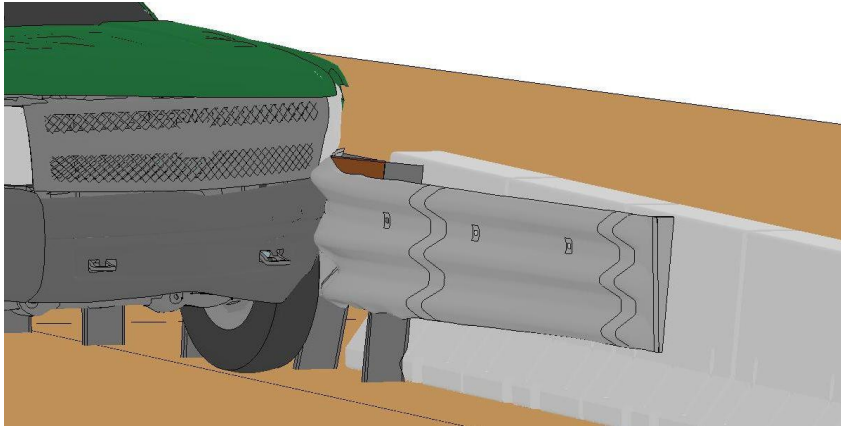
t = 50 ms
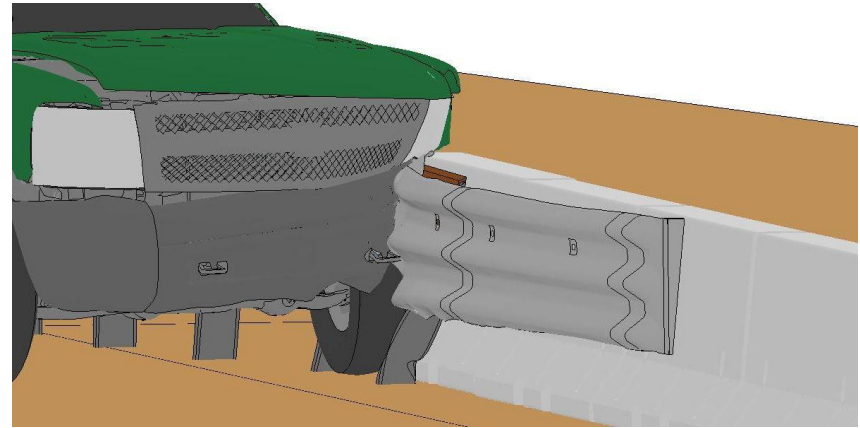
t = 80 ms
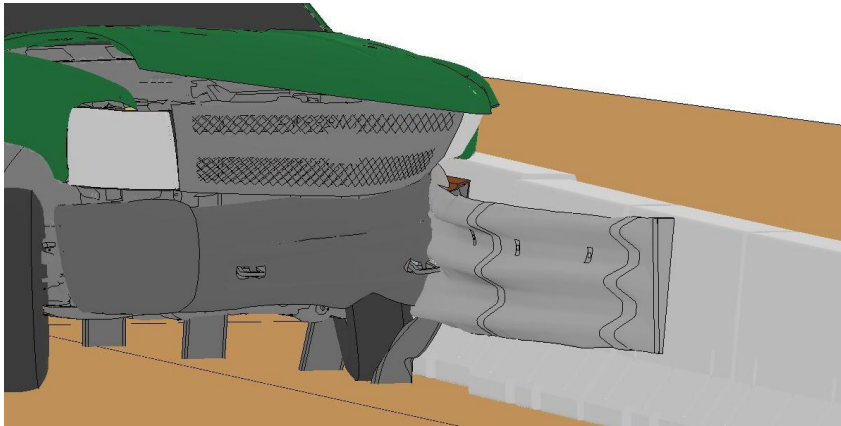
t = 100 ms
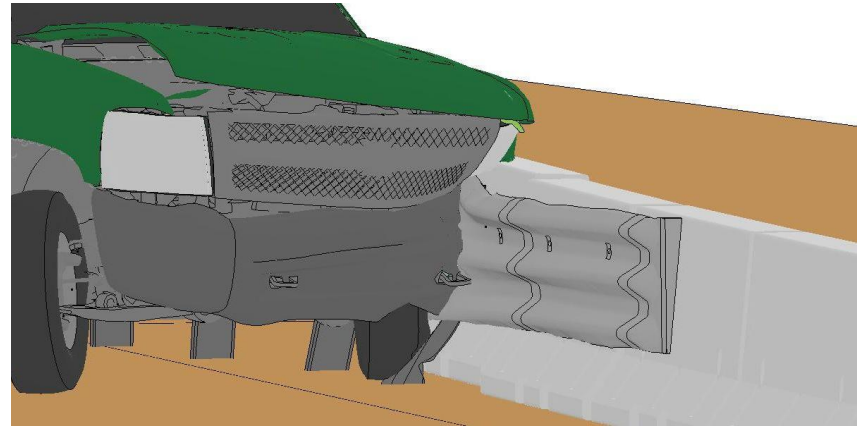
t = 110 ms

Figure 57. Post Wedging and Wheel Snag at Impact Location No. 5

8.4 Occupant Risk

Although researchers observed wheel snag on guardrail posts installed in front of the PCB system, there were no occupant risk values that exceeded or were within 20% of the MASH limits, as shown in Table 12. Researchers determined that longitudinal and lateral OIVs and ORAs were not a concern for the thrie beam end shoe configuration.

Table 12. Occupant Risk Results – Thrie Beam End Shoe

Impact Location	OIV ft/s (m/s)		ORA g's	
	Longitudinal	Lateral	Longitudinal	Lateral
1	-19.13 (-5.83)	-19.36 (-5.90)	-15.20	-15.57
2	-18.64 (-5.68)	-17.78 (-5.42)	11.70	-10.17
3	-18.37 (-5.60)	-21.85 (-6.66)	-10.96	-9.02
4	-16.70 (-5.09)	-20.47 (-6.24)	-12.36	-4.52
5	-24.02 (-7.32)	-17.52 (-5.34)	-8.65	-8.30
6	-21.72 (-6.62)	-18.08 (-5.51)	-9.38	-8.80
7	-20.80 (-6.34)	-19.09 (-5.82)	-12.55	-10.85
8	-15.55 (-4.74)	-16.96 (-5.17)	13.03	-8.61
9	-16.08 (-4.90)	-17.19 (-5.24)	-9.55	-8.50
MASH Limits	≤ 40 (12.2)	≤ 40 (12.2)	≤ 20.49	≤ 20.49

8.5 Pocketing Angle

The increased stiffness and height of the thrie beam allowed for lower pocketing angles, as shown in Table 13. None of the pocketing angles for the nine impact locations exceeded the recommended value of 23 degrees. However, the pocketing angles for impact location nos. 6 and 7 were within 20% of the recommended value.

Table 13. Pocketing Angle Results – Thrie Beam End Shoe

Impact Location	Pocketing		
	Angle	Time (ms)	Location
1	3.3°	110	Centerline of Post No. 6
2	5.2°	50	9 ft – 3.7 in. Upstream from End Shoe
3	8.8°	120	9 ft – 3.7 in. Upstream from End Shoe
4	12.9°	200	9 ft – 3.7 in. Upstream from End Shoe
5	15.0°	70	1 ft – 10.4 in. Upstream from Centerline of Post No. 1
6	18.9°	120	2 ft – 7.1 in. Downstream from Centerline of Post No. 2
7	21.5°	130	2 ft – 9.1 in. Upstream from Centerline of Post No. 2
8	17.9°	200	2 ft – 7.2 in. Downstream from Centerline of Post No. 3
9	15.0°	200	2 ft – 7.1 in. Downstream from Centerline of Post No. 4
Recommended Limits	23.0°	N/A	N/A

*Yellow cells denote values within 20% of MASH or recommended limits

The higher pocketing angles associated with impact location nos. 6 and 7 were due to the outward bowing of the thrie beam and limited rotation of posts located in front of the PCB system when impacted upstream of the PCBs, as shown in Figure 58.
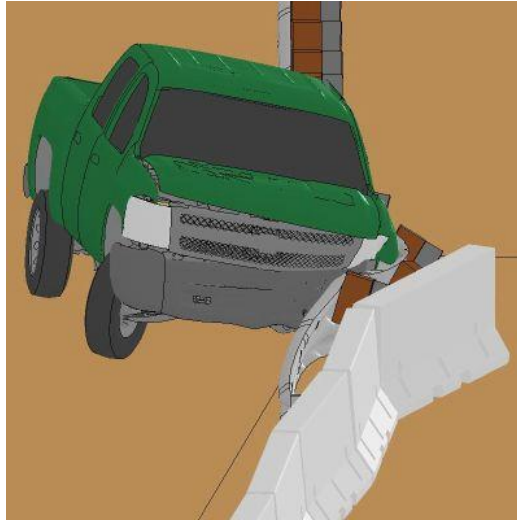
Figure 58. Bowing of Thrie Beam at Impact Location No. 7

8.6 Discussion

Upon full investigation of the simulation results, it was determined that the increased nominal rail height and stiffness of the thrie beam aided in the capture of the vehicle. Slight vehicle instabilities and higher pocketing angles were observed for some impact locations. The posts installed in front of the PCB system showed a tendency to wedge against the face of the PCBs and cause wheel snag and slight vehicle climb. Also, the lack of a blocked connection between the thrie beam rail and the PCBs caused bowing of the rail and higher pocketing angles. Researchers observed improvements in this configuration as compared to the modified G4(1S) configurations, and its performance suggested a high possibility for meeting the MASH TL-3 full-scale crash testing criteria. In order to provide several options and potentially decrease vehicle instabilities and pocketing angle concerns, researchers decided to next remove posts in

front of the PCB system and install blockouts and additional attachment bolts at 6 ft – 3

in. (1,905 mm) post spacings between the face of the PCBs and thrie beam.

CHAPTER 9 THRIE BEAM WITH FULLY-BLOCKED RAIL

9.1 Introduction

Following the initial thrie beam investigation, several design modifications were made in order to improve system performance. Due to wheel snag and wedging of the guardrail posts against the face of the PCBs, the guardrail posts located in front of the PCBs were removed. In order to eliminate bowing of the thrie beam, blockouts and post bolt attachments were installed at standard 6 ft – 3 in. (1,905 mm) increments between the thrie beam and PCBs. The fully-blocked rail thrie beam configuration was simulated for impacts at nine different locations, as shown in Figure 59.
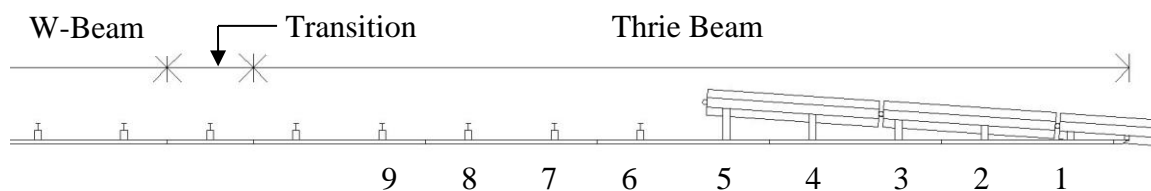
Figure 59. Thrie Beam with Fully-Blocked Rail – Impact Locations

9.2 Model Modifications

9.2.1 Post Removal and Spacer Block Implementation

Upon removal of two posts in front of the PCB system, there were five locations where installation of a blockout was necessary between the thrie beam and PCBs. Due to the 15H:1V PCB flare and sloped face of the F-shape PCBs, the geometry of the blockouts required a 5.81-degree vertical taper along with a 3.81 degree longitudinal cut, as shown in Figure 60.

3.81°

5.81°

(a)   (b)
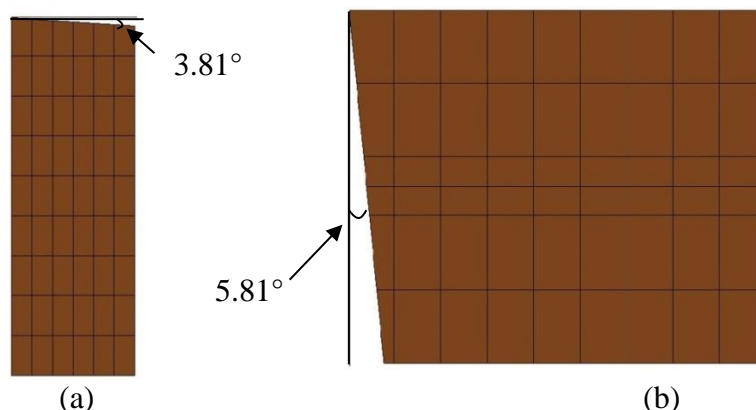
Figure 60. Blockout Slope Geometry (a) Longitudinal (b) Vertical

In order to create the five blockouts for this configuration, one blockout was created and meshed. Then, it was scaled to fit the other four locations, as shown in Figure 61. The corresponding blockout depths are shown in Table 14.
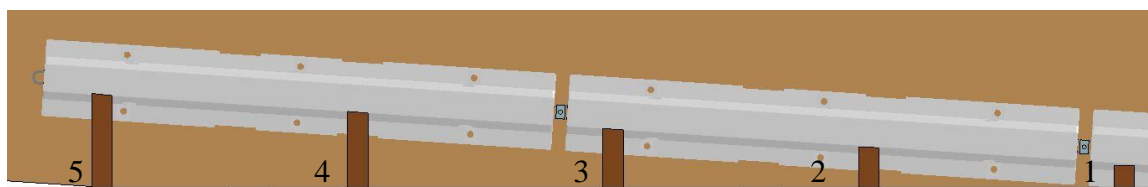
Figure 61. Spacer Block Locations and Depths

Table 14. Thrie Beam with Fully-Blocked Rail Blockout Depths

Blockout No.	Depth, in. (mm)
1	6½ (165)
2	12 (305)
3	17⅜ (441)
4	22⅜ (568)
5	28¼ (718)

The blockouts were modeled using the same simplified wood material as used for the other blockouts in the thrie beam model. Due to the complicated fracture mechanics of wood, a reliable material formulation that accurately simulates wood fracture has yet to be developed. Therefore, the blockouts had no failure criteria. Along with blockouts, guardrail bolts were installed and scaled to fit each new blockout location. The blockout

bolts were modeled to be connected directly to the face of the PCB segments. If oversized blockouts are used in the final design, expanded research must be conducted to configure the guardrail bolt to PCB attachment for use in a full-scale vehicle crash testing program.

9.3 Vehicle Behavior

The thrie beam with fully-blocked rail configuration captured and redirected the vehicle for all nine impact locations, and vehicle stability was acceptable as angles did not exceed the MASH limits for roll and pitch. Also, wheel snag on the PCBs was not observed for any of the nine impact locations, as shown in Table 15. However, the roll angle for impact location no. 3 was within 20% of the MASH limit and had not reached the maximum angle prior to the conclusion of the simulation. Researchers initially determined that the vehicle would have rolled over. However, upon further inspection, the excessive roll motion was deemed unrealistic, and it was likely caused by the lateral stiffness of the vehicle's rear suspension when the back end of the vehicle impacted the thrie beam. No extensive research has been performed to validate the rear suspension of the Chevrolet Silverado pickup model. Previous simulation results have indicated that the rear suspension is overly stiff and can over-predict roll angles as well as occupant risk values when the back end of the vehicle impacts a barrier system. Therefore, it was determined that the vehicle rotation angles would not have exceeded the MASH limits for the thrie beam with fully-blocked rail configuration.

Table 15. Vehicle Behavior Results – Thrie Beam with Fully-Blocked Rail

Impact Location	Roll	Pitch	Yaw	Wheel Snag on PCBs?
1	27.5°	24.5°[1]	40.3°	No
2	25.6°	14.1°	45.8°	No
3	67.4°[1]	26.0°[1]	66.8°	No
4	17.0°	9.3°	39.9°	No
5	13.8°	7.8°	37.2°	No
6	19.2°[1]	10.4°	55.4°[1]	No
7	22.9°	11.1°[1]	48.1°[1]	No
8	34.8°	15.8°	40.0°[1]	No
9	48.0°	13.2°	38.1°	No
MASH Limits	< 75°	< 75°	N/A	N/A

[1]Maximum value was not reached prior to conclusion of simulation
*Yellow cells denote values within 20% of MASH or recommended limits

9.4 Occupant Risk

The occupant risk values for the thrie beam with fully-blocked rail configuration did not exceed the MASH limits for any of the nine impact locations, as shown in Table 16. However, the maximum longitudinal ORA for impact location no. 9 was -16.85 g's, which falls within 20% of the MASH limit of 20.49 g's. This high ORA value occurred after the vehicle became airborne upon redirection and impacted the ground. Researchers determined that a more stable vehicle capture and redirection, that does not allow the vehicle to become airborne, was necessary to reduce this high longitudinal ORA.

Table 16. Occupant Risk Results – Thrie Beam with Fully-Blocked Rail

Impact Location	OIV ft/s (m/s)		ORA g's	
	Longitudinal	Lateral	Longitudinal	Lateral
1	-20.73 (-6.32)	-19.03 (-5.80)	-11.19	-11.75
2	-23.52 (-7.17)	-18.73 (-5.71)	-9.48	-10.63
3	-31.20 (-9.51)	-22.34 (-6.81)	-7.14	-11.11
4	-27.76 (-8.46)	-16.93 (-5.16)	-13.55	-6.32
5	-29.10 (-8.87)	-18.54 (-5.65)	-7.53	-6.37
6	-28.31 (-8.63)	-16.73 (-5.10)	-10.13	-6.03
7	-26.15 (-7.97)	-19.65 (-5.99)	-13.78	7.17
8	-17.81 (-5.43)	-17.75 (-5.41)	-8.28	-8.83
9	-16.31 (-4.97)	-17.39 (-5.30)	-16.85	-8.69
MASH Limits	≤ 40 (12.2)	≤ 40 (12.2)	≤ 20.49	≤ 20.49

*Yellow cells denote values within 20% of MASH or recommended limits

9.5 Pocketing Angle

The oversized blockouts were installed with the intention of initiating PCB displacement earlier in the impact event, which would reduce pocketing at impact locations upstream from the PCB system. However, the maximum pocketing angle at impact location no. 7 exceeded the recommended value of 23 degrees, as shown in Table 17. Further, the maximum pocketing angle at impact location no. 8 was within 20% of 23 degrees.

Table 17. Pocketing Angle Results – Thrie Beam with Fully-Blocked Rail

Impact Location	Pocketing		
	Angle	Time (ms)	Location
1	2.9°	80	Centerline of Post No. 6
2	11.0°	50	2 ft – 7.1 in. Downstream of Centerline of Blockout No. 4
3	15.2°	70	2 ft – 9.2 in. Upstream of Centerline of Blockout No. 2
4	15.6°	70	1 ft – 10.5 in. Upstream of Centerline of Blockout No. 3
5	14.7°	70	1 ft – 10.4 in. Upstream of Centerline of Blockout No. 4
6	17.5°	60	2 ft – 9.2 in. Upstream of Centerline of Blockout No. 5
7	25.4°	120	11.8 in. Upstream of Centerline of Blockout No. 5
8	18.7°	190	1 ft – 8.5 in. Downstream of Centerline of Post No. 1
9	15.9°	190	2 ft – 7.1 in. Downstream of Centerline of Post No. 2
Recommended Limits	23.0°	N/A	N/A

*Yellow cells denote values within 20% of MASH or recommended limits
*Red cells denote values that exceed MASH or recommended limits

While the oversized blockouts engaged the PCBs earlier in the impact event than observed in the configurations with posts in front of PCBs, there was still a delay between vehicle impact with the thrie beam and the onset of PCB displacement. This delay resulted from the significant inertia that must be overcome prior to PCB displacement. As such, the vehicle greatly deformed the thrie beam upstream from the PCB system and led to high pocketing angles prior to PCB displacement, as shown in

Figure 62. It was determined that PCB displacement should be initiated even earlier in the impact event.
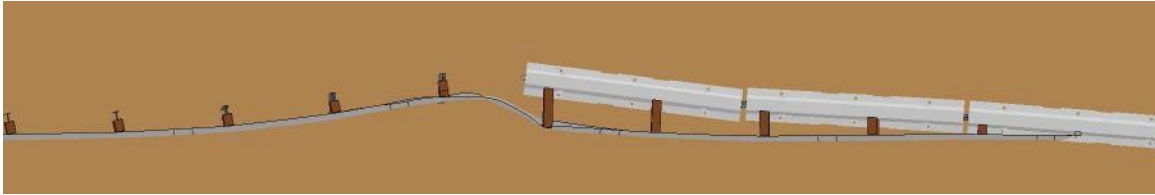
Figure 62. Pocketing Angle for Impact Location No. 7 at 120 ms

9.6 Discussion

While the blocked connection allowed for earlier engagement of the PCB system, high pocketing angles continued to occur. It was determined that PCB displacement should occur even sooner in the impact event. Therefore, the next step involved the attachment of a cantilever beam to the front face of the most upstream PCB, which would allow the guardrail posts to rotate into the cantilever beam and initiate PCB displacement.

CHAPTER 10 THRIE BEAM WITH FULLY-BLOCKED RAIL AND CANTILEVER BEAM

10.1 Introduction

Due to high pocketing angles found in the thrie beam with fully-blocked rail configuration, researchers decided that the PCB displacement needed to be initiated earlier in the impact event. Thus, a cantilever beam was installed on the front face of the most upstream PCB. This configuration used a transition to thrie beam with fully-blocked rail, similar to the previous configuration. The thrie beam with fully-blocked rail and cantilever beam was impacted at the same nine impact locations as used for the previous configuration, as shown in Figure 63.
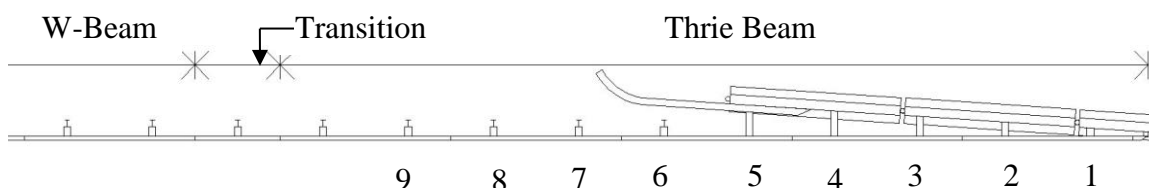
Figure 63. Thrie Beam with Fully-Blocked Rail and Cantilever Beam – Impact Locations

10.2 Model Modifications

10.2.1 Cantilever Beam

A 15-ft (4,572-mm) long cantilever beam was used to initiate displacement of the PCB system. This length was chosen to ensure that a post will be able to rotate into the cantilever beam regardless of PCB placement. For the 15-ft (4,572-mm) beam, a 6 ft (1,829 mm) segment was attached to the face of the PCB, 6 ft (1,829 mm) was a straight cantilever, and the last 3 ft (914 mm) was curved backward to prevent vehicle snag on the end. The cantilever beam was 6 in. (152 mm) deep x 8 in. (203 mm) tall x ¼ in. (6.35 mm) thick and was installed 30 in. (762 mm) above the groundline, as shown in Figure 64.
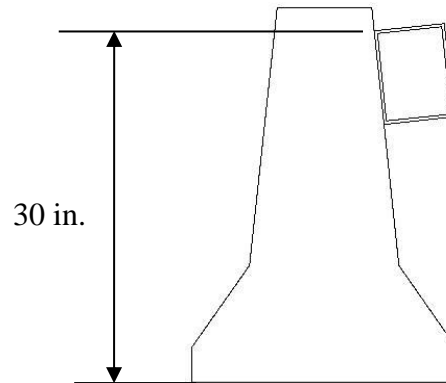
Figure 64. Cantilever Beam Attached to PCB

The cantilever beam was modeled using ASTM A36 steel. The cantilever beam was meshed to have similar mesh size as the PCB segments in order to allow for a good contact interface, as shown in Figure 65. The cantilever beam was rigidly attached to the face of the PCB segment. This simplified connection was chosen in the interest of time to allow for the simulation of the most design concepts. If the final design concept utilized a cantilever beam, a full moment analysis would be undertaken to design both the final cross-section size and a proper connection of the cantilever beam to the PCB.
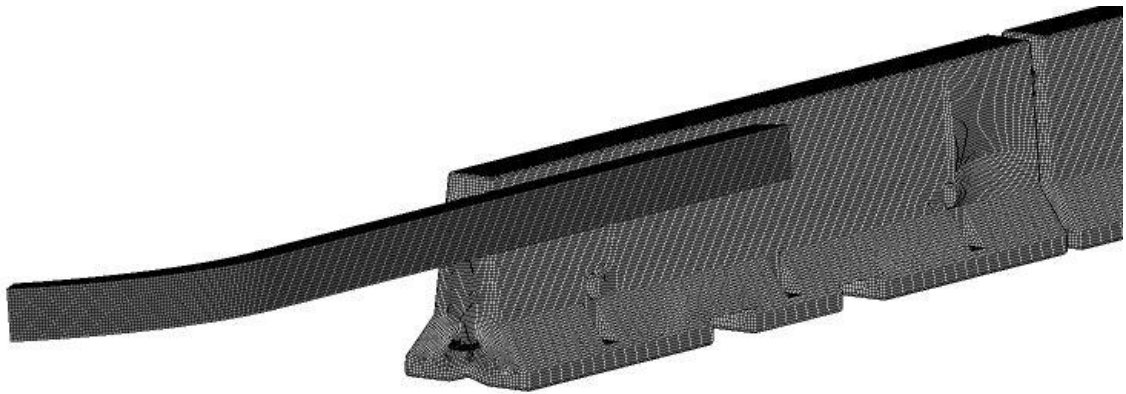
Figure 65. Cantilever Beam Mesh and Attachment

10.3 Vehicle Behavior

None of the vehicle stability measures for the thrie beam with fully-blocked rail and cantilever beam configuration exceeded the MASH limits, and no wheel snag was found on the PCBs for any of the nine impact locations, as shown in Table 18. While the vehicle was captured and redirected for all nine impact locations, the roll angle for impact location no. 3 was 65.3 degrees and had not reached a maximum value prior to the conclusion of the simulation. Researchers believe that the vehicle would have likely rolled over. However, upon further inspection, the excessive roll motion was deemed unrealistic and was likely caused by the exaggerated stiffness of the vehicle's rear suspension when the back end of the vehicle impacted the thrie beam. This finding revealed that the MASH limits would not likely be exceeded.

Table 18. Vehicle Behavior Results – Thrie Beam with Fully-Blocked Rail and Cantilever Beam

Impact Location	Roll	Pitch	Yaw	Wheel Snag on PCBs?
1	31.6°	25.7°[1]	40.2°	No
2	26.9°	14.4°	45.8°	No
3	65.3°[1]	29.8°[1]	62.2°[1]	No
4	25.4°	15.7°	40.0°	No
5	22.3°	6.1°	33.1°	No
6	9.0°	5.9°	35.2°[1]	No
7	28.8°	10.3°	40.2°	No
8	32.8°	12.9°	37.3°[1]	No
9	49.0°	14.2°	38.4°	No
MASH Limits	< 75°	< 75°	N/A	N/A

[1]Maximum value was not reached prior to conclusion of simulation
*Yellow cells denote values within 20% of MASH or recommended limits

10.4 Occupant Risk

The occupant risk values for the thrie beam with fully-blocked rail and cantilever beam configuration were relatively low for all nine impact locations, except for the longitudinal OIV at impact location no. 6, as shown in Table 19.

Table 19. Occupant Risk Results – Thrie Beam with Fully-Blocked Rail and Cantilever Beam

Impact Location	OIV ft/s (m/s)		ORA g's	
	Longitudinal	Lateral	Longitudinal	Lateral
1	-20.11 (-6.13)	-18.86 (-5.75)	-13.29	-14.14
2	-24.05 (-7.33)	-18.54 (-5.65)	-8.88	-10.73
3	-31.27 (-9.53)	-22.28 (-6.79)	-13.50	-8.82
4	-28.41 (-8.66)	-17.62 (-5.37)	-8.31	-7.93
5	-29.30 (-8.93)	-17.13 (-5.22)	-7.79	-5.07
6	-40.52 (-12.35)	-11.42 (-3.48)	-6.49	-9.14
7	-24.02 (-7.32)	-19.16 (-5.84)	-12.67	-5.43
8	-19.72 (-6.01)	-18.64 (-5.68)	-11.21	-8.06
9	-16.17 (-4.93)	-17.45 (-5.32)	-8.90	-9.76
MASH Limits	≤ 40 (12.2)	≤ 40 (12.2)	≤ 20.49	≤ 20.49

*Red cells denote values that exceed MASH or recommended limits

The longitudinal OIV at impact location no. 6 was -40.52 ft/s (-12.35 m/s), which exceeded the maximum allowable limit of 40 ft/s (12.2 m/s) as outlined in MASH. The

longitudinal OIV reached this elevated level as a result of vehicle snag on one of the oversized blockouts, as shown in Figure 66. While these oversized blockouts eliminate the bowing of the rail, they also present an opportunity for vehicle snag. Wood blockouts in full-scale crash testing would likely fracture upon impact, but the blockouts in the LS-DYNA model have no failure criteria due to wood modeling limitations. Therefore, researchers determined that the vehicle snag on the blockout was not a physical phenomenon and likely would not occur in a full-scale crash testing program.

Figure 66. Vehicle Snag on Blockout for Impact Location No. 6 at 90 ms

10.5 Pocketing Angle

The cantilever beam was implemented in order to initiate PCB displacement earlier in the impact event and reduce pocketing angles. The maximum pocketing angles, as found in Table 20, do not exceed the recommended value of 23 degrees. However, impact location nos. 7 and 8 yielded maximum pocketing angles within 20% of 23 degrees. As compared to the previous configuration without the cantilever beam, the pocketing angle for impact location no. 7 was reduced from 25.4 degrees to 20.5 degrees, which led researchers to determine that the installation of the cantilever beam helped reduce pocketing angles.

Table 20. Pocketing Angle Results – Thrie Beam with Fully-Blocked Rail and Cantilever Beam

Impact Location	Pocketing		
	Angle	**Time (ms)**	**Location**
1	2.9°	80	Centerline of Post No. 6
2	10.9°	50	2 ft – 7.1 in. Downstream of Centerline of Blockout No. 4
3	15.1°	70	2 ft – 9.2 in. Upstream of Centerline of Blockout No. 2
4	15.5°	70	1 ft – 10.5 in. Upstream of Centerline of Blockout No. 3
5	15.2°	70	1 ft – 10.4 in. Upstream of Centerline of Blockout No. 4
6	18.3°	60	2 ft – 9.2 in. Upstream of the Centerline of Blockout No. 5
7	20.5°	120	2 ft – 7.1 in. Downstream of Centerline of Post No. 1
8	20.0°	130	1 ft – 10.4 in. Upstream of Centerline of Post No. 1
9	16.7°	200	2 ft – 7.1 in. Downstream of Centerline of Post No. 2
Recommended Limits	23.0°	N/A	N/A

*Yellow cells denote values within 20% of MASH or recommended limits

10.6 Discussion

The cantilever beam was installed to the most upstream PCB with the intention of reducing maximum pocketing angles by initializing PCB displacement earlier in the impact event. The simulation results showed that the cantilever beam did reduce maximum pocketing angles. However, the maximum pocketing angles for impact location nos. 7 and 8 were still within 20% of the recommended value. Also, the

longitudinal OIV for impact location no. 6 exceeded the MASH limit. It was determined that this result was due to vehicle snag on one of the oversized blockouts installed between the thrie beam and PCBs. This value was likely due to the lack of failure criteria for the blockouts in the model. These blockouts would likely fracture in full-scale crash testing, and the longitudinal OIV would likely be much lower. Based on the results of the thrie beam with fully-blocked rail and cantilever beam, this configuration likely demonstrated the highest probability of meeting the MASH testing criteria for any system investigated so far. However, pocketing was still the primary concern, and researchers continued to explore ways to reduce maximum pocketing angles.

CHAPTER 11 NESTED THRIE BEAM WITH FULLY-BLOCKED RAIL

11.1 Introduction

Thus far, the use of thrie beam, removal of posts in front of PCB system, additional blockouts at each post location between the thrie beam and PCBs, and installation of a cantilever beam to the upstream end of the PCB system had each improved the performance of the transition when compared to the baseline system. However, maximum pocketing angles had remained a concern for every configuration so far. In order to further reduce pocketing concerns upstream from the end of the PCB system, the thrie beam was nested in front of the PCB system, as shown in Figure 67. The nested thrie beam with fully-blocked rail configuration was impacted at the same nine impact locations as the three previous designs.
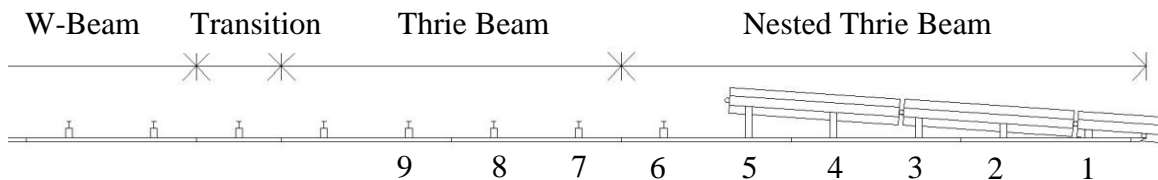
Figure 67. Nested Thrie Beam with Fully-Blocked Rail – Impact Locations

11.2 Model Modification

11.2.1 Nested Thrie Beam

The final three sections of thrie beam were nested. This change was incorporated by doubling the thickness of each section as well as the bolt hole areas from a single 12-gauge (2.66-mm) rail section to two nested 12-gauge (2.66-mm) rail sections. Researchers determined that stiffening the rail ahead of the PCB system would reduce the amount of vehicle penetration into the thrie beam system upstream from the PCB system, which would reduce the maximum rail pocketing angles.

11.3 Vehicle Behavior

The simulation results for the nested thrie beam with fully-blocked rail configuration indicated that the vehicle was captured and redirected for all nine impact locations. However, vehicle stability degraded with this modification, as shown in Table 21. The roll angle for impact location no. 2 was 96.9 degrees and had not reached a maximum value prior to conclusion of the simulation. Also, the roll angle for impact location no. 1 was within 20% of the MASH limit and had not reached a maximum value prior to conclusion of the simulation. Researchers felt the vehicle would have likely rolled over at both impact locations. However, upon further inspection, the excessive roll motion was deemed unrealistic and was likely caused by the exaggerated stiffness of the vehicle's rear suspension when the back end of the vehicle impacted the nested thrie beam. The increased stiffness of the nested thrie beam further accentuated the response of the vehicle's rear suspension, which caused even higher roll angles than were seen in previous designs. This finding led researchers to determine that the MASH limits would not likely be exceeded.

Table 21. Vehicle Behavior Results – Nested Thrie Beam with Fully-Blocked Rail

Impact Location	Roll	Pitch	Yaw	Wheel Snag on PCBs?
1	$71.4°^{1}$	$26.3°^{1}$	$37.9°$	No
2	$96.9°^{1}$	$27.3°$	$40.7°$	No
3	$37.6°$	$10.1°$	$35.4°$	No
4	$36.0°$	$7.4°$	$35.5°$	No
5	$31.0°$	$7.8°$	$35.6°$	No
6	$33.4°$	$10.5°$	$38.1°$	No
7	$32.3°$	$12.0°$	$43.5°$	No
8	$41.1°$	$13.3°$	$39.8°$	No
9	$42.3°$	$12.8°$	$37.6°$	No
MASH Limits	$< 75°$	$< 75°$	N/A	N/A

[1]Maximum value was not reached prior to conclusion of simulation
*Yellow cells denote values within 20% of MASH or recommended limits
*Red cells denote values that exceed MASH or recommended limits

11.4 Occupant Risk

The occupant risk values for the nested thrie beam with fully-blocked rail configuration did not exceed or come within 20% of the MASH limits for any of the nine impact locations, as shown in Table 22. These relatively low OIV and ORA values led researchers to believe that the nested thrie beam had improved the safety performance of the transition, and occupant risk values would likely meet the MASH TL-3 criteria.

Table 22. Occupant Risk Results – Nested Thrie Beam with Fully-Blocked Rail

Impact Location	OIV ft/s (m/s)		ORA g's	
	Longitudinal	Lateral	Longitudinal	Lateral
1	-18.21 (-5.55)	-19.62 (-5.98)	-13.30	-13.03
2	-14.90 (-4.54)	-18.31 (-5.58)	-14.42	-6.69
3	-18.54 (-5.65)	-22.11 (-6.74)	-5.86	-9.66
4	-15.35 (-4.68)	-18.37 (-5.60)	-4.67	-7.02
5	-17.39 (-5.30)	-20.80 (-6.34)	-4.42	-5.95
6	-18.96 (-5.78)	-17.36 (-5.29)	-5.70	-8.41
7	-23.20 (-7.07)	-20.41 (-6.22)	-6.77	-7.13
8	-20.14 (-6.14)	-18.60 (-5.67)	-10.09	-10.19
9	-16.96 (-5.17)	-17.55 (-5.35)	-10.12	-8.88
MASH Limits	≤ 40 (12.2)	≤ 40 (12.2)	≤ 20.49	≤ 20.49

11.5 Pocketing Angle

The nested thrie beam was installed to stiffen the rail in an attempt to reduce pocketing angles. The pocketing angles for all nine impact locations can be found in Table 23, and none of the maximum pocketing angles exceeded the recommended value of 23 degrees. The maximum pocketing angle at impact location no. 7 was 20.3 degrees, which is within 20% of 23 degrees. Compared to the thrie beam with fully-blocked rail

configuration, the maximum pocketing angles at every impact location was reduced, thus the nested thrie beam was successful in reducing maximum pocketing angles.

Table 23. Pocketing Angle Results – Nested Thrie Beam with Fully-Blocked Rail

Impact Location	Pocketing		
	Angle	Time (ms)	Location
1	2.9°	70	Centerline of Post No. 6
2	2.9°	100	Centerline of Post No. 6
3	7.2°	300	2 ft – 7.1 in. Downstream of Centerline of Blockout No. 2
4	10.1°	330	2 ft – 7.1 in. Downstream of Centerline of Blockout No. 2
5	8.9°	350	9.7 in. Downstream of Centerline of Blockout No. 2
6	11.9°	160	9.7 in. Downstream of Centerline of Blockout No. 4
7	20.3°	120	2 ft – 7.2 in. Downstream of Centerline of Post No. 1
8	16.3°	160	9.7 in. Downstream of Centerline of Post No. 1
9	14.2°	120	2 ft – 9.1 in. Upstream of Centerline of Post No. 2
Acceptable Limits	23.0°	N/A	N/A

*Yellow cells denote values within 20% of MASH or recommended limits

11.6 Discussion

The nested thrie beam with fully-blocked rail configuration reduced the maximum pocketing angles below those observed in previously simulated design concepts. While the occupant risk values remained well below the MASH limits, impact location nos. 1 and 2 yielded maximum roll angles that were either in excess of the MASH limits or believed would likely have exceeded MASH limits. However, due to unrealistic rear

suspension behavior that has plagued this vehicle model in the past, researchers feel that the those angles would likely be much lower. These results led researchers to determine that this transition design had the highest possibility of successfully meeting the TL-3 MASH full-scale crash testing criteria.

CHAPTER 12 PCBs BEHIND NESTED THRIE BEAM

12.1 Introduction

While there were several configurations for the Flared PCB – Modified G4(1S) design concept that had a chance of success, a second design concept was developed and simulated to determine its likelihood for success. The Parallel PCB – Modified G4(1S) design concept presented to the TAC members, as noted in CHAPTER 3, utilized modified G4(1S) guardrail attached to the F-shape PCB system with two PCB segments installed parallel to and behind the guardrail system. However, based on the simulation results from the Flared PCB – Modified G4(1S) design concept and subsequent configurations along with engineering judgment, several of the design modifications were implemented into the initial system. The modified G4(1S) guardrail exhibited a low propensity for vehicle capture due to its low top rail height, thus a transition to thrie beam was installed. While the single thrie beam aided in the vehicle capture, it exhibited high pocketing angles upstream from the PCB system, and nested thrie beam was installed for the final five rail sections in the transition. Also, posts installed in front of PCBs tended to wedge against the PCBs, causing wheel snag and vehicle instabilities. Therefore, all of the posts in front of the PCBs were removed, and blockouts were installed at standard 6 ft – 3 in. (1,905 mm) post spacings, as shown in Figure 68. Two PCB segments were installed parallel to and behind the nested thrie beam system before transitioning to the 15H:1V flared PCB system.
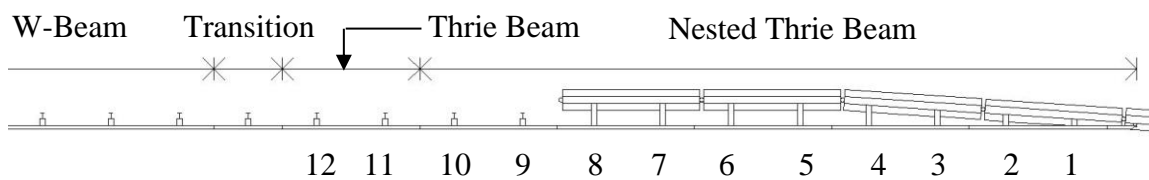
Figure 68. PCBs Behind Nested Thrie Beam – Impact Locations

12.2 Vehicle Behavior

The PCBs behind nested thrie beam configuration captured and redirected the vehicle with no wheel snag on the PCBs for all twelve impact locations, as shown in Table 24. However, the roll angle for impact location no. 11 exceeded the MASH limit and had not reached a maximum value prior to conclusion of the simulation. Also, the roll angle for impact location no. 12 was within 20% of the MASH limit. Upon further inspection, the excessive roll motion was deemed unrealistic and was likely caused by the exaggerated stiffness of the vehicle's rear suspension when the back end of the vehicle impacted the nested thrie beam. For this reason, researchers determined that the MASH limits would not likely be exceeded at these two impact locations, and the vehicle would likely have been safely redirected.

Table 24. Vehicle Behavior Results – PCBs Behind Nested Thrie Beam

Impact Location	Roll	Pitch	Yaw	Wheel Snag on PCBs?
1	58.7°[1]	27.3°[1]	42.5°	No
2	31.3°	18.2°	42.0°	No
3	44.1°	9.5°	36.8°	No
4	29.2°	9.2°	38.1°	No
5	35.1°	9.0°	35.8°	No
6	20.3°	7.8°	35.5°	No
7	28.5°	7.1°	35.0°	No
8	24.6°	8.4°	34.4°	No
9	33.1°	10.4°	35.7°	No
10	26.3°	7.4°	37.7°	No
11	83.3°[1]	19.2°	40.6°	No
12	68.5°	18.1°	40.1°	No
MASH Limits	< 75°	< 75°	N/A	N/A

[1]Maximum value was not reached prior to conclusion of simulation
*Yellow cells denote values within 20% of MASH or recommended limits
*Red cells denote values that exceed MASH or recommended limits

12.3 Occupant Risk

The occupant risk evaluation for the PCBs behind nested thrie beam configuration

yielded results with two values within 20% of the MASH limits, as shown in Table 25.

The maximum longitudinal ORA for impact location nos. 1 and 12 were 18.88 and -17.41

g's, respectively. These high ORA values occurred as the vehicle became airborne upon

redirection and impacted the ground. Researchers determined that a more stable vehicle

capture and redirection was necessary to reduce the high longitudinal ORA values.

Table 25. Occupant Risk Results – PCBs Behind Nested Thrie Beam

Impact Location	OIV ft/s (m/s)		ORA g's	
	Longitudinal	Lateral	Longitudinal	Lateral
1	-14.60 (-4.45)	-17.65 (-5.38)	18.88	-12.14
2	-17.29 (-5.27)	-21.92 (-6.68)	-11.85	-10.97
3	-15.81 (-4.82)	-19.23 (-5.86)	-4.17	-6.64
4	-16.96 (-5.17)	-20.31 (-6.19)	-5.28	-15.16
5	-18.80 (-5.73)	-18.31 (-5.58)	-7.89	-8.45
6	-17.75 (-5.41)	-20.37 (-6.21)	4.17	-10.19
7	-15.88 (-4.84)	-19.16 (-5.84)	-5.03	-5.96
8	-16.60 (-5.06)	-20.34 (-6.20)	-5.65	-5.24
9	-20.21 (-6.16)	-18.47 (-5.63)	-6.16	-8.82
10	-17.91 (-5.46)	-19.85 (-6.05)	-11.60	-8.95
11	-18.50 (-5.64)	-19.23 (-5.86)	16.35	-7.99
12	-18.60 (-5.67)	-17.88 (-5.45)	-17.41	-10.43
MASH Limits	≤ 40 (12.2)	≤ 40 (12.2)	≤ 20.49	≤ 20.49

*Yellow cells denote values within 20% of MASH or recommended limits

12.4 Pocketing Angle

One reason for installing two PCBs parallel to and behind the nested thrie beam

was to engage PCBs early in the impact event using oversized blockouts, thus reducing

pocketing angles. The pocketing angles for all twelve impact locations can be found in

Table 26, and none of the maximum pocketing angles exceeded or came within 20% of the recommended value of 23 degrees. This finding showed that nesting of thrie beam and PCB segments running parallel to and behind the guardrail had helped to reduce pocketing angles.

Table 26. Pocketing Angle Results – PCBs Behind Nested Thrie Beam

Impact Location	Pocketing		
	Angle	Time (ms)	Location
1	2.8°	110	Centerline of Post No. 5
2	4.4°	140	3 ft – 7.9 in. Upstream of Centerline of Blockout No. 1
3	7.2°	140	3 ft – 7.9 in. Upstream of Centerline of Blockout No. 1
4	10.1°	290	3 ft – 7.9 in. Upstream of Centerline of Blockout No. 1
5	10.4°	400	3 ft – 7.9 in. Upstream of Centerline of Blockout No. 1
6	8.5°	480	3 ft – 7.9 in. Upstream of Centerline of Blockout No. 1
7	8.9°	320	2 ft – 7 in. Downstream of Centerline of Blockout No. 5
8	8.0°	310	2 ft – 9.2 in. Upstream of Centerline of Blockout No. 5
9	12.1°	60	2 ft – 7.1 in. Downstream of Centerline of Post No. 1
10	18.2°	110	2 ft – 7.1 in. Downstream of Centerline of Post No. 1
11	15.3°	150	9.7 in. Downstream of Centerline of Post No. 1
12	12.7°	160	1 ft – 8.5 in. Downstream of Centerline of Post No. 2
Recommended Limits	23.0°	N/A	N/A

12.5 Discussion

Upon full investigation of the simulation findings for PCBs behind nested thrie beam configuration, impact location nos. 11 and 12 yielded maximum roll angles that were either in excess of or within 20% of the MASH limits. However, due to unrealistic rear suspension behavior that has plagued this vehicle model in the past, those values would likely be much lower. At impact location nos. 1 and 12, the longitudinal ORAs were within 20% of the MASH limit due to the vehicle impacting the ground after becoming airborne. Based on these findings, researchers had a high amount of confidence that the PCB behind guardrail with nested thrie beam configuration would successfully pass MASH criterion. Based on the results found for the cantilever beam configuration, researchers decided to install a cantilever beam and further investigate its safety performance.

CHAPTER 13 PCBs BEHIND NESTED THRIE BEAM WITH CANTILEVER BEAM

13.1 Introduction

Due to the success observed with installing a cantilever beam in the thrie beam with fully-blocked rail and cantilever beam configuration of the Flared PCB – Modified G4(1S) design concept, and the marginal results associated with PCBs behind nested thrie beam configuration, the same cantilever beam was installed to the most upstream PCB to improve results. This system utilized a similar setup as used in the previous configuration with a transition from modified G4(1S) guardrail to thrie beam and nested thrie beam placed in front of the PCB system, as shown in Figure 69. The cantilever beam was again 15 ft (4,572 mm) long. This configuration was impacted at the same twelve impact locations.
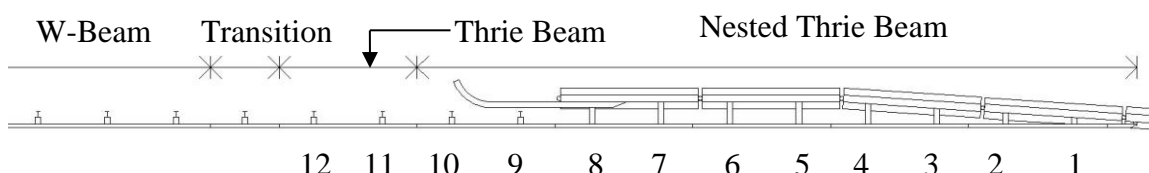
Figure 69. PCB Behind Guardrail with Nested Thrie and Cantilever Beam – Impact Locations

13.2 Vehicle Behavior

The PCBs behind nested thrie beam and cantilever beam configuration captured and redirected the vehicle with no wheel snag on the PCBs, as shown in Table 27. However, the roll angle for impact location no. 1 was 88.7 degrees and had not reached a maximum value prior to conclusion of the simulation. Also, the roll angle for impact location no. 12 was within 20% of the MASH limit. However, upon further inspection, the excessive roll motion was deemed unrealistic and was likely caused by the

exaggerated stiffness of the vehicle's rear suspension when the back end of the vehicle impacted the nested thrie beam. The results were very similar to those observed for the previous configuration, and both were believed capable of safely redirecting the vehicle for all impact locations.

Table 27. Vehicle Behavior Results – PCBs Behind Nested Thrie Beam with Cantilever Beam

Impact Location	Roll	Pitch	Yaw	Wheel Snag on PCBs?
1	88.7°[1]	23.3°[1]	40.3°	No
2	39.4°	19.9°	37.6°	No
3	44.3°	7.9°	33.6°	No
4	25.3°	8.6°	34.4°	No
5	37.8°	7.5°	35.9°	No
6	21.3°	7.9°	34.3°	No
7	28.6°	10.7°	35.6°	No
8	26.0°	8.1°	33.7°	No
9	24.1°	9.4°	35.4°	No
10	48.1°	15.5°	38.5°	No
11	45.3°	11.3°	37.1°	No
12	61.8°	16.7°	41.1°	No
MASH Limits	< 75°	< 75°	N/A	N/A

[1]Maximum value was not reached prior to conclusion of simulation
*Yellow cells denote values within 20% of MASH or recommended limits
*Red cells denote values that exceed MASH or recommended limits

13.3 Occupant Risk

The occupant risk values for the PCBs behind nested thrie beam and cantilever beam configuration revealed two values within 20% of the MASH limits, as shown in Table 28. The maximum longitudinal ORA for impact location nos. 1 and 12 were -16.70 g's and -16.92 g's, respectively. These high ORA values occurred after the vehicle became airborne upon redirection and impacted the ground. Researchers determined that a more stable vehicle capture and redirection was necessary to reduce these high ORA values.

Table 28. Occupant Risk Results – PCBs Behind Nested Thrie Beam with Cantilever Beam

Impact Location	OIV ft/s (m/s)		ORA g's	
	Longitudinal	Lateral	Longitudinal	Lateral
1	-14.80 (-4.51)	-17.33 (-5.28)	-13.09	-16.70
2	-18.90 (-5.76)	-23.13 (-7.05)	-12.88	-13.88
3	-17.65 (-5.38)	-20.37 (-6.21)	4.23	-6.33
4	-17.29 (-5.27)	-20.41 (-6.22)	-5.26	-12.56
5	-16.40 (-5.00)	-19.00 (-5.79)	-5.64	-6.77
6	-18.18 (-5.54)	-20.41 (-6.22)	-4.78	-7.08
7	-19.49 (-5.94)	-17.65 (-5.38)	-6.82	-8.12
8	-17.42 (-5.31)	-20.34 (-6.20)	-4.56	-5.54
9	-19.90 (-5.76)	-18.60 (-5.67)	-6.46	-6.76
10	-17.98 (-5.48)	-20.14 (-6.14)	-4.54	-6.55
11	-19.85 (-6.05)	-19.82 (-6.04)	-8.40	-6.73
12	-19.49 (-5.94)	-18.44 (-5.62)	-16.92	-10.57
MASH Limits	≤ 40 (12.2)	≤ 40 (12.2)	≤ 20.49	≤ 20.49

*Yellow cells denote values within 20% of MASH or recommended limits

13.4 Pocketing Angle

The pocketing angles for all twelve impact locations can be found in Table 29, and none of the maximum pocketing angles exceeded or came within 20% of the recommended value of 23 degrees. When compared to the results from the previous configuration without the cantilever beam, the maximum pocketing angles were not significantly different. Researchers believe that both configurations exhibited a high probability to redirect the vehicle with acceptable pocketing angles.

13.5 Discussion

Upon full investigation of the simulation findings for the PCBs behind nested thrie beam and cantilever beam system, impact location nos. 1 and 12 yielded maximum roll angles that were either in excess of or within 20% of the MASH limits. However, due to unrealistic rear suspension behavior that has plagued this vehicle model in the past, those values would likely be much lower. At impact location nos. 1 and 12, the longitudinal ORA were within 20% of the MASH limit due to the vehicle impacting the ground after becoming airborne. The maximum pocketing angles for all twelve impact locations were very comparable to the results observed for the previous design concept. Thus, the installation of the cantilever beam did not significantly improve the results of the transition and was an unnecessary addition.

Table 29. Pocketing Angle Results – PCBs Behind Nested Thrie Beam with Cantilever Beam

Impact Location	Pocketing		
	Angle	Time (ms)	Location
1	2.8°	100	Centerline of Post No. 5
2	4.7°	150	3 ft – 7.9 in. Upstream of Centerline of Blockout No. 1
3	6.6°	290	3 ft – 7.9 in. Upstream of Centerline of Blockout No. 1
4	9.7°	280	3 ft – 7.9 in. Upstream of Centerline of Blockout No. 1
5	9.2°	360	3 ft – 7.9 in. Upstream of Centerline of Blockout No. 1
6	8.5°	320	2 ft – 9.2 in. Upstream of Centerline of Blockout No. 3
7	8.6°	340	2 ft – 7 in. Downstream of Centerline of Blockout No. 5
8	7.7°	310	2 ft – 9.2 in. Upstream of Centerline of Blockout No. 5
9	8.2°	70	2 ft – 7.1 in. Downstream of Centerline of Post No. 1
10	11.4°	110	2 ft – 7.1 in. Downstream of Centerline of Post No. 1
11	18.3°	110	2 ft – 7.2 in. Downstream of Centerline of Post No. 2
12	15.7°	160	1 ft – 8.5 in. Downstream of Centerline of Post No. 2
Recommended Limits	23.0°	N/A	N/A

CHAPTER 14 SIMULATION RESULTS DISCUSSION

14.1 Introduction

Following simulation of the Flared PCB − Modified G4(1S) design concept, the Parallel PCB − Modified G4(1S) design concept, and subsequent configurations, MwRSF researchers reviewed and ranked each configuration within each design concept based on metrics for vehicle behavior, occupant risk, and rail pocketing. These rankings were presented to and discussed with the TAC for future consideration.

14.2 Flared PCB – Modified G4(1S) Design Concept

The Flared PCB − Modified G4(1S) design concept utilized an attachment of the modified G4(1S) directly to the 15H:1V flared F-shape PCB system using a W-beam end shoe connection. Researchers quickly realized that the modified G4(1S) system lacked the height and stiffness to safely capture and redirect the vehicle without rail pocketing concerns. Thus, a transition to thrie beam was included in the design, which yielded improved vehicle stability. However, posts had a tendency to wedge against the PCBs and caused elevated occupant risk values, and rail pocketing angles were also high. Posts were removed due to their tendency to wedge against PCBs. Blockouts were installed at a standard 6 ft − 3 in. (1,905 mm) post spacing in the next configuration.

The thrie beam with fully-blocked rail configuration yielded results with improved vehicle stability and occupant risk values but with high rail pocketing values. The pocketing behavior was caused by slow displacement of the PCBs at the beginning of the simulation. Therefore, the next configuration included a cantilever beam that was attached to the front face of the PCB system, which was intended to initiate PCB displacement when impacted by rotated posts within the thrie beam system. This

configuration yielded similar vehicle stability and occupant risk values to the configuration without the cantilever beam, but the cantilever beam helped to improve pocketing angles. However, there were still two impact locations that yielded marginal pocketing angles. Thus, researchers nested the thrie beam in front of the PCBs. The nesting of the rail was intended to stiffen the guardrail system ahead of the PCB system and lower the rail pocketing angles.

The nested thrie beam with fully-blocked rail configuration yielded improved pocketing angles, and only one impact location had a pocketing angle of marginal concern. Based on these results, the Flared PCB − Modified G4(1S) configurations were ranked, as shown below:

  (1) Nested Thrie Beam with Fully-Blocked Rail;

  (2) Thrie Beam with Fully-Blocked Rail and Cantilever Beam;

  (3) Thrie Beam End Shoe;

  (4) Thrie Beam with Fully-Blocked Rail; and

  (5) Modified G4(1S) End Shoe.

14.3 Parallel PCB − Modified G4(1S) Design Concept

The Parallel PCB − Modified G4(1S) design concept involved the modified G4(1S) guardrail system attaching to the 15H:1V flared PCB system with two PCB segments placed parallel to and behind the modified G4(1S) system. The guardrail posts within the modified G4(1S) system remained in front of PCB segments placed parallel to and behind the guardrail and were intended to initiate PCB displacement after rotation. Based on findings obtained for the first design concept and using engineering judgment, modifications were implemented into the initial configuration. The rail height of the

modified G4(1S) guardrail system proved incapable of vehicle capture and redirection, and it was transitioned to thrie beam. Also, the single thrie beam yielded high rail pocketing angles, so nested thrie beam was installed in front of the PCB system. Also, guardrail posts installed in front of the PCB system showed a tendency to wedge against PCBs and cause vehicle instabilities as well as elevated occupant risk values. Therefore, all of the guardrail posts installed in front of PCBs were removed, and blockouts were installed behind the nested thrie beam at standard 6 ft − 3 in. (1,905 mm) centers. The nested thrie beam with fully-blocked rail configuration yielded two marginal longitudinal ORA values but with acceptable vehicle stability and rail pocketing angles. In an attempt to improve the simulation results, a cantilever beam was installed to the front face of the most upstream PCB. This configuration yielded similar results for the vehicle behavior, occupant risk, and rail pocketing. Thus, it was concluded that the cantilever beam did not significantly improve the transition system and should not be used. Therefore, the Parallel PCB − Modified G4(1S) configurations were ranked in this order:

(1) PCBs Behind Nested Thrie Beam and

(2) PCBs Behind Nested Thrie Beam with Cantilever Beam.

14.4 Transition Design Discussion

These findings were presented to the TAC members. It was recommended that both the nested thrie beam with fully-blocked rail design concept and the PCBs behind nested thrie beam design concept would have a high likelihood of successfully meeting TL-3 of MASH. It was also noted that the thrie beam with fully-blocked rail and cantilever beam, thrie beam end shoe connection, and thrie beam with fully-blocked rail design concepts along with the PCBs behind nested thrie beam with cantilever beam

design concept had a marginal likelihood of meeting TL-3 of MASH. Finally, the W-beam end shoe connection design concept had a low likelihood of meeting TL-3 of MASH.

Once the simulation results for the first two design concepts were presented to the TAC members with rankings and recommendations, a discussion about feasibility and complexity followed. It was voiced by the TAC members that the some of the designs were overly complex and labor intensive. Therefore, the TAC members recommended that the modified G4(1S) be replaced with MGS. It was predicted that the taller top mounting height of the MGS would aid in vehicle capture and redirection and not require a transition to thrie beam. Other TAC recommendations included the installation of blockouts to the back of the guardrail posts installed in front of the PCB system in order to engage the PCBs earlier in the impact event and initiate PCB displacement. Another TAC recommendation was to install a blockout from the back of the guardrail post to the front of the cantilever beam. Therefore, a simulation study was conducted on a transition system that included MGS instead of modified G4(1S) guardrail.

14.5 Flared PCB – MGS Design Concept

Based on the concern that was expressed about the complexity of installing thrie beam, nested rail, and a cantilever beam in the first two design concepts, researchers explored the option of using the 31-in. (787-mm) tall Midwest Guardrail System (MGS). Researchers believed that an increased top rail height would improve vehicle capture and redirection. Similar to the Flared PCB – Modified G4(1S) design concept, the MGS was attached to the 15VH:1 flared F-shape PCB system using a W-beam end shoe connection. The 15H:1V flared PCB system extended behind the guardrail system, as shown in

Figure 70. The two posts that remained in front of the PCBs were intended to aid in PCB displacement. Upon impact, the posts were expected to rotate backward into the PCBs and initiate PCB displacement, which would reduce vehicle climb and instabilities. Based on the results, several modifications could be made to the transition system to improve its likelihood of success. These modifications included: blockouts installed from back of guardrail posts to PCBs; installation of a cantilever beam to front face of most upstream PCB; a blockout installed from the back of guardrail post to cantilever beam; nesting of rail components; removal of posts in front of PCBs; and installation of blockouts between rail and PCBs.
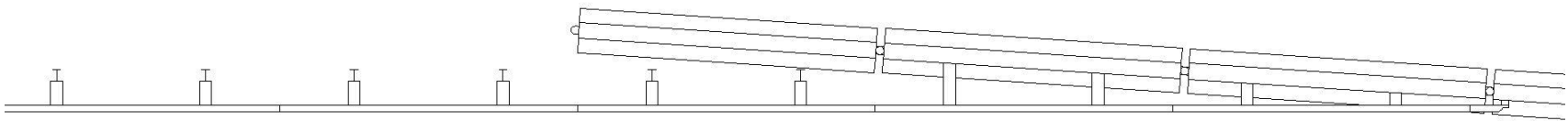
Notes:
(1) Blockouts may be installed from back of guardrail posts to PCBs.
(2) Cantilever beam may be installed on most upstream PCB.
(3) Blockout may be installed from back of guardrail post to cantilever beam.
(4) Nesting of rail components may be required.
(5) May require blockouts between W-beam guardrail and PCBs where post removal was required.

Figure 70. Flared PCB – MGS Design Concept

147

CHAPTER 15 MIDWEST GUARDRAIL SYSTEM (MGS) END SHOE

15.1 Introduction

A third design concept was pursued using the Midwest Guardrail System (MGS) in the place of the modified G4(1S) guardrail and thrie beam systems. The 31-in. (787-mm) high MGS with 12-in. (305-mm) deep blockouts was attached to the fourth F-shape PCB segment using the 30-in. (762-mm) long W-beam end shoe connection. Two guardrail posts remained in front of the PCB system, and blockouts were installed on 6 ft – 3 in. (1,905 mm) centers between the rail and PCBs where posts interfered with PCB placement and were removed. The layout of the MGS end shoe configuration and ten impact locations are shown in Figure 71.
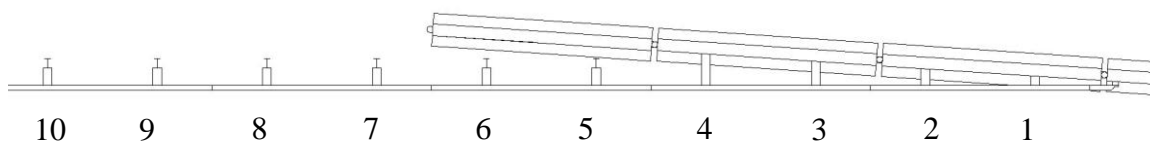
Figure 71. MGS End Shoe – Impact Locations

15.2 Vehicle Behavior

The MGS end shoe configuration captured and redirected the vehicle for all ten impact locations, and none of the roll, pitch, or yaw angles exceeded or were within 20% of the MASH limits, as shown in Table 30. Wheel snag on the PCB was found at impact location nos. 8 and 9. While, there is no criterion associated with wheel snag on the PCBs, it was monitored because prior testing has indicated that wheel snag can lead to vehicle instabilities and increased decelerations. In this configuration, wheel snag was minor and did not cause vehicle instability or excessive deceleration. Thus, the MGS end shoe configuration would likely meet the TL-3 MASH criteria in terms of vehicle stability.

Table 30. Vehicle Behavior Results – MGS End Shoe

Impact Location	Roll	Pitch	Yaw	Wheel Snag on PCBs?
1	49.9°[1]	40.6°[1]	40.7°	No
2	26.5°	14.0°	42.8°[1]	No
3	7.7°	9.6°	46.9°[1]	No
4	8.1°	8.8°	47.2°[1]	No
5	6.0°	6.5°	29.1°[1]	No
6	4.6°	8.2°	38.6°[1]	No
7	6.2°	5.4°	41.8°	No
8	9.9°	9.3°	42.7°[1]	Yes
9	16.8°	10.8°	47.2°	Yes
10	12.0°	8.8°	43.5°[1]	No
MASH Limits	< 75°	< 75°	N/A	N/A

[1]Maximum value was not reached prior to conclusion of simulation
*Yellow cells denote values within 20% of MASH or recommended limits

15.3 Occupant Risk

The occupant risk evaluation for the MGS end shoe configuration yielded results with two values within 20% of the MASH limits, as shown in Table 31. The maximum OIVs for impact location nos. 3 and 5 were -32.55 ft/s (-9.92 m/s) and -35.66 ft/s (-10.87 m/s) respectively. Due to the higher rail height of the MGS, the bumper of the pickup truck protruded underneath the W-beam rail upon impact. As the vehicle deformed the MGS, the wheel engaged the F-shape PCB system. This contact led to vehicle climb up the PCB face, which caused the bumper to lift and twist the W-beam as well as allowed

vehicle snag on the blockouts in front of the PCBs, as shown in Figure 72. This twisting and lifting of the W-beam guardrail caused concern for rail rupture and system failure. This behavior was not seen in either the modified G4(1S) or thrie beam configurations, because neither allowed the vehicle's bumper to protrude underneath the rail.

Table 31. Occupant Risk Results – MGS End Shoe

Impact Location	OIV ft/s (m/s)		ORA g's	
	Longitudinal	Lateral	Longitudinal	Lateral
1	-19.23 (-5.86)	-19.00 (-5.79)	-12.18	-9.95
2	-27.26 (-8.31)	-20.01 (-6.10)	-5.74	-9.63
3	-32.55 (-9.92)	-16.86 (-5.14)	-10.94	-8.70
4	-30.15 (-9.19)	-18.37 (-5.60)	-8.59	-7.60
5	-35.66 (-10.87)	-17.16 (-5.23)	-10.35	-8.30
6	-27.43 (-8.36)	-16.47 (-5.02)	-15.32	-10.73
7	-22.87 (-6.97)	-17.65 (-5.38)	-9.75	-8.75
8	-20.96 (-6.39)	-19.88 (-6.06)	-15.36	-9.06
9	-15.42 (-4.70)	-16.83 (-5.13)	-11.57	-11.28
10	-15.29 (-4.66)	-16.80 (-5.12)	-9.27	-9.13
MASH Limits	≤ 40 (12.2)	≤ 40 (12.2)	≤ 20.49	≤ 20.49

*Yellow cells denote values within 20% of MASH or recommended limits
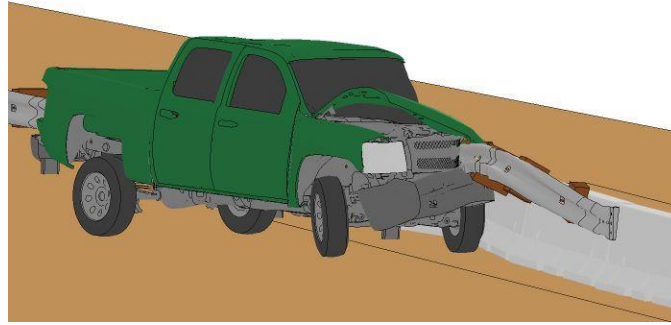
Figure 72. W-Beam Lifting and Twisting for Impact Location No. 5 at 140 ms

15.4 Pocketing Angle

The pocketing angles for all ten impact locations can be found in Table 32, and the maximum pocketing angles for all of the impact locations upstream of the PCB system either exceeded or were within 20% of the recommended value of 23 degrees. Upon impact, the guardrail posts began to rotate, and the two posts located in front of the PCBs rotated and contacted the PCBs. While this post rotation initiated PC displacement, it also severely slowed the post rotation, which caused high pocketing angles, as shown in Figure 73.

Table 32. Pocketing Angle Results – MGS End Shoe

Impact Location	Pocketing		
	Angle	Time (ms)	Location
1	1.0°	60	Centerline of Post No. 1
2	11.5°	60	2 ft – 6.8 in. Downstream of Centerline of Blockout No. 2
3	14.6°	60	2 ft – 10.0 in. Upstream of Centerline of Blockout No. 2
4	15.2°	70	2 ft – 9.5 in. Upstream of Centerline of Blockout No. 3
5	16.8°	70	3 ft – 6.0 in. Downstream of Centerline of Post No. 1
6	17.9°	120	2 ft – 7.4 in. Downstream of Centerline of Post No. 1
7	21.3°	120	2 ft – 6.8 in. Downstream of Centerline of Post No. 2
8	21.3°	130	2 ft – 9.0 in. Upstream of Centerline of Post No. 2
9	24.7°	200	2 ft – 7.4 in. Downstream of Centerline of Post No. 3
10	19.9°	270	2 ft – 7.4 in. Downstream of Centerline of Post No. 3
Recommended Limits	23.0°	N/A	N/A

*Yellow cells denote values within 20% of MASH or recommended limits
*Red cells denote values that exceed MASH or recommended limits
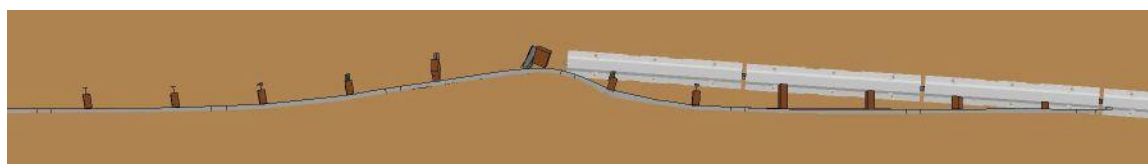
Figure 73. Pocketing Angle for Impact Location No. 9 at 200 ms

15.5 Discussion

Upon full investigation of the simulation findings for MGS end shoe configuration, it was determined that the taller MGS improved vehicle engagement and yielded much lower vehicle stability values than observed for both the modified G4(1S) and thrie beam systems. However, at impact location nos. 3 and 5, the longitudinal OIVs were within 20% of the MASH limit, which was caused by vehicle snag on the blockouts and lifting and twisting of the W-beam. This lifting and twisting of the W-beam guardrail had potential to result in rail rupture. The four impact locations upstream from the PCB system yielded maximum pocketing angles either in excess or within 20% of the recommended value of 23 degrees. Based on these findings, it was determined that the MGS end shoe configuration had a marginal chance of success. There were pocketing and occupant risk concerns for this system, so researchers explored options to reduce both issues.

CHAPTER 16 MGS WITH BLOCKOUTS BEHIND POSTS

16.1 Introduction

Inertial resistance of the PCB system and subsequent vehicle pocketing were the primary concerns for the MGS end shoe configuration. Blockouts were added to the back of two guardrail posts installed in front of the PCBs. By eliminating the gap between the guardrail posts and face of the PCBs, the PCBs were predicted to begin displacing earlier in the impact event. The layout for the MGS with blockouts behind posts configuration and ten impact locations are shown in Figure 74.
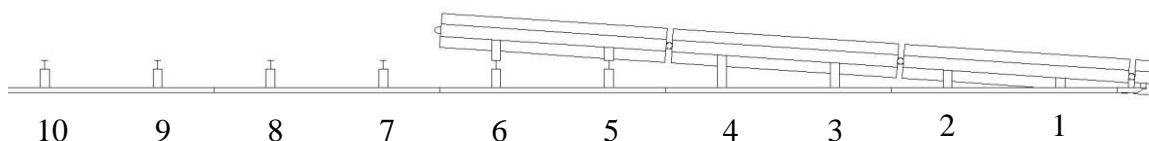
Figure 74. MGS with Blockouts Behind Posts – Impact Locations

16.2 Model Modifications

16.2.1 Blockouts behind Posts

One blockout was installed from the back of each of the two guardrail posts installed in front of the PCB system. The geometry of the blockouts required a 5.81-degree vertical taper along with a 3.81-degree longitudinal cut similar to the blockouts shown in Figure 60. The two blockouts were 6 in. (152 mm) wide x 14¼ in. (362 mm) long and had depths of 13½ in. (343 mm) and 8½ in. (216 mm), as shown in Figure 75.
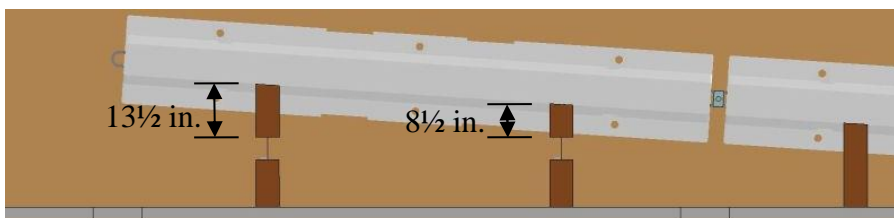
Figure 75. Blockouts Behind Posts Depths

The blockouts were made of the same simplified wood material as used in the previous blockouts. Due to modeling limitations and complex fracture mechanics of

wood, failure was not defined for these blockouts. The blockouts were rigidly attached to the backside of the posts using spotwelds with no failure criteria. The blockouts were not attached to the PCBs as they were intended to initiate displacement but not provide continuity between the two systems.

16.3 Vehicle Behavior

The MGS with blockouts behind posts configuration captured and redirected the vehicle for all ten impact locations, and none of the roll, pitch, or yaw angles exceeded or were within 20% of the MASH limits, as shown in Table 33. Wheel snag on the PCBs was found at impact location no. 8. The wheel snag was minor and did not cause vehicle instability or excessive deceleration.

Table 33. Vehicle Behavior Results – MGS with Blockouts Behind Posts

Impact Location	Roll	Pitch	Yaw	Wheel Snag on PCBs?
1	37.3°	30.3°[1]	40.3°	No
2	19.2°[1]	13.4°	48.8°[1]	No
3	7.1°	9.4°	46.4°[1]	No
4	7.3°	9.6°	26.8°	No
5	7.8°	7.7°	30.8°[1]	No
6	7.7°	6.5°	34.8°[1]	No
7	6.9°	12.2°	57.1°[1]	No
8	7.7°	11.5°	46.2°[1]	Yes
9	14.9°	7.8°	41.9°[1]	No
10	13.0°	8.2°	45.2°[1]	No
MASH Limits	< 75°	< 75°	N/A	N/A

[1]Maximum value was not reached prior to conclusion of simulation
*Yellow cells denote values within 20% of MASH or recommended limits

16.4 Occupant Risk

The occupant risk evaluation for the MGS with blockouts behind posts configuration yielded five values within 20% of the MASH limits, as shown in Table 34. The maximum longitudinal OIVs for impact location nos. 3, 4, and 5 were -32.05 ft/s (-9.77 m/s), -32.45 ft/s (-9.89 m/s), and -33.01 ft/s (-10.06 m/s) respectively. Also, the maximum ORAs for impact location nos. 7 and 8 were -17.21 g's and -19.55 g's, respectively. These elevated ORAs occurred after the vehicle's bumper protruded underneath the W-beam with the wheel engaged with the PCBs and causing vehicle climb. The vehicle climb caused lifting and twisting of the rail as well as vehicle snag on the blockouts between the rail and the PCBs. This twisting and lifting of the W-beam guardrail also caused concern for rail rupture and system failure.

Table 34. Occupant Risk Results – MGS with Blockouts Behind Posts

Impact Location	OIV ft/s (m/s)		ORA g's	
	Longitudinal	Lateral	Longitudinal	Lateral
1	-19.49 (-5.94)	-18.83 (-5.74)	12.79	-10.30
2	-27.99 (-8.53)	-20.57 (-6.27)	-8.28	-9.61
3	-32.05 (-9.77)	-17.65 (-5.38)	-9.63	-10.43
4	-32.45 (-9.89)	-16.99 (-5.18)	-10.03	-7.22
5	-33.01 (-10.06)	-17.62 (-5.37)	-11.08	5.84
6	-23.95 (-7.30)	-15.85 (-4.83)	-15.31	-7.22
7	-27.10 (-8.26)	-19.75 (-6.02)	-17.21	-8.13
8	-20.11 (-6.13)	-18.27 (-5.57)	-19.55	-9.48
9	-16.27 (-4.96)	-17.85 (-5.44)	-9.88	-7.40
10	-15.65 (-4.77)	-17.09 (-5.21)	-8.32	-8.40
MASH Limits	≤ 40 (12.2)	≤ 40 (12.2)	≤ 20.49	≤ 20.49

*Yellow cells denote values within 20% of MASH or recommended limits

16.5 Pocketing Angle

The pocketing angles for all ten impact locations can be found in Table 35, and the maximum pocketing angles for all of the impact locations upstream of the PCB system either exceeded or were within 20% of the recommended value of 23 degrees. The blockouts on the backside of the guardrail posts and placed in front of the PCBs were installed in order to initiate PCB displacement earlier in the impact event. However, these blockouts created a stiffened area, which actually increased the majority of the maximum pocketing angles.

Table 35. Pocketing Angle Results – MGS with Blockouts Behind Posts

Impact Location	Pocketing		
	Angle	Time (ms)	Location
1	1.0°	60	Centerline of Post No. 1
2	11.6°	60	2 ft – 6.8 in. Downstream of Centerline of Blockout No. 2
3	14.6°	60	2 ft – 10.0 in. Upstream of the Centerline of Blockout No. 2
4	15.0°	70	2 ft – 9.5 in. Upstream of Centerline of Blockout No. 3
5	15.6°	60	3 ft – 6.0 in. Downstream of Centerline of Post No. 1
6	16.2°	140	2 ft – 7.4 in. Downstream of Centerline of Post No. 1
7	27.3°	120	2 ft – 6.8 in. Downstream of Centerline of Post No. 1
8	26.2°	110	2 ft – 7.4 in. Downstream of Centerline of Post No. 3
9	28.6°	190	2 ft – 7.4 in. Downstream of Centerline of Post No. 3
10	19.6°	280	2 ft – 7.4 in. Downstream of Centerline of Post No. 3
Recommended Limits	23.0°	N/A	N/A

*Yellow cells denote values within 20% of MASH or recommended limits
*Red cells denote values that exceed MASH or recommended limits

The maximum pocketing angle at impact location no. 9 was 28.6 degrees, which was well above the recommended value of 23 degrees. The maximum pocketing angles were increased with the blockout installation; since, these posts must overcome both the post-soil forces and PCB inertia prior to the initiating PCB displacement. The delay in PCB displacement allowed the vehicle to greatly deform the MGS and pocketed within

the guardrail upstream from the PCB system before the PCBs began to displace. The sequentials of impact location no. 9, as shown in Figure 76, indicate that the PCBs had not begun to displace at 100 ms after impact. By 200 ms, the vehicle is near the upstream end of the PCB system, and the maximum vehicle pocketing has occurred, while the PCBs have just begun displacing.

16.6 Discussion

Upon full investigation of the simulation findings for the MGS with blockouts behind posts configuration, it was determined that blockout installation between the backside of guardrail posts and the PCBs increased occupant risk values as well as maximum pocketing angles. At impact location nos. 3, 4, and 5, the longitudinal OIVs were within 20% of the MASH limit. Also, at impact location nos. 7 and 8, the longitudinal ORAs were within 20% of the MASH limits. The four impact locations upstream from the PCB system yielded maximum pocketing angles either in excess or within 20% of the recommended value of 23 degrees. Based on these findings, it was determined that blockouts placed behind posts increased the likelihood of failure for the transition and thus were not recommended. Researchers continued to explore other options to initiate PCB displacement earlier in the impact event.

0 ms
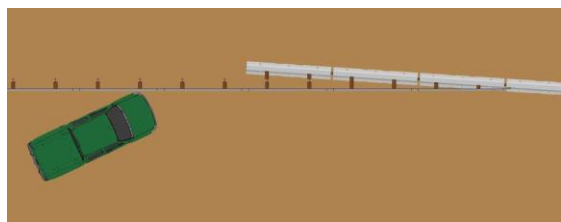
100 ms

200 ms

300 ms

400 ms

500 ms
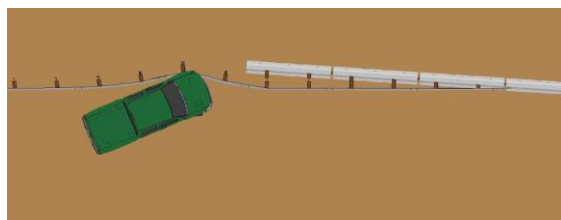
600 ms

700 ms

800 ms
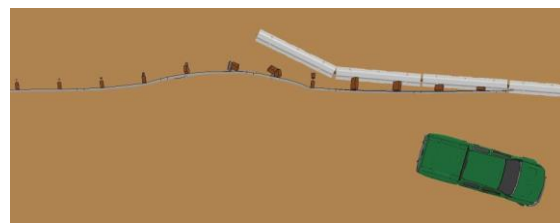
900 ms

Figure 76. MGS with Blockouts Behind Posts Sequentials, Impact Location No. 9

CHAPTER 17 MGS WITH CANTILEVER BEAM

17.1 Introduction

Previously, the installation of a cantilever beam on the upstream PCB had demonstrated some success in reducing pocketing concerns in the Flared PCB − Modified G4(1S) design concept. Thus, a cantilever beam was installed to the most upstream PCB to investigate if it improved the performance of the transition. This configuration utilized an MGS system with W-beam end shoe connected to the fourth PCB segment with two guardrail posts installed in front of the PCB system, blockouts installed at 6 ft − 3 in. (1,905 mm) centers, and a cantilever beam attached to the most upstream PCB. The configuration, as shown in Figure 77, was impacted at the same ten impact locations as previously used. The cantilever beam conformed to the same 15-ft (4,572-mm) long section that was previously used.
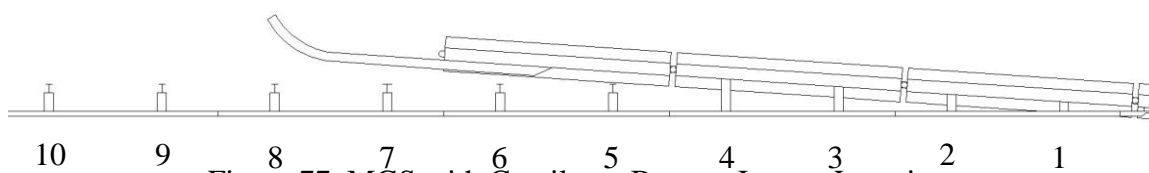
Figure 77. MGS with Cantilever Beam − Impact Locations

17.2 Vehicle Behavior

The MGS with cantilever beam configuration captured and redirected the vehicle for all ten impact locations, and none of the roll, pitch, or yaw angles exceeded or were within 20% of the MASH limits, as shown in Table 36. It was also found that there was no wheel snag on the upstream end of the PCB system. Therefore, researchers determined that the MGS with cantilever beam configuration would likely meet the TL-3 MASH criteria for vehicle stability.

Table 36. Vehicle Behavior Results – MGS with Cantilever Beam

Impact Location	Roll	Pitch	Yaw	Wheel Snag on PCBs?
1	47.6°	43.1°[1]	40.8°	No
2	12.3°	11.4°	39.9°	No
3	8.0°	10.0°	51.8°[1]	No
4	10.7°[1]	10.2°	46.2°[1]	No
5	6.7°	7.9°	31.0°[1]	No
6	5.0°[1]	8.2°	38.6°[1]	No
7	7.9°	9.6°	42.3°	No
8	7.6°	9.1°	43.4°[1]	No
9	9.4°	7.1°	47.3°[1]	No
10	14.5°	8.7°	41.7°[1]	No
MASH Limits	< 75°	< 75°	N/A	N/A

[1]Maximum value was not reached prior to conclusion of simulation

17.3 Occupant Risk

The simulation results for the MGS with cantilever beam configuration showed only one impact location with an occupant risk value within 20% of the MASH limits, as shown in Table 37. The maximum longitudinal OIV for impact location no. 5 was -36.52 ft/s (-11.13 m/s). This elevated OIV occurred after the vehicle's bumper protruded underneath the MGS and allowed the wheel to engage the PCBs, thus causing vehicle climb. The vehicle climb caused lifting and twisting of the rail as well as vehicle snag on the blockouts between the rail and PCBs. This twisting and lifting of the W-beam guardrail caused concern for rail rupture and system failure.

Table 37. Occupant Risk Results – MGS with Cantilever Beam

Impact Location	OIV ft/s (m/s)		ORA g's	
	Longitudinal	Lateral	Longitudinal	Lateral
1	-19.39 (-5.91)	-18.96 (-5.78)	-9.92	-7.71
2	-27.76 (-8.46)	-20.28 (-6.18)	-7.10	-10.26
3	-27.66 (-8.43)	-16.50 (-5.03)	-12.84	-6.85
4	-30.25 (-9.22)	-17.19 (-5.24)	-6.87	-7.34
5	-36.52 (-11.13)	-17.13 (-5.22)	-13.75	-9.08
6	-27.46 (-8.37)	-16.21 (-4.94)	-12.94	-8.77
7	-31.30 (-9.54)	-14.44 (-4.40)	-16.30	-11.94
8	-19.68 (-6.00)	-18.24 (-5.56)	-13.88	-11.02
9	-21.33 (-6.50)	-18.08 (-5.51)	-12.17	-8.93
10	-15.03 (-4.58)	-16.86 (-5.14)	-12.62	-11.48
MASH Limits	≤ 40 (12.2)	≤ 40 (12.2)	≤ 20.49	≤ 20.49

*Yellow cells denote values within 20% of MASH or recommended limits

17.4 Pocketing Angle

The pocketing angles for all ten impact locations can be found in Table 38. The maximum pocketing angles for the impact locations upstream from the PCB system either exceeded or were within 20% of the recommended value. While these values are concerning, the collective results show that the cantilever beam helped to lower

pocketing angles at almost every impact location over what was observed for the two previous MGS configurations.

Table 38. Pocketing Angle Results – MGS with Cantilever Beam

Impact Location	Pocketing		
	Angle	Time (ms)	Location
1	1.0°	120	Centerline of Post No. 1
2	11.6°	60	2 ft – 6.8 in. Downstream of Centerline of Blockout No. 2
3	14.6°	60	2 ft – 10.0 in. Upstream of Centerline of Blockout No. 2
4	15.1°	70	2 ft – 9.5 in. Upstream of Centerline of Blockout No. 3
5	16.8°	70	3 ft – 6.0 in. Downstream of Centerline of Post No. 1
6	17.8°	120	2 ft – 7.4 in. Downstream of Centerline of Post No. 1
7	19.0°	130	2 ft – 6.8 in. Downstream of Centerline of Post No. 2
8	21.3°	220	2 ft – 6.8 in. Downstream of Centerline of Post No. 2
9	20.8°	120	2 ft – 6.8 in. Downstream of Centerline of Post No. 4
10	24.0°	190	2 ft – 6.8 in. Downstream of Centerline of Post No. 4
Recommended Limits	23.0°	N/A	N/A

*Yellow cells denote values within 20% of MASH or recommended limits
*Red cells denote values that exceed MASH or recommended limits

17.5 Discussion

Upon full investigation of the simulation findings for the MGS with cantilever beam configuration, the cantilever beam was found to reduce occupant risk values and

pocketing angles. Only impact location no. 5 had a longitudinal OIV within 20% of the MASH limit. Also, the four impact locations upstream from the PCB system still yielded pocketing angles either in excess or within 20% of the recommended value of 23 degrees. Based on these findings, the MGS with cantilever beam configuration had the highest propensity for successfully meeting TL-3 of MASH out of the MGS configurations thus far. However, other options were explored to initiate PCB displacement earlier in the impact event and reduce pocketing angles.

CHAPTER 18 MGS WITH BLOCKOUT TO CANTILEVER BEAM

18.1 Introduction

The MGS with cantilever beam configuration showed that the installation of a cantilever beam aided in reducing pocketing angles. Thus, it was further explored with modifications. The greatest pocketing concerns occurred at impact locations upstream from the PCB system, which were related to delayed PCB displacement. A blockout was installed to the backside of the guardrail post located in front of the cantilever beam in order to engage it earlier in the impact event. The configuration layout, as shown in Figure 78, was impacted at the same ten impact locations as previously used.
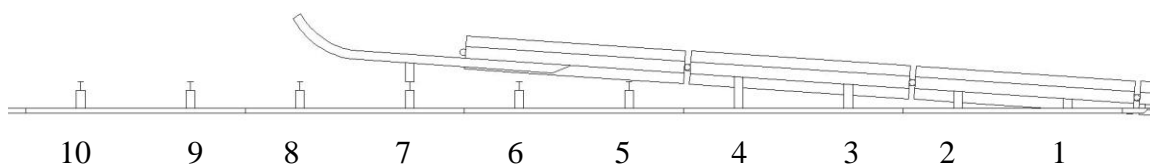
Figure 78. MGS with Blockout to Cantilever Beam – Impact Locations

18.2 Model Modifications

18.2.1 Blockout to Cantilever Beam

One blockout was installed between the back of the guardrail post and to the front of the cantilever beam, which was attached to the most upstream PCB. The geometry of the spacer blocks required a 5.81-degree vertical taper along with a 3.81-degree longitudinal cut similar to the blockouts shown in Figure 60. The blockout was 6 in. (152 mm) wide x 14¼ in. (362 mm) long and had a depth of 12½ in. (343 mm), as shown in Figure 79.
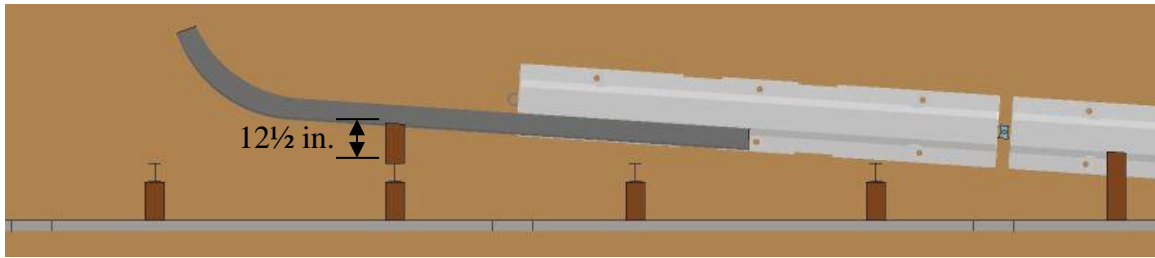
Figure 79. Blockout to Cantilever Beam Depth

The blockout was made of the same simplified wood material as used for the previous blockouts. Due to modeling limitations and complex fracture mechanics of wood, failure was not defined for this blockout. The blockout was rigidly attached to the backside of the post using spotwelds without failure criteria. The blockout was not attached to the cantilever beam as it was intended to initiate PCB displacement and not provide continuity between the two barrier systems.

18.3 Vehicle Behavior

The MGS with a blockout to the cantilever beam configuration captured and redirected the vehicle for all ten impact locations, and none of the roll, pitch, or yaw angles exceeded or were within 20% of the MASH limits, as shown in Table 39. No wheel snag was found on the upstream end of the PCB system. Therefore, the MGS with a blockout to the cantilever beam configuration would likely meet the TL-3 MASH criteria for vehicle stability.

Table 39. Vehicle Behavior Results – MGS with Blockout to Cantilever Beam

Impact Location	Roll	Pitch	Yaw	Wheel Snag on PCBs?
1	44.0°	40.7°[1]	40.4°	No
2	24.4°	14.6°	40.8°[1]	No
3	9.0°	12.6°[1]	55.4°[1]	No
4	6.9°	9.2°	33.1°[1]	No
5	8.6°	9.8°	15.4°	No
6	5.5°	9.2°	38.8°[1]	No
7	9.1°	7.1°	40.6°	No
8	12.8°	10.9°	42.8°[1]	No
9	10.9°	7.4°	44.8°[1]	No
10	13.3°	9.0°	41.9°[1]	No
MASH Limits	< 75°	< 75°	N/A	N/A

[1]Maximum value was not reached prior to conclusion of simulation

18.4 Occupant Risk

The occupant risk results for the MGS with a blockout to the cantilever beam configuration yielded one value within 20% of the MASH limits, as shown in Table 40. The maximum longitudinal OIV for impact location no. 5 was -35.99 ft/s (-10.97 m/s). This elevated OIV occurred after the vehicle's bumper protruded underneath the W-beam rail and allowed the wheel to engage the PCBs, thus causing vehicle climb. The vehicle climb caused lifting and twisting of the rail as well as vehicle snag on the blockouts between the rail and PCBs. This twisting and lifting of the W-beam guardrail caused concern for rail rupture and system failure.

Table 40. Occupant Risk Results – MGS with Blockout to Cantilever Beam

Impact Location	OIV ft/s (m/s)		ORA g's	
	Longitudinal	Lateral	Longitudinal	Lateral
1	-19.23 (-5.86)	-18.83 (-5.74)	-11.75	-9.10
2	-27.36 (-8.34)	-20.11 (-6.13)	9.67	-9.55
3	-29.92 (-9.12)	-16.44 (-5.01)	-10.82	-6.80
4	-29.99 (-9.14)	-17.85 (-5.44)	-8.70	-7.97
5	-35.99 (-10.97)	-17.03 (-5.19)	-9.41	-5.50
6	-27.69 (-8.44)	-15.72 (-4.79)	-11.30	-10.45
7	-20.47 (-6.24)	-17.95 (-5.47)	-10.65	-7.01
8	-22.08 (-6.73)	-17.13 (-5.22)	-15.86	-11.40
9	-18.27 (-5.57)	-17.49 (-5.33)	-10.86	-7.69
10	-15.68 (-4.78)	-17.45 (-5.32)	-10.26	-8.59
MASH Limits	≤ 40 (12.2)	≤ 40 (12.2)	≤ 20.49	≤ 20.49

*Yellow cells denote values within 20% of MASH or recommended limits

18.5 Pocketing Angle

The pocketing angles for all ten impact locations can be found in Table 41, and the pocketing angles for all of the impact locations upstream from the PCB system either exceeded or were within 20% of the recommended value of 23 degrees. For the most

part, the blockout installation between the back of the guardrail post and the front of the

cantilever beam caused the pocketing angles to increase instead of decrease.

Table 41. Pocketing Angle Results – MGS with Blockout to Cantilever Beam

Impact Location	Pocketing		
	Angle	Time (ms)	Location
1	1.0°	160	Centerline of Post No. 1
2	11.5°	60	2 ft – 6.8 in. Downstream of Centerline of Blockout No. 2
3	14.6°	60	2 ft – 10.0 in. Upstream of Centerline of Blockout No. 2
4	15.2°	70	2 ft – 9.5 in. Upstream of Centerline of Blockout No. 3
5	16.8°	70	3 ft – 6.0 in. Downstream of Centerline of Post No. 1
6	18.1°	130	2 ft – 7.4 in. Downstream of Centerline of Post No. 1
7	20.8°	120	2 ft – 6.8 in. Downstream of Centerline of Post No. 2
8	20.6°	200	2 ft – 6.8 in. Downstream of Centerline of Post No. 2
9	24.4°	110	2 ft – 6.8 in. Downstream of Centerline of Post No. 4
10	26.0°	190	2 ft – 6.8 in. Downstream of Centerline of Post No. 4
Recommended Limits	23.0°	N/A	N/A

*Yellow cells denote values within 20% of MASH or recommended limits
*Red cells denote values that exceed MASH or recommended limits

The maximum pocketing angle at impact location no. 9 was 26.0 degrees which is

well above the recommended value of 23 degrees. Similar to the MGS with blockouts

behind the posts transition system and as found in Chapter 16, the maximum pocketing

angles increased because the blockout installation stiffened the system; since, the post must overcome both the post-soil forces and PCB inertia prior to deflection. When the vehicle impacted upstream from the blockout that was attached to the cantilever beam, the rotation of the guardrail post was slowed or resisted. The sequentials for impact location no. 10, as shown in Figure 80, indicate that the PCBs had not begun to displace at 100 ms after impact. By 200 ms, the vehicle is just upstream from the cantilever beam, PCBs have just begun to displace, and the maximum pocketing angle of 26.0 degrees had occurred.

18.6 Discussion

Upon full investigation of the simulation findings for the MGS with blockout to cantilever beam configuration, the addition of the blockout had a negative effect on performance even though the cantilever beam helped reduce occupant risk values and pocketing angles. Three of the four impact locations upstream from the PCB system yielded higher pocketing angles than observed with the cantilever beam alone. Based on these findings, the blockout installation between the back of a guardrail post and to the front of the cantilever beam was not recommended for further testing and evaluation. Therefore, other options were explored to initiate PCB displacement earlier in the impact event and reduce pocketing angles.

0 ms

500 ms

100 ms

600 ms

200 ms

700 ms

400 ms

800 ms

400 ms

900 ms
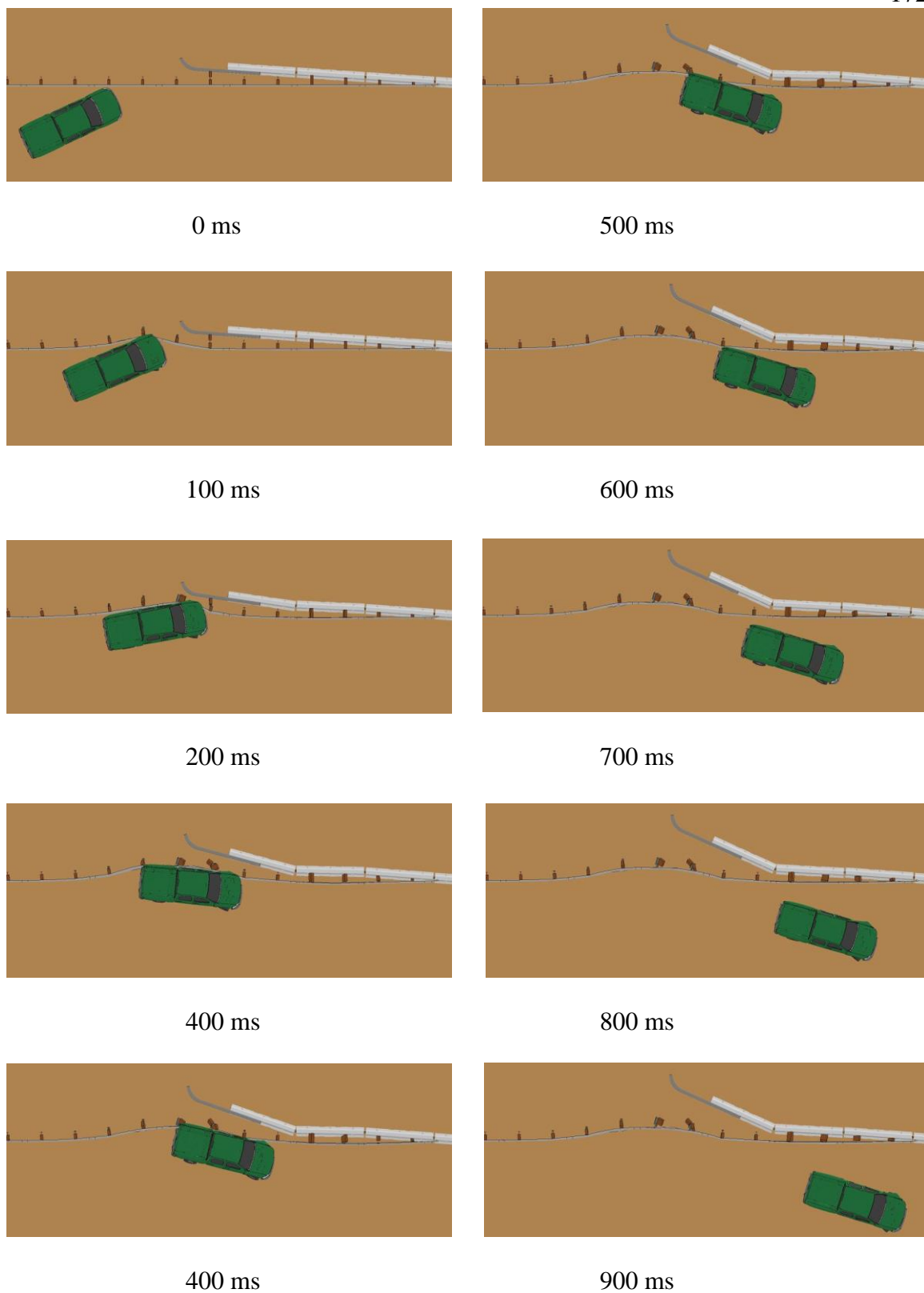
Figure 80. MGS with Blockout to Cantilever Beam Sequentials, Impact Location No. 10

CHAPTER 19 NESTED MGS

19.1 Introduction

While the installation of a cantilever beam to the most upstream PCB was successful in reducing pocketing angles, some pocketing angles still exceeded or within 20% of the recommended value of 23 degrees for impact locations upstream from the PCB system. Therefore, nested MGS was considered in front of the PCB system in order to further stiffen the guardrail ahead of the PCBs and help reduce rail pocketing. The nested MGS layout and ten impact locations are shown in Figure 81.
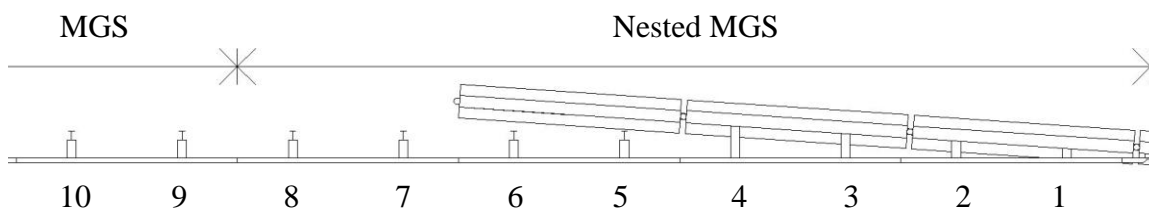
Figure 81. Nested MGS – Impact Locations

19.2 Vehicle Behavior

The nested MGS configuration captured and redirected the vehicle for all ten impact locations, and none of the roll, pitch, or yaw angles exceeded or were within 20% of the MASH limits, as shown in Table 42. No wheel snag on the PCBs was found. Therefore, the nested MGS configuration would likely meet the TL-3 MASH criteria for vehicle stability.

Table 42. Vehicle Behavior Results – Nested MGS

Impact Location	Roll	Pitch	Yaw	Wheel Snag on PCBs?
1	42.7°	26.0°	42.4°	No
2	25.3°	13.9°	35.9°[1]	No
3	42.8°	14.7°	38.5°	No
4	26.1°	9.7°	40.9°	No
5	5.2°	6.2°	36.4°[1]	No
6	14.7°	7.8°	35.6°[1]	No
7	17.8°	5.8°	37.2°[1]	No
8	25.3°	8.2°	40.0°[1]	No
9	28.7°	12.3°	43.0°	No
10	25.0°	9.1°[1]	41.0°	No
MASH Limits	< 75°	< 75°	N/A	N/A

[1]Maximum value was not reached prior to conclusion of simulation

19.3 Occupant Risk

The occupant risk results for the nested MGS configuration did not yield values exceeding or within 20% of the MASH limits, as shown in Table 43. No vehicle snag on oversized blockouts or lifting and twisting of W-beam was observed in the nested MGS configuration. The increased stiffness of the nested MGS did not allow the vehicle's bumper to deform as far into the guardrail system, which reduced vehicle climb on the PCBs. Thus, the nested MGS configuration would likely meet the TL-3 MASH criteria for occupant risk.

Table 43. Occupant Risk Results – Nested MGS

Impact Location	OIV ft/s (m/s)		ORA g's	
	Longitudinal	Lateral	Longitudinal	Lateral
1	-16.47 (-5.02)	-20.11 (-6.13)	-15.20	-15.86
2	-21.26 (-6.48)	-21.33 (-6.50)	-6.65	-9.73
3	-18.54 (-5.65)	-20.77 (-6.33)	-8.25	-5.85
4	-22.54 (-6.87)	-20.90 (-6.37)	-6.69	-5.12
5	-23.52 (-7.17)	-19.75 (-6.02)	8.57	-7.52
6	-19.49 (-5.94)	-21.33 (-6.50)	-10.73	-8.22
7	-16.63 (-5.07)	-18.96 (-5.78)	-7.90	-11.48
8	-16.63 (-5.07)	-18.80 (-5.73)	-7.08	-10.49
9	-18.90 (-5.76)	-16.54 (-5.04)	-10.49	-12.08
10	-16.34 (-4.98)	-16.90 (-5.15)	-9.20	-9.72
MASH Limits	≤ 40 (12.2)	≤ 40 (12.2)	≤ 20.49	≤ 20.49

19.4 Pocketing Angle

The pocketing angles for all ten impact locations can be found in Table 44, and none of the pocketing angles for the impact locations upstream from the PCB system exceeded or were within 20% of the recommended value of 23 degrees. This finding was a major improvement over any other MGS configuration; since, it was the first system that yielded pocketing angles significantly below the recommended value of 23 degrees.

Thus, the nesting of the MGS in front of the PCB system had significantly improved pocketing angles. As a result, full-scale crash testing of this configuration should reveal a reduced potential for vehicle pocketing and excessive rail loads.

Table 44. Pocketing Angle Results – Nested MGS

Impact Location	Pocketing		
	Angle	Time (ms)	Location
1	1.5°	80	1 ft – 8.8 in. Downstream of Centerline of Post No. 1
2	7.0°	70	2 ft – 6.8 in. Downstream of Centerline of Blockout No. 2
3	7.7°	150	2 ft – 6.8 in. Downstream of Centerline of Blockout No. 2
4	10.6°	330	2 ft – 6.8 in. Downstream of Centerline of Blockout No. 2
5	12.7°	60	3 ft – 6.0 in. Downstream of Centerline of Post No. 1
6	14.5°	120	2 ft – 7.4 in. Downstream of Centerline of Post No. 1
7	13.3°	120	2 ft – 9.5 in. Upstream of Centerline of Post No. 1
8	15.1°	120	2 ft – 9.0 in. Upstream of Centerline of Post No. 2
9	18.1°	190	2 ft – 7.4 in. Downstream of Centerline of Post No. 3
10	13.2°	170	1 ft – 8.1 in. Downstream of Centerline of Post No. 4
Recommended Limits	23.0°	N/A	N/A

19.5 Discussion

Upon full investigation of the simulation findings, the nested MGS significantly improved the performance of the transition system. No vehicle stability, occupant risk, or

pocketing angles exceeded or were within 20% of the MASH limits or recommended values. These findings demonstrated that the nested MGS configuration had a high likelihood to meet the MASH TL-3 full-scale crash test criteria.

CHAPTER 20 MGS WITH FULLY-BLOCKED RAIL

20.1 Introduction

In the interest of providing the safest transition design, several variations of the MGS and PCB configuration were explored. Some of the early MGS configurations revealed wheel snag on the upstream on end of the PCB and decreased post rotation due to contact with the face of the PCBs, thus slowing initiation of PCB displacement. Since some success was observed in post removal in front of the PCBs and blockout installation between the thrie beam and PCBs of previous configurations, these modifications were implemented with the MGS. The posts in front of the PCBs were removed, blockouts were installed in their place, and the MGS configuration was impacted at the same ten impact locations, as shown in Figure 82.
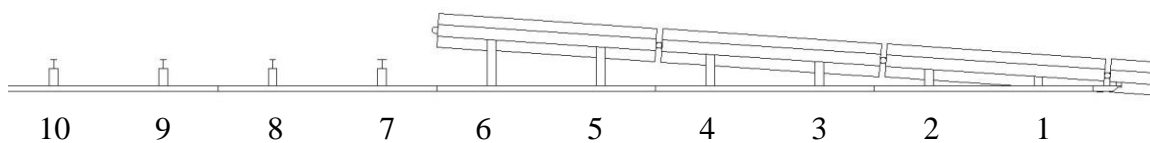
Figure 82. MGS with Fully-Blocked Rail – Impact Locations

20.2 Model Modifications

20.2.1 Post Removal and Blocked Connection

Upon removal of two posts in front of the PCB, there were six locations where blockout implementation was necessary between the rail and PCBs. Due to the 15H:1V flare of the PCB system and the sloped face of the F-shape PCBs, the geometry of the blockouts required a 5.81-degree vertical taper along with a 3.81-degree longitudinal cut, as shown in Figure 60. In order to create the six blockouts for this configuration, one blockout was generated and meshed. Then, it was scaled to fit each of the other five locations, as shown in Figure 83. The corresponding blockout depths are also shown in Table 45.
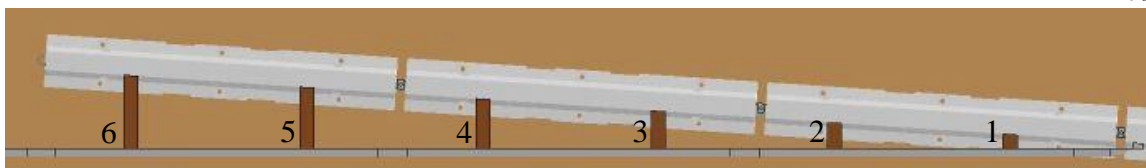
Figure 83. MGS with Fully-Blocked Rail Blockout Setup

Table 45. MGS with Fully-Blocked Rail Blockout Depths

Blockout No.	Depth, in. (mm)
1	6⅜ (162)
2	11 (279)
3	16⅛ (410)
4	21⅜ (543)
5	26¼ (667)
6	31¼ (794)

The blockouts were modeled using the same simplified wood material as used for the other blockouts. Due to the complicated fracture mechanics of wood, a reliable material formulation has yet to be developed that can accurately model wood fracture. Therefore, the blockouts had no failure criteria. Along with blockouts, guardrail bolts were installed and scaled to fit each new blockout location. The blockout bolts were modeled to connect directly to the face of the PCB segments. If these oversized blockouts are used in the final design, additional research must be conducted to determine the final configuration for the guardrail bolt to PCB attachment prior to full-scale crash testing.

20.3 Vehicle Behavior

The MGS with fully-blocked rail configuration captured and redirected the vehicle for all ten impact locations, and none of the roll, pitch, or yaw angles exceeded or were within 20% of the MASH limits, as shown in Table 46. No wheel snag on the PCBs was found. Therefore, the MGS with fully-blocked rail configuration would likely meet the TL-3 MASH criteria for vehicle stability.

Table 46. Vehicle Behavior Results – MGS with Fully-Blocked Rail

Impact Location	Roll	Pitch	Yaw	Wheel Snag on PCBs?
1	50.4°	42.4°[1]	41.0°	No
2	28.6°[1]	13.0°	41.6°[1]	No
3	30.6°[1]	15.8°[1]	66.0°[1]	No
4	8.5°	9.9°	36.4°[1]	No
5	9.1°	6.7°	39.0°	No
6	13.4°	4.9°	39.7°[1]	No
7	11.4°	6.3°	32.7°[1]	No
8	11.2°	4.2°	33.4°[1]	No
9	7.0°	5.0°	40.7°	No
10	11.3°	8.3°	42.6°[1]	No
MASH Limits	< 75°	< 75°	N/A	N/A

[1]Maximum value was not reached prior to conclusion of simulation

20.4 Occupant Risk

The occupant risk evaluation for the MGS with fully-blocked rail configuration yielded one value within 20% of the MASH limits, as shown in Table 47. The maximum longitudinal OIV for impact location no. 7 was -37.37 ft/s (-11.39 m/s). This elevated OIV occurred because after the vehicle's bumper protruded underneath the MGS and allowed the wheel engage the PCBs, thus resulting in vehicle climb. The vehicle climb caused lifting and twisting of the rail as well as vehicle snag on the blockouts between the

rail and PCBs. This twisting and lifting of the MGS caused concern for rail rupture and system failure.

Table 47. Occupant Risk Results – MGS with Fully-Blocked Rail

Impact Location	OIV ft/s (m/s)		ORA g's	
	Longitudinal	Lateral	Longitudinal	Lateral
1	-19.09 (-5.82)	-18.80 (-5.73)	-11.56	-6.98
2	-27.46 (-8.37)	-19.65 (-5.99)	9.50	-9.71
3	-25.52 (-7.78)	-16.86 (-5.14)	-9.82	-7.93
4	-30.05 (-9.16)	-16.83 (-5.13)	-11.96	-6.60
5	-29.72 (-9.06)	-18.21 (-5.55)	-10.20	-7.77
6	-28.94 (-8.82)	-17.32 (-5.28)	-13.27	-5.27
7	-37.37 (-11.39)	-10.33 (-3.15)	-13.35	-6.71
8	-22.38 (-6.82)	-18.93 (-5.77)	-14.24	-6.00
9	-16.27 (-4.96)	-17.91 (-5.46)	-10.41	-7.66
10	-15.12 (-4.61)	-16.96 (-5.17)	-8.21	-9.24
MASH Limits	≤ 40 (12.2)	≤ 40 (12.2)	≤ 20.49	≤ 20.49

*Yellow cells denote values within 20% of MASH or recommended limits

20.5 Pocketing Angle

The pocketing angles for all ten impact locations can be found in Table 48, and pocketing angles for all of the impact locations upstream from the PCB system either

exceeded or were within 20% of the recommended value of 23 degrees. The removal of two posts in front of the PCB system and installation of a blocked connection caused pocketing angles to increase over those observed for several of the configurations with two posts in front of the PCBs. This finding demonstrated that installation of a fully-blocked connection was not successful in reducing pocketing angles.

Table 48. Pocketing Angle Results – MGS with Fully-Blocked Rail

Impact Location	Pocketing		
	Angle	Time (ms)	Location
1	1.2°	100	2 ft – 7.4 in. Downstream of Centerline of Post No. 3
2	11.6°	60	2 ft – 6.8 in. Downstream of Centerline of Blockout No. 2
3	14.9°	70	2 ft – 10.0 in. Upstream of Centerline of Blockout No. 2
4	15.4°	70	2 ft – 9.5 in. Upstream of Centerline of Blockout No. 3
5	15.4°	60	3 ft – 6.0 in. Downstream of Centerline of Post No. 1
6	15.0°	70	2 ft – 9.5 in. Upstream of Centerline of Post No. 1
7	18.4°	60	2 ft – 9.0 in. Upstream of Centerline of Post No. 2
8	28.7°	120	2 ft – 7.4 in. Downstream of Centerline of Post No. 3
9	28.0°	190	2 ft – 7.4 in. Downstream of Centerline of Post No. 3
10	18.6°	200	2 ft – 9.5 in. Upstream of Centerline of Post No. 1
Recommended Limits	23.0°	N/A	N/A

*Yellow cells denote values within 20% of MASH or recommended limits
*Red cells denote values that exceed MASH or recommended limits

20.6 Discussion

Upon full investigation of the simulation findings for the MGS with fully-blocked rail configuration, removal of two posts in front of PCBs and installation of a fully-blocked connection did not increase the potential for the configuration to meet TL-3 of MASH. The longitudinal OIV for impact location no. 7 was within 20% of the MASH limits. Also, pocketing angles for all four impact locations upstream from the PCB system exceeded or were within 20% of the recommended value of 23 degrees. Therefore, other options were explored to create a safe transition design.

CHAPTER 21 MGS WITH FULLY-BLOCKED RAIL AND CANTILEVER BEAM

21.1 Introduction

Since the replacement of two posts with blockouts in front of the PCB system did not reduce pocketing angles nor improve the transition, a cantilever beam was installed to the most upstream PCB. The MGS with fully-blocked rail and cantilever beam configuration was simulated at the same ten impact locations, as shown in Figure 84. The cantilever beam was 15ft (4,572 mm) long and the same as used in the previous configurations.
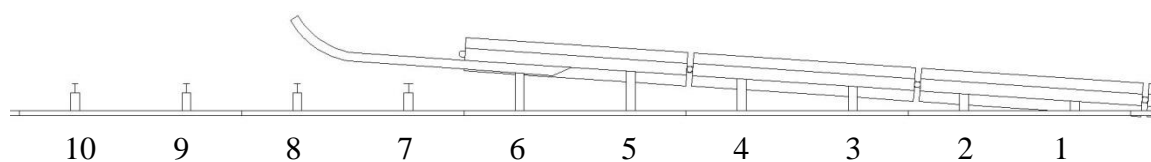
Figure 84. MGS Fully-Blocked Rail and Cantilever Beam – Impact Locations

21.2 Vehicle Behavior

The MGS with fully-blocked rail and cantilever beam configuration captured and redirected the vehicle for all ten impact locations. However, the roll angle for impact location no. 1 was within 20% of the MASH limit, and it had not reached a maximum value prior to conclusion of simulation, as shown in Table 49. Upon further inspection, the excessive roll motion was deemed unrealistic and likely caused by the exaggerated stiffness of the vehicle's rear suspension when the back end of the vehicle impacted the W-beam. This finding led to the conclusion that the MASH limits would not likely be exceeded, and this configuration would likely meet the TL-3 MASH vehicle stability criteria for all impact locations.

Table 49. Vehicle Behavior Results – MGS with Fully-Blocked Rail and Cantilever
Beam

Impact Location	Roll	Pitch	Yaw	Wheel Snag on PCBs?
1	61.3°[1]	47.4°[1]	40.7°	No
2	20.3°	14.3°	40.4°	No
3	7.6°	9.9°	49.2°[1]	No
4	7.0°	8.3°	36.7°[1]	No
5	6.9°	6.4°	40.7°	No
6	9.4°	4.9°	35.5°	No
7	4.5°	5.9°	17.3°[1]	No
8	5.9°	4.7°	35.0°	No
9	6.2°	3.5°	39.6°[1]	No
10	13.6°	8.1°	39.6°	No
MASH Limits	< 75°	< 75°	N/A	N/A

[1]Maximum value was not reached prior to conclusion of simulation
*Yellow cells denote values within 20% of MASH or recommended limits

21.3 Occupant Risk

The occupant risk results for the MGS with fully-blocked rail and cantilever beam configuration yielded one value within 20% of the MASH limits, as shown in Table 50. The maximum longitudinal OIV for impact location no. 7 was -37.57 ft/s (-11.45 m/s). This elevated OIV occurred after the vehicle's bumper protruded underneath MGS and allowed the wheel to engage the PCBs, thus resulting in vehicle climb. The vehicle climb caused lifting and twisting of the MGS as well as vehicle snag on the blockouts between

the rail and PCBs. This twisting and lifting of the MGS caused concern for rail rupture and system failure.

Table 50. Occupant Risk Results – MGS with Fully-Blocked Rail and Cantilever Beam

Impact Location	OIV ft/s (m/s)		ORA g's	
	Longitudinal	Lateral	Longitudinal	Lateral
1	-19.23 (-5.86)	-18.80 (-5.73)	13.14	10.30
2	-27.20 (-8.29)	-19.82 (-6.04)	7.39	-9.93
3	-29.82 (-9.09)	-16.93 (-5.16)	11.61	-6.46
4	-29.79 (-9.08)	-16.96 (-5.16)	-11.02	-6.84
5	-29.00 (-8.84)	-17.62 (-5.37)	-8.91	-8.43
6	-31.10 (-9.48)	-16.60 (-5.06)	-15.21	-5.19
7	-37.57 (-11.45)	-13.19 (-4.02)	-10.68	-7.69
8	-22.97 (-7.00)	-19.52 (-5.95)	-11.00	-5.95
9	-21.26 (-6.48)	-17.72 (-5.40)	-12.45	-8.96
10	-15.09 (-4.60)	-17.16 (-5.23)	-8.98	-9.04
MASH Limits	≤ 40 (12.2)	≤ 40 (12.2)	≤ 20.49	≤ 20.49

*Yellow cells denote values within 20% of MASH or recommended limits

21.4 Pocketing Angle

The pocketing angles for all ten impact locations can be found in Table 51. While the majority of the pocketing angles decreased with the use of the cantilever beam, the

pocketing angles for all of the impact locations upstream from the PCB system exceeded

or were within 20% of the recommended value of 23 degrees.

Table 51. Pocketing Angle Results – MGS with Fully-Blocked Rail and Cantilever Beam

Impact Location	Pocketing		
	Angle	Time (ms)	Location
1	1.3°	100	2 ft – 7.4 in. Downstream of Centerline of Post No. 3
2	11.6°	60	2 ft – 6.8 in. Downstream of Centerline of Blockout No. 2
3	14.8°	70	2 ft – 10.0 in. Upstream of Centerline of Blockout No. 2
4	15.4°	70	2 ft – 9.5 in. Upstream of Centerline of Blockout No. 3
5	15.3°	60	3 ft – 6.0 in. Downstream of Centerline of Post No. 1
6	14.6°	60	2 ft – 9.5 in. Upstream of Centerline of Post No. 1
7	18.5°	60	2 ft – 9.0 in. Upstream of Centerline of Post No. 2
8	22.8°	120	2 ft – 7.4 in. Downstream of Centerline of Post No. 3
9	23.2°	200	2 ft – 7.4 in. Downstream of Centerline of Post No. 3
10	22.8°	190	2 ft – 6.8 in. Downstream of Centerline of Post No. 4
Recommended Limits	23.0°	N/A	N/A

*Yellow cells denote values within 20% of MASH or recommended limits
*Red cells denote values that exceed MASH or recommended limits

21.5 Discussion

Upon full investigation of the simulation findings for the MGS with fully-blocked

rail and cantilever beam configuration, the installation of the cantilever beam successfully

reduced pocketing angles. The longitudinal OIV for impact location no. 7 was within 20% of the MASH limits, a somewhat minor concern. Based on these findings, the MGS with fully-blocked rail and cantilever beam configuration had the second highest probability of successfully meeting the TL-3 criteria outlined in MASH, just behind the nested MGS configuration.

CHAPTER 22 FLARED PCB – MGS DESIGN CONCEPT SUMMARY

22.1 Introduction

Upon completion of the simulation study for the Flared PCB – MGS design concept, the results were reviewed and compared, as was previously completed for the Flared PCB – Modified G4(1S) and the Parallel PCB – Modified G4(1S) design concepts in CHAPTER 14.

22.2 Flared PCB – MGS Design Concept

The Flared PCB – MGS design concept was similar to the Flared PCB – Modified G4(1S) design concept except MGS was connected to the 15H:1V flared PCB system in lieu of modified G4(1S). The MGS was connected to the upstream end of the fourth PCB segment with three PCBs extending behind the rail. Although simulation results for the modified G4(1S) indicated that posts in front of PCBs would deform and wedge against the face of PCBs, the higher MGS was believed capable to capture and redirect the 2270P vehicle with reduced instabilities. Thus, two posts remained in front of the PCB system. Posts were removed when they interfered with placement of the PCB system, but blockouts were installed in their place.

Simulation results for the MGS end shoe configuration yielded high occupant risk values due to vehicle snag, and pocketing angles were a concern for impacts upstream from the PCB system. To initiate PCB displacement earlier in the event, blockouts were installed from the back of posts to the face of the PCBs. Simulation results for the MGS with blockouts behind posts configuration indicated that the additional blockouts stiffened the barrier system as the posts had to overcome post-soil resistance, PCB inertial resistance, as well as barrier friction. This increased resistance resulted in high

pocketing angles upstream from the PCB system and elevated occupant risk values, which led to the conclusion that blockouts from posts to PCBs should not be used.

The next configuration utilized a cantilever beam on the upstream PCB to allow specific posts to rotate into and contact the cantilever beam in order to initiate PCB displacement. The simulation results for the MGS with cantilever beam configuration indicated that pocketing angles were reduced for impacts upstream from the PCB system, but they were still too high.

For the next configuration, a blockout was installed between a post and the cantilever beam, which could initiate PCB displacement earlier in the event. However, simulation results for the MGS with blockout to cantilever beam configuration indicated that the blockout to the cantilever beam stiffened the barrier system as the post had to overcome post-soil resistance, PCB inertial resistance, as well as barrier friction. As such, a blockout between the cantilever beam should not be used.

In the next configuration, the MGS was nested upstream and in front of the PCB system, which would stiffen the barrier system and lower pocketing angles. The simulation results for the nested MGS configuration showed that occupant risk values and pocketing angles were reduced to acceptable levels for all impact locations. Some of the early configurations indicated that vehicle snag occurred on PCBs, and the next configuration attempted to alleviate snag by removal of posts in front of PCBs but with blockouts installed in their place.

The simulation results for the MGS with fully-blocked rail configuration indicated that vehicle snag on PCBs was eliminated, but pocketing angles were significantly higher for impacts upstream from the PCB system. Therefore, a final configuration utilized a

cantilever beam on the most upstream PCB. The simulation results for the MGS with fully-blocked rail and cantilever beam configuration indicated that vehicle snag on PCBs did not occur. Although pocketing angles decreased, they were still marginal. Based on these results, the Flared PCB – MGS configurations were ranked, as shown below:

(1) Nested MGS;

(2) MGS with Fully-Blocked Rail and Cantilever Beam;

(3) MGS with Cantilever Beam;

(4) MGS with Blockout to Cantilever Beam;

(5) MGS End Shoe;

(6) MGS with Fully-Blocked Rail; and

(7) MGS with Blockouts Behind Posts.

CHAPTER 23 SELECTION OF PREFERRED DESIGN ALTERNATIVES

23.1 Introduction

Previously, the Flared PCB − Modified G4(1S), Parallel PCB − Modified G4(1S), and Flared PCB − MGS design concepts were simulated with several configurations. These configurations were summarized within their respective design concept. Now, all three design concepts with their respective configurations will be summarized and ranked together in order to select preferred design alternatives.

23.2 Design Summary and Selection

In order to select preferred design alternatives, a summary of results for all three design concepts with subsequent configurations was prepared, as shown in Tables 52 and 53. The maximum value for each evaluation metric was tabulated at each configuration. The minimum value for each metric was then highlighted within each design concept in order to better understand which configurations represented the safest transition design. Several metrics were also noted, including number of impact locations with values exceeding the MASH or recommended limit, number of impact locations with values within 20 percent of the MASH or recommended limit, and number of values that were deemed realistic or likely representative of a physical phenomenon. As previously explained, several high roll angles and occupant risk values were attributed to an overly stiff rear suspension in the Chevrolet Silverado pickup truck model. They were not deemed accurate and thus should not be heavily considered when selecting preferred design alternatives.

As each design concept was discussed, the configurations were weighed by the number of highlighted cells that each possessed, the number of values that exceeded or

Table 52. Summary of Design Concepts and Configurations

Design Concepts	Configurations [No. of Impact Locations]	Roll [X,Y,Z]	Pitch [X,Y,Z]	Yaw	OIV ft/s (m/s) [X,Y,Z]		ORA g's [X,Y,Z]		Wheel Snag on PCBs? [X]	Max. Pocketing Angle [X,Y,Z]
					Longitudinal	Lateral	Longitudinal	Lateral		
Flared PCB - Modified G4(1S)	Baseline [6]	106.4°[1] [3,0,3]	42.7°[1] [0,0,0]	90.1°[1]	-38.68 (-11.79) [0,1,1]	-19.49 (-5.94) [0,0,0]	-81.87 [3,0,3]	17.27 [0,1,1]	Yes [3]	N/A
	Modified G4(1S) End Shoe [6]	133.6°[1] [3,0,3]	32.6° [0,0,0]	44.2°	-28.02 (-8.54) [0,0,0]	-20.44 (-6.23) [0,0,0]	-23.62 [1,0,1]	-11.42 [0,0,0]	Yes [1]	23.1° [1,2,3]
	Thrie Beam End Shoe [9]	56.5°[1] [0,0,0]	24.6°[1] [0,0,0]	41.4°[1]	-24.02 (-7.32) [0,0,0]	-20.47 (-6.24) [0,0,0]	-15.20 [0,0,0]	-15.57 [0,0,0]	No	21.5° [0,2,2]
	Thrie Beam with Fully-Blocked Rail [9]	67.4°[1] [0,1,0]	26.0°[1] [0,0,0,]	66.8°	-31.20 (-9.51) [0,0,0]	-22.34 (-6.81) [0,0,0]	-16.85 [0,1,1]	-11.75 [0,0,0]	No	25.4° [1,1,2]
	Thrie Beam with Fully-Blocked Rail and Cantilever Beam [9]	65.3°[1] [0,1,0]	29.8°[1] [0,0,0,]	62.2°[1]	-40.52 (-12.35) [1,0,0]	-22.28 (-6.79) [0,0,0]	-13.50 [0,0,0]	-14.14 [0,0,0]	No	20.5° [0,2,2]
	Nested Thrie Beam with Fully-Blocked Rail [9]	96.9°[1] [1,1,0]	27.3° [0,0,0,]	43.5°	-23.20 (-7.07) [0,0,0]	-22.11 (-6.74) [0,0,0]	-14.42 [0,0,0]	-13.03 [0,0,0]	No	20.3° [0,1,1]
Parallel PCB - Modified G4(1S)	PCBs Behind Nested Thrie Beam [12]	83.3°[1] [1,1,0]	27.3°[1] [0,0,0]	42.5°[1]	-20.21 (-6.16) [0,0,0]	-21.92 (-6.68) [0,0,0]	18.88 [0,2,2]	-12.14 [0,0,0]	No	18.2° [0,0,0]
	PCBs Behind Nested Thrie Beam with Cantilever Beam [12]	88.7°[1] [1,1,0]	23.3°[1] [0,0,0]	41.1°	-19.90 (-5.76) [0,0,0]	-23.13 (-7.05) [0,0,0]	-16.92 [0,1,1]	-16.70 [0,1,1]	No	18.3° [0,0,0]
MASH or Recommended Limit		< 75°	< 75°	N/A	≤ 40 (12.2)	≤ 40(12.2)	≤ 20.49	≤ 20.49	N/A	< 23°

[1]Maximum value was not reached prior to conclusion of simulation

X – Number of values that exceeded MASH or recommended limit

Y – Number of values within 20% of MASH or recommended limit

Z – Sum of X and Y values that were deemed physical (real) phenomenon and not modeling limitations

Table 53. Summary of Design Concepts and Configurations (cont.)

Design Concepts	Configurations [No. of Impact Locations]	Roll [X,Y,Z]	Pitch [X,Y,Z]	Yaw [X,Y,Z]	OIV ft/s (m/s) [X,Y,Z]		ORA g's [X,Y,Z]		Wheel Snag on PCBs? [X]	Max. Pocketing Angle [X,Y,Z]
					Longitudinal	Lateral	Longitudinal	Lateral		
Flared PCB - MGS	MGS End Shoe [10]	49.9°[1] [0,0,0]	40.6°[1] [0,0,0]	47.2°	-35.66 (-10.87) [0,2,2]	-20.01 (-6.10) [0,0,0]	-15.36 [0,0,0]	-11.28 [0,0,0]	Yes [2]	24.7° [1,3,4]
	MGS with Blockouts Behind Posts [10]	37.3° [0,0,0]	30.3°[1] [0,0,0]	57.1°[1]	-33.01 (-10.06) [0,3,3]	-20.57 (-6.27) [0,0,0]	-19.55 [0,2,2]	-10.43 [0,0,0]	Yes [1]	28.6° [3,1,4]
	MGS with Cantilever Beam [10]	47.6° [0,0,0]	43.1°[1] [0,0,0]	51.8°[1]	-36.52 (-11.13) [0,1,1]	-20.28 (-6.18) [0,0,0]	-16.30 [0,0,0]	-11.94 [0,0,0]	No	24.0° [1,3,4]
	MGS with Blockout to Cantilever Beam [10]	44.0° [0,0,0]	40.7°[1] [0,0,0]	55.4°[1]	-35.99 (-10.97) [0,1,1]	-20.11 (-6.13) [0,0,0]	-11.75 [0,0,0]	-11.40 [0,0,0]	No	26.0° [2,2,4]
	Nested MGS [10]	42.8° [0,0,0]	26.0° [0,0,0]	43.0°	-23.52 (-7.17) [0,0,0]	-21.33 (-6.50) [0,0,0]	-15.20 [0,0,0]	-15.86 [0,0,0]	No	18.1° [0,0,0]
	MGS with Fully-Blocked Rail [10]	50.4° [0,0,0]	42.4°[1] [0,0,0]	66.0°[1]	-37.37 (-11.39) [0,1,1]	-19.65 (-5.99) [0,0,0]	-14.24 [0,0,0]	-9.71 [0,0,0]	No	28.7° [2,2,4]
	MGS with Fully-Blocked Rail and Cantilever Beam [10]	61.3°[1] [0,1,0]	47.4°[1] [0,0,0]	49.2°[1]	-37.57 (-11.45) [0,1,1]	-19.82 (-6.04) [0,0,0]	-15.21 [0,0,0]	10.30 [0,0,0]	No	23.2° [1,3,4]
MASH or Recommended Limit		< 75°	< 75°	N/A	≤ 40 (12.2)	≤ 40 (12.2)	≤ 20.49	≤ 20.49	N/A	< 23°

[1]Maximum value was not reached prior to conclusion of simulation

X – Number of values that exceeded MASH or recommended limit

Y – Number of values within 20% of MASH or recommended limit

Z – Sum of X and Y values that were deemed physical (real) phenomenon and not modeling limitations

▢ Maximum metric value for Flared PCB – Modified G4(1S) Design Concept

▢ Maximum metric value for Parallel PCB – Modified G4(1S) Design Concept

▢ Maximum metric value for Flared PCB – MGS Design Concept

were within 20% of MASH or recommend limits, amount of vehicle snag, practicality, and ease of installation.

The tabulated results were used to rank the configurations within each design concept, as well as to establish whether each configuration had a high, moderate, or low likelihood of success, as shown in Table 54.

Table 54. Ranking of Design Configurations

Rank	Flared PCB – Modified G4(1S)	Parallel PCB – Modified G4(1S)	Flared PCB – MGS
1	Nested Thrie Beam with Fully-Blocked Rail	PCBs Behind Nested Thrie Beam	Nested MGS
2	Thrie Beam with Fully-Blocked Rail and Cantilever Beam	PCBs Behind Nested Thrie Beam with Cantilever Beam	MGS with Fully-Blocked Rail and Cantilever Beam
3	Thrie Beam End Shoe		MGS with Cantilever Beam
4	Thrie Beam with Fully-Blocked Rail		MGS with Blockout to Cantilever Beam
5	Modified G4(1S) End Shoe		MGS End Shoe
6	Baseline		MGS with Fully-Blocked Rail
7			MGS with Blockouts Behind Posts

	High Likelihood of Success
	Moderate Likelihood of Success
	Low Likelihood of Success

Based on the rankings, it was determined that nested MGS stood above other configurations. It was the only configuration within all three design concepts which yield results without concerns for vehicle behavior, occupant risk, or pocketing angle that exceeded or were within 20% of the MASH or recommended values. Also, nesting of MGS would significantly increase the ease of installation as compared to several other

promising configurations, which may include a W-beam guardrail transition to thrie beam or fabrication and installation of a special cantilever beam. Thus, nested MGS was selected as the preferred alternative and recommended for full-scale crash testing and evaluation.

CHAPTER 24 CRITICAL IMPACT POINT (CIP) STUDY

24.1 Impacts Near End Shoe Attachment

Once a preferred design alternative was chosen for full-scale crash testing and evaluation, further computer simulation was conducted in order to determine a Critical Impact Point (CIP). The first portion of the CIP study was to determine the behavior of the transition system when impacted near the location of the end shoe attachment. Therefore, the nested MGS was simulated for impacts at the end shoe and at four 6 ft – 3 in. (1905 mm) spacings farther downstream, as shown in Figure 85.
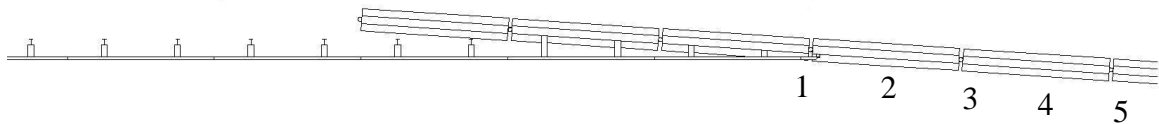
Figure 85. Impact Locations Near End Shoe Attachment

Since the nested MGS was not impacted, pocketing angles were not calculated or considered for the CIP investigation near the end shoe. Therefore, only vehicle behavior and occupant risk values were evaluated, as shown in Table 55. The simulation results showed that the vehicle would remain upright throughout and following the impact event with very little instability for all five impact locations. However, three of the five impact locations displayed lateral ORAs within 20% of the MASH limit. Upon further investigation, these high ORAs occurred late in the impact event after the back end of the vehicle had impacted the PCB system. As noted previously, these high ORAs were likely due to an overly stiff rear suspension of the vehicle model and not representative of a physical phenomenon. Therefore, researchers had high confidence that impacts near the end shoe would allow the nested MGS to safely capture and redirect the vehicle with vehicle stability and occupant risk values within the MASH TL-3 limits.

Table 55. Results for Impacts Near the End Shoe Attachment

Impact Location	Roll	Pitch	Yaw	OIV ft/s (m/s)		ORA g's	
				Longitudinal	Lateral	Longitudinal	Lateral
1	34.4°	28.1°[1]	39.9°	-16.21 (-4.94)	-23.06 (-7.03)	-12.34	-20.25
2	39.9°	26.0°[1]	40.6°	-13.58 (-4.14)	-17.78 (-5.42)	-14.63	-16.45
3	36.7°	26.7°[1]	41.4°	-16.44 (-5.01)	-23.13 (-7.05)	12.04	-14.39
4	14.1°	18.5°	44.1°	-15.22 (-4.64)	-17.49 (-5.33)	-11.22	-8.94
5	35.6°	27.2°[1]	42.2°	-16.40 (-5.00)	-23.00 (-7.01)	-11.78	-17.72

[1]Maximum value was not reached prior to conclusion of simulation

*Yellow cells denote values within 20% of MASH or recommended limits

24.2 Critical Attachment Location

The second portion of the CIP study was to determine the critical attachment location of the MGS to PCB system. The primary concern associated with different attachment locations was the number of posts in front of PCBs that could cause vehicle snag, vehicle instabilities, or elevated pocketing angles. Since, it was determined that the MGS must attach to the fourth PCB segment, three attachment locations were considered for the critical attachment location study, as shown in Figure 86.

Case 1 – MGS attached to upstream end of fourth PCB segment

Case 2 – MGS attached to fourth PCB segment to allow most upstream PCB segment to just miss being contacted by post rotation in front of it

Case 3 – MGS attached to fourth PCB segment to allow most upstream PCB segment to be engaged by post rotation in front of it

Case 1 was chosen as guardrail attachment to the upstream end of the fourth PCB would provide for the least amount of PCB length extending behind the rail and the greatest opportunity for vehicle snag on the upstream end of the PCB system. Case 2 was chosen because extending PCB segments behind the rail without allowing another guardrail post to engage the PCB segment could increase vehicle pocketing upstream from the PCB system. Case 3 was chosen to evaluate whether extending PCB segments behind the rail and allowing another post to engage the PCB segment could cause vehicle snag on the post as well as vehicle instabilities.
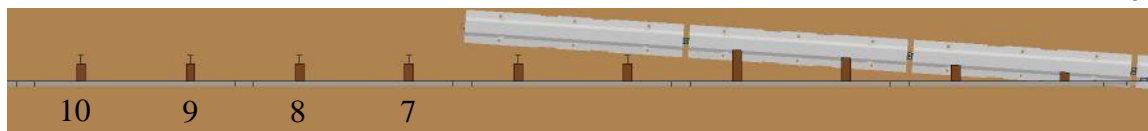
Case 1
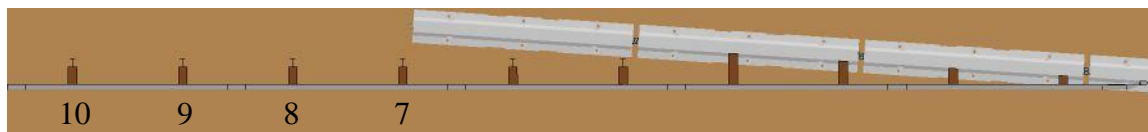
Case 2
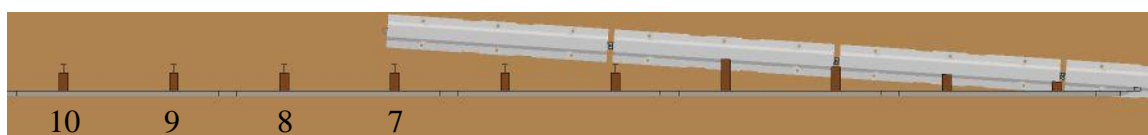
Case 3
Figure 86. Critical Attachment Cases and Impact Locations

Each case was simulated at four locations near the upstream end of the PCB system, and vehicle behavior values, occupant risk values, and pocketing angles were compiled and compared against each other, as shown in Table 56. The maximum value for each metric was then highlighted within each case to determine which would provide a worst-case attachment location. Both vehicle stability results and occupant risk values were found to be well below the MASH limits for all three cases. Thus, these criteria were not used in the determination of the critical attachment location. Therefore, maximum pocketing angles were used to determine the critical attachment location. For this investigation, it was concluded that Case 1 yielded the highest pocketing angles as well as longitudinal OIV and longitudinal ORA, and should be used as the critical attachment location for the CIP study.

Table 56. Simulation Results – Critical Attachment Location

	Impact Location	Roll	Pitch	Yaw	OIV ft/s (m/s)		ORA g's		Wheel Snag on PCBs?	Pocketing		
					Longitudinal	Lateral	Longitudinal	Lateral		Max. Angle	Time	Location
Case 1	7	17.8°	5.8°	37.2°[1]	-16.63 (-5.07)	-18.96 (-5.78)	-7.90	-11.48	No	13.3°	120	2 ft 9.5 in. Upstream of Centerline of Post No. 1
	8	25.3°	8.2°	40.0°[1]	-16.63 (-5.07)	-18.80 (-5.73)	-7.08	-10.49	No	15.1°	120	2 ft 9.0 in. Upstream of Centerline of Post No. 2
	9	28.7°	12.3°	43.0°	-18.90 (-5.76)	-16.54 (-5.04)	-10.49	-12.08	No	18.1°	190	2 ft 7.4 in. Downstream of Centerline of Post No. 3
	10	25.0°	9.1°[1]	41.0°	-16.34 (-4.98)	-16.90 (-5.15)	-9.20	-9.72	No	13.2°	170	1 ft 8.1 in. Downstream of Centerline of Post No. 4
Case 2	7	16.9°	5.6°	37.7°[1]	-16.83 (-5.13)	-19.29 (-5.88)	-8.09	-9.98	No	12.7°	110	2 ft - 6.8 in. Downstream of Centerline of Post No. 2
	8	33.6°	9.5°	38.2°[1]	-16.31 (-4.97)	-19.32 (-5.89)	10.14	-12.19	No	15.4°	120	2 ft - 9.0 in. Upstream of Centerline of Post No. 2
	9	23.9°	8.3°	39.8°[1]	-13.06 (-3.98)	-17.59 (-5.36)	-8.98	-8.10	No	14.5°	180	2 ft - 7.4 in. Downstream of Centerline of Post No. 3
	10	25.6°	7.5°	37.4°[1]	-12.93 (-3.94)	-17.32 (-5.28)	-6.17	-8.69	No	12.0°	180	2 ft - 6.8 in. Downstream of Centerline of Post No. 4
Case 3	7	16.3°	6.5°	37.6°[1]	-16.90 (-5.15)	-19.49 (-5.94)	-6.42	-8.85	No	12.8°	130	2 ft - 9.5 in. Upstream of Centerline of Post No. 1
	8	15.6°	6.3°	40.9°[1]	-14.96 (-4.56)	-18.67 (-5.69)	-9.15	-9.31	No	13.7°	130	1 ft - 10.5 in. Upstream of Centerline of Post No. 2
	9	25.6°	7.1°	39.0°[1]	-13.58 (-4.14)	-18.37 (-5.60)	-7.45	-9.79	No	12.4°	120	2 ft - 10.5 in. Upstream of Centerline of Post No. 3
	10	25.8°	8.3°	38.8°	-13.16 (-4.01)	-17.55 (-5.35)	-7.33	-9.39	No	11.9°	180	2 ft - 6.8 in. Downstream of Centerline of Post No. 4

[1]Maximum value was not reached prior to conclusion of simulation

Maximum metric value for Case 1
Maximum metric value for Case 2
Maximum metric value for Case 3

24.3 Critical Impact Location

Once a critical attachment location was determined, the final portion of the CIP study was to find the worst-case impact location for use in a full-scale crash testing and evaluation program. Case 1 was chosen as the worst-case attachment location and was actually used in simulating the ten impacts for the nested MGS configuration in CHAPTER 19. Therefore, the simulation results from the original ten impact locations were reviewed again to determine the CIP. Due to the vehicle behavior and occupant risk values being well below the MASH limits, maximum pocketing angles were primarily evaluated for the nested MGS configuration. Impact location no. 9 had the highest pocketing angle of 18.1 degrees. Therefore, the general CIP region was selected near impact location no. 9, and further simulations were conducted at 18¾ in. (476 mm) intervals (i.e., quarter-post spacings) between impact location nos. 8 and 10. The vehicle stability, occupant risk, and pocketing angle results for these additional impact locations are shown in Table 57. The maximum value for each metric was then highlighted to aid in the selection of the CIP.

It was found that impact location no. 9 had the highest roll, pitch, yaw, longitudinal OIV, lateral ORA, and pocketing angle. Therefore, future full-scale crash testing of the nested MGS configuration should utilize impact location no. 9 as the CIP.

Table 57. Simulation Results – Additional Critical Impact Point Investigation

Impact Location	Roll	Pitch	Yaw	OIV ft/s (m/s)		ORA g's		Wheel Snag on PCBs?	Pocketing		
				Longitudinal	Lateral	Longitudinal	Lateral		Max. Angle	Time	Location
8	25.3°	8.2°	40.0°[1]	-16.63 (-5.07)	-18.80 (-5.73)	-7.08	-10.49	No	15.1°	120	2 ft 9.0 in. Upstream of Centerline of Post No. 2
8¼	22.2°	7.9°	40.6°[1]	-15.55 (-4.74)	-18.57 (-5.66)	-11.62	-9.09	No	16.7°	140	2 ft 9.0 in. Upstream of Centerline of Post No. 2
8½	21.2°	8.0°	40.3°[1]	-14.07 (-4.29)	-18.83 (-5.74)	-9.78	-9.47	No	16.7°	150	2 ft 7.4 in. Downstream of Centerline of Post No. 3
8¾	18.7°	8.9°	42.1°	-15.19 (-4.63)	-18.67 (-5.69)	-9.87	-8.84	No	17.6°	170	2 ft 7.4 in. Downstream of Centerline of Post No. 3
9	28.7°	12.3°	43.0°	-18.90 (-5.76)	-16.54 (-5.04)	-10.49	-12.08	No	18.1°	190	2 ft 7.4 in. Downstream of Centerline of Post No. 3
9¼	22.3°	9.2°	41.3°	-15.06 (-4.59)	-17.49 (-5.33)	-9.60	-8.97	No	15.1°	200	1 ft 8.8 in. Downstream of Centerline of Post No. 3
9½	22.8°	8.0°	40.3°	-15.22 (-4.64)	-19.26 (-5.87)	-6.82	-8.54	No	13.1°	210	1 ft 8.8 in. Downstream of Centerline of Post No. 3
9¾	23.4°	8.1°	39.6°[1]	-16.08 (-4.90)	-19.16 (-5.84)	-7.58	-9.36	No	12.7°	150	1 ft 8.1 in. Downstream of Centerline of Post No. 4
10	25.0°	9.1°[1]	41.0°	-16.34 (-4.98)	-16.90 (-5.15)	-9.20	-9.72	No	13.2°	170	1 ft 8.1 in. Downstream of Centerline of Post No. 4
MASH Limits	< 75°	< 75°	N/A	≤ 40 (12.2)	≤ 40 (12.2)	≤ 20.49	≤ 20.49	N/A	N/A	N/A	N/A

[1]Maximum value was not reached prior to conclusion of simulation

24.4 Minimum Length for PCB Installation

For the prior LS-DYNA analyses, simulations have been conducted using a PCB system configured with sixteen segments. Historically, F-shape PCB barrier systems have been simulated, tested, and evaluated using sixteen segments and with impact near the center of the system. Further, MwRSF has previously recommended that eight barrier segments be installed upstream and downstream from this impact location, and thus it has become an unofficial length of need. Therefore and for this study, a simulation was performed at the CIP (i.e. impact location no. 9) using eight PCB segments instead of thirteen downstream from the end shoe attachment. For now, eight PCB segments would be the minimum downstream length of need until further analysis or testing is conducted to demonstrate otherwise. The end shoe was attached to the upstream end of the fourth PCB segment with three PCB segments extending upstream and behind the MGS. When considering eight PCBs installed downstream, a total of eleven PCB segments were used to configure the modified PCB installation. The simulation results, as shown in Table 58, yielded values that were very similar to the CIP investigation which used sixteen PCB segments. The barrier system captured and redirected the 2270P pickup truck without vehicle snag on the PCB system. The vehicle stability indicators, occupant risk values, or pocketing angles did not exceed or come within 20% of the MASH or recommended limits.

Table 58. Simulation Results – CIP Investigation with 11 PCBs – Impact Location No. 9

Roll	Pitch	Yaw	OIV ft/s (m/s)		ORA g's		Pocketing		
			Longitudinal	Lateral	Longitudinal	Lateral	Max. Angle	Time (ms)	Location
29.7°	8.7°	40.5°	-15.26 (-4.65)	-18.21 (-5.55)	-7.33	-8.91	17.9°	190	2 ft 7.4 in. Downstream of Centerline of Post No. 3

For the study, the longitudinal displacement of the eleventh and last (i.e. downstream) PCB segment in the eleven and sixteen PCB systems were recorded. The eleventh PCB segment displaced 1.7 in. (43 mm) longitudinally while the sixteenth PCB segment displaced 2.7 in. (69 mm) longitudinally, in the sixteen PCB system. The eleventh PCB segment displaced 4.3 in. (109 mm) longitudinally, in the eleven PCB system. This increased longitudinal displacement was not believed to adversely affect the performance of the nested MGS transition system. Thus, an eleven PCB system was deemed suitable for future full-scale crash testing.

Also considered for this study were the maximum rail forces at several locations throughout the length of the MGS. The locations and corresponding maximum rail forces are shown in Figure 87 and Table 59, respectively. The maximum rail force throughout the system was 270.9 kN, which occurred just downstream of the impact location. The maximum rail force near the end shoe attachment location was 227.9 kN. These rail forces were tracked in order to aid in future connection design for blockouts to PCBs and for W-beam end shoe to PCB.
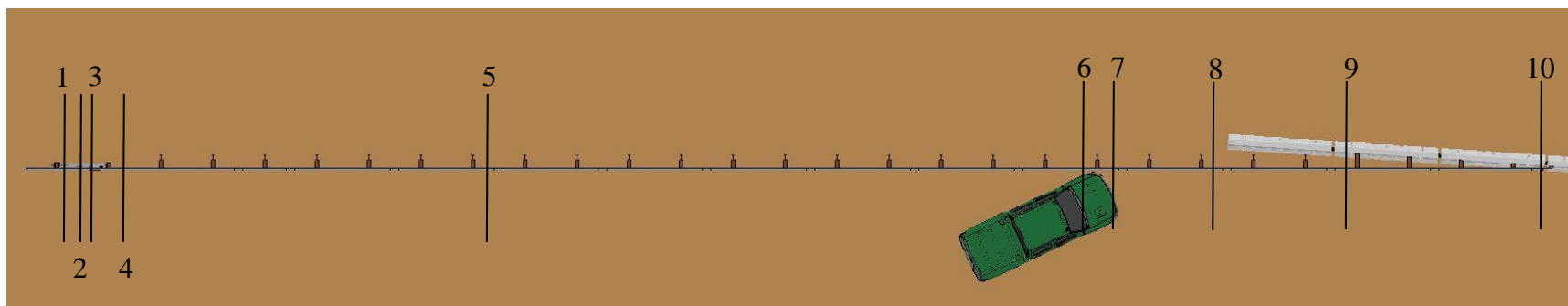
Figure 87. Maximum Rail Force Locations

Table 59. Maximum Rail Forces for CIP with 11 PCB Segments

Location No.	Maximum Rail Force (kN)
1 (Through Anchor Cable)	119.7
2	24.5
3	122.4
4	154.4
5	245.5
6	265.2
7	270.9
8	231.1
9	226.2
10	227.9

24.5 Reverse-Direction Impact Scenarios

Previously, it was discussed that the primary transition consisted of guardrail extending up to PCBs, but that reverse-direction impacts should be considered within the scope of the project. When a preferred design alternative was selected, it was also deemed necessary to perform a simulation study on reverse-direction, TL-3 impacts with 2270P vehicle and into the transition system. Therefore, the nested MGS was subjected to reverse-direction impacts at seven locations, as shown in Figure 88. One impact scenario occurred at the end shoe attachment, three locations occurred at 6 ft − 3 in. (1,905 mm) centers upstream from the end shoe attachment on the PCB system, and three locations occurred at 6 ft − 3 in. (1,905 mm) centers downstream from the end shoe attachment on the nested MGS. These seven impact locations were chosen in an attempt to encompass all portions of the system.
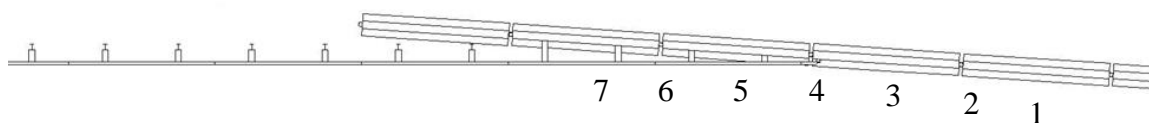
Figure 88. Reverse-Direction Impact Scenarios

24.5.1 Simulation Results

The system captured and redirected the vehicle for all seven impact locations, and none of the vehicle stability values exceeded or were within 20% of the MASH limits, as shown in Table 60. However, the lateral ORA for impact location no. 2 was 16.49 g's, which was within 20% of the MASH limit of 20.49 g's. Upon further inspection, the lateral ORA was deemed unrealistic, likely due to the exaggerated stiffness of the vehicle's rear suspension after the back end of the vehicle impacted the W-beam. This finding led to the determination that the MASH limits would not likely be exceeded.

One concern with the reverse-direction impact scenario was that the vehicle could impact the PCB system and climb the face of PCBs, thus increasing the propensity for the vehicle to override the MGS or become unstable and roll over. While the vehicle did not override the MGS in any of the seven simulated impact locations, the time sequentials for impact location no. 2, as shown in Figure 89, depicted that this concern was not unfounded. At 100 ms, the vehicle had impacted the transition system and begun to climb the face of the PCB. By 200 ms, the vehicle had begun to interact with the MGS, and the bottom of the wheel was approximately at the height of the bottom of the nested MGS. However, by 300 ms, the vehicle had redirected, and MGS override was no longer a concern. These findings led to the determination that the nested MGS configuration would likely contain and redirect the test vehicle and meet TL-3 of MASH. Full-scale crash testing should be conducted in the reverse direction at impact location no. 2 due to the concern for system override.

Table 60. Simulation Results – Reverse-Direction Impact Scenarios

Impact Location	Roll	Pitch	Yaw	OIV ft/s (m/s)		ORA g's	
				Longitudinal	Lateral	Longitudinal	Lateral
1	27.2°	25.8°[1]	33.9°	-7.51 (-2.29)	14.67 (4.47)	-10.36	15.04
2	34.3°	18.1°	32.2°	-8.96 (-2.73)	17.78 (5.42)	-10.89	16.49
3	25.7°	11.9°	36.7°	-12.04 (-3.67)	15.87 (4.84)	11.63	11.95
4	15.2°	12.9°	38.6°	-17.29 (-5.27)	19.23 (5.86)	-10.68	5.87
5	22.0°	10.1°	36.9°	-17.55 (-5.35)	19.85 (6.05)	9.62	6.39
6	29.4°	8.5°	36.8°	-18.21 (-5.55)	-18.04 (-5.50)	-5.90	7.33
7	16.9°	6.7°	37.3°	-19.75 (-6.02)	17.75 (5.41)	-7.50	-7.20

[1]Maximum value was not reached prior to conclusion of simulation

*Yellow cells denote values within 20% of MASH or recommended limits

0 ms

500 ms

100 ms

600 ms

200 ms

700 ms

300 ms

800 ms

400 ms

900 ms
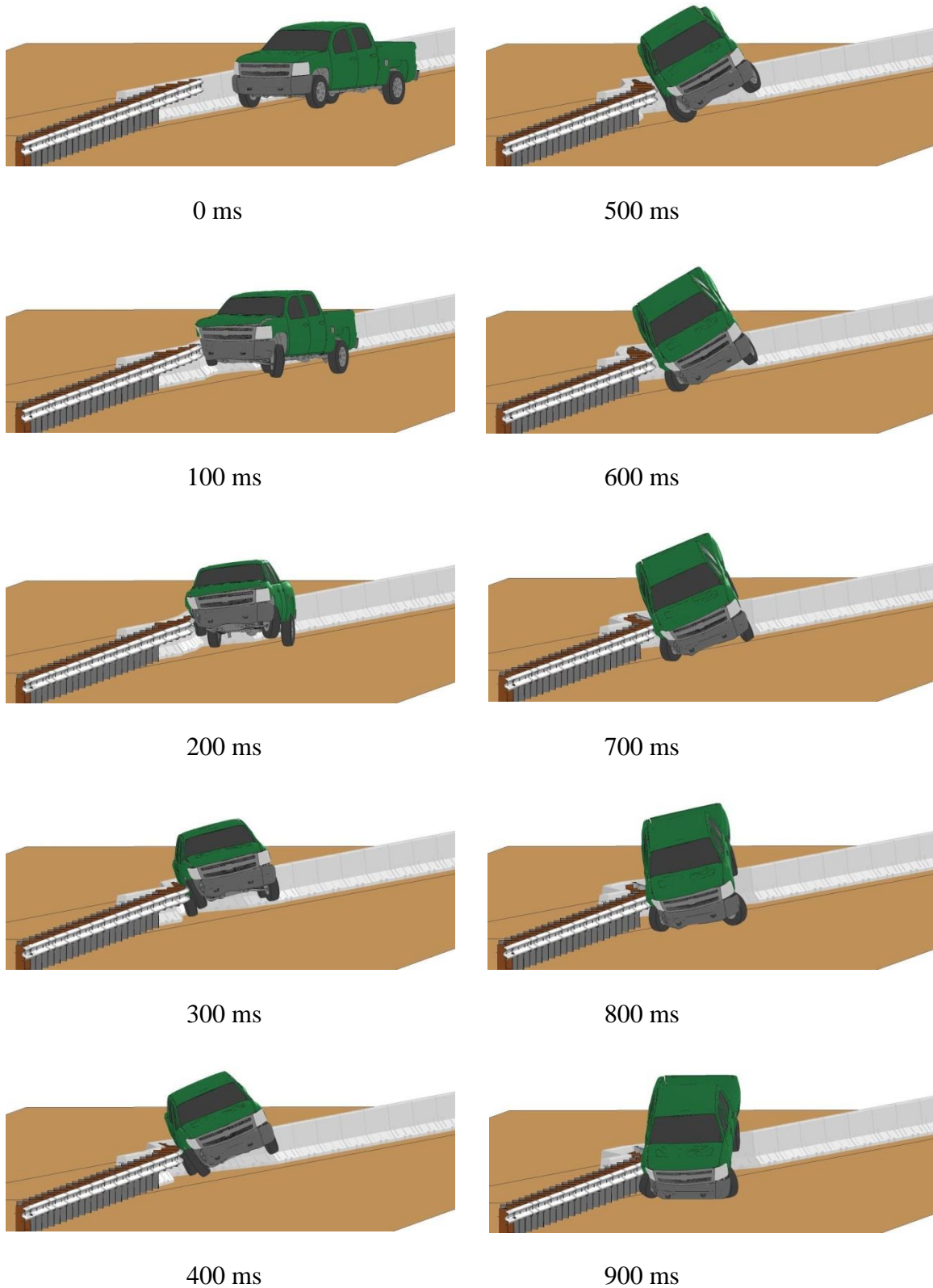
Figure 89. Reverse-Direction Impact Sequentials, Impact Location No. 2

CHAPTER 25 SUMMARY, CONCLUSIONS, AND RECOMMENDATIONS

25.1 Summary and Conclusions

The research objectives were to determine performance and design constraints and to develop a stiffness transition between PCBs and W-beam guardrail that will significantly improve safety for the motoring public and workers within construction zones. The stiffness transition was designed and simulated according to the AASHTO MASH Test Level 3 impact safety criteria. Design concepts were developed and refined through the use of LS-DYNA computer simulation.

Prior to conducting the simulation effort, TAC members provided several design constraints for which the transition should be configured. The modified G4(1S) guardrail was preferred for use; since, it represented the current guardrail standard in Nebraska, which would allow for a simpler retrofit to PCBs. In order to limit damage to the roadway surface and reduce installation time, it was preferred that the PCBs remain free-standing and not be anchored or pinned to the roadway surface. Since PCB placement may occur compacted, crushed limestone, concrete, or asphalt, all three base conditions deserve consideration for the design concepts and subjected to a full-scale crash testing program. Soil grading and terrain were also considered. If PCBs were to be placed on native soil, a minimum lateral width of 4 ft (1,219 mm) and depth of compacted, crushed limestone should be used, or similar, behind the PCB installation due to concerns of PCBs settling or gouging into soft or saturated, native soil.

25.1.1 Design Concept Development

Within these constraints, design concepts were developed and presented to the TAC members. Ease of installation and simplicity were high on the list of priorities. Thus

all of the design concepts were presented in their simplest form, although several potential configurations were presented and may be required in order to improve system performance. The potential configurations included: transition to thrie beam; removal of posts in front of PCBs; blocked connection between rail and PCBs; a cantilever beam attached to the most upstream PCB; nesting of rail; blockouts from the back of posts to the PCBs; and blockout from the back of post to cantilever beam. Five design concepts were originally presented to the TAC members for consideration, as denoted in CHAPTER 3. The pros and cons for each concept were weighed, and design concepts were ranked based on feasibility, ease of installation, and likelihood of success, as denoted below:

(1) Flared PCB – Modified G4(1S);

(2) Parallel PCB – Modified G4(1S);

(3) Beam Attachment Between PCB and Modified G4(1S);

(4) PCB Offset from Modified G4(1S); and

(5) Stiffened PCB and Modified G4(1S).

These rankings served as a guide for making system decisions during the simulation process. Due to project constraints and sponsor priorities, only the first two design concepts and subsequent configurations for each were simulated in the initial study. The results are discussed below.

25.1.2 Flared PCB – Modified G4(1S)

The Flared PCB – Modified G4(1S) design concept used a W-beam end shoe to attach the modified G4(1S) directly to the 15H:1V flared F-shape PCB system. Simulation results quickly showed that the rail height of the modified G4(1S) was

inadequate to safely capture and redirect the vehicle. Thus, a transition to thrie beam was utilized in all of the following configurations, which showed a higher propensity for vehicle capture and redirection. Other configurations were considered to alleviate post wedging against PCBs, slow initiation of PCB displacement, and high pocketing angles. Five configurations were simulated for the Flared PCB – Modified G4(1S) design concept, and the results were analyzed, compared, and ranked, as shown below:

      (1) Nested Thrie Beam with Fully-Blocked Rail;

      (2) Thrie Beam with Fully-Blocked Rail and Cantilever Beam;

      (3) Thrie Beam End Shoe;

      (4) Thrie Beam with Fully-Blocked Rail; and

      (5) W-Beam End Shoe.

25.1.3 Parallel PCB – Modified G4(1S)

When the Parallel PCB – Modified G4(1S) design concept was presented to the TAC members, it depicted the modified G4(1S) guardrail attached to the 15H:1V flared PCB system with two PCB segments placed parallel to and behind the modified G4(1S). The posts of the modified G4(1S) remained in front of PCBs. These posts were intended to initiate PCB displacement through rotation. Based on the results from the Flared PCB – Modified G4(1S) design concept and using engineering judgment, modifications were made to this design. The rail height of the modified G4(1S) proved incapable of vehicle capture and redirection, and it was transitioned to thrie beam. Also, the single thrie beam yielded high pocketing angles, and nested thrie beam was installed ahead of the PCB system. Also, posts in front of the PCBs showed a tendency to wedge against PCBs and cause vehicle instabilities and elevated occupant risk values. Thus, all of the posts in front

of PCBs were removed, and blockouts were installed in their place. The PCBs behind nested thrie beam configuration yielded two longitudinal ORAs that were marginal but with acceptable vehicle stability and pocketing angles. A cantilever beam was installed to the most upstream PCB to investigate if it would improve safety performance. The PCBs behind nested thrie beam with cantilever beam configuration yielded values similar to the previous configuration in vehicle behavior, occupant risk, and pocketing angles. Based on these results, the Parallel PCB − Modified G4(1S) configurations were analyzed and ranked, as shown below:

(1) PCBs Behind Nested Thrie Beam and

(2) PCBs Behind Nested Thrie Beam with Cantilever Beam

25.1.4 Design Concept Summary

The results from the Flared PCB − Modified G4(1S) and the Parallel PCB − Modified G4(1S) design concepts and subsequent configurations were presented to the TAC members for consideration. The pros and cons for each configuration were considered, and TAC members determined that several of the configurations were too complex with a transition to thrie beam, installation and fabrication of a cantilever beam, and/or nesting of the rail. Based on the simulation finding that the rail height of the modified G4(1S) was inadequate to capture the vehicle, TAC members advised the use of the Midwest Guardrail System (MGS) in lieu of the modified G4(1S). It was predicted that the taller MGS would improve vehicle capture and redirection without the need to transition from W-beam to thrie beam.

25.1.5 Flared PCB – MGS

The Flared PCB – MGS design concept was similar to the Flared PCB – Modified G4(1S) design concept, except that a taller MGS system was now attached to the 15H:1V flared PCB system. Although the modified G4(1S) had indicated that posts in front of PCBs would lead to wedging of posts against PCBs, the taller rail height of the MGS was believed capable to capture the vehicle and reduce vehicle instabilities, so two posts remained in front of PCBs. Posts were removed when they interfered with placement of PCBs, and blockout were installed in their place. Simulation results for the MGS end shoe configuration indicated that occupant risk values were high due to vehicle snag, and pocketing angles were high for impact locations upstream from the PCB system. Several configurations were considered to alleviate high occupant risk values, pocketing angles, and slow initiation of PCB displacement. Seven configurations were simulated for the Flared PCB – MGS design concept, and the results were analyzed, compared, and ranked, as shown below:

(1) MGS with Nested W-Beam;

(2) MGS with Fully-Blocked Rail and Cantilever Beam;

(3) MGS with Cantilever Beam;

(4) MGS End Shoe Connection;

(5) MGS with Blockout to Cantilever Beam;

(6) MGS with Fully-Blocked Rail; and

(7) MGS with Blockouts Behind Posts.

25.1.6 Design Selection

After simulating of the three design concepts, the results were compared against each other, and the configurations were ranked within each design concept. These rankings were presented to the TAC members for consideration, and a unanimous decision was reached to move forward with the nested MGS configuration. This decision was made based on the simulation results, which indicated that all of the vehicle behavior values, occupant risk values, and pocketing angles were well below the MASH or recommended limits for all impact locations. No other configuration yielded similar results, which provided confidence that the nested MGS would meet the MASH TL-3 impact safety standards. Also, the TAC members were pleased with the ease of installation as it would not require any new components other than a few brackets for supporting or attaching blockouts to the face of the PCBs.

25.1.7 CIP Study

The final portion of this study was to conduct a simulation effort to find the CIP for the selected design alternative for later use in the full-scale crash testing program. This process was completed through a number of steps. First, the nested MGS was subjected to impacts near the end shoe connection to ensure that the vehicle would be safely captured and redirected for impacts on the 15H:1V flared PCB system alone. The results indicated that the vehicle was safely captured and redirected for all five impact locations near the end shoe.

The next portion of the CIP study was to determine the critical attachment location between the nested MGS and the PCB system. It was determined that a minimum of three PCB segments should be installed behind and upstream from the

nested MGS that is attached to the PCB system in order to provide adequate longitudinal barrier tension to capture and redirect the vehicle as well as prevent vehicle snag on the upstream end of the PCB system. Thus, the critical attachment location should occur on the fourth PCB segment. Three attachment locations were simulated for investigating the critical attachment location. These locations included: (1) the end shoe attached to the upstream end of the fourth PCB to allow for the minimum PCB length behind the MGS; (2) the end shoe attached toward the center of the fourth PCB segment such that one more post upstream of the PCB system would just miss the most upstream PCB segment upon rotation; (3) the end shoe attached toward the center of the fourth PCB segment, but such that the one more post upstream of the PCB system would impact the most upstream PCB upon rotation. Each attachment location was simulated at four impact locations near the upstream end of the PCB system. The results indicated that the first attachment location, corresponding to a minimum PCB length behind the MGS, provided the most critical attachment location.

The next part of the CIP study was to find the critical impact location. The simulation results presented in CHAPTER 19 indicated that impact location no. 9 yielded some of the higher occupant risk values and the highest pocketing angle. Thus, it was determined that the CIP would be near impact location no. 9, and the nested MGS configuration was subjected to impacts at 18¾ in. (476 mm) centers between impact location nos. 8 and 10. Based on the simulation results, impact location no. 9 still yielded the highest pocketing angle and several of the occupant risk values. Therefore, the CIP was determined to occur at impact location no. 9.

Researchers wanted to refine the system even further to recommend the shortest design. Therefore, a simulation effort was conducted to investigate a reduced-length, PCB installation. The original configuration for testing and evaluation of the F-shape PCB system used a sixteen-PCB system with impacts near the center of the installation. In order to investigate a reduced length, three PCBs were upstream and eight PCBs were installed downstream from the end shoe attachment to the PCB system, thus resulting in a total of eleven PCBs. This nested MGS with a reduced-length PCB installation was impacted at the CIP location. Results indicated that the nested MGS configuration was not adversely affected with the minimum PCB installation.

The final portion of the CIP study was to investigate reverse-direction impacts into the nested MGS transition system. The nested MGS was subjected to reverse-direction impacts at seven locations spaced on 6 ft − 3 in. (1,905 mm) centers upstream from the end shoe attachment through 6 ft − 3 in. (1,905 mm) centers downstream from the end shoe attachment, including one impact at the end shoe attachment. The simulation results indicated that the vehicle was safely captured and redirected for all seven impact locations. However, the reverse-direction simulations indicated that a future full-scale crash testing program should include an evaluation at impact location no. 2. First, it showed the most vehicle climb on the PCB system. Second, a vehicle wheel was near the top of the MGS and could lead to MGS override.

25.2 Recommendations

A second phase of the research project will focus on the final design, fabrication, and full-scale crash testing of the TL-3 transition between MGS guardrail and F-shaped PCBs. It is anticipated that three full-scale crash tests would be required to fully evaluate

the transition system. These crash tests would include MASH test designation nos. 3-20 and 3-21, which are used to evaluate the barrier transition with a 1100C small car and a 2270P pickup truck, respectively. In addition, it is anticipated that a reverse-direction impact according to test designation no. 3-21 would be used with the 2270P test vehicle to evaluate the transition when installed in two-way traffic applications.

Based on this research, the nested MGS configuration was recommended for evaluation using a full-scale crash testing program. In addition, the nested MGS should use an attachment location configured per Case 1, which represented the minimum PCB length behind the MGS. Also, the W-beam end shoe should be attached to the upstream end of the fourth PCB segment with three PCB segments extending behind the nested MGS. A minimum of five 12-ft 6-in. (3,810 mm) long, W-beam sections should be nested upstream from the end shoe. For testing purposes, the transition should consist of at least a twenty-five post, MGS system and an eleven segment PCB system at a 15H:1V flare. The critical impact point should occur at impact location no. 9 (i.e., the centerline of fifth guardrail post upstream from end shoe attachment) for test designation no. 3-21. The reverse-direction test scenario should use impact location no. 2 (i.e., 12 ft − 6 in. (3,810 mm) longitudinally upstream from the end shoe attachment) for test designation no. 3-21.

A simulation effort involving impacts with the 1100C small car was not conducted. As noted in CHAPTER 5, the 2270P test vehicle was deemed more critical than the 1100C small car, for the concept development phase, due the likelihood of increased barrier deflections, rail and anchor loads, rail pocketing, and wheel snag.

Therefore, test designation no. 3-11 for the full-scale crash testing program should use MASH procedures for determining a critical impact point.

25.2.1 Future Research

The current nested MGS model utilized simplified connections between the blockouts and PCBs. The blockout bolts were attached directly to the face of the PCB segments, which would not be possible in the actual configuration. Thus, design of the actual connection must be completed in order to properly attach the blockouts to the PCBs. Also, an attachment wedge was used to rigidly attach the W-beam end shoe to the face of the PCB, which may be challenging in the actual configuration. Thus, a connection must be designed between the W-beam end shoe and the PCB.

Upon completion of a full-scale vehicle crash testing program, further validation and refinement of the nested MGS model is recommended. While this overall transition configuration utilized two different system models that had been separately validated using results from full-scale crash testing, their dynamic impact behaviors when connected to one another have not been validated with actual crash testing. When this physical test data becomes available, an opportunity will exist to improve the accuracy of the FEA barrier system model.

Throughout the simulation process, a number of modeling difficulties were encountered. These difficulties along with remedies were documented and compiled. Examples and a further explanation may be found in Appendix C.

CHAPTER 26 REFERENCES

1. Bielenberg, B.W., Faller, R.K., Rohde, J.R., Reid, J.D., Sicking, D.L., and Holloway, J.C., *Development of Tie-Down and Transition Systems for Temporary Concrete Barrier on Asphalt Road Surfaces*, MwRSF Report No. TRP-03-180-06, Midwest Roadside Safety Facility, University of Nebraska-Lincoln, February 2007.

2. Wiebelhaus, M.J., Terpsma, R.J., Lechtenberg, K.A., Reid, J.D., Faller, R.K., Bielenberg, R.W., Rohde, J.R., and Sicking, D.L., *Development of a Temporary Concrete Barrier to Permanent Concrete Median Barrier Approach Transition*, MwRSF Report No. TRP-03-208-10, Midwest Roadside Safety Facility, University of Nebraska-Lincoln, July 2010.

3. Bryden, J.E., and Phillips, R.G., *Roadside Barriers for Bridge-Pier Protection,* Research Report 117, Engineering Research and Development Bureau, New York State Department of Transportation, Albany, Dec. 1984.

4. Bryden, J.E., and Phillips, R.G., *Roadside Barriers for Bridge-Pier Protection,* Transportation Research Record 1024, Washington, D.C., 1985

5. *Manual for Assessing Safety Hardware (MASH)*, American Association of State Highway and Transportation Officials (AASHTO), Washington, D.C., 2009.

6. Hallquist, J.O. *LS-DYNA Keyword User's Manual, Volume I*. Livermore, CA: Livermore Software Technology Corporation. 2007.

7. Marzougui, D., Buyuk, M., and Kan, S., *Performance Evaluation of Portable Concrete Barriers*, NCAC Report 2007-R-004, National Crash Analysis Center (NCAC), January 2007.

8. Faller, R.K., Rohde, J.R., Rosson, B.T., Smith, R.P., and Addink, K.H., *Development of a TL-3 F-Shape Temporary Concrete Median Barrier,* MwRSF Report No. TRP-03-64-96, Midwest Roadside Safety Facility, University of Nebraska-Lincoln, December 1996.

9. Polivka, K.A., Faller, R.K., Sicking, D.L., Rohde, J.R., Bielenberg, B.W., Reid, J.D., and Coon, B.A., Performance Evaluation of the Free-Standing Temporary Barrier – Update to NCHRP 350 Test No. 3-11 with 28" C.G. Height (2214TB-2), MwRSF Report No. TRP-03-174-06, Midwest Roadside Safety Facility, University of Nebraska-Lincoln, October 2006.

10. Beason, W.L., and Bullard, D.L., Jr., *Development of a Limited-Slip Portable Concrete Barrier Connection*, Research Report 1959-1, Texas Transportation Institute, College Station, TX, November 1993.

11. Jewell, J., Weldon, G., and Peter, R., *Compliance Crash Testing of K-Rail Used in Semi-Permanent Installations*, Final Report No. FWHA/CA/OR-99/07, State of California Department of Transportation, October 1999.

12. Bielenberg, B.W., Faller, R.K., Reid, J.D., Holloway, J.C., Rohde, J.R., and Sicking, D.L., *Development of a Tie-Down System for Temporary Concrete Barriers*, MwRSF Report No. TRP-03-115-02, Midwest Roadside Safety Facility, University of Nebraska-Lincoln, August 2002.

13. Polivka, K.A., Faller, R.K., Rohde, J.R., Holloway, J.C., Bielenberg, B.W., and Sicking, D.L., *Development and Evaluation of a Tie-Down System for the Redesigned F-Shape Concrete Temporary Barrier*, MwRSF Report No. TRP-03-134-03, Midwest Roadside Safety Facility, University of Nebraska-Lincoln, August 2003.

14. Sheikh, N.M., Bligh, R.P., and Menges, W.L, *Crash Testing and Evaluation of the 12 ft Pinned F-Shape Temporary Barrier*, Research Report 405160-3-1, Texas Transportation Institute, College Station, TX, April 2008.

15. Howard, C.N., Stolle, C.J., Lechtenberg, K.A., Faller, R.K., Reid, J.D., and Sicking, D.L., *Dynamic Evaluation of a Pinned Anchoring System for New York State's Temporary Concrete Barriers*, MwRSF Report No. TRP-03-216-09, Midwest Roadside Safety Facility, University of Nebraska-Lincoln, September 2009.

16. Lechtenberg, K.A., Faller, R.K., Reid, J.D., and Sicking, D.L., *Dynamic Evaluation of a Pinned Anchoring System for New York State's Temporary Concrete Barriers – Phase II*, MwRSF Report No. TRP-03-224-10, Midwest Roadside Safety Facility, University of Nebraska-Lincoln, January 2010.

17. Rosenbaugh, S.K., Bielenberg, R.W., Faller, R.K., Reid, J.D., Rohde, J.R., Sicking, D.L., Lechtenberg, K.A., and Holloway, J.C., *Termination and Anchorage of Temporary Concrete Barriers*, MwRSF Report No. TRP-03-209-09, Midwest Roadside Safety Facility, University of Nebraska-Lincoln, October 2009.

18. Abu-Odeh, A.Y., Kim, K.M., and Bligh, R.P, *Guardrail Deflection Analysis, Phase I: (2010-2011),* Research Report 405160-24, Texas Transportation Institute, College Station, TX, August 2011.

19. Faller, R.K., Reid, J.D., Rohde, J.R., Sicking, D.L., and Keller, E.A., *Two Approach Guardrail Transitions for Concrete Safety Shape Barriers*, MwRSF Report No. TRP-03-69-98, Midwest Roadside Safety Facility, University of Nebraska-Lincoln, May 1998.

20. Polivka, K.A., Faller, R.K., Sicking, D.L., Rohde, J.R., Bielenberg, B.W., Reid, J.D., and Coon, B.A., Performance Evaluation of the Guardrail to Concrete Barrier Transition – Update to NCHRP 350 Test No. 3-21 with 28" C.G. Height (2214T-1), MwRSF Report No. TRP-03-175-06, Midwest Roadside Safety Facility, University of Nebraska-Lincoln, October 2006.

21. Eller, C.M., Polivka, K.A., Faller, R.K., Sicking, D.L., Rohde, J.R., Reid, J.D., Bielenberg, R.B., and Allison, E.M., *Development of the Midwest Guardrail System*

(MGS) W-Beam to Thrie Beam Transition Element, MwRSF Report No. TRP-03-167-07, Midwest Roadside Safety Facility, University of Nebraska-Lincoln, November 2007.

22. Polivka, K.A., Faller, R.K., Reid, J.D., Sicking, D.L., Rohde, J.R., and Holloway, J.C., *Crash Testing of Missouri's W-Beam to Thrie Beam Transition Element,* MwRSF Report No. TRP-03-93-00, Midwest Roadside Safety Facility, University of Nebraska-Lincoln, September 2000.

23. Arrington, D.R., Bligh, R.P., and Menges, W.L., *MASH Test 3-21 on TL-3 Thrie Beam Transition without Curb,* Research Report No. 9-1002-12-3, Texas Transportation Institute, College Station, TX, July 2013.

24. Rosenbaugh, S.K., Lechtenberg, K.A., Faller, R.K., Sicking, D.L., Bielenberg, R.W., and Reid, J.D., *Development of the MGS Approach Guardrail Transition Using Standardized Steel Posts*, MwRSF Report No. TRP-03-210-10, Midwest Roadside Safety Facility, University of Nebraska-Lincoln, December 2010.

25. Beason, W.L., Sheikh, N.M., Bligh, R.P., and Menges, W.L, *Development of a Low-Profile to F-Shape Transition Barrier Segment*, Research Report 0-5527-1, Texas Transportation Institute, College Station, TX, September 2006.

26. Stoughton, R.L., Parks, D.M., Stoker, J.R., Nordlin, E.F., *Vehicular Impact Tests of Precast Concrete Median Barriers with Corrugated Ends and Tensioned Cables*, Final Report No. FWHA-CA-TL-78-13, State of California Department of Transportation, June 1978.

27. Van Kirk, J.L, Stoughton, R.L., Stoker, J.R., and Nordlin, E.F., *Vehicular Impact Test on Steel Channel-Beams Spanning a Gap in a Continuous Concrete Median Barrier*, Final Report No. CA-TL-79-01, State of California Department of Transportation, February 1979.

28. Addink, K.H., Pfeifer, B.G., and Rohde, J.R., *Development of a Temporary Barrier System for Off-Road Applications*, MwRSF Report No. TRP-03-66-98, Midwest Roadside Safety Facility, University of Nebraska-Lincoln, March 1998.

29. Stolle, C.J., Polivka, K.A., Faller, R.K., Sicking, D.L., Bielenberg, R.W., Reid, J.D., Rohde, J.R., Allison, E.M., and Terpsma, R.J., *Evaluation of Box Beam Stiffening of Unanchored Temporary Concrete Barriers,* MwRSF Report No. TRP-03-202-08, Midwest Roadside Safety Facility, University of Nebraska-Lincoln, March 2008.

30. Jowsa, E.R., Faller, R.K., Rosenbaugh, S.K., Sicking, D.L., and Reid, J.D., *Safety Investigation and Guidance for Retrofitting Existing Approach Guardrail Transitions*, MwRSF Report No. TRP-03-266-12, Midwest Roadside Safety Facility, University of Nebraska-Lincoln, August, 2012.

31. Polivka, K.A., Faller, R.K., Sicking, D.L., Reid, J.D., Rohde, J.R., Holloway, J.C., Bielenberg, R.W., and Kuipers, B.D., *Development of the Midwest Guardrail System (MGS) for Standard and Reduced Post Spacing and in Combination with Curbs*, MwRSF Research Report No. TRP-03-139-04, Midwest Roadside Safety Facility, University of Nebraska-Lincoln, September 2004.

32. Julin, R.D., Reid, J.D., Faller, R.K., and Mongiardini, M., *Determination of the Maximum MGS Mounting Height – Phase II Detailed Analysis Using LS-DYNA®*, MwRSF Report No. TRP-03-274-12, Midwest Roadside Safety Facility, University of Nebraska-Lincoln, December 2012.

33. Soyland, K., Faller, R.K., Holloway, J.C., and Sicking, D.L., *Development and Testing of an Approach Guardrail Transition to a Single Slope Concrete Median Barrier,* MwRSF Report No. TRP-03-47-95, Midwest Roadside Safety Facility, University of Nebraska-Lincoln, November 1995

APPENDICES

Appendix A.   PCB Evaluation Results

The results from NCAC's computer simulation study that were used to evaluate the performance of PCB systems are found in this appendix. The results include ride-down acceleration, ride-down velocity, barrier rotation angle, and barrier displacement. The results are compiled by barrier type: F-shape; New Jersey shape; single slope; vertical shape; and inverted shape.
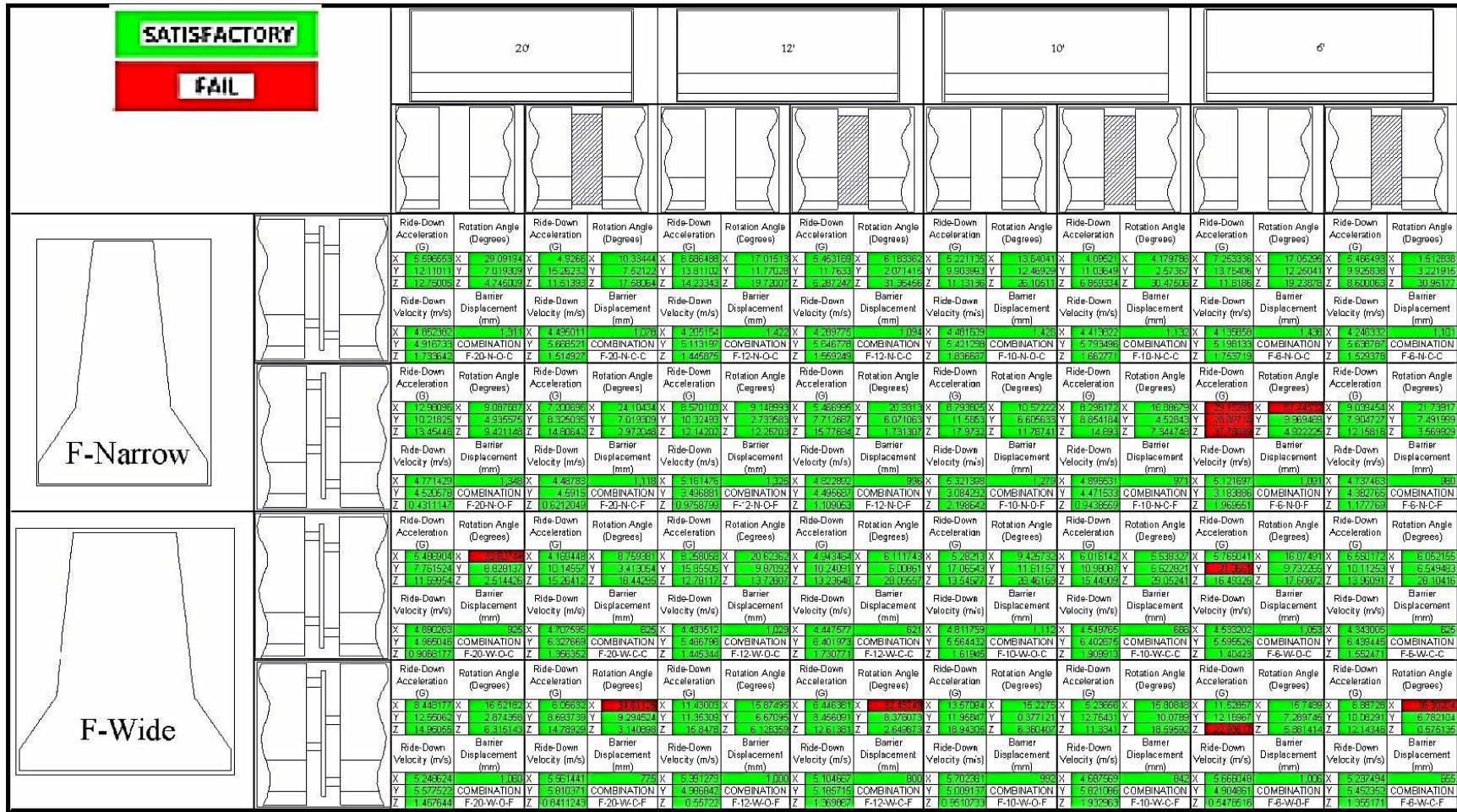
Figure A-1. F-Shape PCB Evaluation [7]

Figure A-2. New Jersey Shape PCB Evaluation [7]

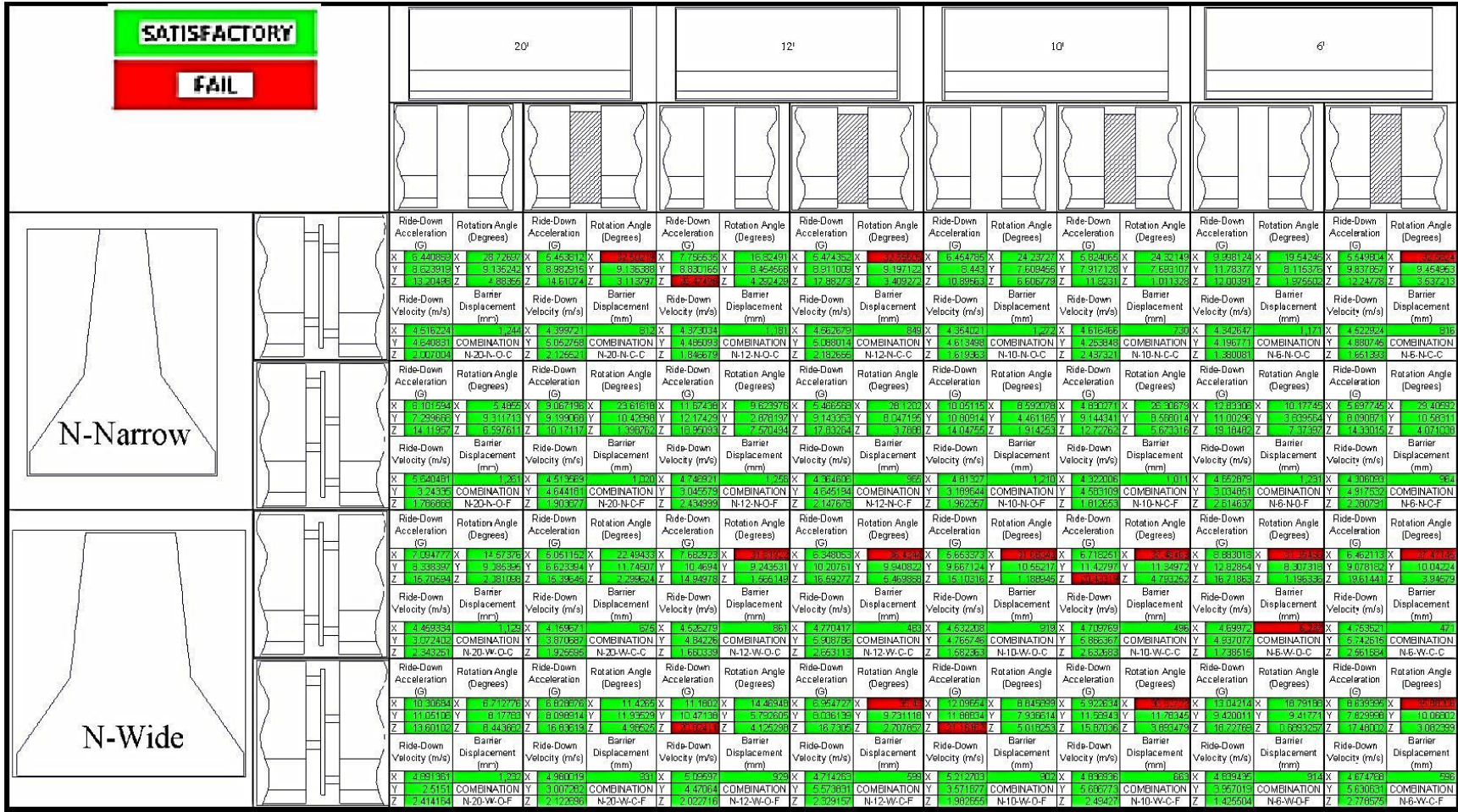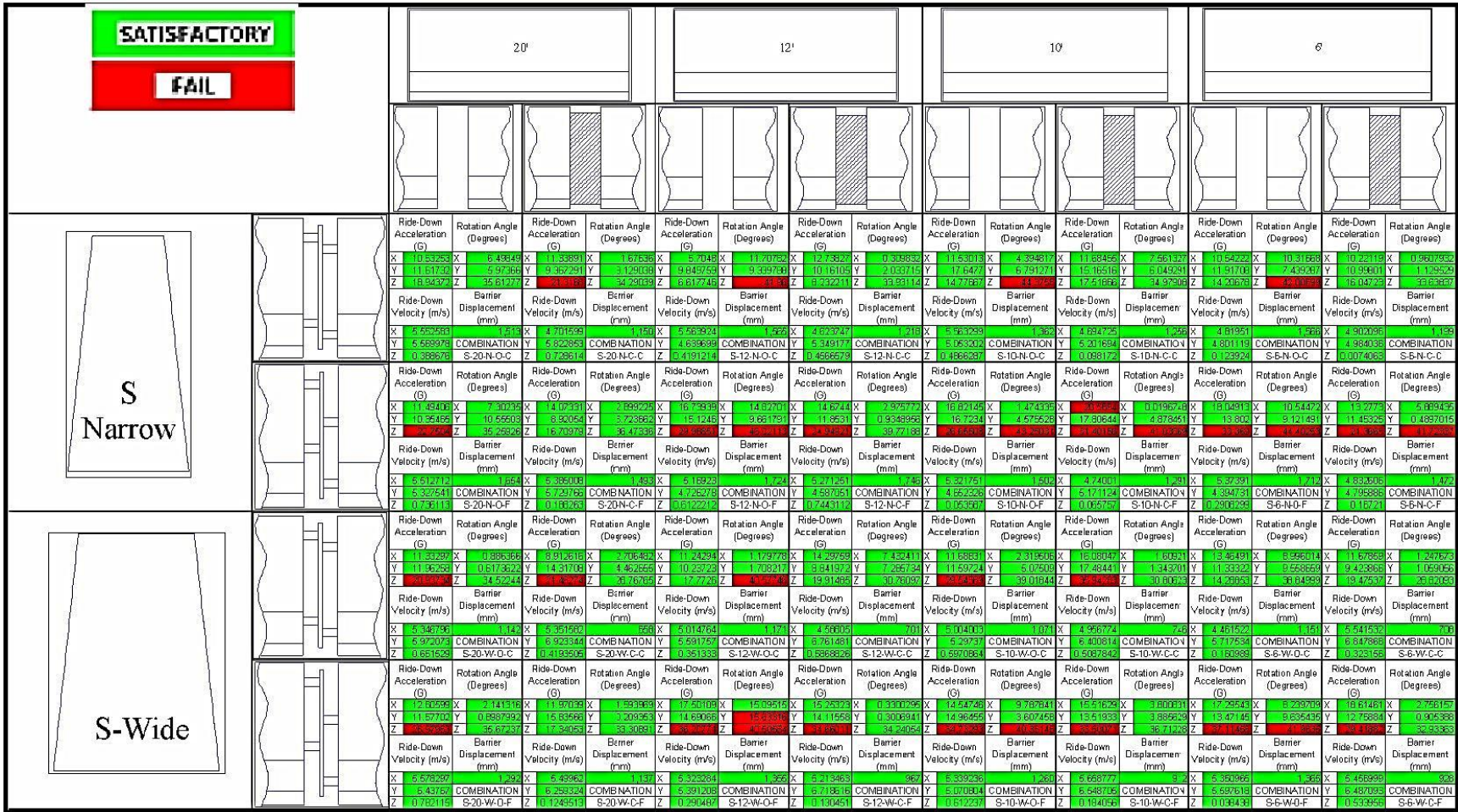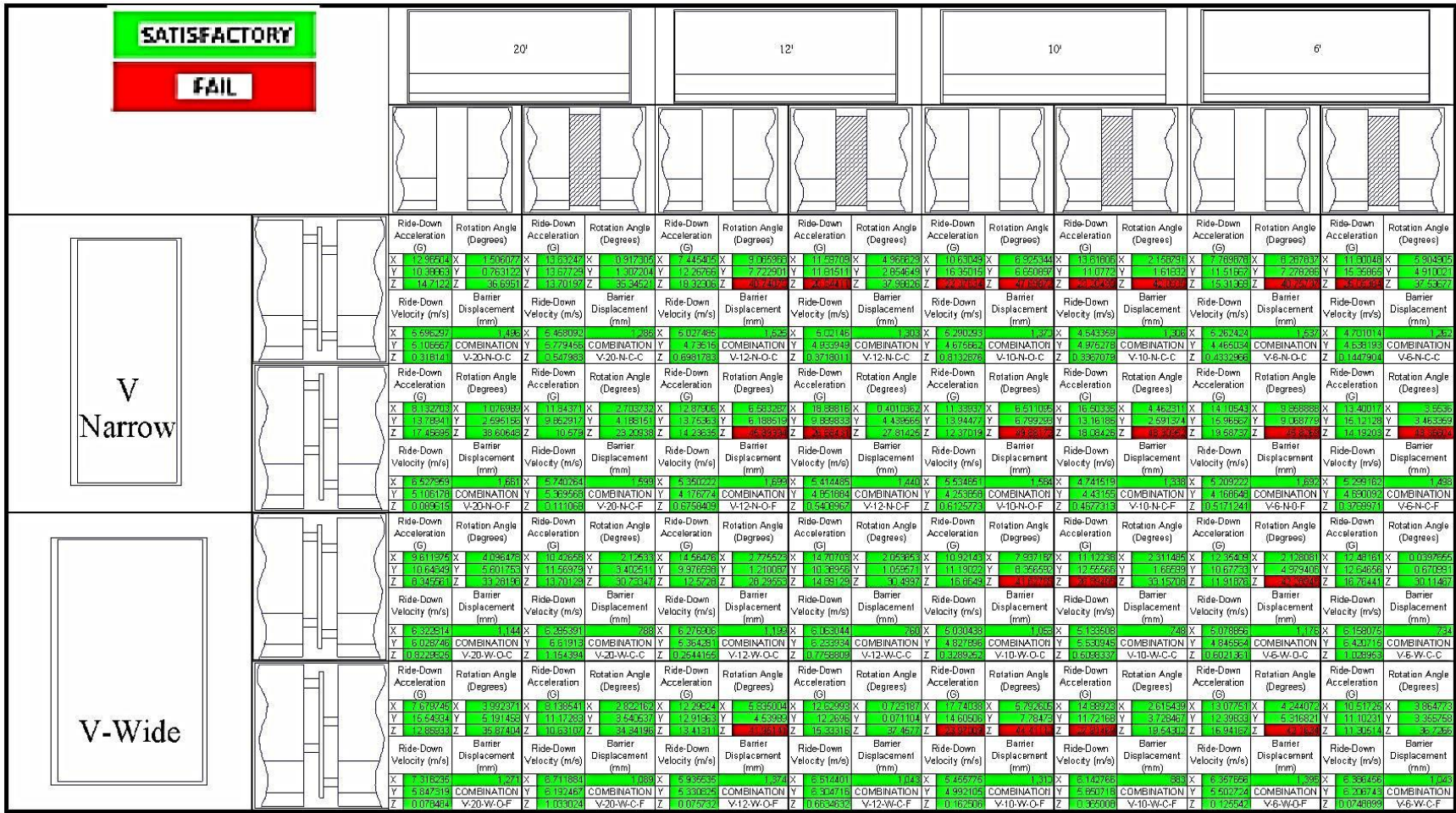Figure A-3. Single Slope PCB Evaluation [7]

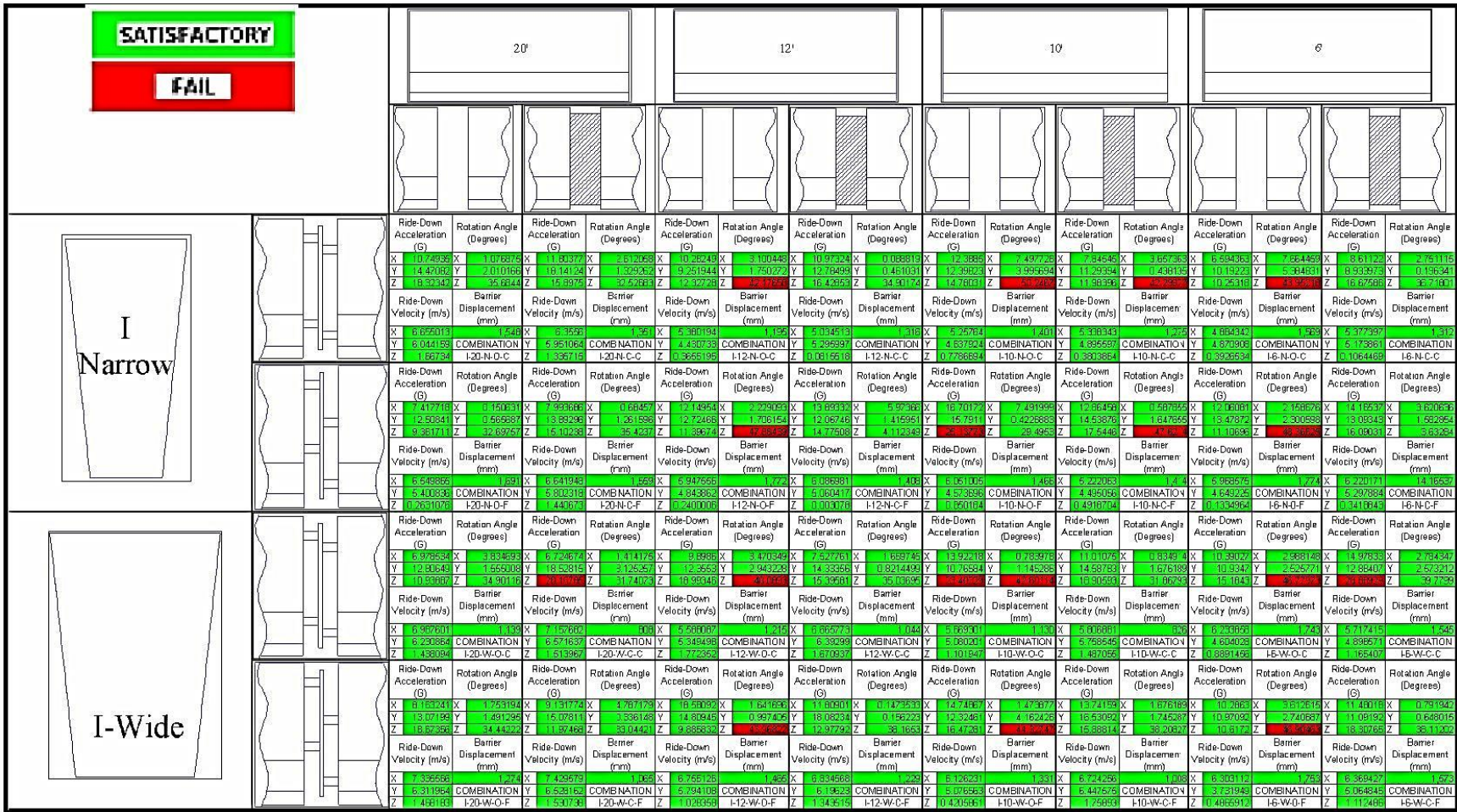Figure A-4. Vertical Shape PCB Evaluation [7]

Figure A-5. Inverted Shape PCB Evaluation [7]

231

Appendix B. W-Beam Guardrail Deflections

The results from TTI's guardrail deflection study are found in this appendix. The results include testing agency, system description, maximum permanent and dynamic deflections, and working width.

Table B-1. W-Beam Guardrail Deflections [18]

Test No. Agency, Year	Rail Height	Post Size and Material	Post Spacing	Blockout	Maximum Deflection Permanent	Maximum Deflection Dynamic	Working Width	FHWA Letter No.	System Configuration
471470-26 TTI, 1994 (18)[1]	27 inches (686 mm)	5 ft-4 inch long 6×8 inch wood	6 ft-3 inch	6×8×14 inch wood	27.2 inches (690 mm)	32.3 inches (820 mm)	N/A	N/A	W-beam, strong post G4(2W) guardrail (*NCHRP 350* 3-11)
405421-1 TTI, 1995 (19)[2]	27.8 inches (706 mm)[3]	6 ft long W6×8.5 steel	6 ft-3 inch	5⅞×7⅞× 14⅛ inch timber	27.6 inches (700 mm)	39.4 inches (1000 mm)	N/A	N/A	Modified W-beam, strong post G4(1S) guardrail (*NCHRP 350* 3-11)
405391-1 TTI, 1995 (20)[1]	27.8 inches (706 mm)[3]	6 ft-3 inch long 7.25 inch dia round wood	6 ft-3 inch	5¾×5 ¾ ×14 inch wood	31.1 inches (790 mm)	43.3 inches (1100 mm)	N/A	N/A	Round wood post G4(2W) guardrail (*NCHRP 350* 3-11)
400001-MPT1 TTI, 1996 (21)[2]	27.8 inches (706 mm)[3]	6 ft long W6×9 steel	6 ft-3 inch	6×7⅞× 14 inch recycled polyethylene block	28.3 inches (720 mm)	44.5 inches (1130 mm)	N/A	N/A	Modified G4(1S) guardrail with recycled blockouts (*NCHRP 350* 3-11)
439637-1 TTI, 1997 (22)[2]	27.8 inches (706 mm)[3]	5 ft-6 inch long W6×9 steel	6 ft-3 inch	6×6×14 inch routed wood	17.7 inches (450 mm)	29.5 inches (750 mm)	N/A	N/A	Modified G4(1S) guardrail (*NCHRP 350* 3-11)
400001-APL1 TTI, 2000 (23)[2]	27.8 inches (706 mm)[3]	4 ft-10.5 inch long 6×7.5 inch recycled plastic	6 ft-3 inch	5⅞×7⅞× 14⅛ inch timber	31.3 inches (795 mm)	53.6 inches (1362 mm)	5.47 ft (1.67 m)	N/A	Modified G4(2W) guardrail with Amity plastic's recycled posts (*NCHRP 350* 3-11)
404201-1 TTI, 2000 (24)[2]	27.8 inches (706 mm)[3]	5 ft-11 inch long 5⅞×7⅞ inch wood	6 ft-3 inch	5⅞ × 7⅞ ×14⅛ inch wood	33.9 inches (860 mm)	40.6 inches (1032 mm)	N/A	N/A	G4(2W) with 100 mm asphaltic curb (*NCHRP 350* 3-11)

Table B-2. W-Beam Guardrail Deflections, Cont. [18]

Test No. Agency, Year	Rail Height	Post		Blockout	Maximum Deflection		Working Width	FHWA Letter No.	System Configuration
		Size and Material	Spacing		Permanent	Dynamic			
473750-3 TTI, 2000 (25)[1]	32.3 inches (820 mm)	5 ft-3 inch long S3×5.7 steel	12 ft-6 inch	N/A	64.6 inches (1640 mm)	83.5 inches (2120 mm)	N/A	N/A	Modified PennDOT Type 2 weak post guiderail (G2) (NCHRP 350 3-11)
400001-CFI1 TTI, 2001 (26)[2]	27.8 inches (706 mm)	5 ft-3 inch long HALCO X-48 steel	6 ft-3 inch	6⅛×7⅞× 14⅛ inch Recycled plastic	12.8 inches (326 mm)	31.9 inches (811 mm)	3.8 ft (1.16 m)	B80	G4 guardrail with HALCO X-48 steel posts and recycled plastic blockouts (NCHRP 350 3-11)
400001-ILP2 TTI, 2001 (27)[2]	27.8 inches (705 mm)	5 ply laminated 5 ft-4 inch long 5⅞×7⅞ inch wood	6 ft-3 inch	5 ply laminated 5⅞ × 7⅞ ×14 inch wood	13.4 inches (340 mm)	31.1 inches (789 mm)	2.87 ft (0.88 m)	B92	G4(2W) guardrail with imperial 5-Lam posts and blockouts (NCHRP 350 3-11)
441622-1 TTI, 2001 (28)[1]	27 inches (686 mm)	6 ft long W6×9 steel	6 ft-3 inch	6×8×14 inch routed wood	13.4 inches (340 mm)	23 inches (584 mm)	3.43 ft (1.05 m)	B64B	Modified G4(1S) guardrail on concrete mow strip (NCHRP 350 3-11)
41-1655-001 E-TECH Inc. 2001 (29)[2]	27.8 inches (706 mm)[3]	5 ft-3 inch long HALCO X-40 Steel	6 ft-3 inch	6⅛×7⅞× 14⅛ inch Recycled plastic	27.6 inches (700 mm)	51.2 inches (1300 mm)	N/A	B80A	G4 guardrail with light weight HALCO X-40 steel posts and recycled plastic blockouts (NCHRP 350 3-11)
441622-2 TTI, 2002 (28)[2]	27 inches (686 mm)	7 inch dia round wood	6 ft-3 inch	6×8×14 inch routed wood	22.4 inches (570 mm)	27.1 inches (688 mm)	3.88 ft (1.18 m)	B64B	G4(2W) guardrail on round posts in mow strip (NCHRP 350 3-11)

Table B-3. W-Beam Guardrail Deflections, Cont. [18]

Test No. Agency, Year	Rail Height	Post		Blockout	Maximum Deflection		Working Width	FHWA Letter No.	System Configuration
		Size and Material	Spacing		Permanent	Dynamic			
400001-MON1 TTI, 2002 (30) [1]	27.8 inches (706 mm)	6-ft long W6×9 steel	6 ft-3 inch	Mondo polymer blocks	10.4 inches (265 mm)	33 inches (837 mm)	3.93 ft (1.2 m)	N/A	Modified G4(1S) guardrail with Mondo Polymer blockouts (*NCHRP 350* 3-11)
NPG-4 MwRS, 2002 (31) [2]	31 inches (787 mm)	6 ft long W6×9 steel	6 ft-3 inch	6×12× 14 inch routed wood	25.7 inches (652 mm)	43.1 inches (1094 mm)	4.13 ft (1.26 m)	B133	Modified MGS (G4(1S) guardrail) (*NCHRP 350* 3-11)
NPG-5 MwRSF, 2002 (31) [2]	31 inches (787 mm)	6 ft long W6×9 steel	6 ft-3 inch	6×12× 14 inch routed wood	24.1 inches (611 mm)	40.3 inches (1024 mm)	4.77 ft (1.45 m)	B133	Same system of NPG-4 with 6 inch tall concrete curb (*NCHRP 350* 3-11)
NPG-6 MwRSF, 2002 (31) [2]	31 inches (787 mm)	6 ft long W6×9 steel	18¾ inch (Post 11-51)	6×12× 14 inch routed wood	12 inches (305 mm)	17.6 inches (447 mm)	3.05 ft (0.93 m)	B133	Modified MGS with reduced post spacing (*NCHRP 350* 3-11)
PR-1 MwRSF, 2002 (32) [2]	27.8 inches (706 mm)	4 ft-5 inch long W6×9 steel	6 ft-3 inch	6×8× 14 inch wood	N/A	38.2 inches (970 mm)	3.31 ft (1.01 m)	B64B	G4(1S) guardrail with posts installed in rock (*NCHRP 350* 3-11)
N/A_1 SwRI, 2002 (33) [1]	27.8 inches (706 mm) [3]	6 ft long O-Post (Posts 12-18)	6 ft-3 inch	5.5×7.7× 14.25 inch routed timber	N/A	40.6 inches (1030 mm)	N/A	B95	O-Post as an alternative to a standard W6×8.5 steel post for use for W-beam guardrail (*NCHRP 350* 3-11)
N/A_2 SwRI, 2002 (34) [1]	27.8 inches (706 mm) [3]	6 ft long O-Post (Posts 12-18)	6 ft-3 inch	5.5×7.7× 14.25 inch routed timber	N/A	43.7 inches (1110 mm)	N/A	B95A	O-Post impacting at the open side (*NCHRP 350* 3-11)

Table B-4. W-Beam Guardrail Deflections, Cont. [18]

Test No. Agency, Year	Rail Height	Post		Blockout	Maximum Deflection		Working Width	FHWA Letter No.	System Configuration
		Size and Material	Spacing		Permanent	Dynamic			
41-1792-001 E-TECH Inc., 2003 (35)[1]	27.8 inches (706 mm)[2]	5 ft-3 inch long HALCO X-44 Steel	6 ft-3 inch	6⅛×7⅞×14¼ inch recycled plastic	23.6 inches (600 mm)	27.6 inches (700 mm)	N/A	B80C	G4 guardrail with light weight, strong HALCO X-44 steel posts (NCHRP 350 3-11)
2214MG -1 MwRSF, 2004 (36)[3]	31 inches (787 mm)	6 ft long W6×9 steel	6 ft-3 inch	6×12×14¼ inch wood	42.9 inches (1089 mm)	57 inches (1447 mm)	4.78 ft (1.46 m)	N/A	Modified MGS guardrail (MASH 3-11)
2214MG -2 MwRSF, 2004 (37)[3]	31 inches (787 mm)	6 ft long W6×9 steel	6 ft-3 inch	6×12×14¼ inch wood	31.6 inches (803 mm)	43.9 inches (1114 mm)	4.05 ft (1.23 m)	N/A	Modified MGS guardrail (MASH 3-11)
2214WB-2 MwRSF, 2005 (38)[1]	27.8 inches (706 mm)	6 ft long W6×9 steel	6 ft-3 inch	6×8×14¼ inch wood	33.3 inches (845 mm)	47.1 inches (1196 mm)	4.58 ft (1.4 m)	N/A	Modified MGS guardrail (MASH 3-11)
220570-2 TTI, 2005 (39)[4]	31 inches (787 mm)	6-ft long W6×8.5 SYLP	6 ft-3 inch	N/A	28.7 inches (730 mm)	40.9 inches (1040 mm)	3.67 ft (1.12 m)	B140	W-beam guardrail on SYLP (G2 guardrail) (MASH 3-11)
220570-8 TTI, 2006 (40)[3]	29 inches (737 mm)	6-ft long W6×8.5 SYLP	6 ft-3 inch	N/A	28.7 inches (730 mm)	37.4 inches (950 mm)	4.04 ft (1.23 m)	N/A	29 inch tall T-31 W-beam guardrail on SYLP (G2 guardrail) (NCHRP 350 3-11)
GMS-1 SwRI, 2006 (41)[4]	31 inches (787 mm)	6-ft long W6×8.5 steel	6 ft-3 inch	N/A	22 inches (560 mm)	35 inches (890 mm)	N/A	B150	Modified G4(1S) Longitudinal Barrier using GMS fastener (MASH 3-11)

Table B-5. W-Beam Guardrail Deflections, Cont. [18]

| Test No. Agency, Year	Rail Height	Post Size and Material	Spacing	Blockout	Maximum Deflection Permanent	Dynamic	Working Width	FHWA Letter No.	System Configuration
MGSDF-1 MwRSF,2006 (42)[1]	31 inches (787 mm)	5 ft-9 inch long 7¼ inch dia Douglas fir wood posts	6 ft-3 inch	6×8× 14¼ inch & 6×5× 14¼ inch wood	35.5 inches (902 mm)	60.2 inches (1529 mm)	5.02 ft (1.53 m)	B175	MGS with Douglas fir wood post (*NCHRP 350* 3-11)
MGSPP-1 MwRSF,2006 (42)[1]	31 inches (787 mm)	5 ft-9 inch long 8 inch dia Ponderosa pine posts	6 ft-3 inch	6×8× 14¼ inch and 6×5× 14¼ inch wood	27.8 inches (705 mm)	37.6 inches (956 mm)	4.05 ft (1.23 m)	B175	MGS with Round Ponderosa pine posts (*NCHRP 350* 3-11)
400001-TGS1 TTI, 2007 (43)[2]	31 inches (787 mm)	6-ft long W6×8.5 steel	6 ft-3 inch	N/A	31 inches (787 mm)	38.4 inches (975 mm)	3.4 ft (1.04 m)	N/A	Trinity Guardrail System (TGS) (*MASH* 3-11)
GMS-6 SwRI, 2007 (44)[2]	27⅝ inches (702 mm)	6-ft long W6×8.5 steel	6 ft-3 inch	N/A	31.9 inches (810 mm)	52 inches (1320 mm)	N/A	B150A	Modified GMS guardrail (*MASH* 3-11)
GMS-7 SwRI, 2007 (45)[2]	27⅝ inches (702 mm)	6-ft long W6×8.5 steel	12 ft-6 inch	N/A	20.9 inches (530 mm)	59.8 inches (1520 mm)	N/A	B150B	Modified GMS guardrail with longer spacing (*MASH* 3-11)
057073112 Holmes Solutions, 2007 (46)[1]	31 inches (787 mm)	6 ft-6 inch long U-channel steel (Nucor Grade SP-80, galvanized)	6 ft-3 inch	N/A	31.5 inches (800 mm)	41.3 inches (1050 mm)	N/A	B162	Nucor strong post W-beam guardrail system without blockout (*MASH* 3-11)

Table B-6. W-Beam Guardrail Deflections, Cont. [18]

Test No. Agency, Year	Rail Height	Post		Blockout	Maximum Deflection		Working Width	FHWA Letter No.	System Configuration
		Size and Material	Spacing		Permanent	Dynamic			
05707b3111 Holmes Solutions, 2007 (46)[1]	27 inches (686 mm)	6 ft-6 inch long U-channel steel (Nucor Grade SP-80)	6 ft-3 inch	4×8×14 in Recycled plastic	35.4 inches (900 mm)	45.3 inches (1150 mm)	N/A	B162	Nucor Strong Post W-beam guardrail system (NCHRP 350 3-11)
0000-0-0-00-1 Holmes Solutions, 2008 (47)[2]	27 inches (686 mm)	6 ft-6 inch long W6×9 steel and 6 ft long U-channel steel[3]	6 ft-3 inch	Original plastic	38.6 inches (980 mm)	56.7 inches (1440 mm)	5.41 ft (1.65 m)	B186	NU-Guard posts mixed in strong post guardrail using Mazda Proceed vehicle (NCHRP 350 3-11)

Appendix C. Modeling Difficulties

Fender Penetration

On several occasions, the left-front fender of the Chevrolet Silverado pickup model penetrated the rail section upon impact, as shown in Figure C-1. This penetration caused the fender to become snagged behind the rail section, which caused a spike in the total energy of the system, as shown in Figure C-2.
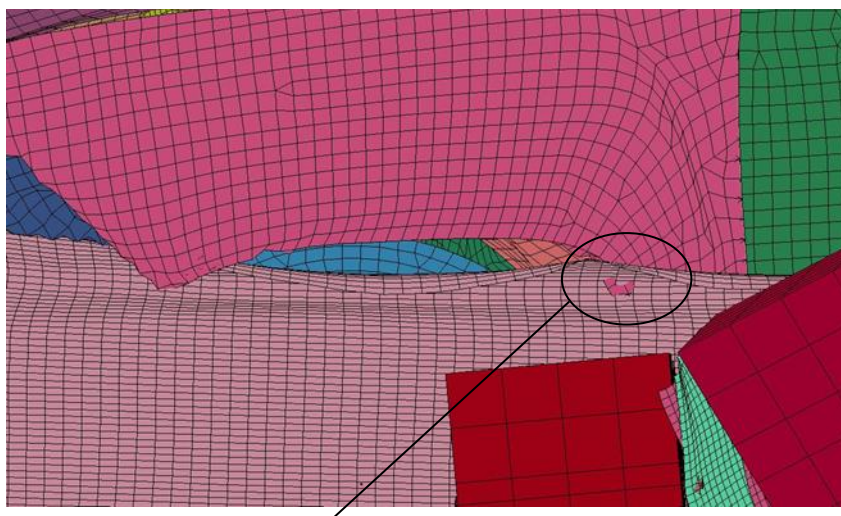
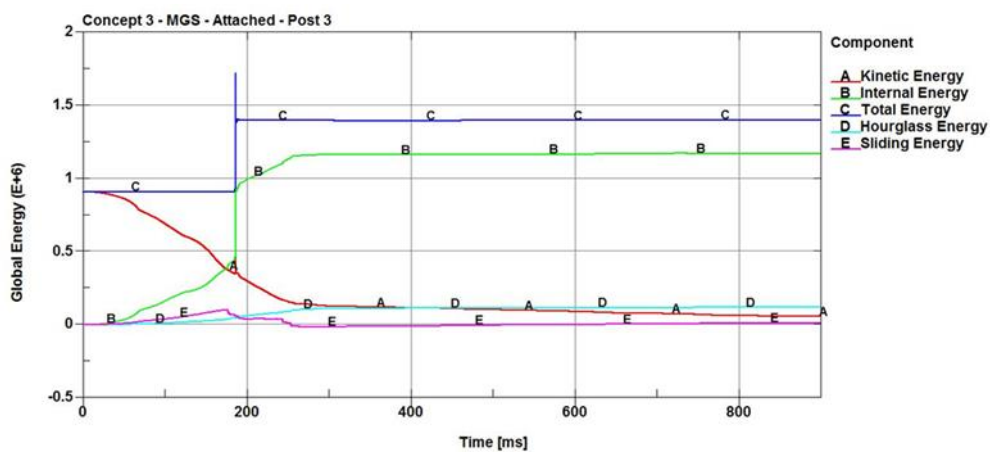Fender Penetration

Figure C-1. Fender Penetration

Figure C-2. Global Energy Plot

In order to alleviate the fender penetration issues, the DT2MS in the *CONTROL_TIMESTEP card was reduced from -1.112e-03 to -0.800e-03 for each occurrence. Reducing this time step eliminated the spike in total energy, and there were no longer any fender penetration concerns.

Blockout Modeling

The blockouts that were used in transition modeling were comprised of solid elements with a material definition of *MAT_ELASTIC. As previously noted, due to complex fracture mechanics of wood material, an LS-DYNA model that accurately reflects the fracture of wood has not been developed. This lack of failure caused deformations of the rail that likely would not occur in actual testing, as shown in Figure C-3. This unrealistic behavior was noted for affected simulations.
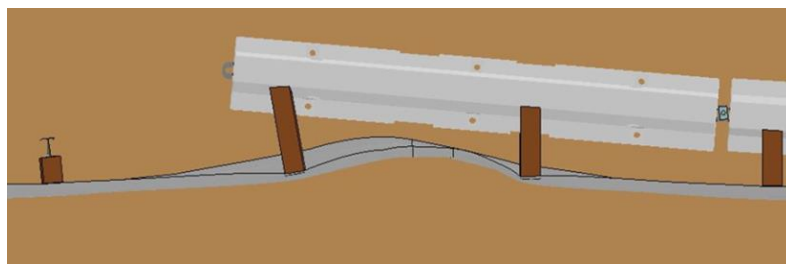

Figure C-3. Localized Kinking Between Oversize Blockouts

Blockout Connection to PCBs

A simplified connection of blockouts to PCBs was modeled using a discrete element connection similar to other bolted connections in the MGS model. The discrete elements were modeled to connect directly to the face of the PCB segment, as shown in Figure C-4. This simplified connection would not be possible in actual testing, so further research is necessary to develop a connection or bracket between blockouts and PCBs prior to full-scale crash testing.

Figure C-4. Blockout Connection to PCBs

W-Beam End Shoe Attachment to PCBs

Similarly, the W-beam end shoe attachment was modeled as a simplified connection. An actual W-beam end shoe could likely be bolted directly to the face of the F-shape PCB segment. However, due to the sloped face of the F-shape PCB in combination with limitations in modeling capabilities, a small attachment wedge was required, as shown in Figure C-5. The attachment wedge was constrained to the PCB segment using *CONSTRAINED_RIGID_BODIES due to the rigid material formulation of both the PCB segment and the attachment wedge. Since the W-beam end shoe was a deformable material, it was constrained to the attachment wedge using *CONSTRAINED_EXTRA_NODE_SET. A failure criterion was not defined for either of these constraint definitions. The attachment wedge and constraints would not be necessary in actual testing, so further research is necessary to develop a connection between the W-beam end shoe and PCB prior to full-scale crash testing.
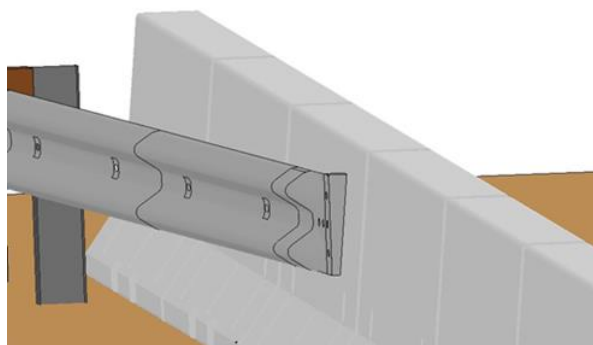

Figure C-5. W-Beam End Shoe Attachment